2011

Integrated Life-Cycle Framework for Optimal Inspection, Monitoring and Maintenance under Uncertainty: Applications to Highway Bridges and Naval Ship Structures

Sunyong Kim
Lehigh University

Integrated Life-Cycle Framework for Optimal Inspection, Monitoring and Maintenance under Uncertainty: Applications to Highway Bridges and Naval Ship Structures

by

Sunyong Kim

A Dissertation
Presented to the Graduate Research Committee
of Lehigh University
in Candidacy for the Degree of
Doctor of Philosophy

in
Structural Engineering

Lehigh University

May 2011

Approved and recommended for acceptance as a dissertation in partial fulfillment of the requirements for the degree of Doctor of Philosophy.

_____
Date

_____
Dr. Dan M. Frangopol
Dissertation Advisor
Professor of Civil and
Environmental Engineering
Lehigh University

_____
Accepted Date

Committee Members:

_____
Dr. John L. Wilson
Committee Chairperson
Professor of Civil and
Environmental Engineering
Lehigh University

_____
Dr. James M. Ricles
Member
Professor of Civil and
Environmental Engineering
Lehigh University

_____
Dr. Ben T. Yen
Member
Professor of Civil and
Environmental Engineering
Lehigh University

_____
Dr. Yunfeng Zhang
Member
Associate Professor of Civil and
Environmental Engineering
University of Maryland

ACKNOWLEDGEMENTS

First of all, I would like to express my appreciation to my advisor Prof. Dan M. Frangopol for his guidance, endless patience and continuous support throughout my Ph.D. program. I am particularly grateful to Prof. Dan M. Frangopol for the opportunity to present fifteen papers for publication in reputable scientific journals. Especially, his frequent and critical guidance kept me on track. As a result, eleven journal papers have already been published, and four are in press, in addition to a book chapter and several conference papers.

My gratitude is extended to Professors Wilson, Yen, Ricles, and Zhang who served on my Ph.D. committee and evaluated my work.

I gratefully acknowledge the support from (a) the National Science Foundation through grants CMS-0638728 and CMS-0639428, (b) the Commonwealth of Pennsylvania, Department of Community and Economic Development, through the Pennsylvania Infrastructure Technology Alliance (PITA), (c) the U.S. Federal Highway Administration Cooperative Agreement Award DTFH61-07-H-00040, and (d) the U.S. Office of Naval Research Contract Number N00014-08-1-0188.

I would like to thank my colleagues for their contributions to parts of this study. I thank Alberto Decò, Duygu Saydam, and Mohamed Soliman for their constructive discussions and comments to improve this study, and warm friendship. I also thank

Benjin Zhu for her contribution in some of the computations. Special thanks to Kihyon Kwon and my previous office mate Nader Okasha for their assistance, encouragement and warm friendship. Furthermore, I would like to thank former and present visiting scholars at Lehigh University including Drs. Alfred Strauss, Ming Liu Andrè D. Orcesi and Paolo Bocchini for their contributions and suggestions.

Finally and most importantly, I offer my sincere thanks and love to my wife Taewoo Koh and my parents Chuljoong Kim and Younghee Oh, to whom this thesis is dedicated.

TABLE OF CONTENTS

LIST OF TABLES

CHAPTER 2

CHAPTER 3

CHAPTER 4

CHAPTER 5

CHAPTER 6

CHAPTER 7

LIST OF FIGURES

CHAPTER 2

CHAPTER 3

CHAPTER 4

CHAPTER 6

CHAPTER 7

APPENDIX

ABSTRACT

Existing engineering structures are continuously deteriorating and their lifetimes are limited. In order to help ensure the structural safety and extend the service life of existing deteriorating structures, significant research efforts for establishing cost-effective maintenance strategies have been made. A life-cycle analysis usually depends on structural assessment and prediction models under uncertainty. The accuracy associated with these models can be considerably improved if the data from structural health monitoring (SHM) are used efficiently. Therefore, integration of SHM into maintenance management has recently been considered as a significant tool for rational maintenance planning.

Improved accuracy of structural performance assessment and prediction by SHM can lead to timely and appropriate maintenance interventions, resulting in reduction of both expected failure cost and expected maintenance cost of deteriorating structural systems. In order to maximize this potential benefit of SHM, information from monitoring has to be used appropriately, and an effective optimum monitoring planning is necessary. Furthermore, lifetime optimization of inspection, monitoring, and maintenance strategies needs to be investigated in a life-cycle management framework.

The main focus of this study is the development of a rational probabilistic integrated framework for optimum inspection, monitoring and maintenance planning.

Based on concepts of probability and reliability, novel approaches to assess and predict the structural performance using SHM data are developed and applied to existing highway bridges. For optimum inspection and monitoring planning under uncertainty, several probabilistic approaches are developed in this study. Optimization formulations for these approaches are based on the concepts of availability, damage detection delay, and time-based safety margin. The inspection or monitoring plan is a solution of a multi-objective optimization problem under uncertainty. The uncertainties associated with damage occurrence and propagation, and quality of inspection method are considered within the optimization problem. These approaches are applied to deteriorating structures (i.e., highway bridges, naval ships) under various deterioration mechanisms (i.e., corrosion, fatigue). Furthermore, considering the effects of probabilities of damage detection and repair on future structural performance, the optimum inspection and maintenance strategy under uncertainty are addressed to extend the lifetime of deteriorating structures.

CHAPTER 1

INTRODUCTION

1.1 Overview of Life-Cycle Analysis

The performance of a structure over its service life undergoes gradual deterioration due to various environmental stressors [Frangopol and Liu 2006]. In order to ensure the structural safety during the service life of a structure, maintenance and risk mitigation are required [Frangopol et al. 2001]. Limited financial resources should be allocated in a rational way so that lifetime structural performance can be improved, and the service life of a structure can be extended [Das 1999]. This requires reliable modeling of loadings, accurate prediction of structural performance, proper estimation of management and maintenance cost over time, and generation of well-balanced solutions [Frangopol and Liu 2006, Schuëller 1998]. Since time-dependent structural deterioration processes under continuously changing environmental conditions are highly uncertain, reliability-based approaches for life-cycle analysis are necessary [Estes et al. 1999, Kong and Frangopol 2003b, and 2005].

1.1.1 Reliability-Based Life-Cycle Analysis

Life-cycle analysis can be referred to a systemic method to evaluate the effects of time-dependent deterioration processes, loading conditions, maintenance and repair actions on the performance of structures and their service lives [Moan 2005,

Frangopol and Liu 2006]. Generally, the evaluation of these effects includes high uncertainties [Frangopol 2011]. In order to treat uncertainties rationally, reliability-based approaches for life-cycle analysis were introduced and investigated by Frangopol et al. (1997a and 1997b), Estes and Frangopol (1999), Kong and Frangopol (2003 and 2005), Ang and De Leon (2005), and Moan (2005), among others. The reliability-based life-cycle analysis can provide (a) the expected total cost including the initial cost, inspection cost, maintenance and repair cost, and cost associated with structural failure during a predefined lifetime; (b) optimum inspection, maintenance and repair times; and (c) the expected structural performance during the service life of a structure.

1.1.2 Prediction of Lifetime Performance under Uncertainty

For the life-cycle analysis, understanding of deterioration mechanism and accurate performance prediction of a deteriorating structure are essential. The deterioration of structures may be caused by combined effects of progressive structure aging, aggressive environmental stressors, and loading conditions. The most common causes of resistance reduction of concrete and steel structures are corrosion and fatigue.

Among the processes to induce deterioration of reinforced concrete (RC) bridges, corrosion of reinforcement in concrete was considered as predominant [Chaker 1992]. A significant amount of effort has been made to predict the propagation of corrosion damage [NCHRP 2005]. However, since the mechanism of RC degradation is highly

dependent on the environment and concrete material properties are uncertain, it is still not possible to accurately predict structural performance of deteriorating RC structures. Several studies focusing on probabilistic service life prediction have been conducted on deteriorating concrete bridges under corrosion [Frangopol et al. 1997a, Enright and Frangopol 1998a; Stewart 2004; Li et al. 2005].

The deterioration of a steel structure over its service life can be the result of fatigue induced by various loadings [Fisher et al. 1998]. The fatigue can cause cracking, and lead to unexpected failure or out-of-service state of a steel structure. This problem is one of the major threats to the structural integrity of deteriorating steel structures [Akpan et al. 2002]. In order to consider uncertainties associated with the loading conditions, environmental stressors, fabrication, and modeling of steel structures subjected to fatigue, several probabilistic approaches have been used to assess and predict the fatigue structural performance [Madsen and Sørensen 1990, Madsen et al. 1991, Soares and Garbatov 1996a and 1996b, Ayyub et al. 2002].

1.1.3 Life-Cycle Optimization

Minimization of life-cycle cost is the most widely used criterion, but in reality multiple and conflicting objectives need to be considered simultaneously [Frangopol and Liu 2006]. For example, structural management decisions should be made by improving structural performance and reducing the life-cycle cost. The management planning of deteriorating structures can be formulated as a multi-objective

optimization problem with several performance indicators including system reliability, availability, condition and safety indices, and cost [Liu and Frangopol 2005a and 2005b, Neves et al. 2006a and 2006b, Okasha and Frangopol 2009 and 2010b]. Structural managers can select one of the solutions from the Pareto optimal set, considering the financial resources and the performance level of the deteriorating structure.

1.2 Problem Statement

The importance of cost-effective maintenance of deteriorating structures under limited funds has been well documented. The topics of establishing management programs to maintain structural safety and serviceability above prescribed thresholds and extend the service life of deteriorating structures are of great interest. These studies require improved modelings of loadings and deterioration processes, accurate prediction of the structural performance, and proper estimation and optimum allocation of inspection, monitoring, and maintenance costs over time [Frangopol and Liu 2006 and 2007, Frangopol 2011].

In the last decades, structural health monitoring (SHM) has been widely applied to determine the location and severity of damage [Chang et al. 2003]. Significant efforts have been focused on technological advancements of SHM, and development of efficient data acquisition and interpretation algorithms for structures including civil infrastructures, naval ship and aircraft structures subjected to various deterioration

mechanisms such as corrosion and fatigue [Chong et al. 2003, Farrar and Worden 2007]. However, the field of integrating SHM concepts and methods into maintenance management of deteriorating structures under uncertainty is still in its infancy. The reliability assessment and prediction using monitored data has been studied only recently [Frangopol 2011].

In general, the uncertainties associated with resistance and load effect for structural assessment are smaller than those associated with structural design due to the availability of information from site-specific response data [Liu et al. 2009a]. Therefore, the application of SHM has a great potential in cost-effective maintenance by reduction of uncertainty. This reduction can lead to preventing unexpected failure of a structure, assessing and predicting structural performance more reliably, and applying appropriate maintenance on time. As a result, it can yield the reduction of both the failure cost and maintenance cost [Frangopol and Messervey 2007, 2009a, 2009b]. However, if the application of SHM is not cost-effective, and the use of SHM data is not efficient, then it will be difficult for structure managers to justify adopting SHM. Therefore, cost-effective monitoring planning and efficient use of SHM data should be considered in a life-cycle management framework. Furthermore, lifetime optimization of inspection, monitoring, and maintenance strategies needs to be investigated.

1.3 Research Objectives

The followings are the main objective of this study:

1. Develop approaches for efficient use of SHM data to assess and predict the structural performance in a life-cycle framework under uncertainty
2. Develop probabilistic approaches for optimum inspection and monitoring planning.
3. Develop probabilistic approaches for lifetime optimization of inspection and repair strategies.

1.4 Benefits and Limitations of the Research

1.4.1 Benefits

- This study addresses probabilistic optimization, system reliability, modeling of uncertainties associated with damage propagation and inspection methods, deterioration models, expected life-cycle costs, non-destructive testing, and SHM in the integrated framework for optimum inspection, monitoring and maintenance planning.
- This study proposes several novel concepts such as the availability of monitoring data, expected damage detection delay, time-based safety margin, and expected extended lifetime of a structure. These concepts are based on (a) reliability, (b) statistics of extremes, (c) decision analysis, (d) probabilistic analysis and prediction of damage occurrence, propagation and detection, and (e) cost

estimation for inspection, monitoring and repair of structures. Even though these concepts have several limitations, they lay down the theoretical background for practical applications.

- The approaches in this study are applied to highway bridges and ship structures subjected to corrosion or fatigue. However, the approaches in this study are general, and can also be applied to any type of structure subjected to various kinds of deterioration processes.

1.4.2 Limitations

- Probabilistic approaches for inspection, monitoring and maintenance planning in this study require the modeling of structural deterioration processes. In general, structural deterioration processes are very complex, and accuracy in these models is desirable. The modeling of the structural deterioration process itself is beyond the scope of this study. However, the proposed approaches for optimum inspection, monitoring, and maintenance planning may be used for updating information after each inspection or monitoring in order to improve the accuracy of the modeling of structural deteriorating processes.
- The optimum monitoring planning includes decisions on (a) types of sensors, (b) location and number of sensors, and (c) operating duration of sensors [Farrar and Worden 2007]. The approaches proposed in this study are associated with the decision on operating duration of sensors, under the assumption that the

appropriate monitoring system for the expected damage is installed at the critical locations.

- Cost estimations in this study are based on several assumptions. For instance, the failure cost representing the monetary loss due to a structural failure should be quantified considering various factors such as loss of life, reconstruction, and users inconvenience, among others [Estes and Frangopol 2005]. However, this study does not attempt to quantify the failure cost. Furthermore, the discount rate of money is assumed constant over time in this study. However, this rate may change over time. Moreover, different government agencies use different discount rates of money. The approaches for optimum inspection, monitoring, and maintenance planning can be affected by the failure cost and the discount rate of money. For this reason, this research includes the effects of several assumptions for cost estimation on the results.
- Maintenance actions depend on the outcome of inspection or monitoring. If the damage is detected, maintenance should be applied as soon as possible. However, in reality, due to the limited financial resources, maintenance may not be applied just after damage detection. In this study, the decision maker's willingness to make repair after damage detection is probability-based. In reality, this willingness depends on availability of funds and competing priorities.
- In this study, the interaction between deteriorating processes such as corrosion and fatigue is not considered. The corrosion and fatigue processes can propagate

simultaneously, leading to a higher deteriorating rate of a structure than the case of separate propagation [Akpan et al. 2002].

1.5 Organization of the Dissertation

- **Chapter 1** serves as introduction.
- **Chapter 2** presents the concepts of the reliability and service life of structures. The system reliability approach and its applications are presented. The effects of time-dependent structural performance on the service life of a structure are studied. Furthermore, the general concepts of optimal management using multi-criteria optimization are provided.
- In **Chapter 3**, the approaches for efficient use of SHM are provided. These are (a) an approach to develop and update prediction functions, and (b) an approach for the assessment and prediction of structural performance using monitoring data. The general concept of reliability described in Chapter 2 is used to develop these two approaches. The mean square fitting to monitored data, acceptance sampling theory, and concept of reliability are used to establish and update prediction functions. Furthermore, in order to assess and predict the structural system performance through series-parallel system modeling, an approach using the long-term monitored strain data is proposed.
- **Chapter 4** proposes a novel approach for the optimum monitoring planning under uncertainty. This approach is based on a bi-objective optimization problem with

two conflicting criteria associated with the maximization of the expected average availability of the monitoring data and minimization of total monitoring cost. In order to solve this bi-objective optimization problem, the genetic algorithm is used. A solution of this problem provides uniform time interval between monitoring activities for an individual structural component. This process is extended to the approach for a structural system, considering reliability importance factors of structural components. In addition, decision analysis theory based on the minimum monetary loss criterion is used as an alternative approach.

- **Chapter 5** presents a probabilistic approach for optimum inspection and monitoring planning to minimize the expected damage detection delay. The formulation of damage detection delay considers the uncertainties associated with damage occurrence and propagation, and quality of inspection method. The optimization problem is formulated with the objective of minimization of the expected damage detection delay. This approach provides non-uniform time intervals between inspections or monitoring activities. The effects of the quality of inspection, number of inspections or monitoring activities, and monitoring duration on the expected damage detection delay are investigated. The bi-objective optimization problem is formulated by simultaneously minimizing the expected damage detection delay and the total inspection and/or monitoring cost. The solution of this bi-objective optimization includes types and time of inspections. A comparison of the cost-effective inspection plans based on a single

type and multiple types of inspections is carried out. Furthermore, an optimum combined inspection / monitoring planning is investigated taking into account the Pareto solution sets associated with all possible combinations of inspection and monitoring.

- **Chapter 6** extends the approach presented in Chapter 5 to cost-based optimum inspection and monitoring planning. This chapter describes the relationship between time-based safety margin and damage detection delay, and the expected total cost. The objective of the optimization problem in this chapter is to minimize the expected total cost consisting of the failure cost and inspection or monitoring cost. The failure cost is based on the time-based failure criterion defined using the damage detection delay and time-based safety margin. Effects of the failure cost on inspection and monitoring scheduling are studied.
- **Chapter 7** presents an approach for an optimum inspection and repair strategy under uncertainty to extend the lifetime of structures. The optimum strategy provided in this chapter consists in the maximization of the expected extended lifetime and the minimization of the expected total maintenance cost. The extended lifetime for a given number of inspections is formulated through a decision tree model. The decision maker's willingness to make repair after damage detection is considered in this decision tree. The effects of inspection quality, repair approach and number of inspections on the expected extended lifetime are investigated.

- **Chapter 8** summarizes this study, draws conclusions, and recommends future research directions.

CHAPTER 2

CONCEPTS OF RELIABILITY, SERVICE LIFE AND LIFE-CYCLE MANAGEMENT OF STRUCTURES

2.1 Introduction

The importance of maintenance for the deteriorating civil infrastructure has been recognized and many engineers have made significant efforts to extend the service life of existing civil structures effectively [Peil 2005, Frangopol 2011]. The service life of a structure is generally affected by its deterioration mechanisms and various environmental stressors under uncertainty [Smoak 2002]. Several probabilistic deterioration models for service life prediction have been presented [Frangopol et al. 1997a, Enright and Frangopol 1998a, Ang and De Leon 2005, Moan 2005]. Based on these models, lifetime optimization methodologies for planning repair strategies of deteriorating structures have been developed to make structural managers decide the priority of maintenance interventions on a deteriorating structure [Frangopol et al. 1997b, Enright and Frangopol 1999b, Estes and Frangopol 1999, 2001]. The expected service life, structural performance during its lifetime, and expected cost can be considered for the maintenance intervention [Frangopol et al. 2001, Kong and Frangopol 2003a].

This chapter provides the concepts of the reliability and service life of civil structures. The system reliability approach and its applications are presented. The effects of time-dependent structural performance on the service life of a structure are

studied. Furthermore, the general concepts of optimal management using multi-criteria optimization are provided.

2.2 Structural Reliability

2.2.1 General Concepts

In general, two types of uncertainties exist at present: aleatoric and epistemic. Due to aleatoric uncertainty (which relates to the inherent randomness of a process) and epistemic uncertainty (which is caused by lack of data and can be reduced by additional information), there always exists a probability of structural failure [Ang and De Leon 2005]. These two types of uncertainties make prediction of service life of a civil structure uncertain as shown in Figure 2.1. Therefore, these uncertainties should be treated in a rational way by using concepts and methods of probability and structural reliability theory [Ang and Tang 1984, 2007].

Uncertainties associated with structural performance can be quantified using the concept of probability. Figure 2.1 shows that the performance of a structure has randomness associated with some physical quantities under uncertainty. This randomness may be identified through a function of a random variable such as probability density function (PDF). The service life, which can be defined as the expected time period for which the performance of a structure is above a target level, has its own PDF.

This section introduces the concept of reliability and its application to define

uncertainty in structural behavior quantitatively. The reliability can be defined as the probability that an item will adequately perform its specified purpose for a specified period of time under specified environmental condition [Leemis 1995] and, in brief, a probabilistic measure of assurance of safe performance [Ang and Tang 1984]. In reality, the reliability problem of engineering systems can be expressed as a problem of supply and demand which are modeled by means of random variables. For instance, if R and S are the resistance and the load effect respectively, characterized by the PDF $f_R(r)$ and $f_S(s)$, respectively, the probability that S will not exceed R, $P(R > S)$, represents the reliability of the structural system (see Figure 2.2). If R and S are statistically independent, the probability of failure, $P(R < S)$, is

$$p_F = \int_0^\infty F_R(s) f_s(s) ds \tag{2.1}$$

where $F_R(s)$ is the cumulative distribution function (CDF) of R. Therefore, the reliability can be formulated as

$$p_S = 1 - \int_0^\infty F_R(s) f_s(s) ds \tag{2.2}$$

As a general case, if R and S are not independent, the probability of failure can be expressed in terms of joint PDF of the random variables R and S, $f_{R,S}(r,s)$, as

$$p_F = \int_0^\infty \left[\int_0^s f_{R,S}(r,s) dr \right] ds \tag{2.3}$$

And the corresponding probability of survival is

$$p_S = \int_0^\infty \left[\int_0^r f_{R,S}(r,s) ds \right] dr \tag{2.4}$$

Safety margin

The difference between resistance and load effect can be defined as safety margin $M = R - S$. The safety margin, M, is a random variable with PDF $f_M(m)$. As shown in Figure 2.3, the area under the PDF upper bounded by $m = 0$ represents the probability of failure

$$p_F = \int_{-\infty}^{0} f_M(m)dm \tag{2.5}$$

Reliability index

The reliability index is defined as (see Figure 2.3)

$$\beta = \frac{\mu_M}{\sigma_M} \tag{2.6}$$

where μ_M and σ_M are the mean and standard deviation of the safety margin, respectively. If R and S are independent, Equation 2.6 becomes

$$\beta = \frac{\mu_R - \mu_S}{\sqrt{\sigma_R^2 + \sigma_S^2}} \tag{2.7}$$

where μ_R, μ_S and σ_R, σ_S are the means and standard deviations, respectively. Furthermore, on the assumption that the safety margin M is normally distributed, the reliability index can be expressed as follows:

$$\beta = \Phi^{-1}(p_S) = \Phi^{-1}(1 - p_F) \tag{2.8}$$

where Φ^{-1} is the inverse of the standard normal cumulative density function. The reliability index may be evaluated by using the first moment (i.e., the mean value) and

the second moment (i.e., the variance). Let the reduced variables of R and S be defined by

$$R' = \frac{X - \mu_R}{\sigma_R} \quad \text{and} \quad S' = \frac{Y - \mu_S}{\sigma_S} \tag{2.9}$$

As shown Figure 2.4, the minimum distance from $M = 0$ to the origin of the space of reduced variables is equal to the reliability index β defined in Equation 2.7.

State function

The state function is related to the safety margin $M = R - S$. In general, the resistance and load effect consist of several variables. In order to generalize the problem considering these variables, the safety margin is formulated as a state function $g(\mathbf{X})$ [Ang and Tang 1984].

$$g(\mathbf{X}) = g(X_1, X_2, \ldots, X_n) \tag{2.10}$$

where $\mathbf{X} = (X_1, X_2, \ldots, X_n)$ is a vector of design variables, and the state function $g(\mathbf{X})$ determines the state as

$[g(\mathbf{X}) > 0] \rightarrow$ Safe state

$[g(\mathbf{X}) < 0] \rightarrow$ Failure state

$[g(\mathbf{X}) = 0] \rightarrow$ Limit state

Considering a two-variable reduced space, the limit state, the safe domain, and the failure domain are illustrated in Figure 2.5.

2.2.2 System Reliability

In general, structures are composed of many components. For each component, its various limit states (such as bending, shear, buckling, etc) may need to be considered. However, reliability of the individual structural component is not enough to guarantee the reliability of a structural system. Therefore, the problem of safety evaluation of existing structures can only be correctly assessed by considering the full structural system. In general, systems composed of multiple connected components can be classified as a series system (Figure 2.6(a)), a parallel system (Figure 2.6(b)), or a combined series-parallel system (Figure 2.6(c)).

Series system

In a series system (see Figure 2.6(a)), failure of any of its components constitutes the failure of the system; therefore, such a system has no redundancy and is also known as "weakest link" system. In other words, the reliability of the system requires that none of its components fail. The probability of failure p_F can be expressed as the probability of union of component failure events

$$p_F = p\left(\bigcup_{i=1}^{N}\left\{g_i\left(\mathbf{X}\right)\le 0\right\}\right) \tag{2.11}$$

The failure probability of the series system depends on the correlation among the safety margins of the components. The two extreme cases are as follows:

(a) for perfectly correlated case: $p_F = \max_{i=1}^{N} p_{Fi}$

(b) for statistically independent case: $p_F = 1 - \prod_{i=1}^{N} (1 - p_{Fi})$

The first-order bounds for the failure probability of a series system are [Cornell 1967]

$$\max_{i=1}^{N} p_{Fi} \le p_F \le 1 - \prod_{i=1}^{N} (1 - p_{Fi}) \tag{2.12}$$

Closer bounds were developed by Ditlevsen (1979) using joint-event probabilities, which accounted for failure mode correlation

$$p_{F1} + \sum_{i=2}^{k} max\left[p_{Fi} - \sum_{j=1}^{i-1} p_{Fij}, 0 \right] \le p_F \le \sum_{i=1}^{k} p_{Fi} - \sum_{i=2}^{k} \max_{j<i} \left[p_{Fij} \right] \tag{2.13}$$

where p_{Fij} is the joint probability of occurrence of the ith and jth failure modes, and k is the number of potential failure modes of a series system. Figures 2.7(a) and (b) show the safe domain, the failure domain, and the limit state of component 1 and component 2, respectively, and in Figure 2.8(a), the safe domain and the failure domain are shown when these two components are linked in series. It should be noted that X_1 and X_2 associated with Figures 2.7 and 2.8 are uncorrelated normal random variables.

Parallel system

Failure of a parallel system (see Figure 2.6(b)) requires failures of all its components. Therefore, if any one of the components survives, the system remains safe. The probability of failure of a parallel system P_f can be expressed as the probability of intersections of component failure events

$$p_F = p\left(\bigcap_{i=1}^{N} \{ g_i(\mathbf{X}) \le 0 \} \right) \tag{2.14}$$

The failure of an *N*-component parallel system depends on the correlation among the safety margins of its components. The two extreme cases are as follows:

(a) for perfectly correlated case: $p_F = \min_{i=1}^{N} p_{Fi}$

(b) for statistically independent case: $p_F = \prod_{i=1}^{N} p_{Fi}$

The first-order bounds for the failure probability of a parallel system are [Ang and Tang 1984]

$$\prod_{i=1}^{N} p_{Fi} \le p_F \le \min_{i=1} p_{Fi} \tag{2.15}$$

Practically, the first-order bounds of the failure probability of a parallel system determined by Equation 2.15 may be too wide to be useful. Therefore, an alternative approach is used as follows [Thoft-Christensen and Murotsu 1986]

$$p_F = \int_{\beta_1}^{\infty}\int_{\beta_2}^{\infty}\cdots\int_{\beta_N}^{\infty} \frac{1}{(2\pi)^{N/2}\sqrt{\det[\rho_{sys}]}} e^{-1/2\{\beta\}[\rho_{sys}]^{-1}\{\beta\}^T} d\{\beta\} \tag{2.16}$$

where $\{\beta\}=\{\beta_1, \beta_2, \ldots, \beta_N\}$, ρ_{sys} is the system correlation matrix, and *N* is the number of members in the system. The safe domain and the reliability index of the parallel system consisting of the two components having the safety domains shown in Figures 2.7(a) and (b) are indicated in Figure 2.8(a). By comparing Figures 2.8(a) and 2.8(b), it can be seen that both the safety domain and the reliability index of the parallel system are larger than those of the associated series system.

Combined system

A combined system can be modeled as a series system of parallel systems or a parallel

system of series systems. Consider a series system consisting of L parallel systems, where each parallel system i has N_i components (Figures 2.6(c)). The probability of overall system failure is given by

$$p_F = p\left(\bigcup_{i=1}^{L}\bigcap_{j=1}^{N_i}\left\{g_{ij}\left(\mathbf{X}\right)\le 0\right\}\right) \tag{2.17}$$

There are several computer programs such as CalREL [Liu et al. 1989] and RELSYS [Estes and Frangopol 1998] able to compute the probability of failure of combined systems.

Reliability importance factor

A structural system is composed of various components with different limit states. In general, the system performance can be assessed by using a series-parallel model. For effective maintenance strategy, it is necessary to rank structural components based on their reliability importance factors [Gharaibeh et al. 2002; Liu and Frangopol 2005c]. For instance, an individual component having the highest probability of failure in a series system has the highest impact on the system reliability. To quantify the impact of reliability of an individual component on the system reliability, the reliability importance factor (RIF) is used. The RIF of component i can be defined as the gradient of system reliability with respect to reliability of component i as [Leemis, 1995]

$$RIF_i = \frac{\partial p_{S,system}}{\partial p_{S,i}} \tag{2.18}$$

where $p_{S,\text{system}}$ = system reliability; and $p_{S,i}$ = reliability of component i. The associated normalized reliability importance factor (NRIF) of component i is defined as [Gharaibeh et al. 2002]

$$NRIF_i = \frac{RIF_i}{\sum_{j=1}^{N} RIF_j} \tag{2.19}$$

where N is the number of components in the system, and $0 \le NRIF_i \le 1.0$. For example, the reliability $p_{S,series}$ of a series system consisting of two statistically independent components is $p_{S,1} \times p_{S,2}$ where, $p_{S,1}$ and $p_{S,2}$ are the reliability of components 1 and 2, respectively. From Equation (2.18), the RIFs of components 1 and 2 become $p_{S,2}$ and $p_{S,1}$, respectively. Therefore, the NRIFs of these components are, according to Equation (2.19), $p_{S,2}$ / ($p_{S,1}$ + $p_{S,2}$) and $p_{S,1}$ / ($p_{S,1}$ + $p_{S,2}$), respectively. However, since most structural systems have correlated components, it could be difficult to formulate the system reliability using component reliability directly.

If the reliability of the system $p_{S,system}$ (i.e., series system, parallel system, or series-parallel system) is provided in terms of the reliabilities of N components as $f(p_{S,1}, p_{S,2}, ..., p_{S,i}, ..., p_{S,N})$, where $p_{S,i} = p_{S,i}(\mathbf{X}_i)$ is the reliability of component i, and $\mathbf{X}_i = \left(X_{i,1}, X_{i,2}, ..., X_{i,n_i}\right)$ is the vector associated with n_i design variables of component i, the gradient of system reliability $p_{S,system}(\mathbf{X})$ with respect to the kth design variable of component i, $X_{i,k}$, is given by the chain rule as follows

$$\frac{\partial p_{S,system}}{\partial X_{i,k}} = \frac{\partial p_{S,system}}{\partial p_{S,1}(\mathbf{X}_1)} \cdot \frac{\partial p_{S,1}(\mathbf{X}_1)}{\partial X_{i,k}} + \frac{\partial p_{S,system}}{\partial p_{S,2}(\mathbf{X}_2)} \cdot \frac{\partial p_{S,2}(\mathbf{X}_2)}{\partial X_{i,k}} + \ldots + \frac{\partial p_{S,system}}{\partial p_{S,N}(\mathbf{X}_N)} \cdot \frac{\partial p_{S,N}(\mathbf{X}_N)}{\partial X_{i,k}} \tag{2.20}$$

When the design variable $X_{i,k}$ is related to only the reliability function of component i, $p_{S,i}(\mathbf{X}_i)$, Equation (2.20) becomes

$$\frac{\partial p_{S,system}}{\partial X_{i,k}} = \frac{\partial p_{S,system}}{\partial p_{S,i}(\mathbf{X}_i)} \cdot \frac{\partial p_{S,i}(\mathbf{X}_i)}{\partial X_{i,k}} \tag{2.21}$$

Therefore, from Equation (2.18), the RIF of component i can be approximated as [Kim and Frangopol 2010]

$$RIF_i = \left(\frac{\partial p_{S,system}}{\partial X_{i,k}} \right) / \left(\frac{\partial p_{S,i}(\mathbf{X}_i)}{\partial X_{i,k}} \right) \approx \left(\frac{\Delta p_{S,system}}{\Delta X_{i,k}} \right) / \left(\frac{\Delta p_{S,i}(\mathbf{X}_i)}{\Delta X_{i,k}} \right) \tag{2.22}$$

Equation (2.22) means that the RIF of component i is the ratio of change in the system reliability to change in the component reliability due to a small change in the variable associated only with the reliability function of component i. Therefore, the RIF can be computed by changing a variable, uncorrelated with other variables, of the state function defined in Equation (2.10). The reliability importance factor can provide useful information for selecting the optimal maintenance strategy.

2.2.3 Application of Structural Reliability

In order to compute the reliability of a structural system, it is first necessary to define the system model. As an example, a four span bridge with four girders in each span is

used (see Figures 2.9(a) and (b)). It is assumed that failure of any two adjacent girders, failure of the deck, or both result in the failure of the superstructure. Failure event of each span can be modeled by the combined model in Figure 2.10(a) and the failure models of the four spans are connected in series system (see Figure 2.10(b)). The reliability analysis of a system can be extended to bridge network reliability. Evaluation of a bridge network is based on connectivity between a start point (A) and an end point (B). Such a network with six bridges is indicated in Figure 2.11(a). The bridge network model is shown in Figure 2.11(b).

2.3 Time-Dependent Reliability and Service Life

2.3.1 Time-Dependent Effects on Structures

An accurate reliability prediction model of a deteriorating structure is necessary to estimate the service life of a civil structure and to allocate the limited maintenance funds optimally for extension of its life. For establishing an accurate modeling of structural deterioration process, it is essential to accurately model both time-dependent mechanisms of resistance and load effect. Four cases are indicated in Figures 2.12(a) to (d) as follows: (a) time-independent resistance and load effect (Figure 2.12(a)); (b) time-dependent resistance and time-independent load effect (Figure 2.12(b)); (c) time-independent resistance and time-dependent load effect (Figure 2.12(c)); and (d) time-dependent resistance and load effect (Figure 2.12(d)). The mean safety margin profiles (i.e., the difference between mean resistance and

mean load effect) associated with the four cases shown in Figures 2.12(a) to (d) are indicated in Figure 2.12(e).

Resistance

Among the factors affecting the deterioration of concrete structures, corrosion is the main factor which may produce crack and spalling as well as loss of bond between concrete and reinforcing steel, and loss of steel section. In general, the deterioration process of reinforced concrete due to corrosion can be described by six steps [Thoft-Christensen 2003]:(a) chloride penetration in the concrete; (b) initiation of the corrosion of the reinforcement; (c) evolution of corrosion of the reinforcement; (d) initial cracking of the concrete; (e) evolution of cracks in the concrete; and (f) spalling. Corrosion in steel structures may be a very significant performance deterioration factor because most of components of a steel structure are exposed to environment directly.

Fatigue in metals can be defined as the process of initiation and growth of cracks under repetitive stresses. If crack growth is allowed, failure of a steel member can occur and this process can take place at stress levels that are less than levels at which failure occurs under static loading condition. Generally the fatigue life of a fabricated steel structure may be determined by three factors as follows [Fisher et al. 1998]: (a) number of loading cycles; (b) stress range at the location of a steel member; and (c) type of detail of a steel member. All these factors can have an important effect on the

service life of a steel structure.

Applied load

Maximum stress reaching yield strength and number of stress cycles exceeding the critical number of cycles can induce failure of a structural system. Therefore, the accuracy of the time- dependent models for prediction of the maximum stress caused by loads and number of stress cycles under live loads is important.

2.3.2 Analysis of Reliability of Deteriorating Structures and Service Life

Performance of a civil structure decreases with time due to load increase, fatigue and/or environmental attack such as corrosion [Ellingwood 2005]. If the stochastic models of loadings and environmental stressors are established over time accurately, the performance deterioration of structural components and of the entire system can be determined.

As an example, consider a series system and a parallel system both consisting of two components as shown in Figure 2.13(a). The time-dependent reliability indices of the two components are indicated in Table. 2.1. The relation between reliability index and probability of failure is determined using Equation 2.8, and the failure probabilities for the series system and parallel system are calculated by Equations 2.12 and 2.15, respectively. Figures 2.13(b) and (c) show each component reliability index and the system reliability indices over time when the correlation between two

members is perfect and when the safety margins of the components are statistically independent. In the perfectly correlated case, the series system reliability is equal to the smaller reliability index (i.e., the reliability index of the less safe member), and the reliability of the parallel system is equal to the larger reliability index (i.e., the reliability index of the most safe member).

As mentioned in section 2.3.1, the deterioration process of the performance of a civil structure depends on the time-dependent resistance and load effect. Figure 2.14 shows the change of the mean safety margin associated with each case in Table 2.2. Under four different deteriorating processes (cases A, B, C and D in Table 2.2), the time-dependent reliability indices are calculated by using Monte Carlo simulation program, MONTE [Kong et al. 2000]. Random variables X_1 and X_3 correspond to resistance and variables X_2 and X_4 are associated with load effect. These four random variables are considered independent. In Figures 2.15(a) to (d), the system reliability index of the series system has the lowest value, and that of parallel system has the largest value at any time. Therefore, the time necessary to reach the target value of reliability index, $\beta_{target} = 2.0$ (i.e., the service life of the system) is the lowest in case of the series system among all four cases. Also, the deteriorating rate associated with case D is the largest as shown in Figure 2.15(d).

These analyses could be utilized to determine: (a) which component has more influence on the system reliability; (b) which component needs inspection, maintenance and repair for effective improvement of system reliability; and (c) when

the maintenance and repair are needed for optimal extension of service life of the system.

2.3.3 Maintenance

To extend the expected service life of a system, effective maintenance is necessary [Frangopol et al., 1997b; and Frangopol et al., 2001; Moan, 2005; Frangopol and Liu, 2007, Okasha and Frangopol 2010b]. Therefore, preventive and/or essential maintenance are performed. Preventive maintenance is a time-based maintenance action, which is applied at predefined time instants to prevent the failure of the system. Preventive maintenance includes replacing small parts, patching concrete, repairing cracks, changing lubricants, and cleaning and painting exposed parts, among others. The essential maintenance is a performance-based action that it is immediately applied when some performance indicators reach predefined target values. In general, the essential maintenance follows an inspection, and includes replacing a bearing, resurfacing a deck, or modifying a girder of bridge. Preventive maintenance tends to be more frequent, less costly, and less efficient from the safety improvement viewpoint than essential maintenance.

A reliability index profile (multi-linear profile) associated with two preventive maintenances and one essential maintenance is presented as shown in Figure 2.16. This profile consists of the followings: (I) structure retains the initial reliability index without any performance deterioration; (II) performance deterioration of the structure

begins with the rate $r^{(0)}_{det}$ until time $T_{main,1}$; (III) first preventive maintenance is applied at time $T_{main,1}$, performance is improved, and deterioration continues but at smaller rate r_{det}, where, $r^{(0)}_{det} > r_{det}$; (IV) effectiveness of first preventive maintenance ends and the rate of the deterioration becomes $r^{(0)}_{det}$; (V) at time $T_{main,2}$, second preventive maintenance is applied, and the steps (III) and (IV) are repeated; and (VI) when the reliability index of structure reaches the target value, β_{target}, the essential maintenance will be applied resulting in a substantial increase of the reliability index, $\beta_{imp,3}$ (i.e., $\beta_{imp,3} > \beta_{imp,2}$, $\beta_{imp,3} > \beta_{imp,1}$). The reliability index profile including maintenance effects can be expressed by non-linear profiles. Based on these characteristics of maintenance, effective maintenance strategy can be formulated as a multi-objective optimization problem in which the objectives are minimizing maintenance cost and maximizing the service life.

2.4 Optimum Maintenance

2.4.1 Optimization of Lifetime Maintenance

The optimum maintenance strategy depends on many factors including the expected service life and the associated assumptions. The reliability of an entire system provides significant information for determination of maintenance strategy rather than the reliability of any individual component [Estes and Frangopol 1999]. To show that the maintenance strategy is mainly based on the reliability of a system, the three options indicated in Table 2.3 are applied to two systems (series and parallel system)

consisting of two perfectly correlated components with time dependent reliability index functions as indicated in Table 2.1.

As shown in Table 2.3, option 1 depends on the lowest reliability index, option 2 depends on the system reliability index, and option 3 considers both component reliability and system reliability. Figure 2.17(a) shows the reliability index profiles during 100 years for the series system. It is assumed that the expected replacement cost for each component is the same, \$1,000, and the failures of the two components are perfectly correlated. Total maintenance cost, C_{main}, can be computed as follows:

$$C_{main} = \sum_{i=1}^{n_{main}} \frac{C_{main,i}}{\left(1 + r_{dis}\right)^{T_{main,i}}} \tag{2.23}$$

where n_{main} = number of maintenance applications, $C_{main,i}$ = cost of ith maintenance, $T_{main,i}$ = time for ith maintenance, and r_{dis} = discount rate of money. The discount rate is assumed r_{dis} = 2 % / year.

• *Repair Option 1 for series system*: The first replacement will be conducted for the component 1 at year 35, the second replacement will be for the component 2 at year 50, and the third replacement will be for the component 1 at year 70. The total maintenance cost associated with the repair option 1 is

$$C_{main} = \frac{1{,}000}{(1+0.02)^{35}} + \frac{1{,}000}{(1+0.02)^{50}} + \frac{1{,}000}{(1+0.02)^{70}} = \$1{,}121.58\,.$$

• *Repair Option 2 for series system*: This system will be replaced entirely at year 35 and 70, when the system reliability index will reach 2.5. The total maintenance cost is

$$C_{main} = \frac{1{,}000 + 1{,}000}{(1+0.02)^{35}} + \frac{1{,}000 + 1{,}000}{(1+0.02)^{70}} = \$1{,}500.11 .$$

• *Repair Option 3 for series system*: Component 1 will be replaced at year 35, component 2 at year 50, and component 1 at year 70. The total maintenance cost associated with option 3 is as follows:

$$C_{main} = \frac{1{,}000}{(1+0.02)^{35}} + \frac{1{,}000}{(1+0.02)^{50}} + \frac{1{,}000}{(1+0.02)^{70}} = \$1{,}121.58 .$$

For the series system, options 1 and 3 are identical. In the series system, the component with the lowest reliability is the most important and controls the system reliability. Therefore, repair options 1 and 3 are the optimum repair strategies for this case (see Figure 2.18).

For the parallel system made of the same two components as the associated series system, the reliability index profiles during the specified service life of 100 years are shown, for each repair option, in Figure 2.17(b). The assumptions and discount rate for the analysis of this parallel system are the same as those used for the analysis of the associated series system.

• *Repair Option 1 for parallel system*: The first replacement will be conducted for the component 1 at year 35, the component 2 will be replaced at year 50, and the third replacement will be for the component 1 at year 70. The total maintenance cost is

$$C_{main} = \frac{1{,}000}{(1+0.02)^{35}} + \frac{1{,}000}{(1+0.02)^{50}} + \frac{1{,}000}{(1+0.02)^{70}} = \$1{,}121.58 .$$

• *Repair Option 2 for parallel system*: This parallel system will be replaced at year 50

and when the system reliability index of this system will reach 2.5. The total maintenance cost is

$$C_{main} = \frac{1{,}000 + 1{,}000}{(1+0.02)^{50}} = \$743.06 .$$

• *Repair Option 3 for parallel system*: At year 50 the system reliability will reach β_{system} = 2.5 and the reliability of component 1 will be 1.0. Therefore, the first replacement for component 1 will be at year 50, and the second for component 2 will be at year 80. The total maintenance cost for repair option 3 is

$$C_{main} = \frac{1{,}000}{(1+0.02)^{50}} + \frac{1{,}000}{(1+0.02)^{80}} = \$576.64 .$$

This parallel system in which the failures of two components are perfectly correlated has the reliability index profile that is governed by the component with the largest reliability. Therefore, repair option 3 can be considered as the optimal maintenance strategy in this example as shown in Figure 2.19. Estes and Frangopol (1999) provided the computational platform for the time-dependent reliability analysis of existing highway bridges and established the basis for the optimum lifetime maintenance approach under uncertainty.

2.4.2 Multi-Criteria Lifetime Optimization

There are many practical applications for life-cycle cost analysis where the designer may want to optimize two or more objectives simultaneously [Frangopol and Liu 2007; Furuta et al. 2006]. For example, decrease cost for maintenance and increase of

structural performance are two conflicting objectives. In this case, multi-criteria optimization should be applied by simultaneously minimizing a set of objective functions. Optimum solutions which are on the minimal boundary of the feasible criterion space are called Pareto optimal set as shown in Figure 2.19. In order to solve the multi-objective optimization problem, the following approaches can be applied as: (a) weighted sum, (b) weighted min-max, (c) weighted global criterion, (d) ε-constraint, and (e) genetic algorithm [Arora 2004]. The characteristics of these approaches are indicated in Table 2.4. Decision on which multi-objective optimization approach is most appropriate depends on user's preferences and efficiency of the computational process for a particular application [Flouda et al. 1999]. Decision makers have to compare different possible solutions from the multi-objective optimization problem and choose the best compromise. Liu and Frangopol (2004, 2005a, 2005b) proposed a multi-objective optimization approach with respect to condition index, safety index, and cumulative maintenance cost. Neves et al. (2006a and 2006b) considered a full probabilistic multi-objective optimization for single maintenance (silane or rebuild) and combined maintenance (silane and rebuild). Considering the objectives of system reliability, redundancy and life-cycle cost, the maintenance interventions was studied by Okasha and Frangopol (2009).

2.5 Summary

This chapter presents concepts of reliability, service life, maintenance and

optimization of structural systems. The service life of a structural system under uncertainty can be predicted using time-dependent reliability analysis. Optimization process can be used to establish optimal maintenance intervention during given target lifetime [Frangopol 2011].

The concepts of probability and structural reliability can provide a rational tool to treat uncertainties (i.e., aleatoric and epistemic) related to structural performance quantitatively. These concepts can be extended to prediction of time-dependent reliability and service life of structural systems considering deteriorating processes. Multi-criteria optimization under uncertainty allows structure managers to actively compare different solution options and choose the one that best balances their objectives and constraints.

Table 2.1 Time-dependent reliability indices

Reliability index at time *t* (years)	
Component 1:	$\beta_1(t) = 6.0 - 0.1t$
Component 2:	$\beta_2(t) = 5.0 - 0.05t$

Table 2.2 State functions of components 1 and 2 with different time-dependent resistance and load effect

	Component 1	**Component 2**
	$g_1 = R_1(t) - S_1(t)$	$g_2 = R_2(t) - S_2(t)$
Case A Time independent R Time independent S	$R_1(t) = X_1$ $S_1(t) = X_2$	$R_2(t) = X_3$ $S_2(t) = X_4$
Case B Time dependent R Time independent S	$R_1(t) = X_1(1-(t/100)^2)$ $S_1(t) = X_2$	$R_2(t) = X_3(1-(t/100)^2)$ $S_2(t) = X_4$
Case C Time independent R Time dependent S	$R_1(t) = X_1$ $S_1(t) = X_2(1+(t/100)^2)$	$R_2(t) = X_3$ $S_2(t) = X_4(1+(t/100)^2)$
Case D Time dependent R Time dependent S	$R_1(t) = X_1(1-(t/100)^2)$ $S_1(t) = X_2(1+(t/100)^2)$	$R_2(t) = X_3(1-(t/100)^2)$ $S_2(t) = X_4(1+(t/100)^2)$
Random variables	X_1; N (μ_1=90, σ_1=15) X_2; N (μ_2=50, σ_2=4.0)	X_3; N (μ_3=80, σ_3=10) X_4; N (μ_4=50, σ_4=5.0)

Note: N = normal distribution; μ_i = mean of random variable X_i; σ_i = standard deviation of random variable X_i

Table 2.3 Performance-based repair options

Option 1	• If the reliability index of a component reaches 2.5, the component will be replaced. • The reliability index of the new component will have the value of initial reliability index of the replaced component.
Option 2	• If the reliability index of a system reaches 2.5, every component will be replaced. • The reliability index of the system will have the value of its initial reliability index.
Option 3	• If the reliability index of a system reaches 2.5 or the reliability index of a component reaches 1.0, the critical component will be replaced with a new component having the same initial reliability index as that of the replaced component. • For a series system, the system reliability is at most equal to the reliability of the weakest component. Conversely, for a parallel system, the system reliability is at least equal to the reliability of the strongest component. For this reason, components will always be replaced when the reliability index of the series system reaches 2.5.

Table 2.4 Characteristics of approaches to multi-objective optimization problem (adapted from Arora 2004)

Approach	Can yield all Pareto set?	Depends on function continuity?	Uses utopia point?	Always yields Pareto optimal point?
(a) Weighted sum	No	Depends on objective functions	Yes	Yes
(b) Weighted min-max	Yes	Same as above	Yes	Yes
(c) Weighted global criterion	No	Same as above	Yes	Yes
(d) ε-constraint	No	Same as above	No	Yes
(e) Genetic algorithm	Yes	No	No	Yes

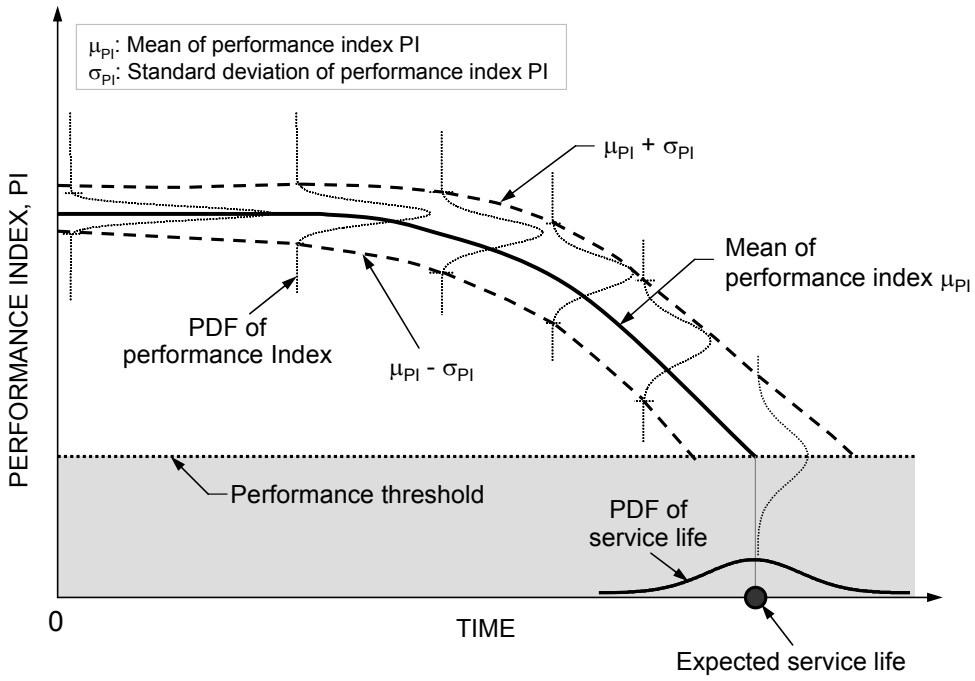

Figure 2.1 Lifetime performance of structure under uncertainty

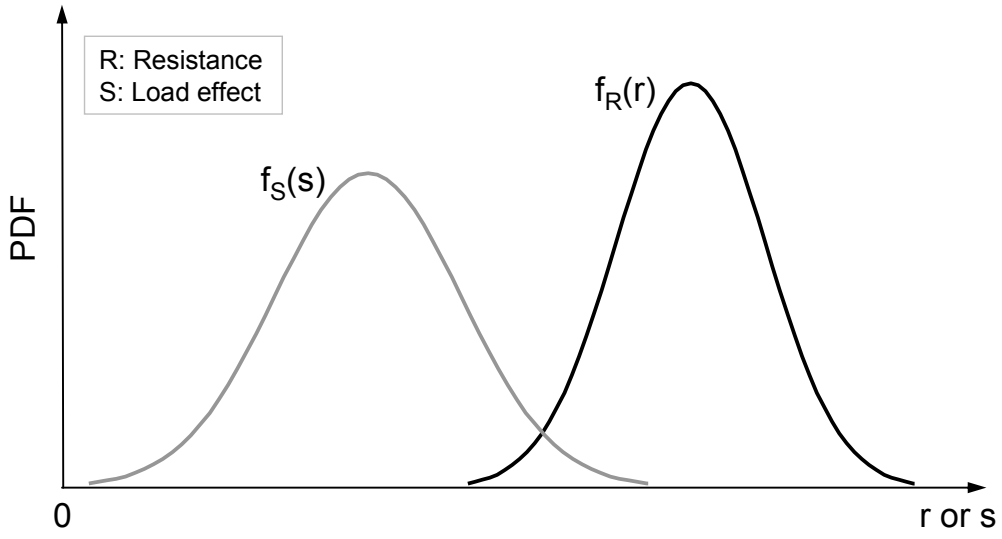

Figure 2.2 Probability density functions of R and S

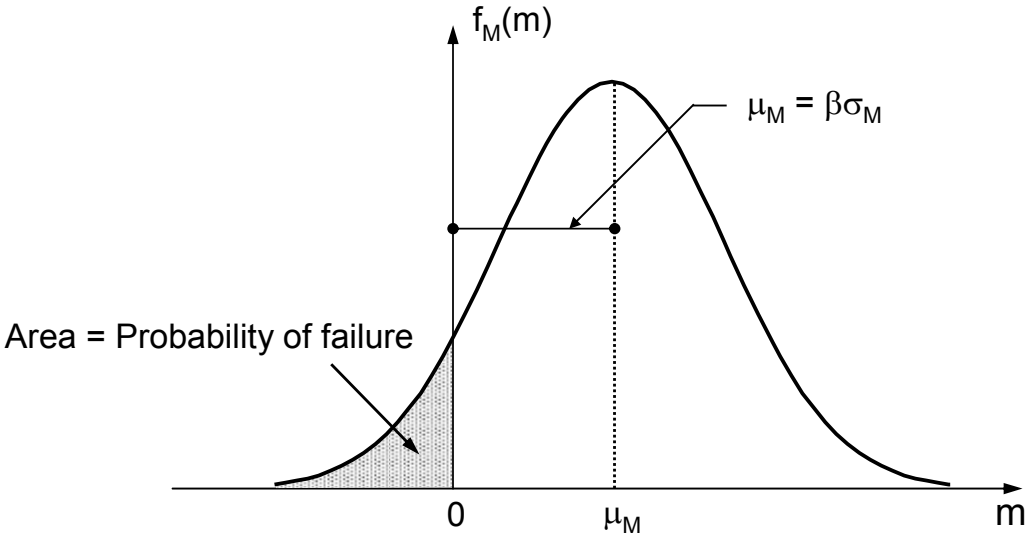

Figure 2.3 Probability density function of safety margin M and the reliability index β

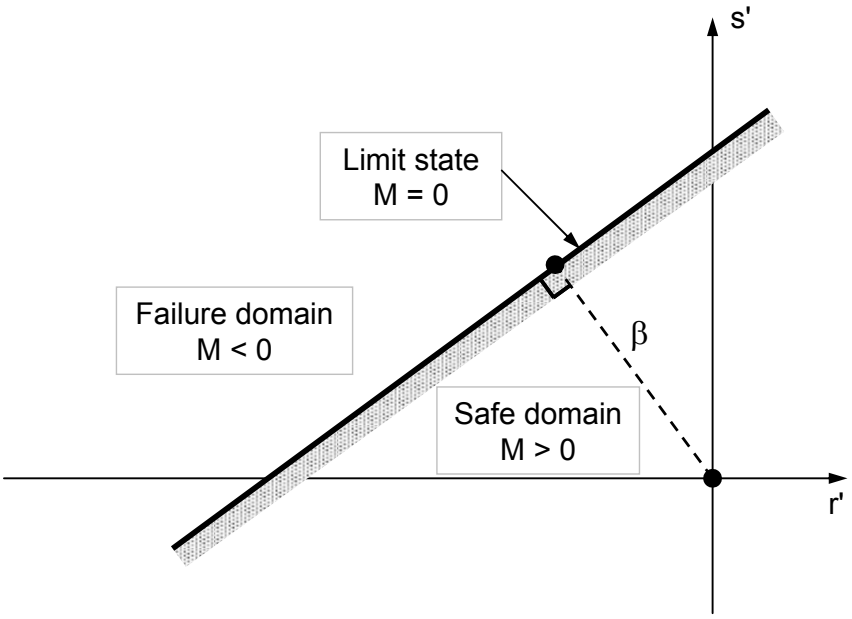

Figure 2.4 Reliability index β in the space of reduced variables R' and S'

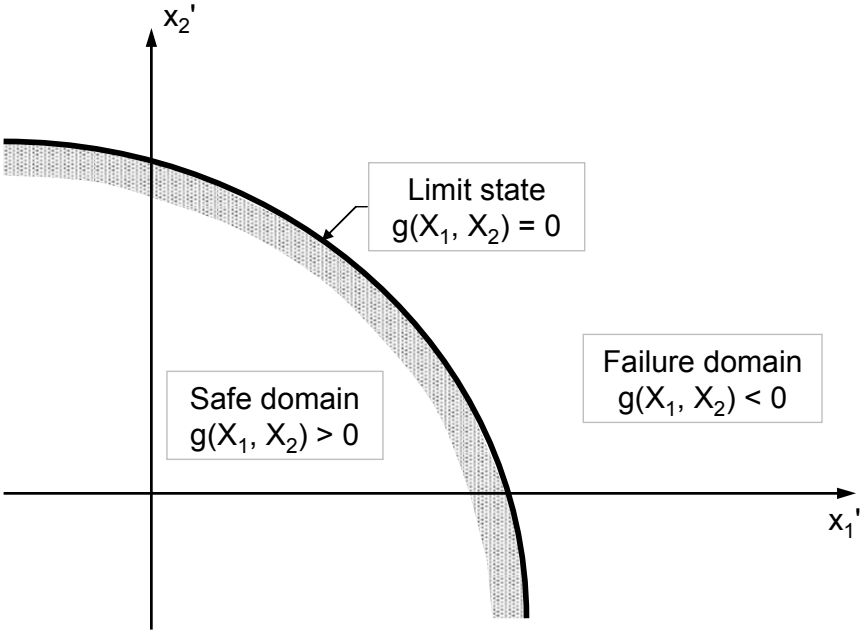

Figure 2.5 State function for limit state, safe state, and failure state in space of reduced variables *X1'* and *X2'*

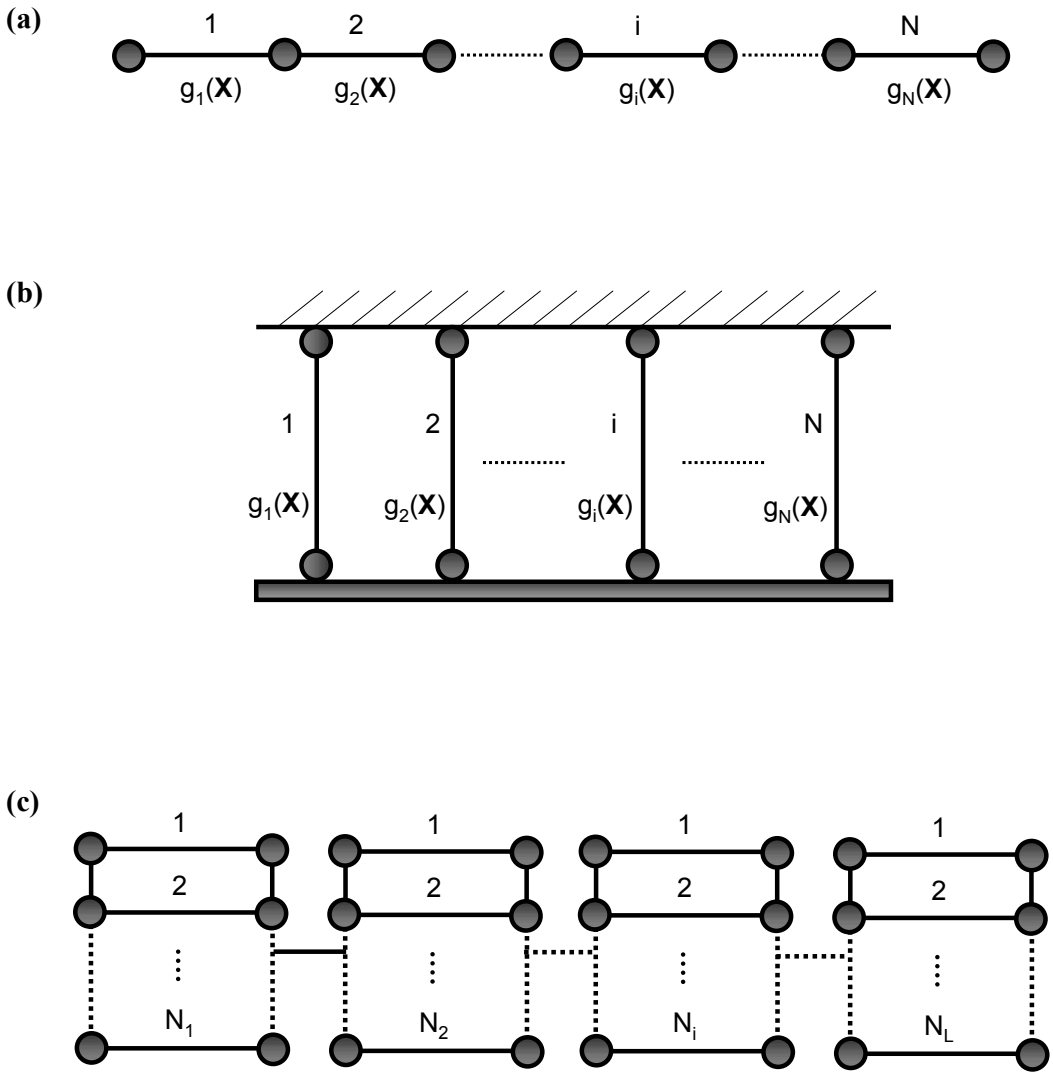

Figure 2.6 (a) Series system; **(b)** parallel system; and **(c)** combined series-parallel system

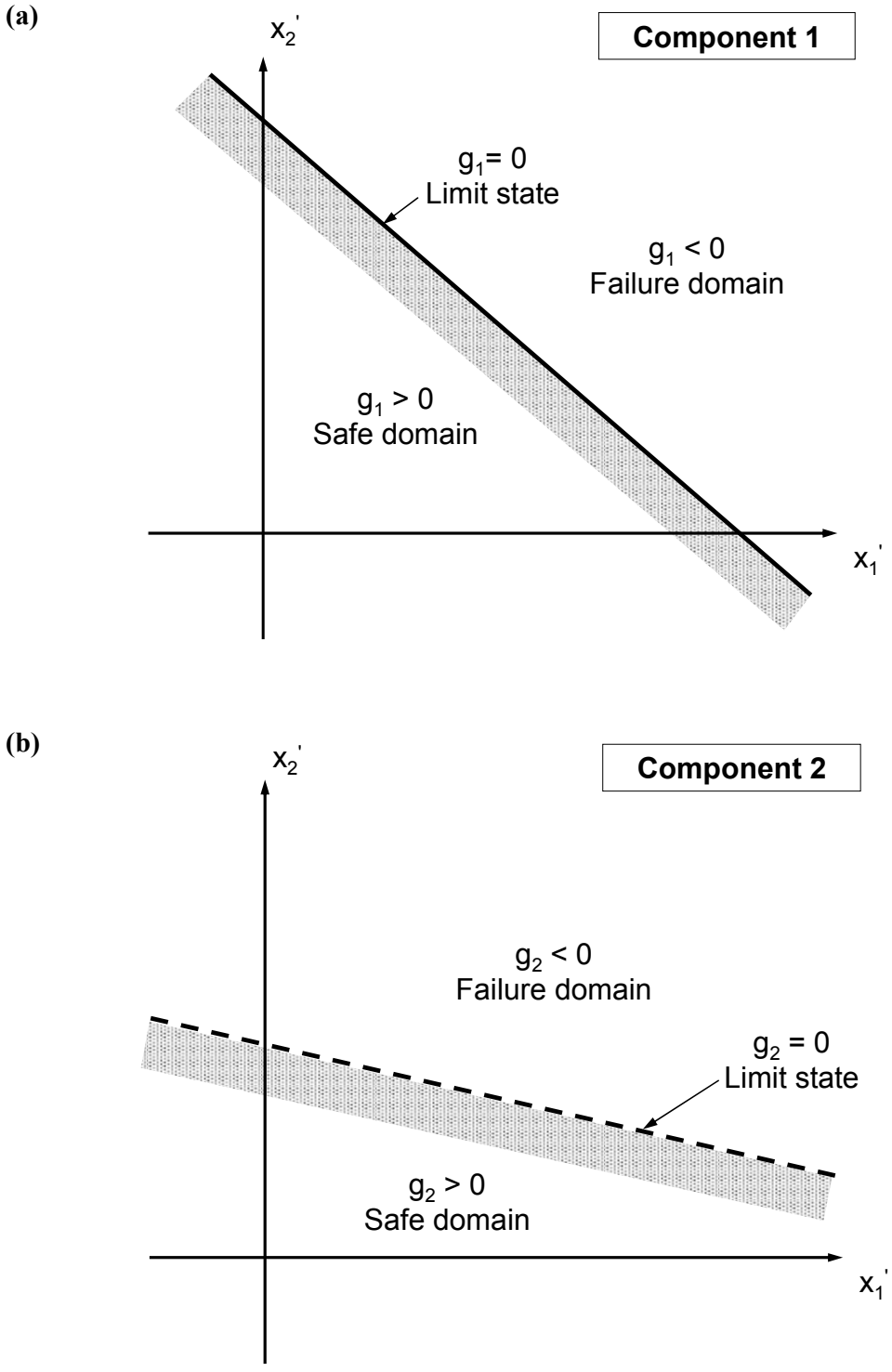

Figure 2.7 Safe and failure spaces for **(a)** component 1; **(b)** component 2

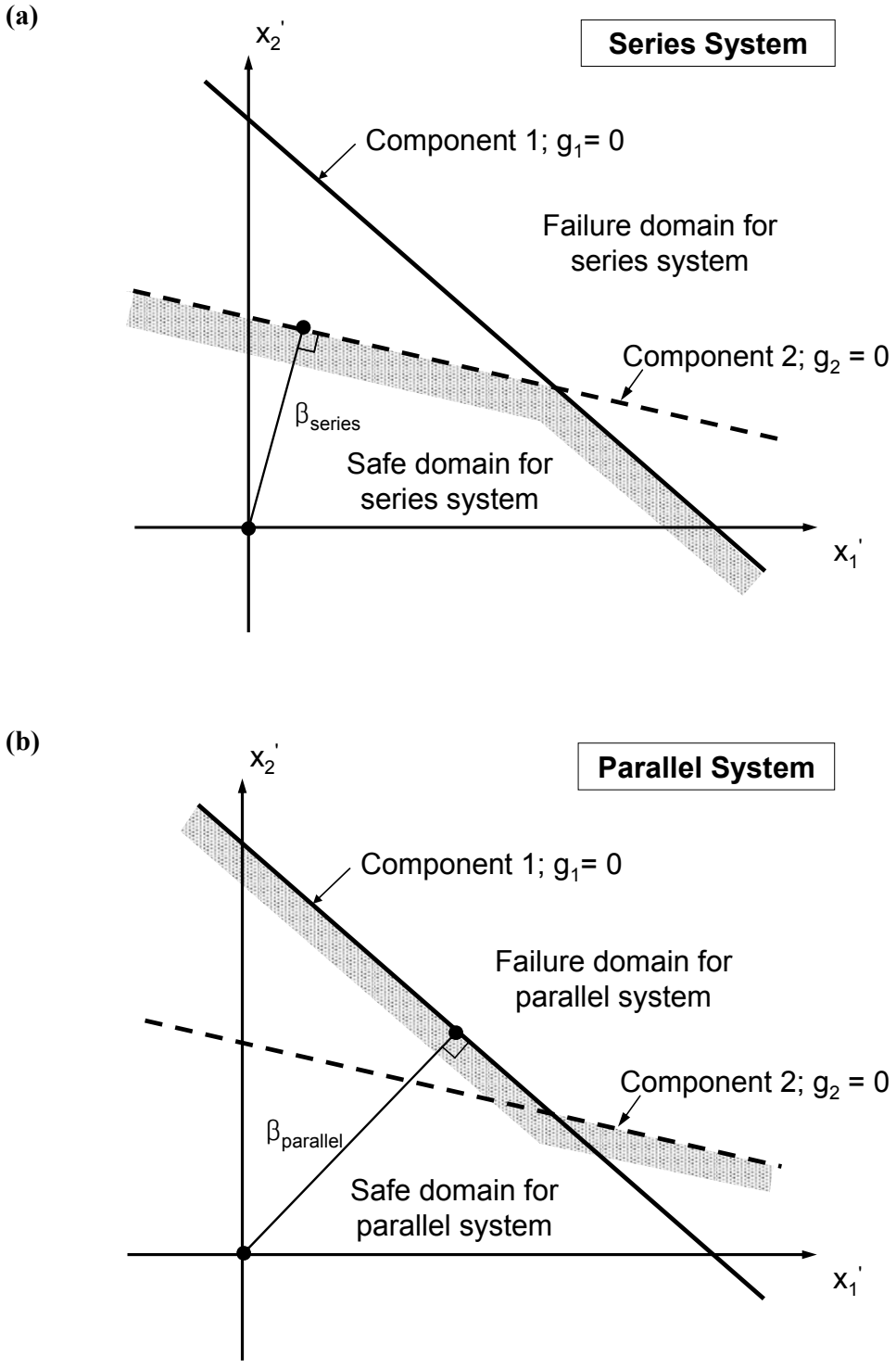

Figure 2.8 Safe and failure spaces for **(a)** series system; **(b)** parallel system

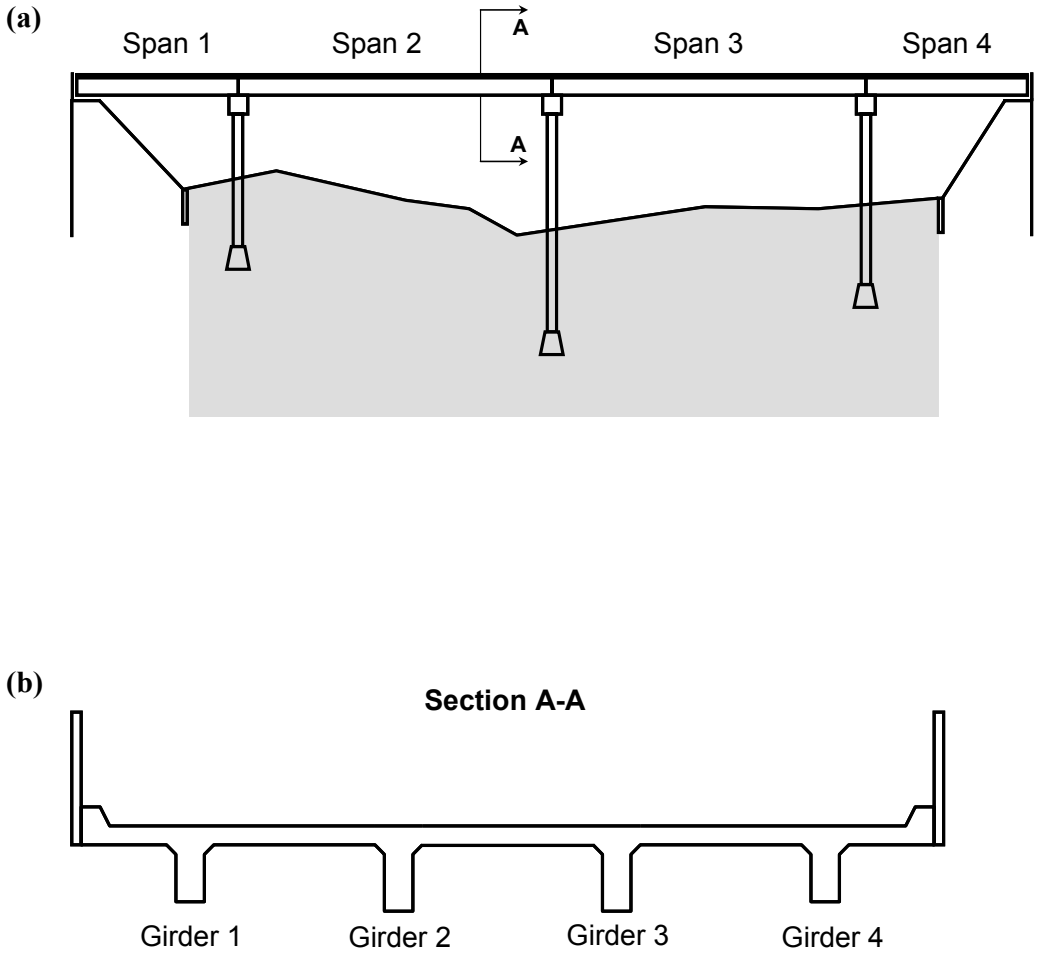

Figure 2.9 (a) Bridge elevation, and **(b)** cross section

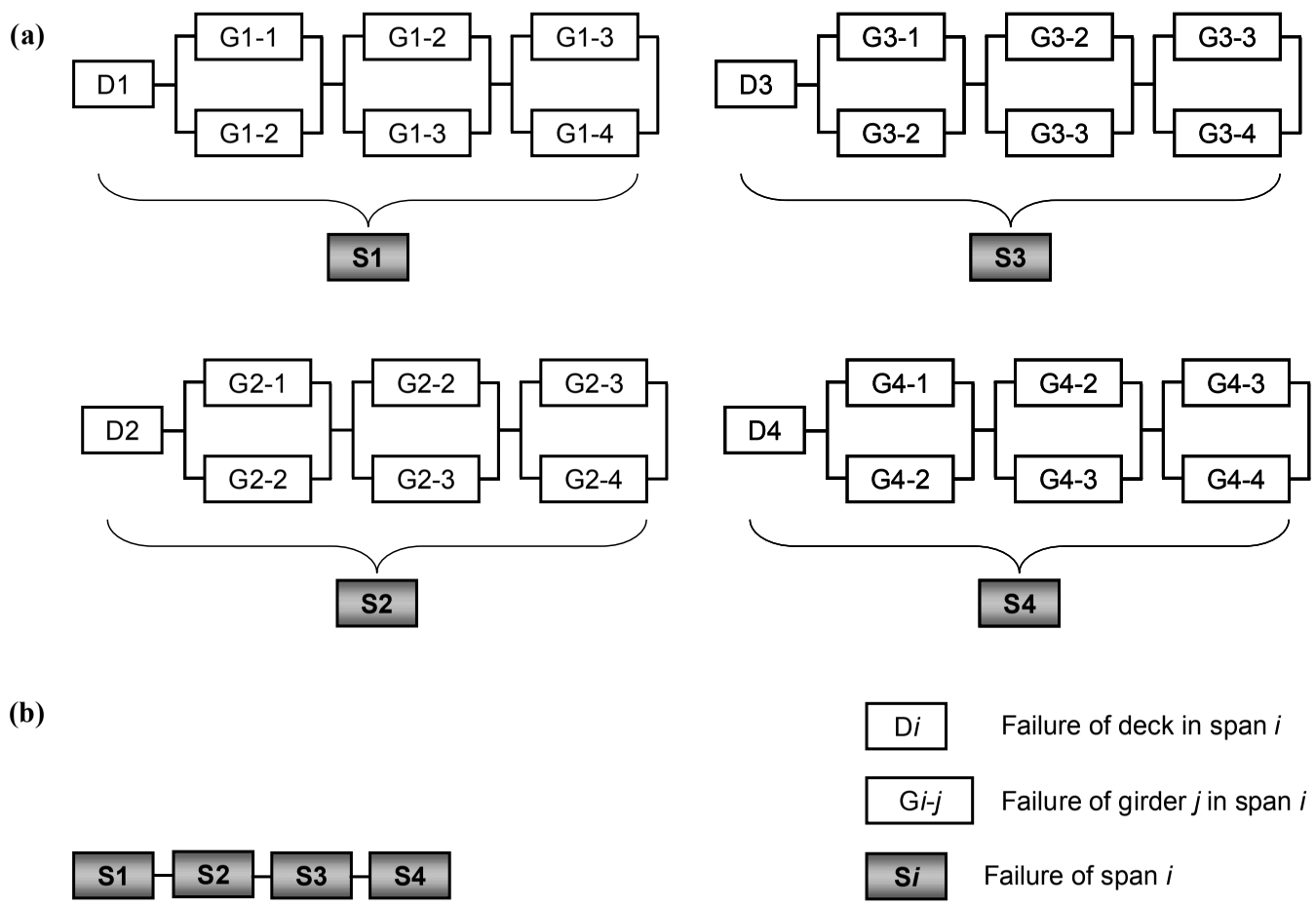

Figure 2.10 (a) Failure model of each span, and **(b)** entire system failure model

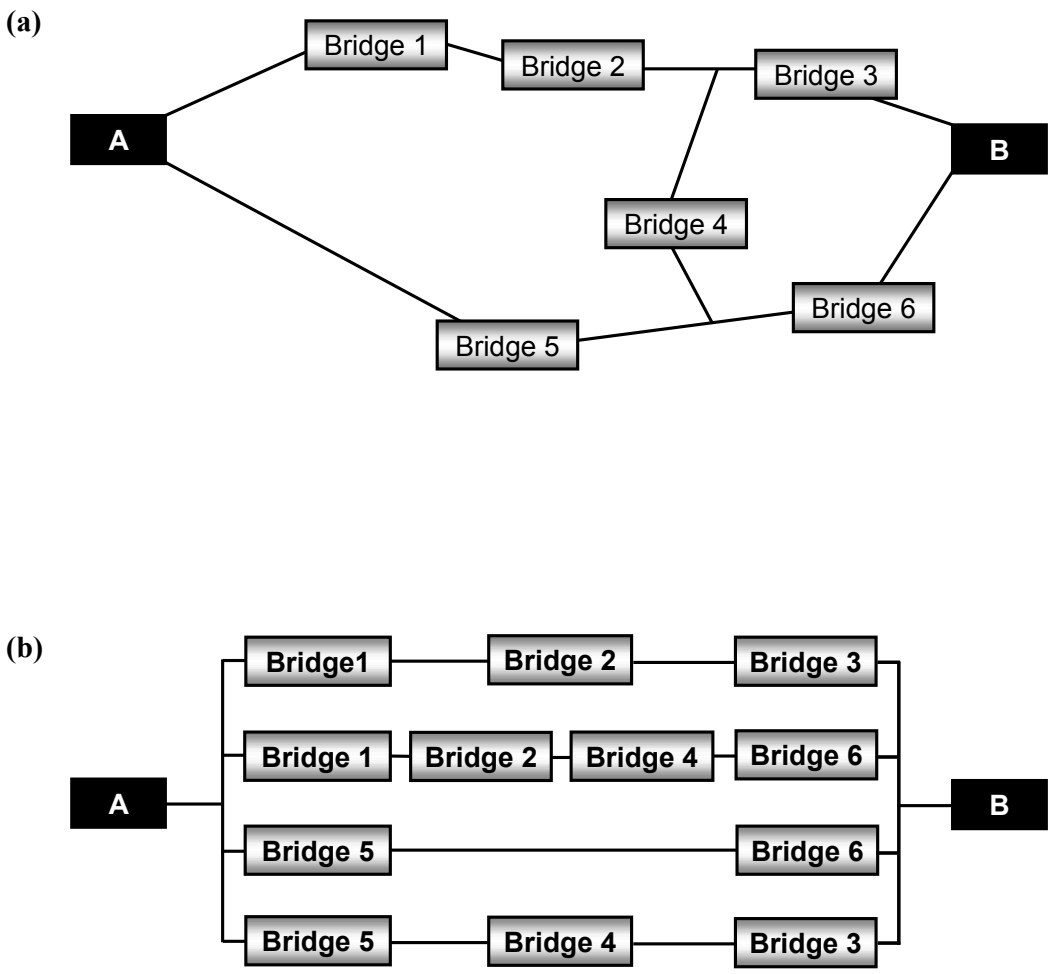

Figure 2.11 (a) Bridge network, and **(b)** series-parallel path model

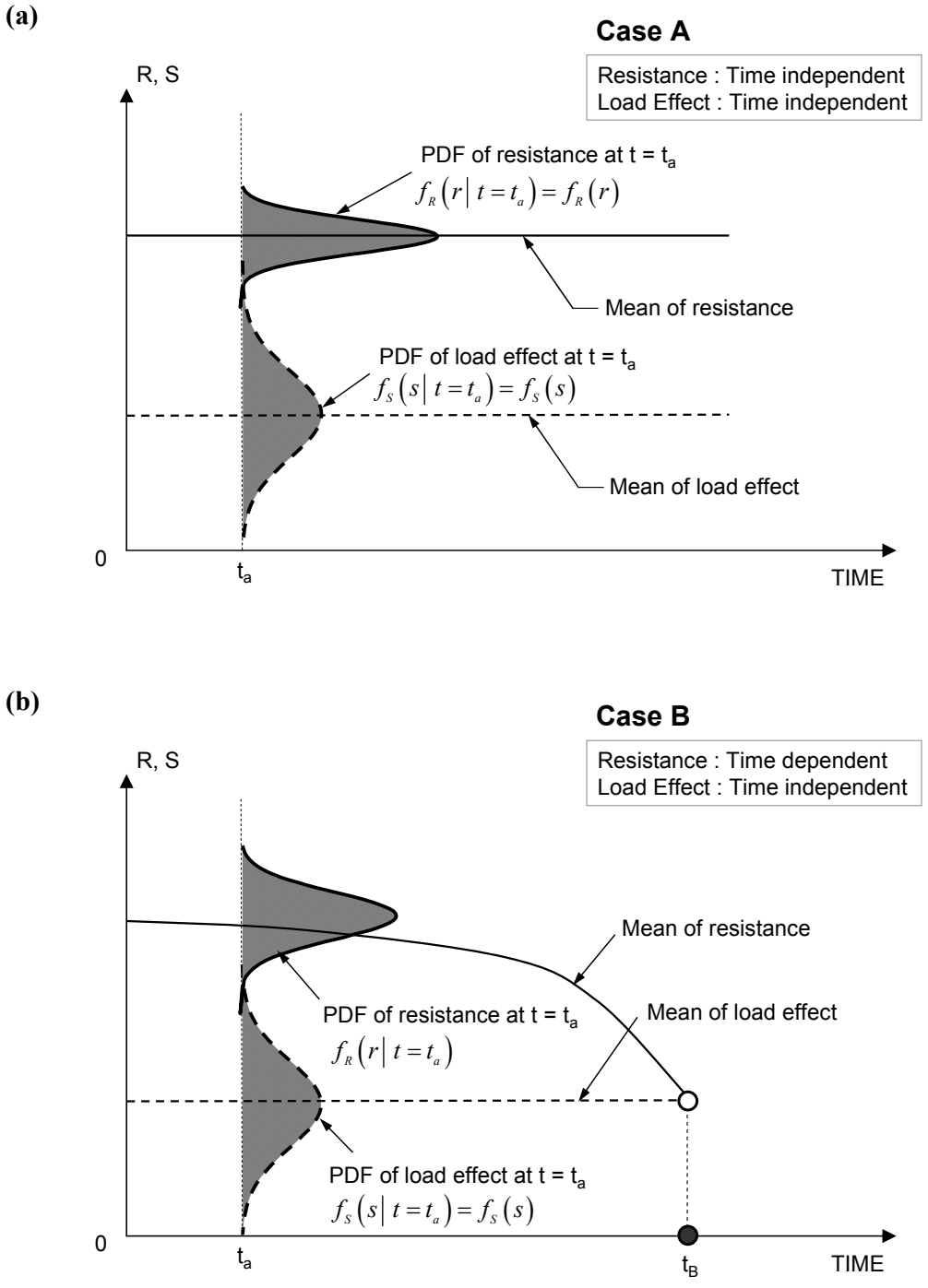

Figure 2.12 Time-independent and time-dependent R and S: **(a)** time-independent; **(b)** time-dependent resistance and time-independent load effect; **(c)** time-independent resistance and time-dependent load effect; **(d)** time-dependent resistance and time-dependent load effect, and **(e)** profiles of mean safety margin of cases (a), (b), (c), and (d)

(c)

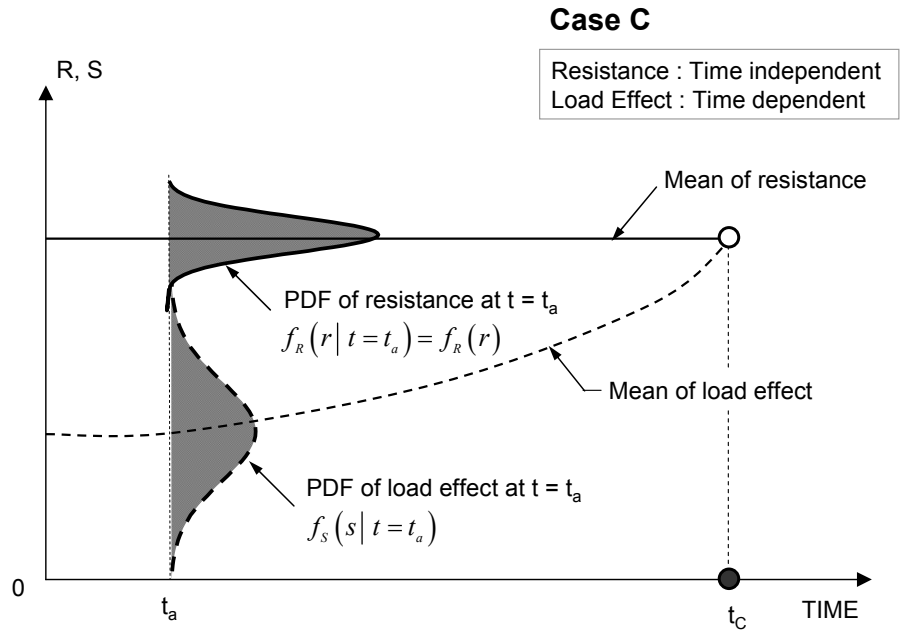

(d)

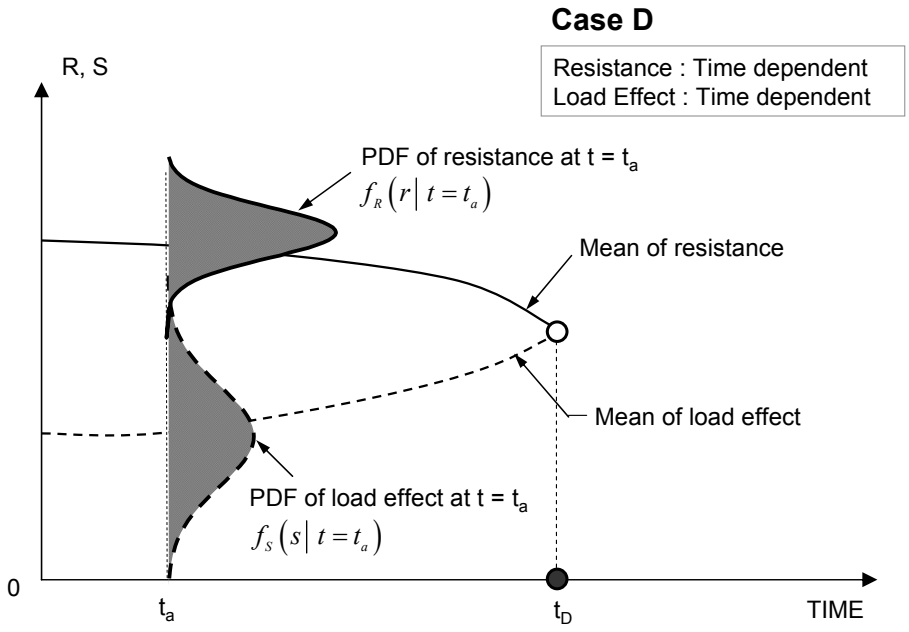

Figure 2.12 Time-independent and time-dependent R and S: **(a)** time-independent; **(b)** time-dependent resistance and time-independent load effect; **(c)** time-independent resistance and time-dependent load effect; **(d)** time-dependent resistance and time-dependent load effect, and **(e)** profiles of mean safety margin of cases (a), (b), (c), and (d) (continued)

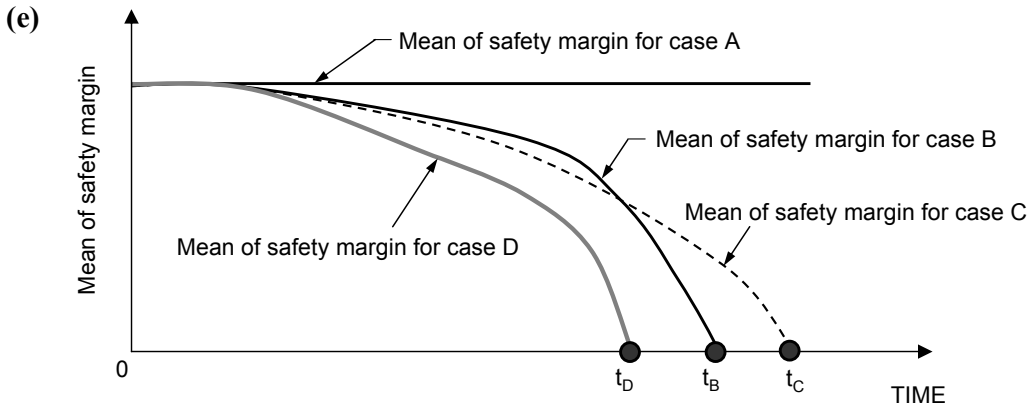

Figure 2.12 Time-independent and time-dependent R and S: **(a)** time-independent; **(b)** time-dependent resistance and time-independent load effect; **(c)** time-independent resistance and time-dependent load effect; **(d)** time-dependent resistance and time-dependent load effect, and **(e)** profiles of mean safety margin of cases (a), (b), (c), and (d) (continued)

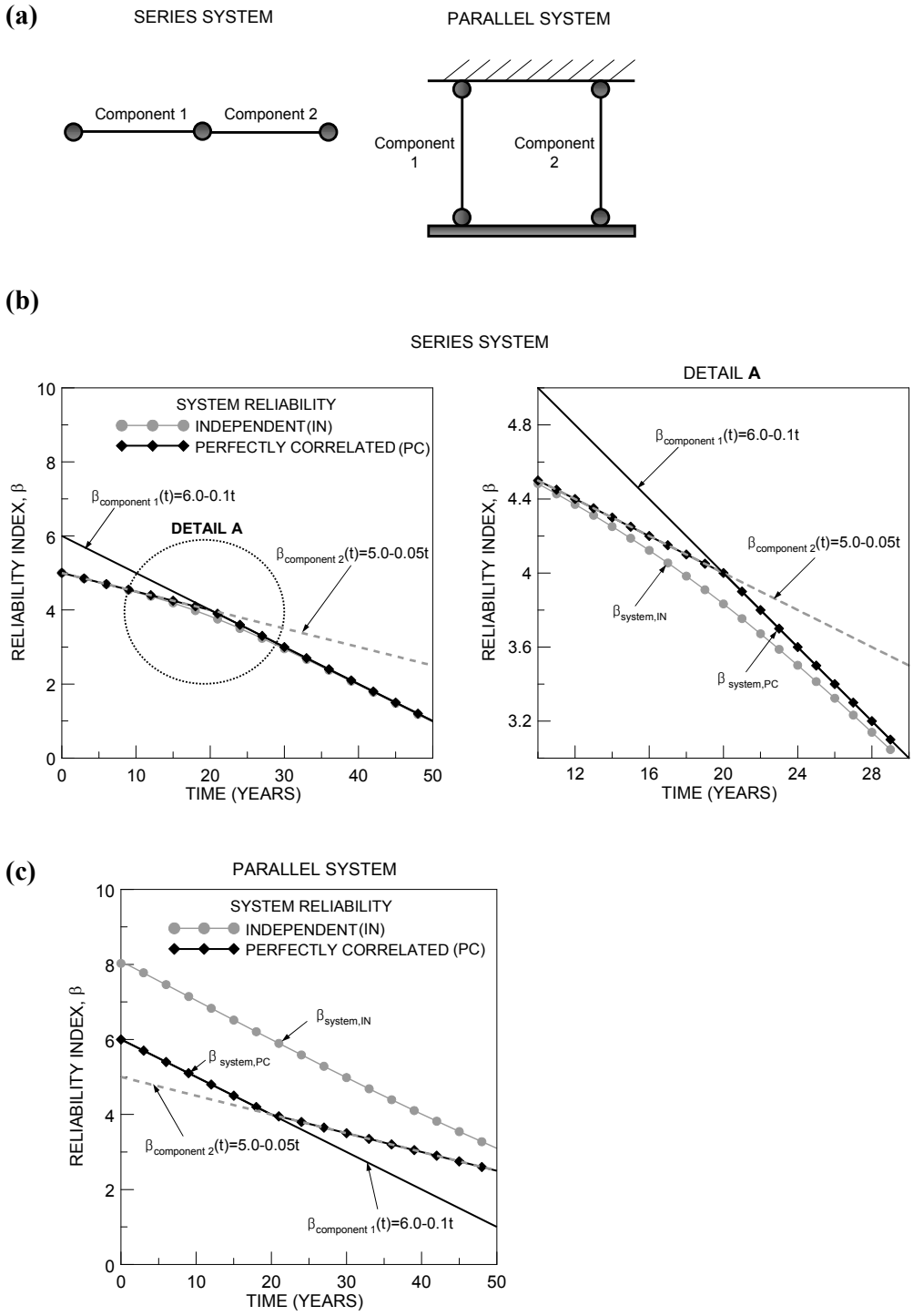

Figure 2.13 (a) Series and parallel systems; **(b)** time-dependent series system reliability index; and **(c)** time-dependent parallel system reliability index

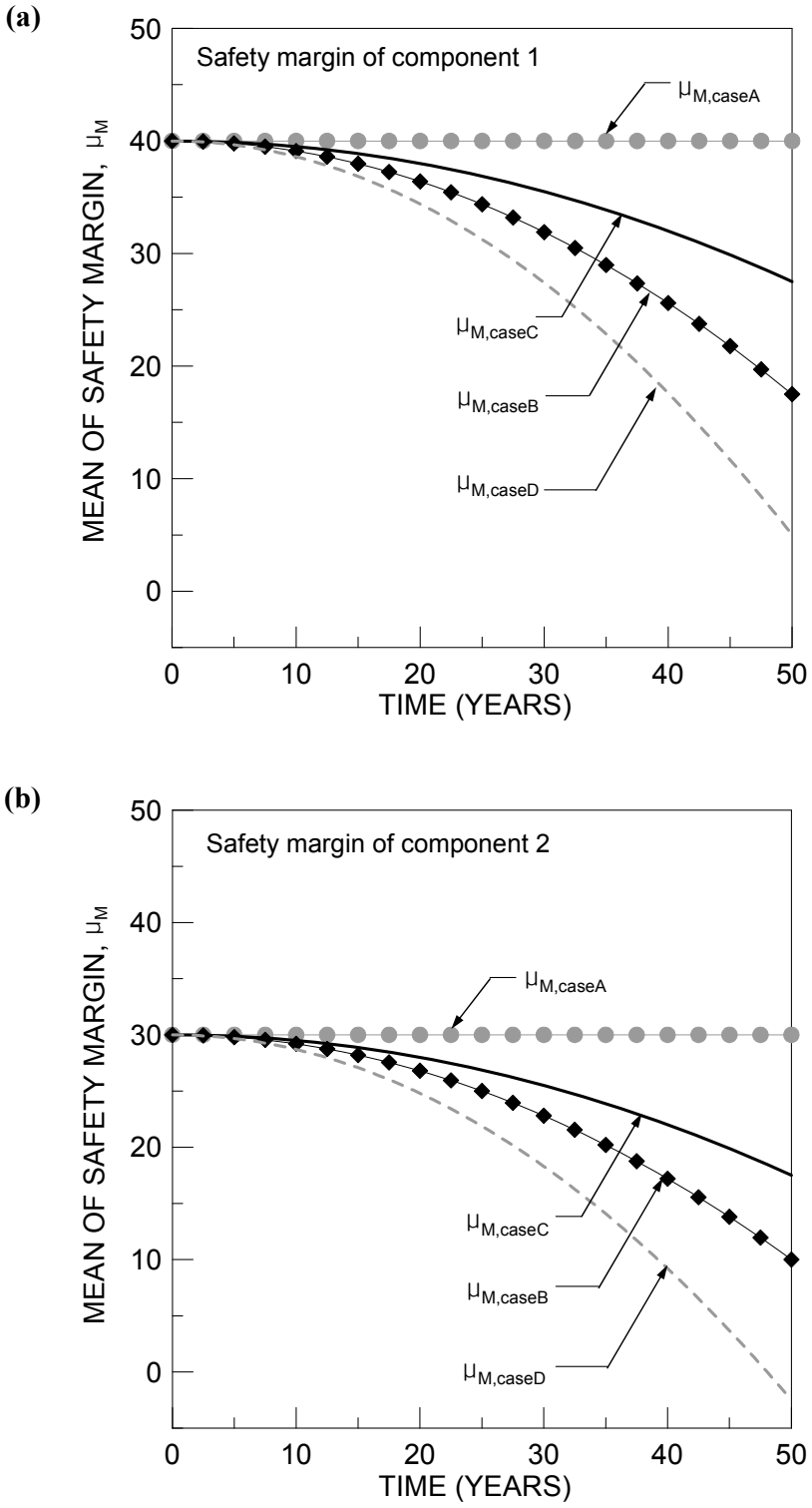

Figure 2.14 Time-dependent safety margins under the cases A, B, C, and D in Table 2.2: **(a)** component 1 and **(b)** component 2

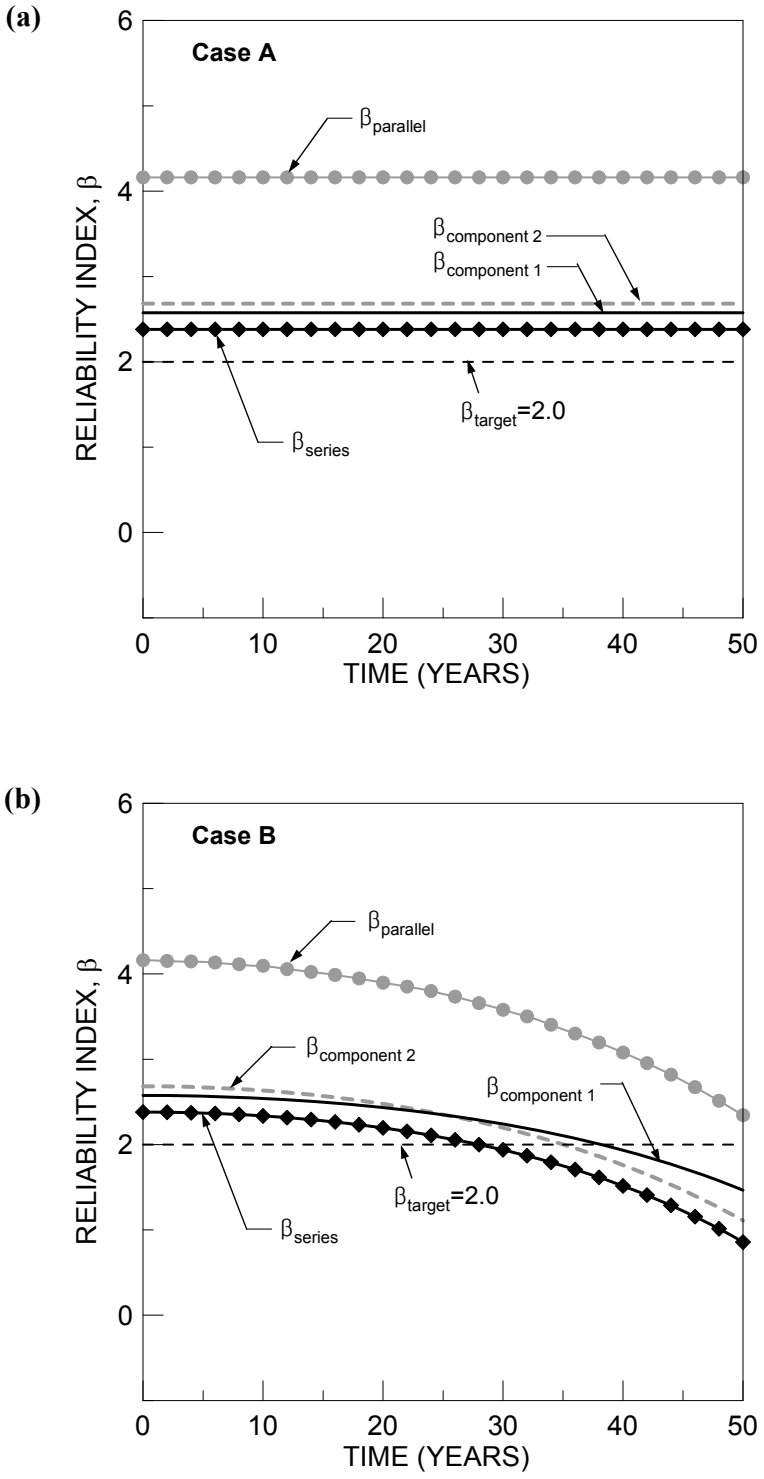

Figure 2.15 Time-dependent reliability index: **(a)** case A, **(b)** case B, **(c)** case C, and **(d)** case D

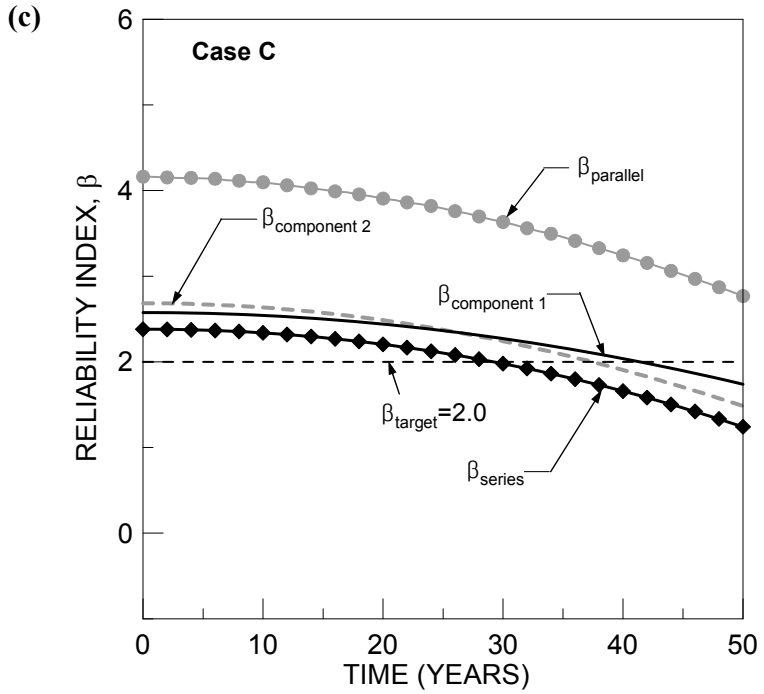

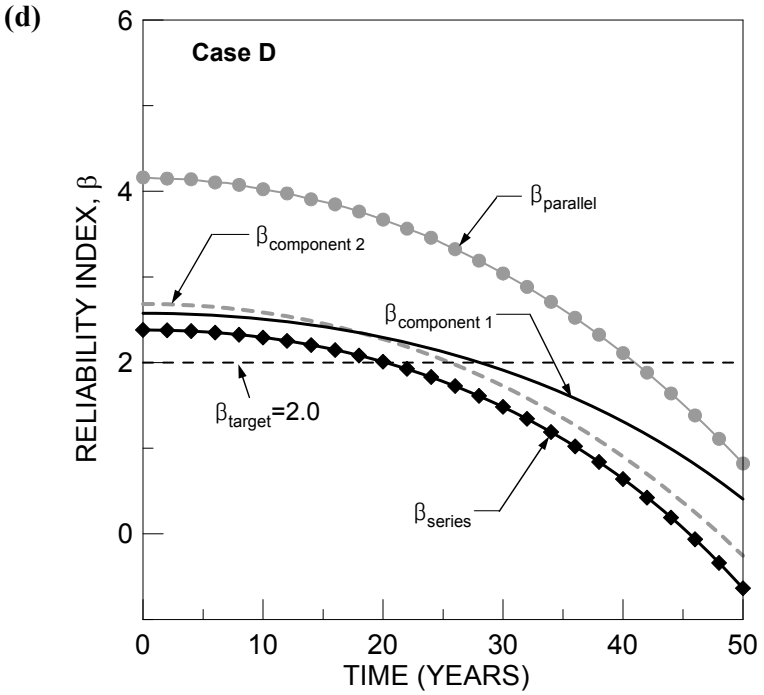

Figure 2.15 Time-dependent reliability index: **(a)** case A, **(b)** case B, **(c)** case C, and **(d)** case D (continued)

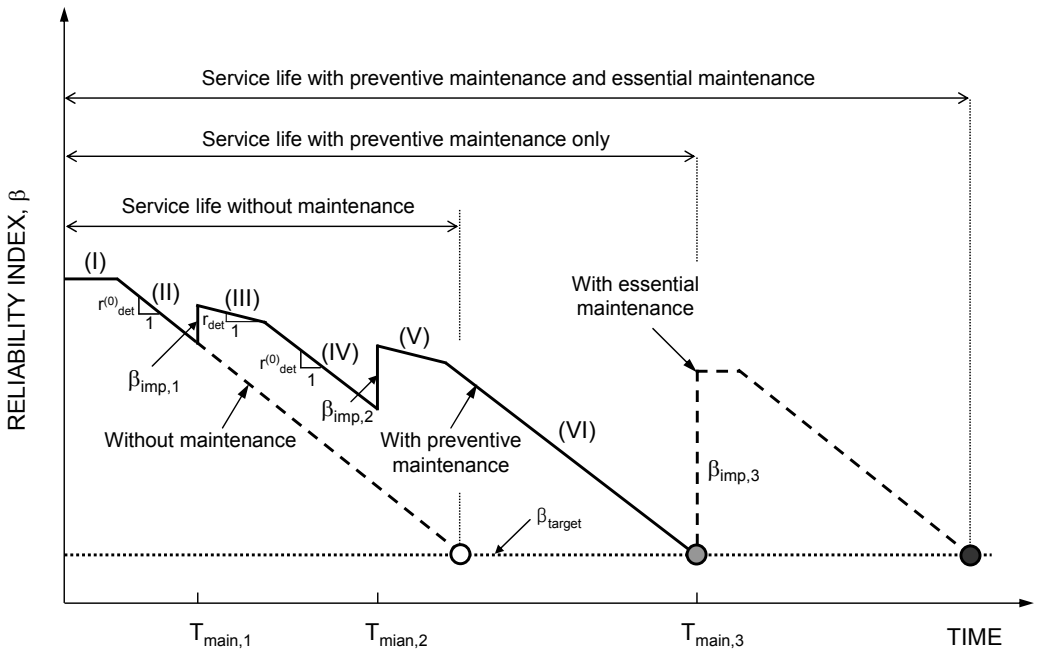

Figure 2.16 Multi-linear reliability index profiles with and without maintenance

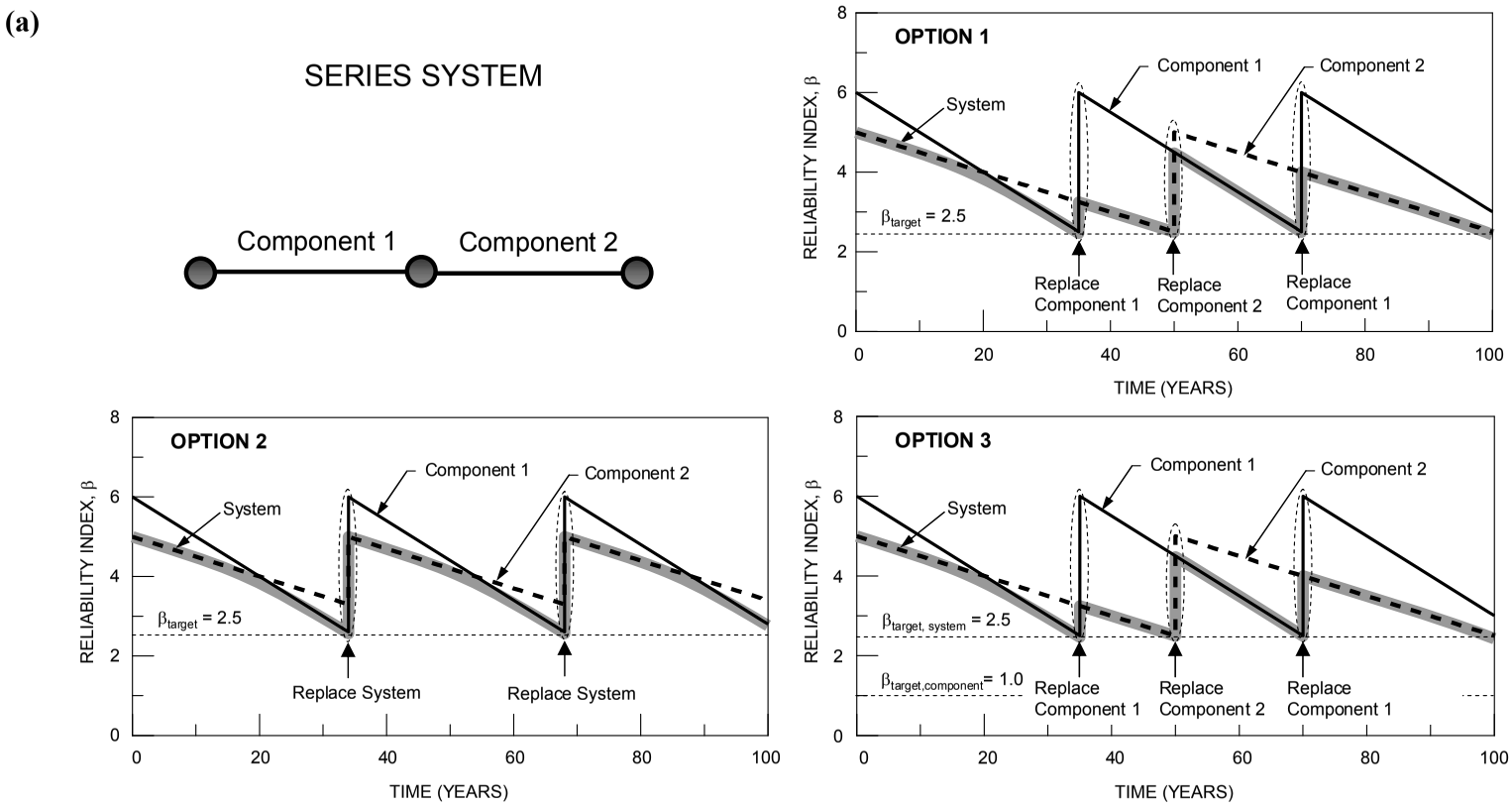

Figure 2.17 Time-dependent reliability index of the three maintenance options in Table 2.3: **(a)** series system, and **(b)** parallel system

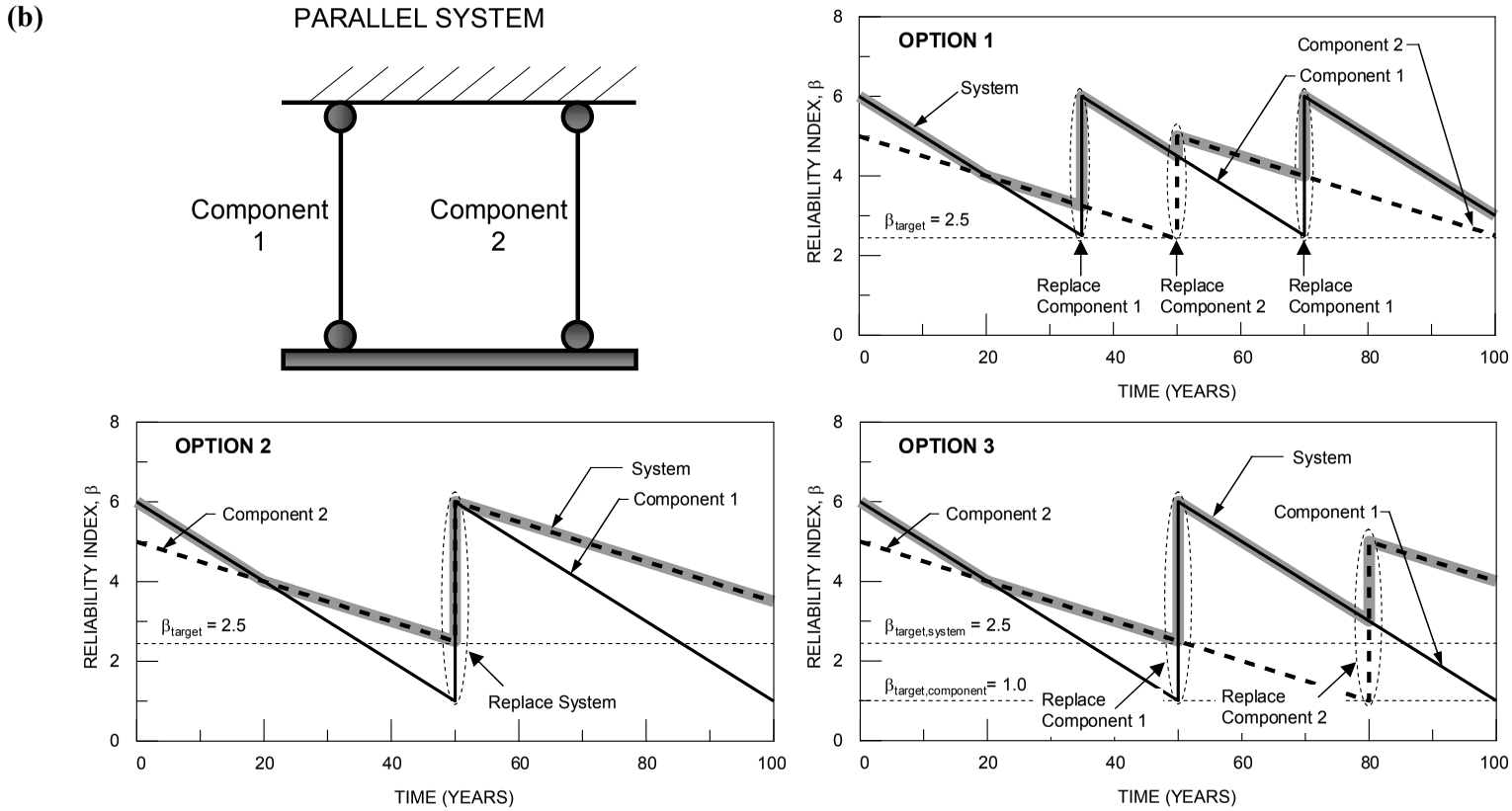

Figure 2.17 Time-dependent reliability index of the three maintenance options in Table 2.3: **(a)** series system, and **(b)** parallel system (continued)

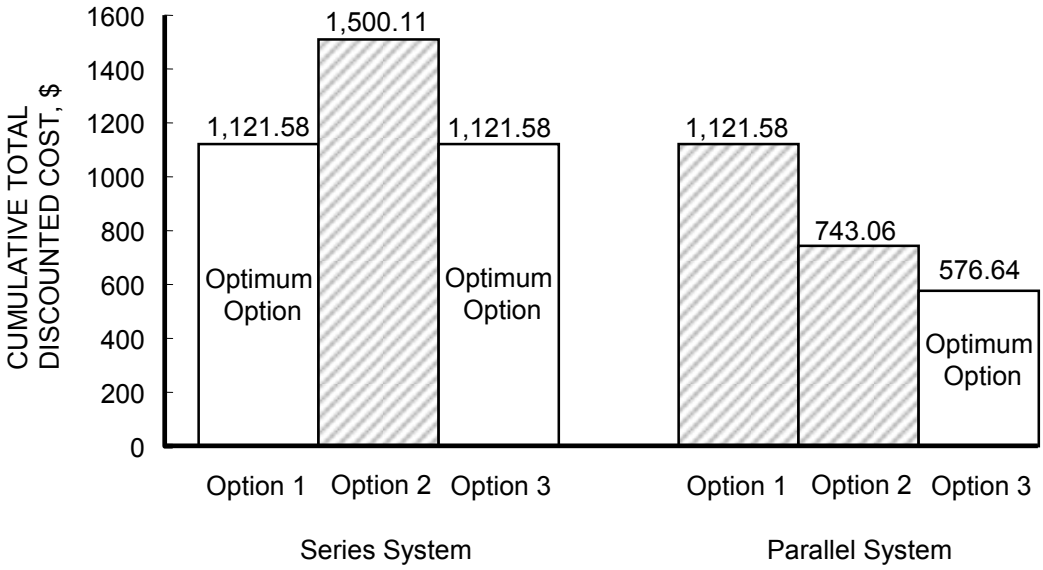

Figure 2.18 Total maintenance cost for series and parallel system under the three maintenance options in Table 2.3

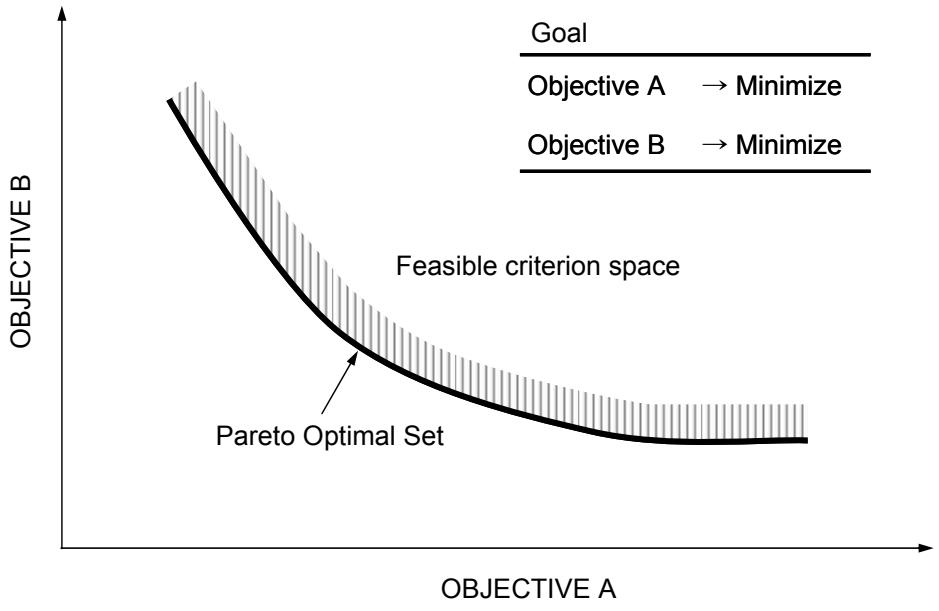

Figure 2.19 Pareto optimal sets: minimize objectives A and B

CHAPTER 3

EFFICIENT USE OF STRUCTURAL HEALTH MONITORING FOR LIFE-CYCLE COST AND PERFORMANCE PREDICTION

3.1 Introduction

In the last decade, structural health monitoring (SHM) has been applied as an attractive tool with various purposes including (a) preventing unexpected structural failure through improved structural performance assessment, (b) predicting the remaining service life of a structure with improved accuracy, and (c) providing the information to support cost-effective maintenance decision processes [Frangopol et al. 2008b, Liu et al. 2009b]. Most of recent research has been focused on technological advancements of SHM, damage detection using SHM, and development of efficient data acquisition and interpretation algorithms [Chong et al. 2003, Farrar and Worden 2007]. Development of the methodology to efficient use of monitoring data for accurate assessment and prediction of the structural performance under uncertainty is needed. This methodology will lead to cost-effective life-cycle maintenance planning.

This chapter presents an approach for the development of prediction functions and a procedure for the performance assessment of structures using monitored extreme data. The updating of prediction functions is based on mean square fitting to monitored extreme data assigned to monitoring periods, while the necessary

monitoring periods are computed from acceptance sampling theory. Furthermore, based on the long-term monitored strain data induced by heavy vehicle traffic on an existing bridge, an efficient approach to assess and predict the structural system performance through series-parallel system modeling is proposed. The correlations among the structural component are directly obtained from monitored strain data. The prediction of structural performance in the future is dependent on the component performance functions considering the monitored data. Sensitivity studies with respect to system modeling, correlations and measurement errors are carried out. The proposed approaches are applied to an existing highway bridge in Wisconsin, which was monitored in 2004 by the Advanced Technology for Large Structural System (ATLSS) Engineering Research Center, a National Engineering Research Center at Lehigh University, Bethlehem, Pennsylvania, USA.

3.2 Structural Health Monitoring for Structural Safety Evaluation

3.2.1 Structural Safety in Design

The structural safety in design is traditionally quantified by comparing the structural capacities, R, with the load effects, S. The deterministic Allowable Stress Design (ASD) adopts the concept of the factor of safety, *F.S.*, where $F.S. = R / S$. The structural safety is achieved by defining the minimum required $F.S.$ from previous experiences and expert opinions. The uncertainties in R and S are somewhat combined, and are implicitly considered when assigning the minimum allowable *F.S.* In current

semi-probabilistic Load Resistance Factored Design (LRFD), such as the LRFD Bridge Design Specification [AASHTO 2007], the Building Code Requirements for Structural Concrete [ACI 318 2005], and the Steel Construction Manual [AISC 325 2005], the concept of the reliability index β is introduced in code calibration. The uncertainties in R and S are considered separately by assigning different load factors, γ_i, and resistance factors ϕ_n through rational calibration procedures, where the target reliability β for each type of structural element (e.g. beam, column, slab) is assigned to maintain an acceptable probability of failure.

One of the important limitations associated with ASD and current LRFD methodologies is the lack of consideration of structural system reliability. In other words, the structural safety in design can be quantified at the level of structural component only, although the analytical models of structural system reliability are ready for adoption [Frangopol et al. 2001]. The absence of the structural system safety considerations in current design codes, with the exception of system factor modifiers in the LRFD Bridge Design Specification [AASHTO 2007], reflects the needs for future efforts to check the analytical models, where SHM may play a vital role.

The probabilistic performance-based design follows the fundamental structural safety concept where the structural safety can be quantified by safety margin $M = R - S$, where R and S are random variables and their uncertainties are fully investigated by advanced analytical and experimental techniques through statistical and probability considerations. Evolution of structural design methodologies from ASD to LRFD to

performance-based system design has revealed the importance of uncertainty consideration in balancing economical and safety aspects of structural designs. It is uncertainty consideration that distinguishes advanced design philosophy from traditional design principles, and yield cost-effective designs while keeping structural reliability level acceptable.

3.2.2 Structural Safety in Evaluation

The structural safety in evaluation of existing structures should be quantified in the same way as that in design of new structures. However, most of current structural safety evaluation practices focus only on condition assessment and evaluation of construction materials. For example, ASCE (2000) provides the general assessment procedures, evaluations of construction materials of concrete, metal, masonry and wood, and documentation formats. ACI 437R-03 (2003) recommends the load testing procedures and criteria, in addition to analytical investigation procedures. Although AASHTO (1989) supports the adoption of the concepts of structural reliability, the structural safety in evaluation is still quantified by using a "notional" truck, which does not represent any actual loading conditions on a bridge. In short, although many structural field tests have been conducted for the purposes of damage detection, verification of finite element models (FEM) among others, the structural safety in evaluation has not been clearly defined and standardized yet [Frangopol et al. 2008a].

It should be worth noting that the uncertainties in the structural capacity R and

the load effect *S* are much different in structural evaluation than in design. In general, the uncertainties in *R* and *S* for structural evaluation are smaller than those associated with structural design due to the availability of site-specified information on structural capacities and loading conditions. Moreover, the live load models in current structural design codes are usually established for general applications with conservative assumptions, although the live loads such as traffic volumes and wind speeds may vary considerably from site to site. The use of actual live loads from structural field investigations including SHM may have a great potential in repair and rehabilitation cost-saving by taking advantages of the differences between the actual live loads and those specified in the live load models.

3.2.3 SHM for Structural Performance Evaluation

SHM can be defined as a long-term observation of the responses of a constructed facility to the changes of its surrounding environment through instrumentation and field testing techniques to assess the current condition and reliability of a structure and predict in future performance. The long-term requirement may be satisfied by measuring and recording the structural responses and changes of the environments either continuously or within a predefined time interval along the service lifetime of the constructed facility. There is an essential difference between SHM and structural field testing, where structural field testing is usually conducted very few times (e.g. once or twice) during the life of a structural system or after occurrences of major

disasters such as earthquake, flood, hurricane, and explosion. The structural responses refer to both mechanical responses (e.g. strain due to change in temperature, stress under traffic loading) and physical changes (e.g. deformation and cracking under fatigue loading, loss in sectional area due to steel corrosion).

Current SHM has been conducted for different purposes, but can be classified as either for condition assessment or for performance evaluation. The condition assessment measures physical, chemical and/or mechanical properties of structural components. The damage state and/or condition index of the important components in a structural system are the typical indicators that can be obtained from condition assessment. The condition assessment techniques have been well developed and documented, particularly by using NDE, but the effects of structural component damage states on structural system safety are seldom studied. The condition assessment results can only affect the structural resistance R. Load effect S still has to be assumed for structural safety evaluation. Therefore, the structural safety under actual loading conditions can not be quantified from condition assessment. However, the condition assessment results are useful to predict future condition and performance of a structural component or system when effectively integrated into carefully developed physical models. On the other hand, the performance evaluation directly measures and records the structural responses subjected to the controlled and/or uncontrolled loading conditions. The combined effects of resistance R and load effect S on structural safety may be evaluated from the performance evaluation,

if the monitoring periods are long enough.

3.3 Benefit of Structural Health Monitoring in Life-Cycle Cost

The most valuable aspects of application of SHM are related to reduction of uncertainty. The reduction of uncertainty can lead to preventing unexpected failure of a structure, assessing and predicting more reliably structural performance, and applying appropriate maintenance on time. As a result, it can allow the reduction of both the failure cost and maintenance cost. The general formulation of the expected life-cycle cost C_{ET} is [Frangopol et al. 1997b]

$$C_{ET} = C_{INI} + C_{PM} + C_{INS} + C_{REP} + C_{FAIL} \tag{3.1}$$

where C_{INI} = initial cost (*i.e.*, design and construction cost), C_{PM} = the expected cost of routine maintenance, C_{INS} = the expected cost of inspection, C_{REP} = the expected cost of repair, and C_{FAIL} = the expected cost of failure. If SHM is applied, the expected total cost C^*_{ET} will be [Frangopol and Messervey 2009a]

$$C^*_{ET} = C^*_{INI} + C^*_{PM} + C^*_{INS} + C^*_{REP} + C^*_{FAIL} + C_{MON} \tag{3.2}$$

where C_{MON} = monitoring cost. From the difference between the expected costs from Equations (3.1) and (3.2), the benefit of SHM, B_{MON}, can be determined as $C_{ET} - C^*_{ET,}$. If the application of SHM does not provide a benefit (i.e., $B_{MON} < 0$), it will be difficult for structure managers to justify adopting SHM. Therefore, efficient use of SHM should be considered, in order to maximize the benefit of SHM.

3.4 Prediction Functions based on Monitoring Extreme Data

Sensors of monitoring systems can provide information at specific locations. Continuous combination of information provided by sensors in space and time can allow the assessment of the space- and time-dependent system performance [Frangopol and Messervey 2009a, 2009b]. Several approaches have been proposed for determining the optimal sensor placement to minimize the number of sensors [Shi et al. 2000 Worden and Burrows 2001, Meo and Zumpano 2005]. However, significant efforts related to the efficient inclusion of monitoring data in the assessment, prediction of structural performance, and optimized intervention planning of maintenance actions are still needed.

SHM to monitor the response of a structural system to external loadings (e.g., live load, temperature) requires a large storage system if all the data are recorded. The size of data depends on the monitoring frequency and the number of installed sensors on the structural system. Generally, in order to reduce the data amount and manage it effectively, the information associated with the extreme physical quantities can be recorded [Mahmoud et al. 2005]. This information can be mainly used to evaluate fatigue structural performance, but can be also used for serviceability performance. The prediction function based on the monitored extreme data can provide helpful information to predict effective stress range and the number of cycles using the relation among the variation of the monitored extreme data in time.

Therefore, the prediction function can be effective for the assessment and prediction of fatigue structural performance [Frangopol et al. 2008b, Strauss et al. 2008].

3.4.1 Prediction Functions

There are numerous prediction functions for the description of structural degradation processes that do not take into account the information available from the monitored extreme data. Most of these functions are based on advanced analytical formulations [Stehno et al. 1987, Teply et al. 2006]. However, the use of the monitored extreme data is necessary for a more accurate estimation of prediction functions f_p. Polynomial approaches of first, second, or higher order can be generally used for defining prediction functions, such as

$$f_P = \sum_{i=0}^{n_{op}} a_i \cdot t^i \qquad n_{op} = 1, 2, 3 \tag{3.3}$$

where a_i = coefficients, n_{op} = order of the polynomial function, and t = time.

3.4.2 Processing Monitoring Data for Prediction Functions

The coefficients a_i in Equation (3.3) can be obtained by using the following three successive steps as:

Step I: *Finding the necessary monitoring period*

The duration of the necessary overall monitoring period t_{md} can be computed based on an accepted probability p of monitored extreme data f_{exm} to overcross the prediction

function f_p (i.e., $f_{exm} > f_p$) per time interval t_i and the confidence level C_{level} associated with this probability. Therefore, it is necessary to define in advance the probability p and the confidence level C_{level} = 1- λ , where λ is the probability that the monitored extreme data is not larger than f_p (i.e., $f_{exm} \leq f_p$). The overall period t_{md} is divided in equal time intervals, e.g., monitoring time periods $t_{i-1} = t_i = t_{i+1}$ as shown in Figure 3.1. The definition of the duration of these intervals depends on the monitoring frequency, the characteristics of the recorded data, the mathematical formulation of the prediction function, and the duration of the overall monitoring period.

The required magnitude of t_{md} can be computed by an acceptance sampling approach as [Ang and Tang 2007]

$$\sqrt{t_{md}} \cdot \left[\Phi^{-1}(p) - \Phi^{-1}(m) \right] = \Phi^{-1}(1-\lambda) \tag{3.4}$$

where $\Phi^{-1}(\cdot)$ = inverse of the standard normal cumulative distribution function, p_{acept} = acceptable fraction of violations during t_{md} (i.e., S_P / t_{md}). S_P represents the number of allowable violating samples (i.e., $f_{exm} > f_p$) during t_{md}. Equation (3.4) can be rearranged as follows

$$\sqrt{t_{md}} = \frac{\Phi^{-1}(1-\lambda)}{\Phi^{-1}(p) - \Phi^{-1}(S_p / t_{md})} \tag{3.5}$$

Step II: Finding the prediction function

Once the monitoring period t_{md} is computed, the coefficients a_i of Equation (3.3) can be obtained. The mean square fitting to the monitored extreme data provides the

coefficients a_i. These coefficients represent the tendency of the monitored extreme data f_{exm}. To match the previously defined criterion (i.e., $S_p = 1$) for the computation of the overall monitoring period t_{md} the prediction function f_p must be moved (see Figure 3.1). This updating is carried out via a new set of coefficients as follows

$$f'_P = \sum_{i=0}^{n_{op}} a'_i \cdot t^i \qquad n_{op} = 1, 2, 3 \tag{3.6}$$

Equation (3.6) represents a translation of the initial prediction function f_p towards the threshold of the investigated physical quantity (see Figure 3.1). The above defined procedure for the location of f'_p does not restrict the magnitude ζ of the violating extreme values f'_{exm} (see Figure 3.1). The constraint on ζ can be given by using the chart method [Levine et al. 2001]. Considering the magnitude ζ, the updated prediction function f'_p for the monitoring duration t_{md} can be obtained. More detail procedure is provided in Frangopol et al. (2008b) and Strauss et al. (2008).

Step III: *Updating the prediction function for successive monitoring periods*

The definition and updating of prediction function f'_p as described previously are based on a single monitored period t_{md}. Monitoring is a continuous process allowing access to the past and the current structural performance assessment. Therefore, in order to account for these aspects, the updating of the prediction functions has to be extended. For instance, a polynomial function associated with the first order will require at least two monitoring periods to determine a prediction function $f_p^{'(t_{i-1},t_i)}$

using the past ($t_{md,i-1}$) and the current ($t_{md,i}$) monitoring information. Therefore, the previous described process for the computation of a'_i should be based on a first order polynomial $f_p^{'(t_{i-1},t_i)}$ spanning at least two periods $t_{md,i-1}$ and $t_{md,i}$ as shown in Figure 3.2.

3.4.3 Application

The I-39 Northbound Bridge over the Wisconsin River was built in 1961 in Wausau, Wisconsin. The bridge carries the northbound traffic of the interstate I-39 as shown in Figure 3.3. It is a five span continuous steel plate girder bridge. The alignments of the horizontal curved girders are symmetric with respect to the mid point of the third span.

The monitoring program for this bridge included the assessment of the strain of specified structural components and, for the entire structure, a controlled testing and long-term assessment. Strain gages as well as linear variable differential magnetic based transformers (LVDTs) were used for the monitoring program [Mahmoud et al. 2005]. More details about the aim and results of the monitoring program are given in Mahmoud et al. (2005). The proposed approach in this section is applied to the monitored data of the sensor CH15. This sensor was mounted on the bottom flange of the Northbound Bridge girder as shown in Figure 3.3. The sensor was located at this position, since the stress concentrations and crack initiations due to the welded flange cover plates associated with field splices are significant at that detail [Mahmoud et al. 2005].

Prediction function for the monitoring period $t_{md,1}$

The duration of the long term monitoring for CH15 installed on the I-39 Northbound Bridge was 97 days [Mahmoud et al. 2005]. In order to obtain prediction functions f'_p in Equation (3.6), it is first necessary to compute the duration of monitoring t_{md}. An accepted probability of violation p = 0.10 per day, with a confidence level C_{level} = 0.975 (i.e., $\lambda = 1 - C_{level} = 0.025$), based on a single violating sample S_p = 1 yields according to Equation (3.5) to a monitoring period $t_{md,1}$ = 22.3 days. Figure 3.4(a) shows the prediction function associated with the monitoring period $t_{md,1}$ = 22.3 days. The coefficients of the first-order prediction function $f_p^{(1)}$ to the extreme values of the monitoring period $t_{md,1}$ = 0 to 22.3 days are a_0 = 24.347 and a_1 = 0.1042. The coefficient a'_0 = 32.5 of the adjusted prediction function $f'^{(1)}_p$, which satisfies the constraint of only one violating sample S_p = 1 within the monitoring period $t_{md,1}$, can be obtained using the chart method.

Prediction functions for successive monitoring periods

In order to take into account the past monitored information, the prediction function $f'^{(1,2)}_p$ can be based on the monitoring periods $t_{md,1}$ and $t_{md,2}$, and the next prediction function $f'^{(2,3)}_p$ based on the periods $t_{md,2}$ and $t_{md,3}$ as shown in Figures 3.4(b) and 3.4(c). Therefore, the updating of the coefficients of the prediction function has been performed by considering the monitored extreme data of the two associated monitored

periods. Figure 3.4(c) shows the previously defined steps for $f'_p{}^{(2,3)}$: (a) fitting the polynomial first order to the monitored extreme data of $t_{md,2}$ and $t_{md,3}$, (b) shifting the polynomial towards the monitored extreme values S_p of $t_{md,2}$ and $t_{md,3}$ by updating a'_0, and (c) verifying the magnitude ζ by using the chart method. It has to be noted that due to the small differences between $f'_p{}^{(1,2)}$ and $f'_p{}^{(2,3)}$ the prediction function $f'_p{}^{(2,3)}$ is replaced by $f'_p{}^{(1,2)}$. Figure 3.4(d) shows the prediction functions of the monitored periods $t_{md,i}$ associated to the sensor CH15 for the whole monitoring program of the I-39 Northbound Bridge.

Reliability profile associated with yield strength

The monitored data and the design data of the I-39 Northbound Bridge provide the basis for the probabilistic assessment with respect to steel yielding. The assessment is strongly influenced by the steel grade. The steel used in the girders of the I-39 Northbound Bridge is M270 Grade 50W. The nominal yield strength of this steel is 345 MPa (50 ksi). The probabilistic analysis requires the mean value and standard deviation of all random variables. For this steel, there have already been performed extensive examinations of probabilistic models for the yield strength, the tensile strength, and their correlation [Strauss et al. 2006]. The probabilistic descriptors of the yield strength for the steel girder σ_{yield} of the I-39 Northbound Bridge are derived from these investigations which yield to a mean value of 380 MPa and a standard deviation of 26.6 MPa. These probabilistic descriptors serve as the mean μ_R and standard

deviation σ_R of the steel resistance R.

The long term monitored data displays the variability of the stresses caused by traffic, temperature, shrinkage, creep and structural changes. The stresses from the dead weight of the steel structure and the concrete deck are not included in the measured data. Therefore, the computation of the reliability index profile β_p associated with the prediction function f'_p defined in Equation (3.6) has to be based on additional information. The reliability index associated with the monitored data of the sensor CH15 can be computed as follows

$$\beta = \frac{\mu_R - \mu_{steel} - \mu_{conc} - \gamma_p \times \mu_p}{\sqrt{\sigma_R^2 + \sigma_{steel}^2 + \sigma_{conc}^2 + \left(\gamma_p \times \sigma_p\right)^2}} \tag{3.7}$$

where μ_p, σ_p = mean and standard deviation of the stress associated with the prediction function f'_p, respectively; μ_{steel}, σ_{steel} = mean and standard deviation of the stress caused by the dead weight of steel, respectively; μ_{conc} , σ_{conc} = mean and standard deviation of the stress caused by the dead weight of concrete, respectively; and γ_p is a factor assigned to the data provided by sensors.

The stresses associated with sensor CH15 are not the maximum stresses representative for the yield strength assessment. Figure 3.3 shows that the sensor CH15 is located out of the middle (maximum stress domain) of the girder in the second lateral span. Several simulations according to different load combinations showed that the traffic load located in the second and fourth span produces the maximum stress in the bottom of the steel girder. The factor γ_p assigned to the

measured sensor data and the stresses to be expected in the middle of the second lateral field, as derived from the numerical simulations, is 1.15. The values of descripters (i.e., resistance: μ_R = 380 MPa and σ_R = 380 × 0.07 = 26.6 MPa , stress by dead weight of steel: μ_{steel} = 116.3 MPa and σ_{steel} = 116.3 × 0.04 = 4.65 MPa, and stress by dead weight of concrete: μ_{conc} = 108.8 MPa and σ_{conc}= 108.8 × 0.04 = 4.35 MPa) yield to

$$\beta_p = \frac{380 - 116.3 - 108.8 - 1.15 \times \mu_p}{\sqrt{26.6^2 + 4.65^2 + 4.35^2 + \left(1.15 \times \sigma_p\right)^2}} = \frac{155 - 1.15 \times \mu_p}{\sqrt{27.35^2 + \left(1.15 \times \sigma_p\right)^2}} \tag{3.8}$$

The adjusted prediction functions $f'_p{}^{(1)}$ to $f'_p{}^{(3,4)}$ in Figure 3.4 of the monitoring periods $t_{md,1}$ to $t_{md,4}$, respectively, lead to the β_p profile according to Equation (3.8) as shown in Figure 3.5. The β_p profile serves for the assessment of the measured physical quantity in time and can also be used as reliability prediction function for a defined time horizon. For instance, Figure 3.5(a) shows the $\beta_p^{(1)}$ profile, based on the monitored extreme data obtained from the first 22.3 days. Figures 3.5(b) to 3.5(d) show the β_p profiles, according to the monitored extreme values of the four periods $t_{md,1}$ to $t_{md,4}$. The use of monitored extreme data allows (a) the reduction of uncertainties associated with numerical models, (b) the validation and updating of existing prediction models, and sometimes, the creation of novel prediction models.

3.5 System Performance Assessment and Prediction Using Monitoring Data

3.5.1 Assessment of Structural Performance

The state function is related to the difference between resistance R and load effect S (i.e., safety margin M). The state function of component i can be formulated in terms of the monitored physical quantity (e.g., stress, strain) as [Liu et al. 2009a and 2009b, Kim and Franopol 2010]

$$g_i(\mathbf{q_i}) = q_{limit,i} - q_{mon,i} \tag{3.9}$$

where $\mathbf{q_i} = (q_{limit,i}, q_{mon,i})$ is a vector of physical quantities of component i, $q_{limit,i}$ = predefined upper limit of physical quantity of component i, and $q_{mon,i}$ = physical quantity obtained from monitoring system installed on the critical location of component i. The predefined limit $q_{limit,i}$ and the monitored physical quantity $q_{mon,i}$ can both be treated as random variables. In this section, the probability that the monitored physical quantity does not exceed the predefined limit serves as the reliability measure.

3.5.2 Prediction of Structural Performance

In order to predict structural performance, a probabilistic approach based on monitored data is applied. If the predefined limit is assumed to be constant over time, $g_i(\mathbf{q_i}, t)$ can be formulated as

$$g_i(\mathbf{q_i}, t) = q_{limit,i} - \zeta_i(t) \times q_{mon,i} \tag{3.10}$$

$\zeta_i(t)$ is defined as the ratio of the expected largest value during future time period t to the largest value obtained during the monitored period [Liu *et al*., 2009a and 2009b]. This ratio can be derived from the recurrent probability using monitored data. If the monitored stress is considered as the physical quantity of interest, the random stress induced by all vehicles crossing a bridge can be assumed as Gaussian. In this case, the largest stress $\sigma_{\max}$, induced by only heavy vehicles, is asymptotically approaching a Gumbel distribution (i.e., double exponential distribution). The CDF of $\sigma_{\max}$ is [Gumbel 1958]

$$F(\sigma_{\max}) = \exp\left[-\exp\left(-\frac{\sigma_{\max} - \lambda_{par}}{\rho_{par}}\right)\right] \tag{3.11}$$

where λ_{par} = location parameter; and ρ_{par} = scale parameter. The largest stress $\sigma_{\max}(N_T)$ among the stresses induced by the expected number of heavy vehicles N_T during future time period T can be predicted from $F(\sigma_{\max}(N_T)) = 1-(1/N_T)$ [Ang and Tang, 1984]. Therefore,

$$\sigma_{\max}(N_T) = \lambda_{par} - \rho_{par} \cdot \ln\left[-\ln(1-\frac{1}{N_T})\right] \tag{3.12}$$

Consequently, the time-dependent function $\zeta_i(t)$ can be obtained as:

$$\zeta_i(t=T) = \max\left\{\frac{\lambda_{par} - \rho_{par} \cdot \ln\left[-\ln\left(1-1/N_T\right)\right]}{\max\left(\sigma_{\max,1}, \sigma_{\max,2}, ..., \sigma_{\max,j}, ..., \sigma_{\max,No}\right)};\ 1.0\right\} \tag{3.13}$$

where $\sigma_{\max,j}$ = monitored maximum stress induced by j-th heavy vehicle on a bridge; and N_o = number of heavy trucks crossing the bridge during the given monitored period T_o. However, there is no guarantee that the largest stress $\sigma_{\max}$ will

asymptotically approach a Gumbel distribution. For this reason, in order to select the most appropriate PDF of the largest stress σ_{max}, the relative goodness of fit tests have to be performed with several candidate distributions.

3.5.3 Application

The proposed approach is applied to an actual bridge over the Wisconsin River (Bridge I-39, Northbound) in Wisconsin. As mentioned in Section 3.4.3, the I-39 Northbound Wisconsin River Bridge is a five-span continuous steel girder bridge. The controlled load tests including crawl tests (speed up to 8 km/h (5 mph)) and dynamic tests (speed up to 108 km/h (65 mph)) were performed between 9 am and 11 am on July 28, 2004, by employing two tri-axle dump trucks with the gross vehicle weights (GVW) of 296.5 kN (67.2 kips) and 329.2 kN (74.6 kips), respectively. This study focuses on the monitored data from Channels 3, 4, 5, and 6 which measured and recorded the structural responses of the east exterior girder (G4), east interior girder (G3), west interior girder (G2), and west exterior girder (G1), respectively. As shown in Figure 3.6, the corresponding sensors were installed at the bottoms of the bottom flanges.

In order to minimize the volume of monitoring data and to consider only the heavy vehicles, recording of the data in Channels 3 and 6 was triggered when the vehicle induced the strain larger than the predefined strain [Mahmoud et al. 2005]. There were a total of 893 events captured during the monitoring period of 95 days

(*i.e.* N_{tt} = 893), of which the 636 heavy vehicles crossed the bridge on the right lane (*i.e.* N_{rt} = 636), and the 249 heavy vehicles crossed the bridge on the left lane (*i.e.* N_{lt} = 249). In addition, there were only 8 occurrences when the heavy vehicles crossed the bridge side-by-side (*i.e.* N_{ss} = 8) during the monitoring period. Figures 3.7(a) to 3.7(d) present the histograms of the recorded 893 maximum stresses, which clearly demonstrate that the individual girders of a multiple girder bridge may have quite different responses to the identical loading patterns from actual heavy vehicle traffics. The frequency diagrams in Figures 3.7(a) and 3.7(d) have two modes, and in Figures 3.7(b) and 3.7(c) have only one mode. This indicates that the exterior girders (G1 and G4) may be more sensitive to the transverse positions of the heavy vehicle traffics than the interior girders (G2 and G3). As indicated in Equation (3.9), the probability that the monitored data from the strain gage do not exceed the predefined limit from controlled test serves as reliability measure in this application.

Assessment of component reliability

Figure 3.8 presents the histograms of the maximum stresses σ_{max} recorded on the east exterior girder (G4) under the right lane (see Figure 3.8(a)), and left lane (see Figure 3.8(b)) heavy vehicle loading conditions. The dash lines in Figure 3.8 represent the best fitting probability function for the histograms, (i.e. the generalized extreme value (GEV) distribution). The GEV distribution is defined as

$$f_X(x) = \frac{1}{\rho_{par}}\left[1+\xi_{par}\left(\frac{x-\lambda_{par}}{\rho_{par}}\right)\right]^{-1/\xi_{par}-1} \cdot \exp\left[-\left(1+\xi_{par}(\frac{x-\lambda_{par}}{\rho_{par}})\right)^{-1/\xi_{par}}\right] \quad (3.14)$$

$$\text{for } \rho_{par} > 0 \text{ and } 0 < \rho_{par} + \xi_{par}(x-\lambda_{par})$$

where ξ_{par} = shape parameter; ρ_{par} = scale parameter; λ_{par} = location parameter. Table 3.1 provides the best fitting values of the GEV parameters and the exceedance probability $P(\sigma_{max,i,j} > \sigma_{limit,i})$ associated with Girder 4. $P(\sigma_{max,i,j} > \sigma_{limit,i})$ means the probability that the maximum monitored stress $\sigma_{max,i,j}$ associated with girder i (i = 1, 2, 3 and 4) under the jth lane loading condition (j = *rt*, *lt* and *ss* represents the loading condition under the right lane, left lane, and side-by-side heavy vehicle traffics, respectively) exceeds the predefined limit $\sigma_{limit,i}$ associated with girder i. In order to consider different loading conditions (right, left and side-by-side lane loadings), the theorem of total probability is applied. The exceedance probability of girder i $P(\sigma_{max,i} > \sigma_{limit,i})$ is expressed as

$$P\left(\sigma_{max,i} > \sigma_{limit,i}\right) = P\left(\left(\frac{N_{rt}}{N_{tt}}\sigma_{max,i,rt} + \frac{N_{lt}}{N_{tt}}\sigma_{max,i,lt} + \frac{N_{ss}}{N_{tt}}\sigma_{max,i,ss}\right) > \sigma_{limit,i}\right) \quad (3.15)$$

Similarly, the best fitting values of the GEV parameters and corresponding $P(\sigma_{max,i} > \sigma_{limit,i})$ for the girders G1, G2 and G3 are also summarized in Table 3.1, where the girder G4 has the highest probability $P(\sigma_{max,4} > \sigma_{limit,4})$ = 0.1432. The predefined stress limit $\sigma_{limit,i}$ in Equation (3.12) can treated as the normal distributed random variable with the mean value equal to the maximum stress measured during the controlled load tests, and the coefficient of variation (COV) is assigned to be 4% (including dispersion of the measurement errors during the controlled load tests).

Considering the measurement error, the state function for component *i* is defined using Equation (3.12) as

$$g_i\left(\boldsymbol{\sigma}_{\mathbf{i}}\right) = \sigma_{limit,i} - C_e \cdot \left(\frac{N_{rt}}{N_{tt}} \cdot \sigma_{max,i,r} + \frac{N_{lt}}{N_{tt}} \cdot \sigma_{max,i,l} + \frac{N_{ss}}{N_{tt}} \cdot \sigma_{max,i,ss} \right) \tag{3.16}$$

where C_e = measurement error factor. The measurement errors factor C_e is assumed to be normally distributed random variable with the mean value of 1.0 and the COV of 0.02.

Assessment of system reliability

The system reliability is assessed by using the series-parallel system model shown in Figure 3.9 (System Models I, II and III). The coefficients of correlation ρ (*X, Y*) are directly obtained from the monitored data *x* and *y* as follows:

$$\rho(X,Y) = \frac{\sum (x-\mu_x)(y-\mu_y)}{\sqrt{\sum (x-\mu_x)^2 \sum (y-\mu_y)^2}} \tag{3.17}$$

where μ_x and μ_y are the mean values of the monitored data *x* and *y*, respectively. Table 3.2 presents the resulting ρ(*X, Y*) for all heavy vehicle loading conditions, based on the actual monitored data. Although ρ(*X, Y*) may vary with time, ρ(*X, Y*) is considered as time-invariant in this study, due to lack of the actual monitored data other than those obtained in 2004. The state function of Equation (3.16) is used to formulate the exceedance probabilities for System Models in Figure 3.9. These probabilities for System Models I, II and III are obtained as 0.002%, 0.012% and 0.483%, respectively, using RELSYS [Estes and Frangopol, 1998]. From this result,

it may be concluded that the proposed approach is sensitive to the system models adopted.

Sensitivity studies

The sensitivity studies with respect to the measurement errors are conducted by varying the standard deviation of the measurement errors factor C_e in Equation (3.13) from 2% up to 8%. Figure 3.10 presents the corresponding exceedance probabilities for System Models I, II and III. It may be concluded that the increases of the measurement errors may result in increasing the probabilities of exceedance, regardless of the types of the system models adopted. In addition, the probabilities of exceedance with both perfect and zero correlations among the random variables in Equation (3.13) are computed for System Model I, II and III, respectively. Figure 3.11 shows that assuming independent random variables (i.e., the coefficients of correlation = 0.0) yields to smaller probabilities of exceedance of the structural system than those based on the actual coefficients of correlation. Conversely, the assumption of perfect correlations (i.e., the coefficients of correlation = 1.0) results in conservative assessment. Thus, it is important to obtain the actual coefficients of correlation directly from the monitored data.

Prediction of system reliability

The exceedance probability of the system is predicted by using Equation (3.13). According to the original monitored data, there were 636 and 249 heavy vehicles captured under the right and left lane traffics, respectively, during the monitoring period of 95 days. Therefore, it is estimated that the annual number of the heavy vehicles are approximately 2,500 on the right lane and 1,000 on the left lane, respectively. Consequently, the total number of the passages of the heavy vehicles in the next t years will be $N_T = 2{,}500 \times t$ for the right lane, and $N_T = 1{,}000 \times t$ for the left lane. Figure 3.12 presents the computed exceedance probabilities of system of the bridge at current time (*i.e.* in 2004) and the predicted probabilities of exceedance during the next 5, 10, 15 and 20 years. It should be noted that the increases in the exceedance probabilities with time in Figure 3.12 are caused by the predicted increases of the load effects from the heavy vehicle traffics only.

3.6 Conclusions

In this chapter, current structural safety approaches for design of new structures and assessment of existing structures are briefly reviewed, and benefit of SHM in life-cycle cost analysis are discussed. Furthermore, this chapter presents an approach for the development of prediction functions and a procedure for the performance assessment of structures based on monitored extreme data. A practical approach to assess and predict structural performance based on SHM is also proposed. The following conclusions can be drawn.

1. The proposed performance prediction functions based on monitoring extreme data can lead to the following benefits as (a) instantaneous inclusion of environmental and degradation processes in the structural reliability assessment; (b) reduction of time in the processing of monitored data of the observed physical quantity; and (c) flexible updating of performance functions associated with the reliability index or to any performance indicator by using acceptance criteria applied to monitored extreme data. This approach can provide an efficient support tool to both designer and owner for the optimum lifetime planning of deteriorating structural systems.
2. The approach based on the newly developed component state function using monitored data is proposed. This approach can effectively assess the structural system performance using the SHM data. However, the system models that combine the bridge component performance functions in different series and parallel forms may greatly affect the results.
3. The success in the structural system performance assessment and prediction using SHM data depends on how correctly and completely the structural system is modeled in terms of all critical components and their contributing response mechanisms.
4. In order to achieve valuable system performance assessment, it is important to obtain the actual coefficients of correlation among the random variables directly from the monitored data.

Table 3.1 Best fitting values for parameters of the GEV probability distributions, and probabilities $P(\sigma_{max,i,j} > \sigma_{limit,i})$ and $P(\sigma_{max,i} > \sigma_{limit,i})$

Girder	Traffic	Parameters of the GEV probability distributions			$P(\sigma_{max,i,j} > \sigma_{limit,i})$	$P(\sigma_{max,i} > \sigma_{limit,i})$
		λ_{par}	σ_{par}	ξ_{par}		
G1	Right Lane	10.02	2.64	0.105	0.007	0.07086
	Left Lane	23.14	3.63	-0.195	0.226	
	Side by Side	23.57	4.90	0.102	0.370	
G2	Right Lane	13.39	2.36	0.104	0.0070	0.01772
	Left Lane	20.04	3.08	-0.096	0.0367	
	Side by Side	22.01	6.21	-0.047	0.2810	
G3	Right Lane	20.97	3.25	-0.036	0.085	0.08312
	Left Lane	13.02	3.16	0.174	0.028	
	Side by Side	25.37	3.12	0.125	0.320	
G4	Right Lane	21.87	2.89	0.051	0.182	0.14319
	Left Lane	9.81	3.96	0.122	0.032	
	Side by Side	24.86	3.71	-0.658	0.425	

Table 3.2 Coefficients of correlation among the monitored data

Girder (Channel)		1 (CH6)			2 (CH5)			3 (CH4)			4 (CH3)		
	Traffic	Right lane	Left lane	Side by side	Right lane	Left lane	Side by side	Right lane	Left lane	Side by side	Right lane	Left lane	Side by side
1	Right lane	1.00	0.00	0.00	0.81	0.00	0.00	0.30	0.00	0.00	0.26	0.00	0.00
	Left lane	0.00	1.00	0.00	0.00	0.78	0.00	0.00	0.31	0.00	0.00	0.15	0.00
	Side by side	0.00	0.00	1.00	0.00	0.00	0.97	0.00	0.00	0.31	0.00	0.00	0.51
2	Right lane	0.81	0.00	0.00	1.00	0.00	0.00	0.53	0.00	0.00	0.42	0.00	0.00
	Left lane	0.00	0.78	0.00	0.00	1.00	0.00	0.00	0.48	0.00	0.00	0.34	0.00
	Side by side	0.00	0.00	0.97	0.00	0.00	1.00	0.00	0.00	0.37	0.00	0.00	0.50
3	Right lane	0.30	0.00	0.00	0.53	0.00	0.00	1.00	0.00	0.00	0.39	0.00	0.00
	Left lane	0.00	0.31	0.00	0.00	0.48	0.00	0.00	1.00	0.00	0.00	0.92	0.00
	Side by side	0.00	0.00	0.31	0.00	0.00	0.37	0.00	0.00	1.00	0.00	0.00	0.80
4	Right lane	0.26	0.00	0.00	0.42	0.00	0.00	0.39	0.00	0.00	1.00	0.00	0.00
	Left lane	0.00	0.15	0.00	0.00	0.34	0.00	0.00	0.92	0.00	0.00	1.00	0.00
	Side by side	0.00	0.00	0.51	0.00	0.00	0.50	0.00	0.00	0.80	0.00	0.00	1.00

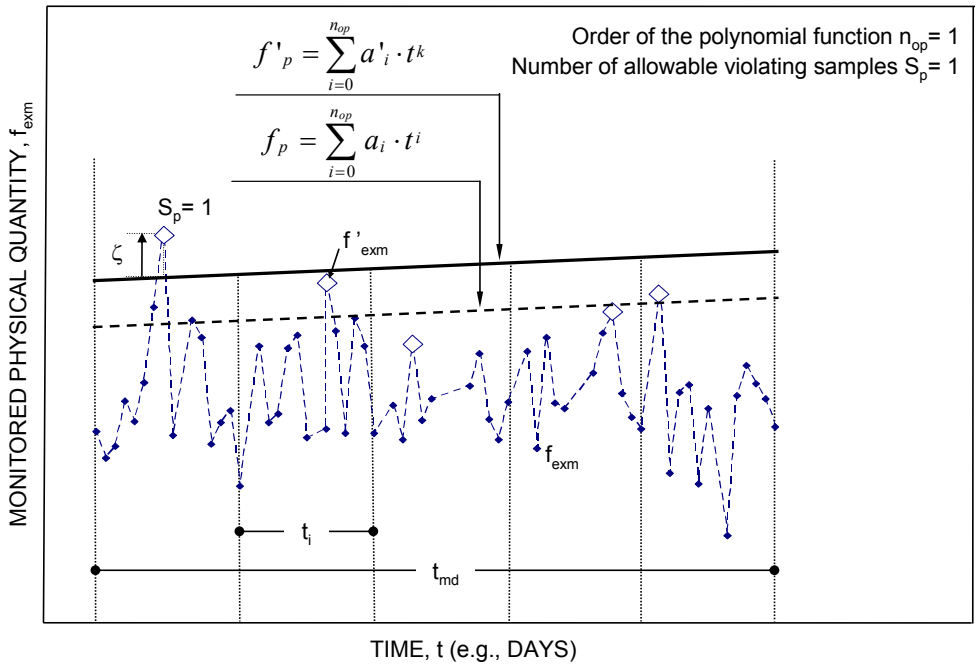

Figure 3.1 Prediction function f_p based on monitored extreme data during t_{md}

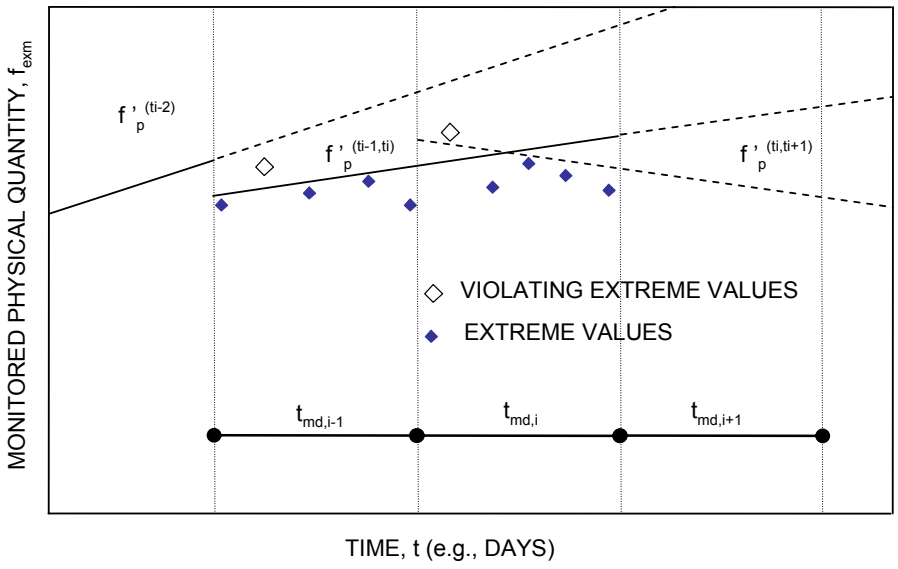

Figure 3.2 Updating the prediction function f_p

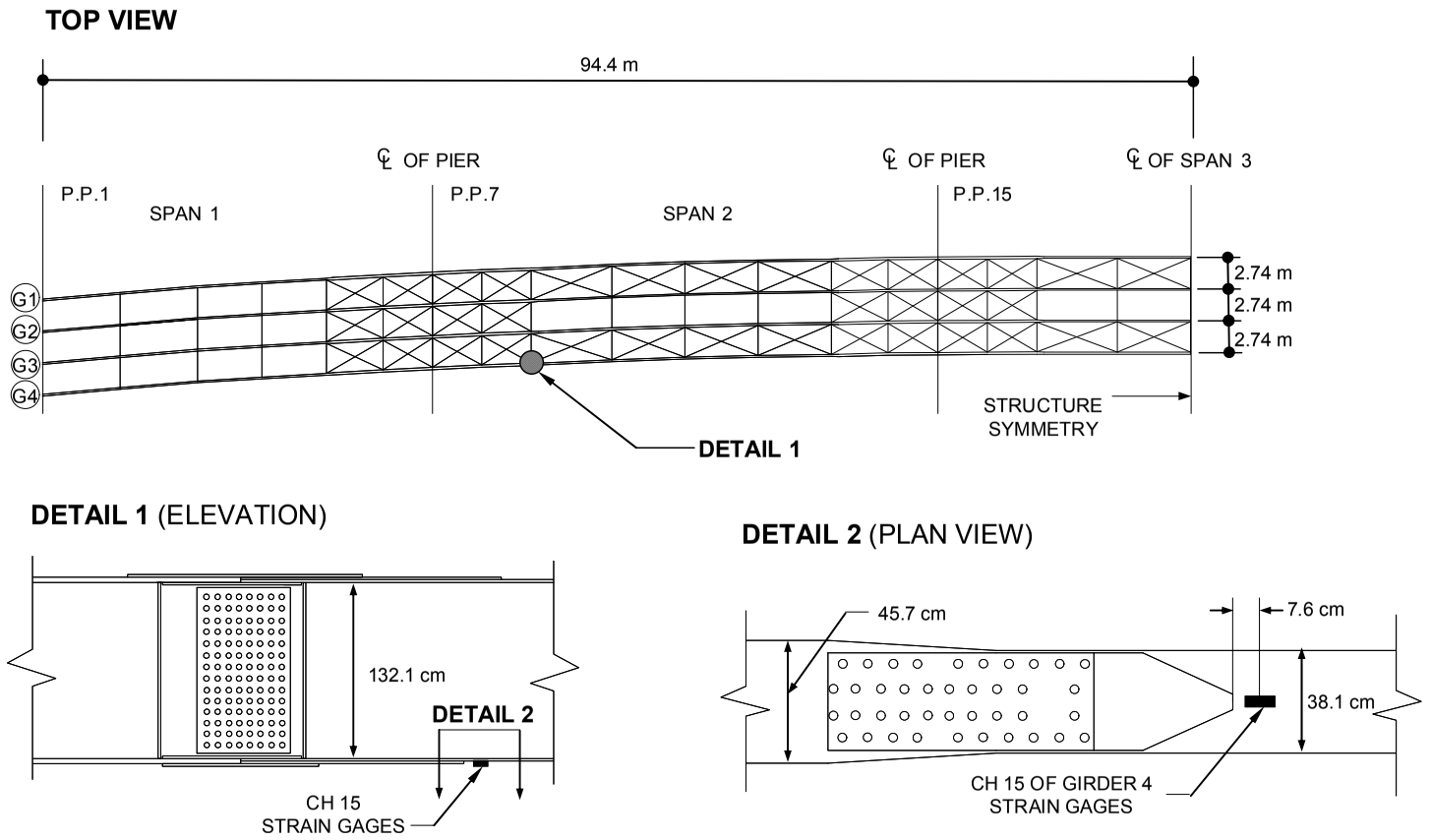

Figure 3.3 I-39 North Bound Bridge: Instrumentation plan of the strain gage, CH15 (adapted from Mahmoud et al. (2005))

(a)

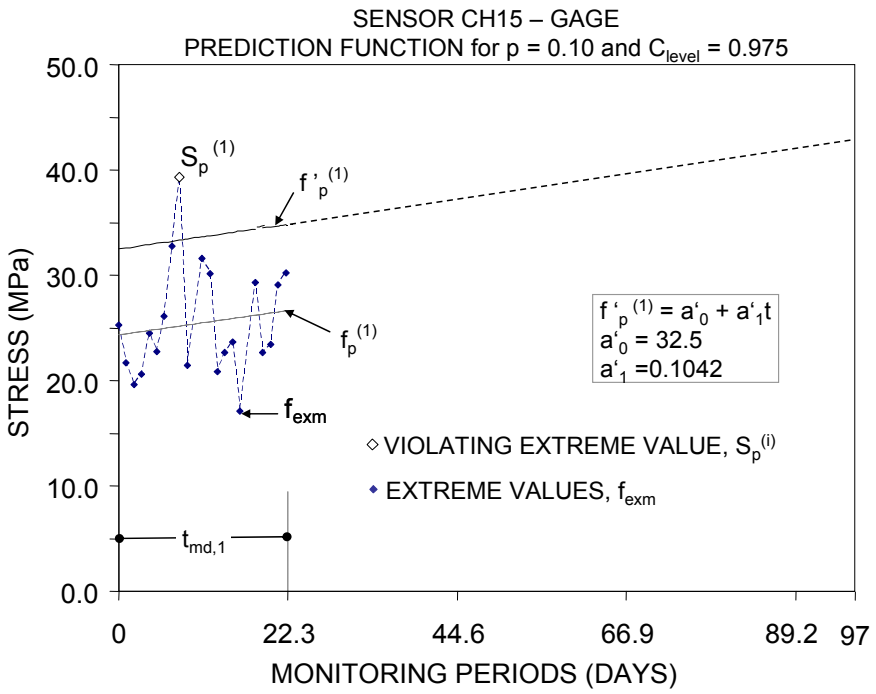

(b)

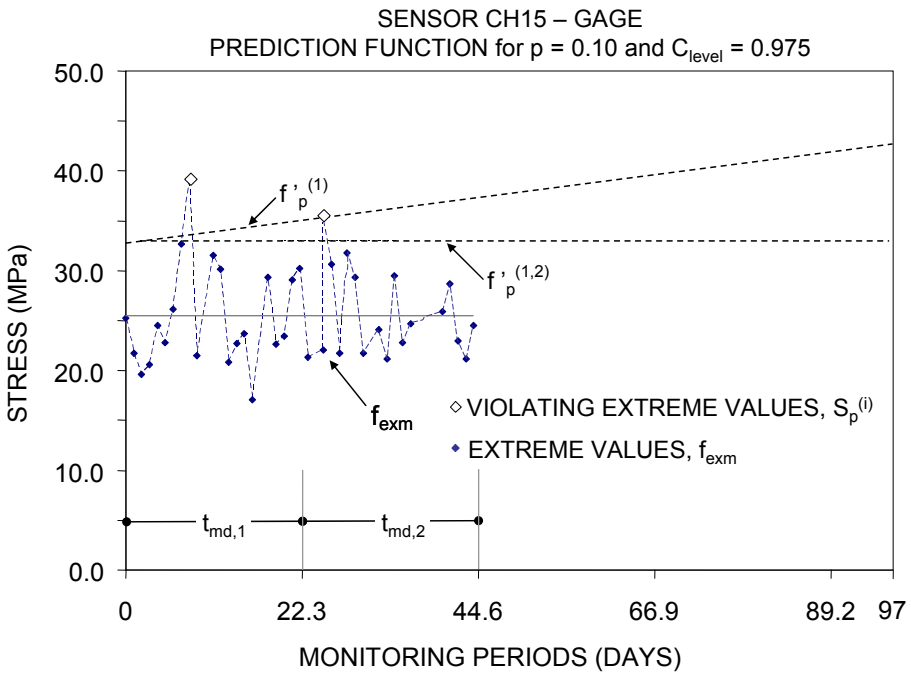

Figure 3.4 Prediction functions: **(a)** $f'_p{}^{(1)}$ of the monitoring period $t_{md,1}$; **(b)** $f'_p{}^{(1,2)}$ of the monitoring periods $t_{md,1}$ and $t_{md,2}$; **(c)** $f'_p{}^{(2,3)}$ of the monitoring periods $t_{md,2}$ and $t_{md,3}$; and **(d)** $f'_p{}^{(3,4)}$ of the monitoring periods $t_{md,3}$ and $t_{md,4}$

(c)

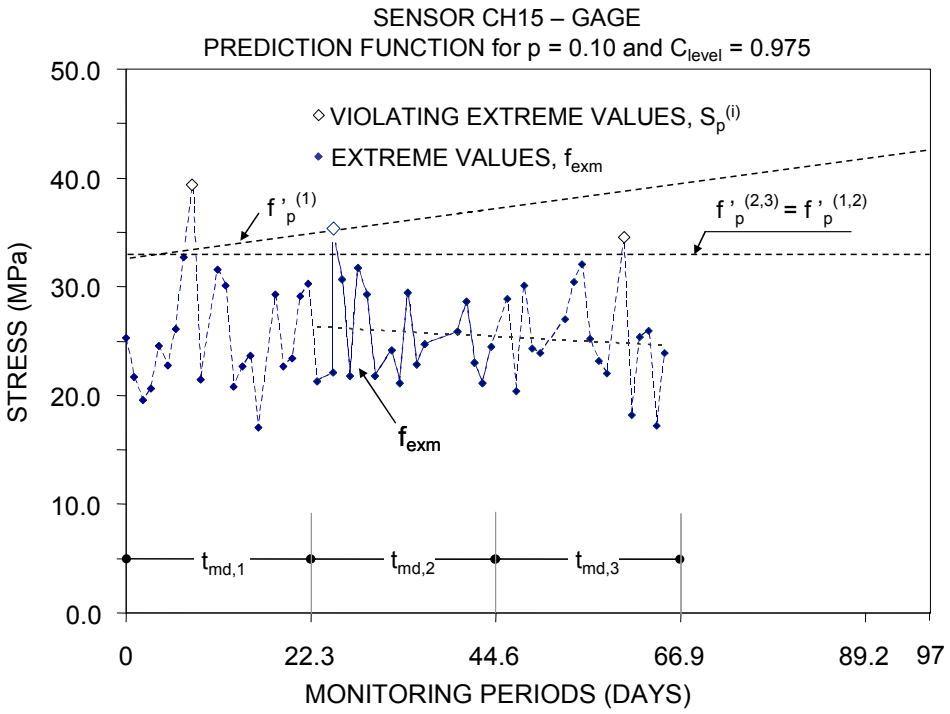

(d)

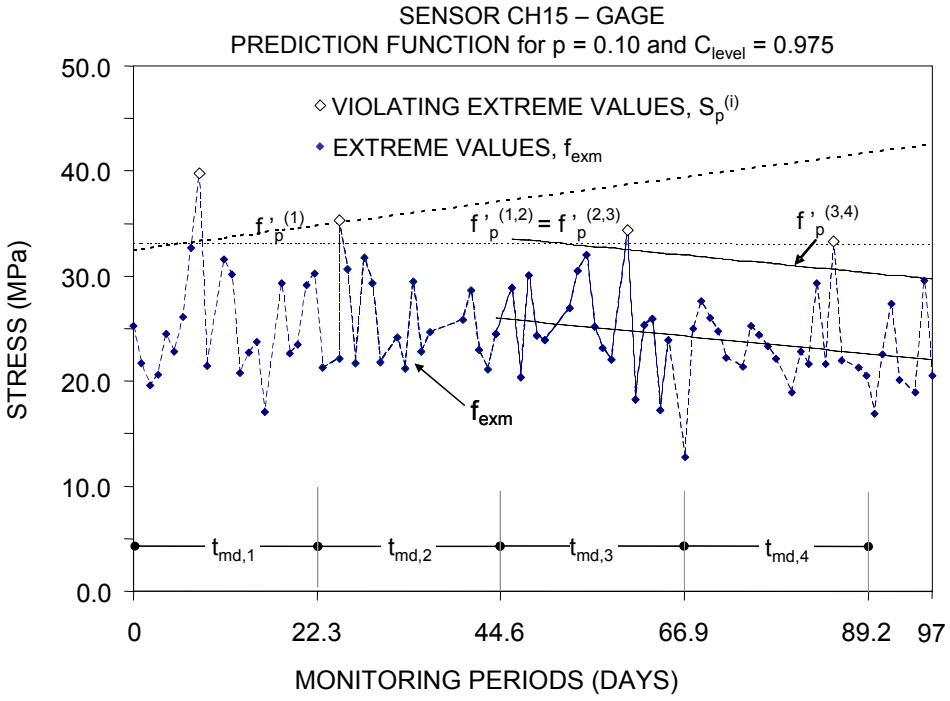

Figure 3.4 Prediction functions: **(a)** $f'_p{}^{(1)}$ of the monitoring period $t_{md,1}$; **(b)** $f'_p{}^{(1,2)}$ of the monitoring periods $t_{md,1}$ and $t_{md,2}$; **(c)** $f'_p{}^{(2,3)}$ of the monitoring periods $t_{md,2}$ and $t_{md,3}$; and **(d)** $f'_p{}^{(3,4)}$ of the monitoring periods $t_{md,3}$ and $t_{md,4}$ (continued)

(a)

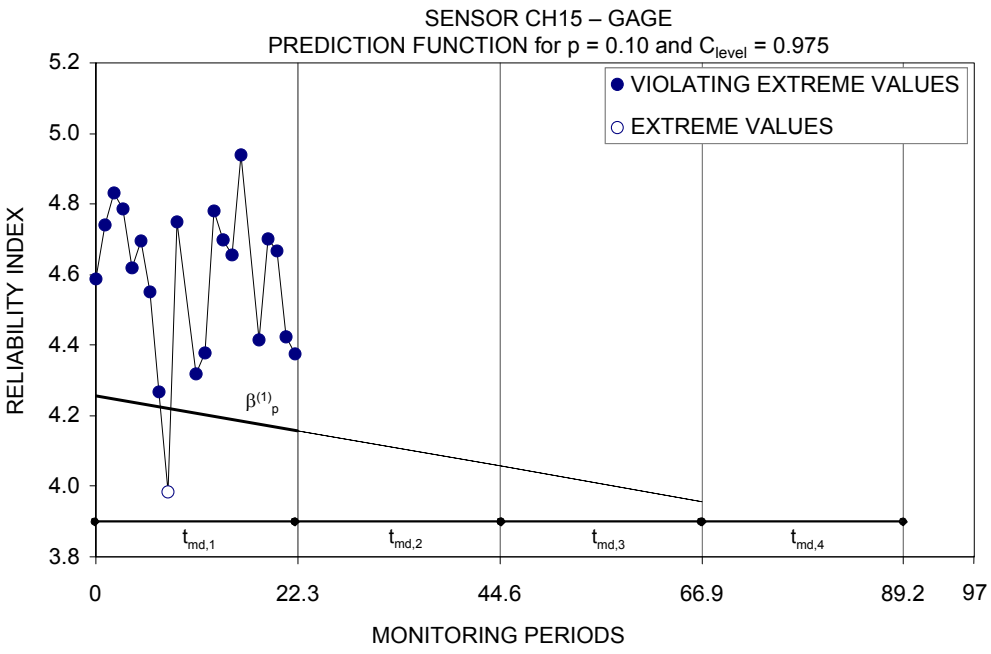

(b)

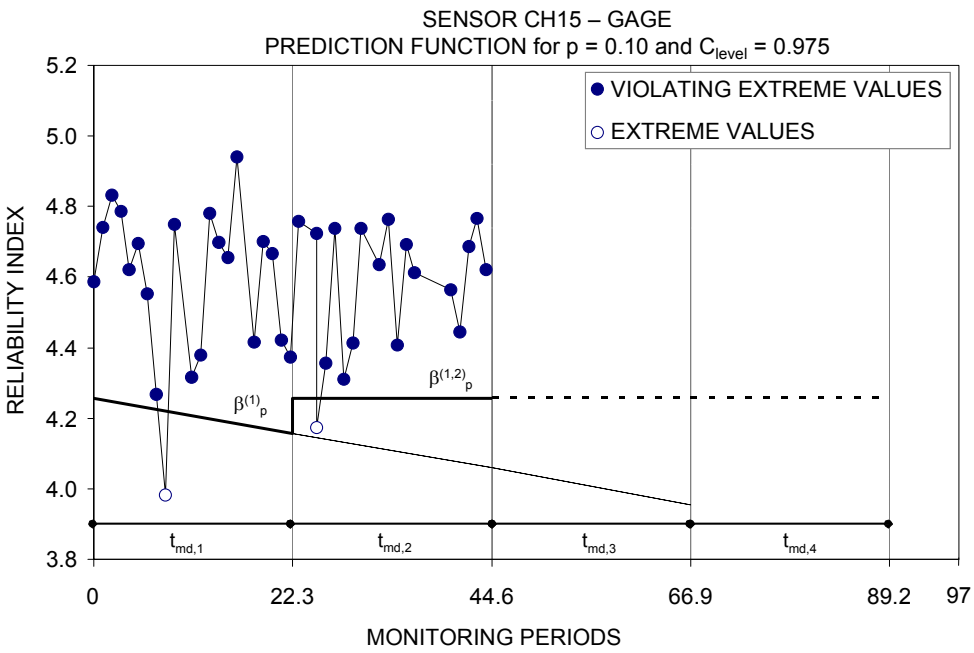

Figure 3.5 Reliability profiles based on **(a)** the prediction function $f'_p{}^{(1)}$; **(b)** the prediction functions $f'_p{}^{(1)}$ and $f'_p{}^{(1,2)}$; **(c)** the prediction functions $f'_p{}^{(1)}$ to $f'_p{}^{(2,3)}$; and **(d)** the prediction functions $f'_p{}^{(1)}$ to $f'_p{}^{(3,4)}$

(c)

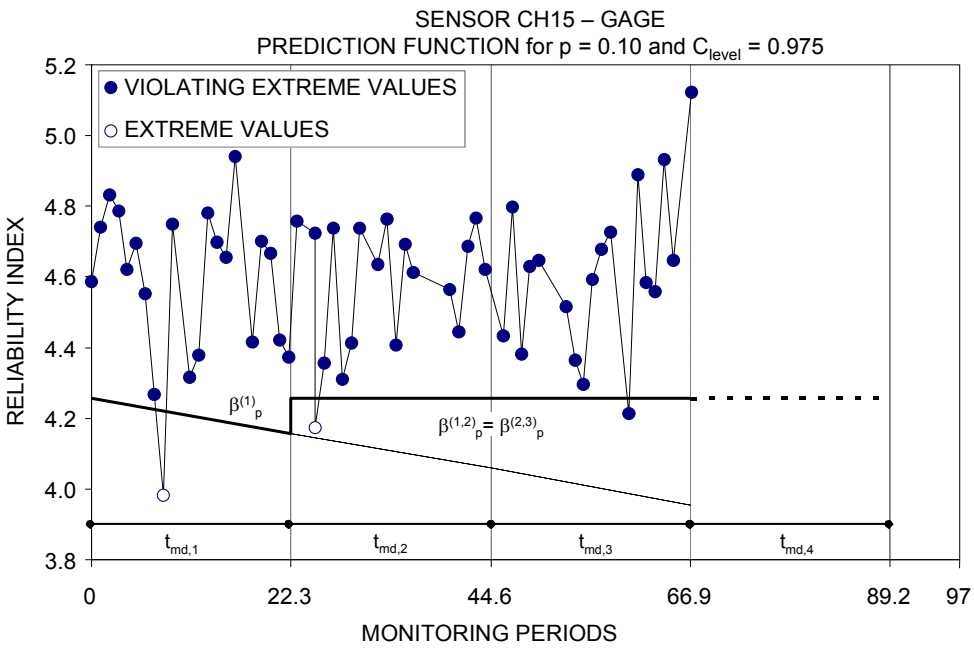

(d)

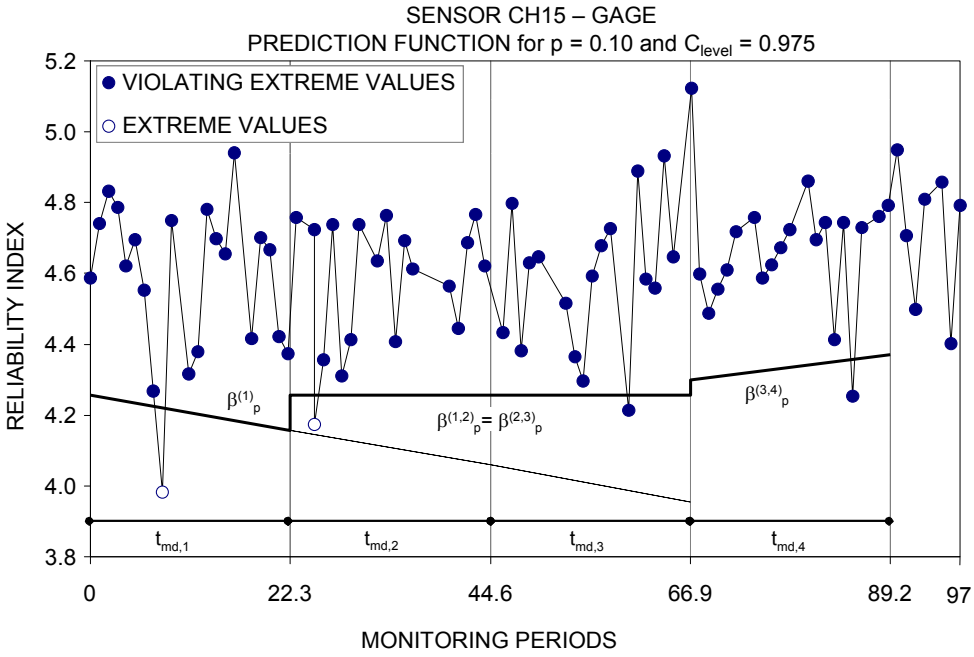

Figure 3.5 Reliability profiles based on **(a)** the prediction function $f'_p{}^{(1)}$; **(b)** the prediction functions $f'_p{}^{(1)}$ and $f'_p{}^{(1,2)}$; **(c)** the prediction functions $f'_p{}^{(1)}$ to $f'_p{}^{(2,3)}$; and **(d)** the prediction functions $f'_p{}^{(1)}$ to $f'_p{}^{(3,4)}$ (continued)

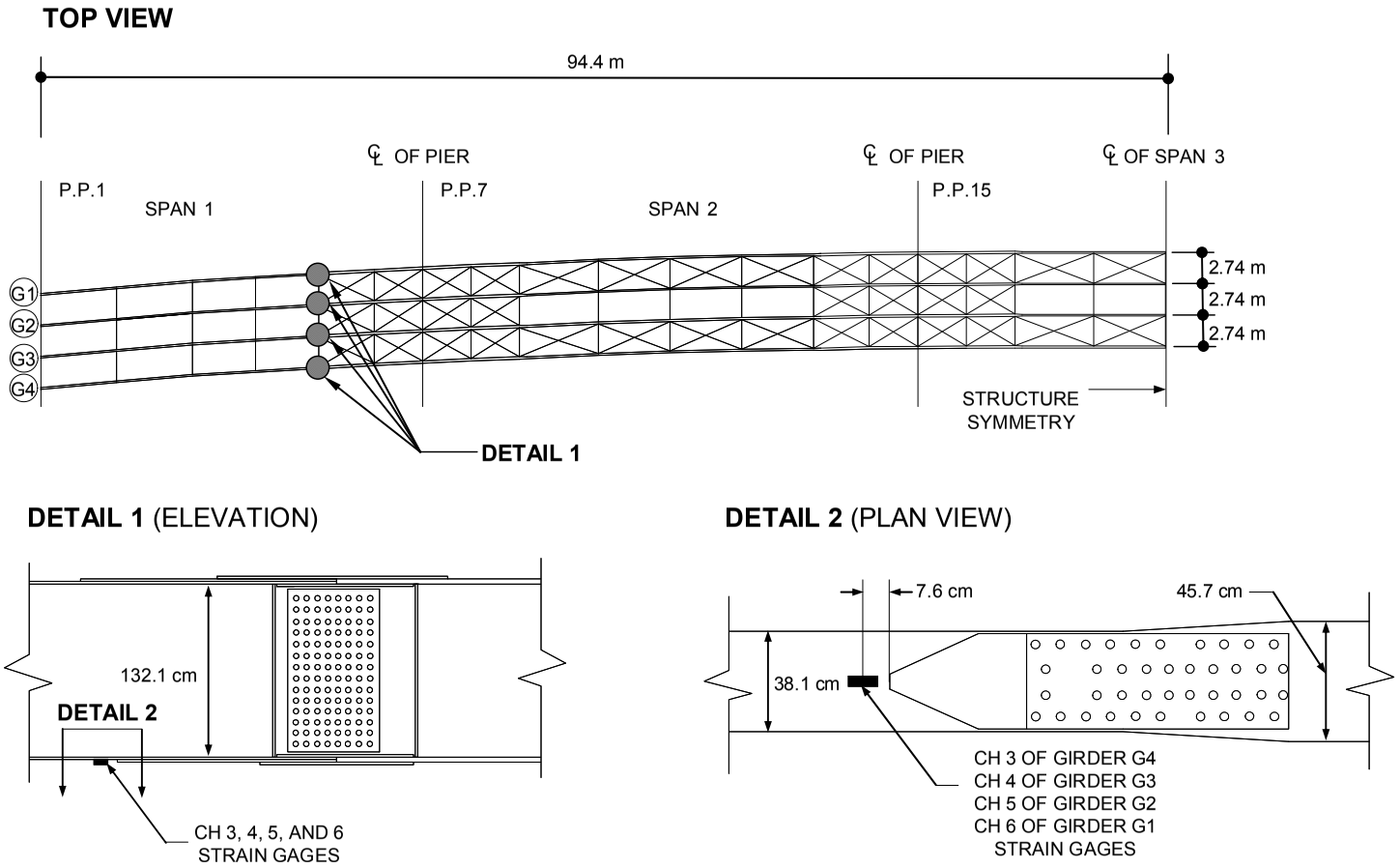

Figure 3.6 I-39 North Bound Bridge: Instrumentation plan of the strain gages, CH1, 2, 3 and 4 (adapted from Mahmoud et al. (2005))

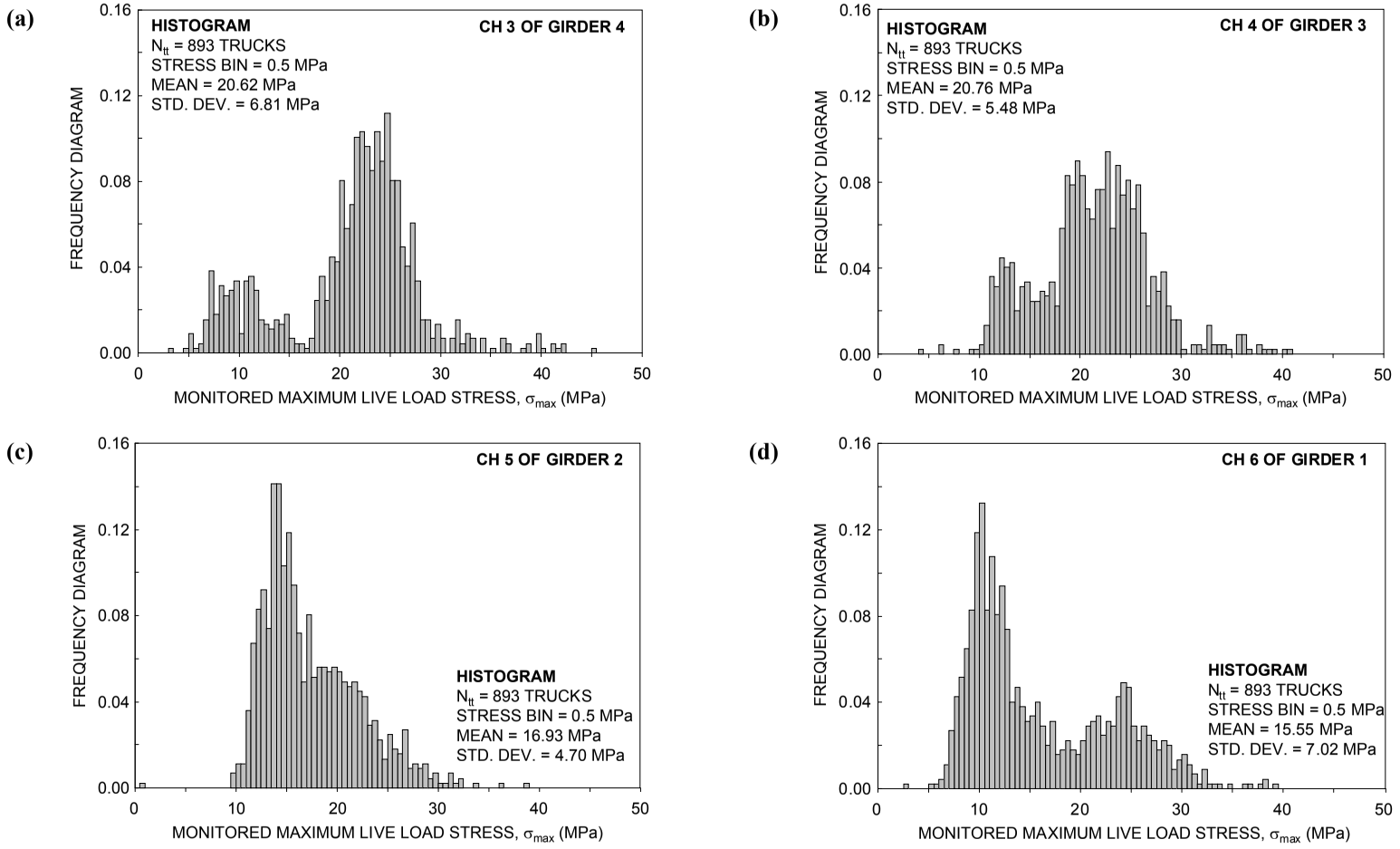

Figure 3.7 Histograms of monitored data from **(a)** CH 3; **(b)** CH 4; **(c)** CH 5; and **(d)** CH 6

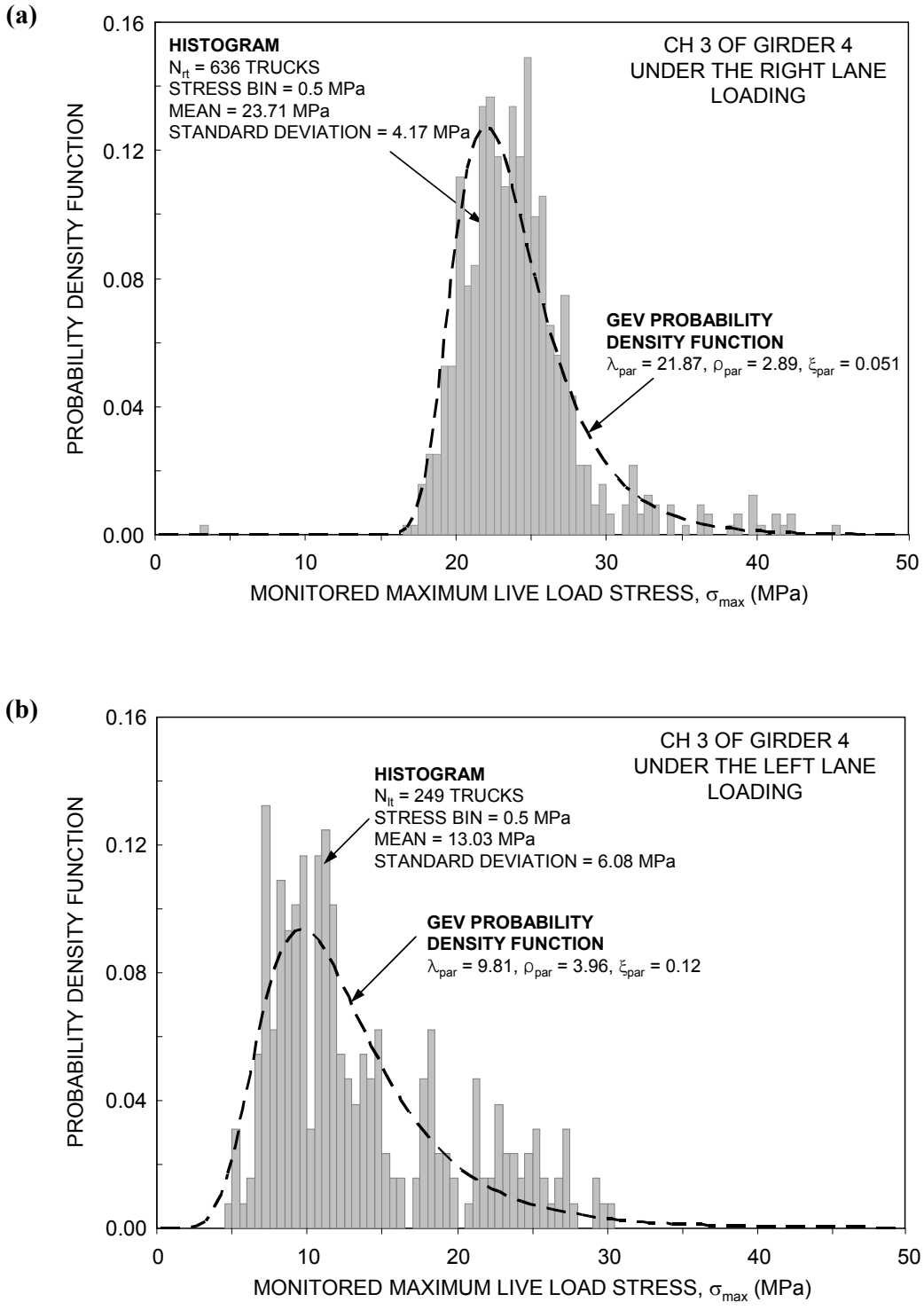

Figure 3.8 Histograms and the GEV PDF of monitored data from CH 3 of Girder 4: **(a)** under the right lane loading; and **(b)** under the left lane loading

(a) **SYSTEM MODEL I**

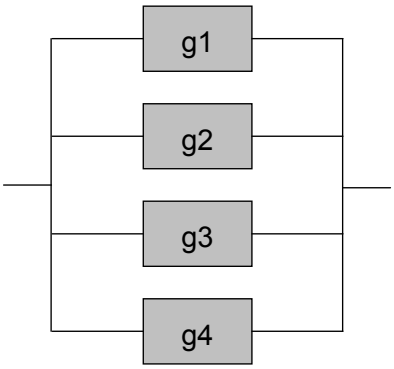

(b) **SYSTEM MODEL II**

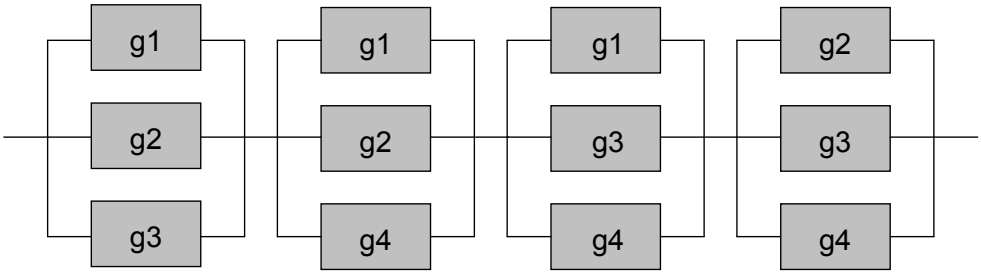

(c) **SYSTEM MODEL III**

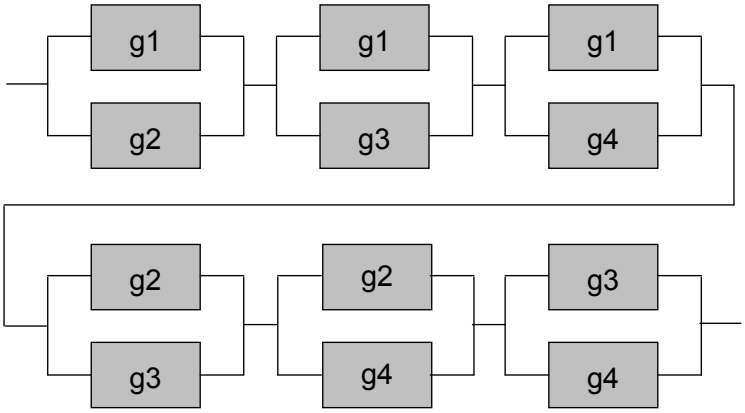

g*i*: Limit state function of girder *i*

Figure 3.9 (a) System model I; **(b)** system model II; and **(c)** system model III

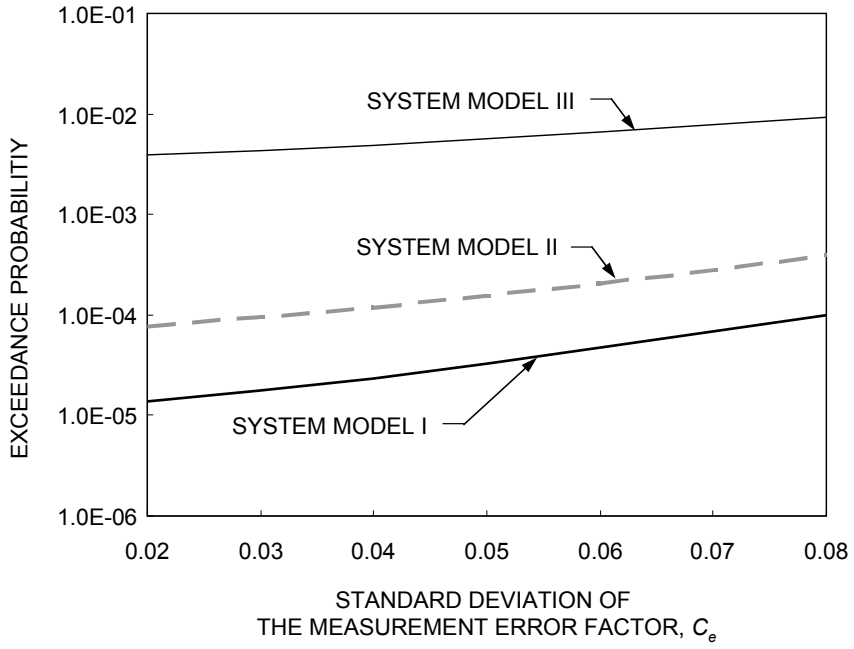

Figure 3.10 Effect of measurement error on exceedance probability of System Models I, II, and III

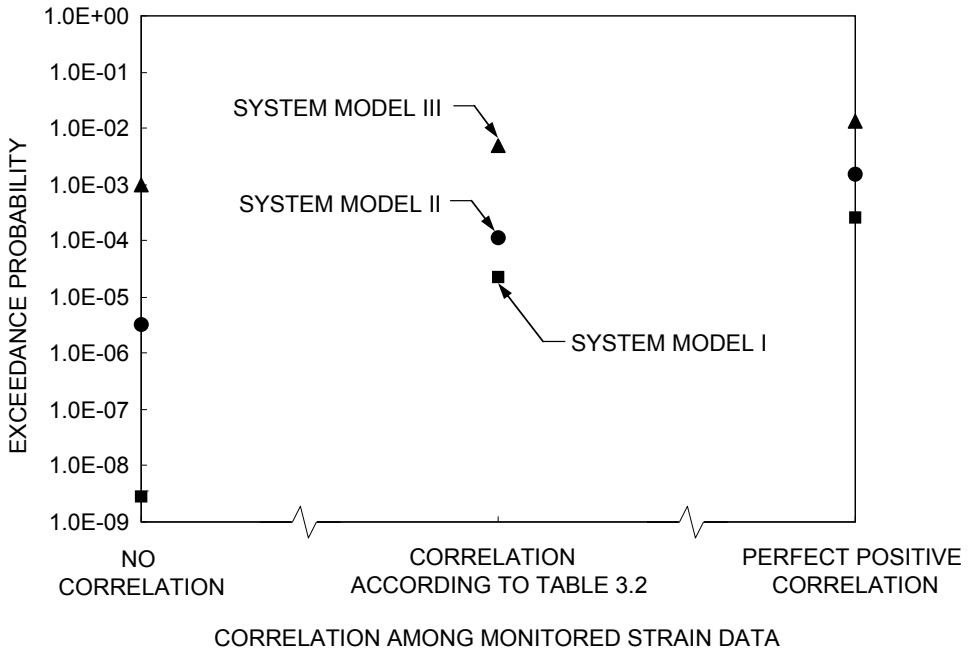

Figure 3.11 Effect of correlation among the monitored strain data on exceedance probability of System Models I, II, and III

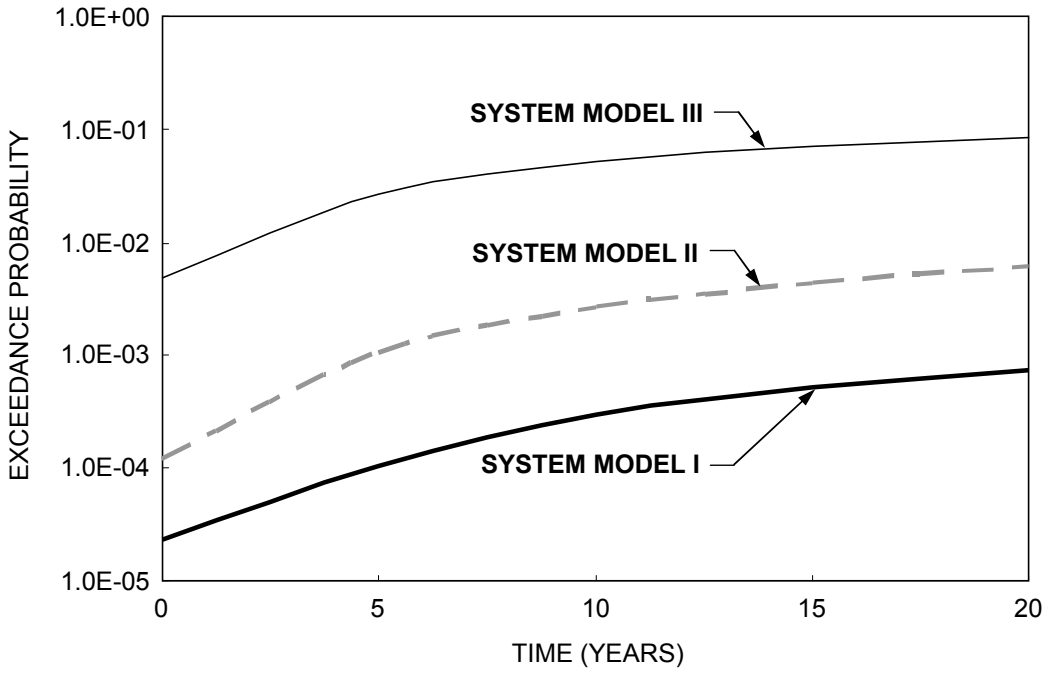

Figure 3.12 Time-dependent exceedance probabilities of System Models I, II, and III

CHAPTER 4

MONITORING PLANNING BASED ON AVAILABILITY OF MONITORING DATA

4.1 Introduction

Uncertainty associated with the life-cycle performance prediction generally increases as the structural performance is predicted further into the future. SHM can substantially reduce the expected failure cost and the expected maintenance cost of deteriorating structural systems by improving the accuracy of predicted structural performance [Frangopol and Messervey 2007]. In order to maximize this potential benefit of SHM, information from monitoring must be used appropriately [Frangopol et al. 2008a and 2008b]. Ideally, continuous monitoring is needed to establish the optimal maintenance plan. However, this is not practical due to economical constraints and limited potential benefit of monitoring program. For this reason, the cost of monitoring and reliable performance prediction can be simultaneously considered in a bi-objective optimization formulation [Kim and Frangopol 2010 and 2011a].

In this chapter, the probability that the performance prediction model based on monitoring data is usable in the future is computed by using the statistics of extremes. This probability represents the availability of the monitoring data over the future non-monitoring period. The optimum availability of the prediction model and optimum monitoring cost can be formulated as an optimization problem with two

conflicting criteria: minimization of the total monitoring cost and maximization of the availability of the monitoring data for performance prediction. This bi-objective optimization problem provides a Pareto solution set (i.e., optimum-balanced monitoring plan). This solution set provides the monitoring plan for an individual component of a structural system. Structural managers can choose the best monitoring plan from the Pareto set according to their preference and purpose. Furthermore, the monitoring plan for a component in a structural system can be changed according to the contribution of the component to the overall system reliability. In order to quantify this contribution, the NRIF of structural components has to be evaluated. Consequently, the total monitoring cost for a structural system has to be allocated based on NRIF. An alternative approach based on decision theory is also proposed. These approaches are applied to the monitored data of the I-39 Northbound Bridge over the Wisconsin River in Wisconsin, USA, obtained by the ATLSS Engineering Research Center at Lehigh University.

4.2 Exceedance Probability for Prediction Model

4.2.1 Statistical Modeling of Extreme Values

The extreme values of random variables can be treated as random variables themselves and have their own probability density function (PDF) that is related to the distribution of the initial variables [Ang and Tang 1984]. The PDF for the

extreme values can be derived from the statistical data associated with the n initial sample values. The maximum value of initial variable X is defined as

$$Y_{max} = max\{X_1, X_2, \ldots, X_n\} \tag{4.1}$$

If the random variables $X_1, X_2, \ldots, X_n$ are assumed to be statistically independent and identically distributed, the cumulative distribution function (CDF) of Y_{max} can be obtained for all n initial values of $X_1, X_2, \ldots, X_n$ as:

$$F_{Y_{max}}(y) \equiv P(Y_{max} \le y) = P(X_1 \le y, X_2 \le y, \ldots, X_n \le y) = \left[F_X(y)\right]^n \tag{4.2}$$

Equation (4.2) represents the exact CDF of the extremes of n samples with identical distribution. As $n \to \infty$, asymptotic (or limiting) forms of Equation (4.2) may converge to a particular distribution type which depends on each end of tail's behavior of the initial distribution. Gumbel (1958) categorized the asymptotic distributions into three types: (a) Type I asymptotic form (i.e., the double exponential form that holds for initial distributions of the exponential type); (b) Type II asymptotic form (i.e., the exponential form); and (c) Type III asymptotic form (i.e., the exponential form with upper bound). For example, the largest values of the initial variables with normal and exponential distributions having exponential tails correspond to Type I asymptotic distribution; Type II asymptotic distribution is the largest value distribution of lognormal distribution with a polynomial tail in the direction of the largest one; and the distribution of the extreme values of a uniform and triangular distributions with an upper or a lower limit converges to the Type III

asymptotic distribution [Ang and Tang 1984]. The three representative distributions mentioned previously are not exhaustive.

4.2.2 Linear Prediction Function and Its Residuals

In order to establish the prediction model, the relation between time (predictor variable) and physical quantity (response variable) can be assumed as a function. The prediction model can be approximated by a first-, second-, or third- order regression function based on the extreme value which can be relevant to the assurance of structural performance as mentioned in Section 3.4. The relationship between the real physical quantity and predictor variables is [Rosenkrantz 1997]

$$O_t = f_p(t) + x_t \tag{4.3}$$

where O_t is observed data at time t, f_p and x_t are the prediction function and the residual between values from the observed data and values from the regression at time t, respectively. As indicated in Equation (3.3), the prediction function can be expressed as $f_p(t) = \sum_{i=0}^{n_{op}} a_i \cdot t^i$, where a_i = coefficient, n_{op} = order of the prediction function, and t = time. As shown in Figure 4.1(a), if the regression model based on monitored data is linear, the order of the function n_{op} should be 1.0 and the coefficients a_1 and a_0 can be obtained by minimizing the sum of the squared residuals (i.e., method of least squares). In general, the residuals between the values from the linear regression model and the actual data can be assumed normally

distributed with mean value 0. This assumption is valid if the data are mutually independent, the number of data is large enough, and the regression model is obtained appropriately [Rosenkrantz 1997].

4.2.3 Exceedance Probability

The extreme values of the residuals (i.e., initial variate) have their own probability distribution. If the residuals are normally distributed, their extreme values can be modeled by the double exponential form as shown in Figure 4.1(b) (i.e.,Type I asymptotic form) [Ang and Tang 1984]. The CDF of the double exponential form for the maximum positive value of the residual is

$$F_{Y_{max}}(y) = P(Y_{max} \le y) = exp\left[-exp\left[-\rho_{max}(y-\lambda_{max})\right]\right] \tag{4.4a}$$

and the CDF associated with the minimum negative value of the residual is

$$F_{Y_{min}}(y) = P(Y_{min} > y) = 1 - exp\left[-exp\left[-\rho_{min}(y-\lambda_{min})\right]\right] \tag{4.4b}$$

where ρ_{max} and ρ_{min} = scale parameters for Y_{max} and Y_{min}, respectively; and λ_{max} and λ_{min} = characteristic maximum and minimum values, respectively, of the initial variables which are the residuals between the predicted values and the observed values. If n samples associated with Equation (4.4a) are chosen as n daily maximum positive residuals (i.e., $Y_{max,1}$, $Y_{max,2}$, ..., $Y_{max,n}$), and if each sample is statistically

independent and identically distributed, according to Equation (4.2), the CDF of the largest value, $Y_{max,n}$, among n samples would be

$$F_{Y_{max,n}}(y) = \left[F_{Y_{max}}(y)\right]^n = exp\left[-exp\left[-\rho_{max}\left(y-\lambda_{max,n}\right)\right]\right] \tag{4.5}$$

where $\lambda_{max,n}$ = characteristic maximum values of Y_{max}. Based on Equation (4.5), the CDF of the maximum value, $Y_{max,N}$, among future N samples can be derived as follows

$$F_{Y_{max,N}}(y) = \left[F_{Y_{max}}(y)\right]^N = \left\{\left[F_{Y_{max}}(y)\right]^n\right\}^{N/n} \tag{4.6}$$

If $\lambda_{max,n}$ is assumed to be $Y_{max,n}$ which is the largest positive residual among n current samples in Equation (4.5), the probability that the maximum positive residual, $Y_{max,N}$, in N future observations will be larger than the maximum positive residual, $Y_{max,n}$, among n current samples is given as [Ang and Tang 1984]

$$P(Y_{max,N} > Y_{max,n}) = 1 - \{[F_{Ymax}(Y_{max,n})]^n\}^{N/n} = 1 - e^{-N/n} \tag{4.7}$$

Since n is the number of daily maximum positive residuals and N is the number of daily maximum positive residuals in the future, the probability that the largest positive residual in the future t days will exceed the largest positive residual among t_{md} monitoring days can be obtained by modifying Equation (4.7) as [Kim and Frangopol 2011a]

$$P_{exd}(t) = 1 - exp\left(-t / t_{md}\right) \tag{4.8}$$

If the residuals between the values from the linear regression model and the actual data are not normally distributed, the procedure associated with Equations (4.4) to (4.7) can be applied after determining the appropriate distribution of the initial variate (i.e., the residuals) through distribution fitting tests. For example, if the extreme value from an initial distribution decays with an exponential tail (i.e., Type I), the exceedance probability is that in Equation (4.8). Furthermore, if the extreme value from an initial distribution decays with a polynomial tail (i.e., Type II), the final formulation of exceedance probability will be as that in Equation (4.8).

In this chapter, Equation (4.8) is assumed as exceedance probability for the monitoring data to predict structural performance. The exceedance probability for the monitoring data based on monitoring duration t_{md} can have different values depending on the number of future exceedances of the maximum positive residual from t_{md} monitoring days. Furthermore, by taking into account the relation between Equation (4.8) and the Poisson process, the probability associated with the number of future exceedances N_{exd} can be expressed as

$$P\left(N_{exd}=n_{exd}\right)=\frac{\left(t/t_{md}\right)^{n_{exd}}}{n_{exd}!}exp\left(-t/t_{md}\right) \tag{4.9}$$

From Equation (4.9), the probability that the number of future exceedances, N_{exd}, will be at least one is

$$P\left(N_{exd}\geq 1\right)=1-P\left(N_{exd}=0\right)=1-exp\left(-t/t_{md}\right) \tag{4.10}$$

which is identical with Equation (4.8). In this manner, the exceedance probability associated with various numbers of future exceedances can be formulated. For instance, the probability that the number of future exceedances will be at least two is

$$P\left(N_{exd} \geq 2\right) = 1 - \left\{P\left(N_{exd} = 0\right) + P\left(N_{exd} = 1\right)\right\} = 1 - \left(\frac{t + t_{md}}{t_{md}}\right) \cdot exp\left(-t / t_{md}\right) \tag{4.11}$$

Similarily, the number of future exceedances of the minimum negative residuals as well as the maximum positive residuals from t_{md} monitoring days can also be considered and formulated using Equation (4.5) to Equation (4.7). The formulation of the exceedance probability considering both the minimum negative residuals and the maximum positive residual can be developed. In this case, the probability that the maximum residuals in the future t days will exceed the largest positive residual among t_{md} monitoring days or the minimum residual in t days will downcross the minimum negative residual among t_{md} days has to be considered. This exceedance probability can be formulated as

$$P_{exd}\left(t\right) = 1 - exp\left(-\frac{2t}{t_{md}}\right) \tag{4.12}$$

Table 4.1 summarizes exceedance probabilities with various numbers of future exceedances.

4.3 Availability of Prediction Model for Monitoring at Regular Time Intervals

The availability of a system can be defined as the probability that the system is in operating state [Ang and Tang 1984]. A system in an operating state can become

non-operating due to deterioration. Conversely, a system in a non-operating state can be returned to an operating state through appropriate repair (see Figure 4.2). The availability of monitoring data for structural performance prediction is defined as the probability that the prediction model based on monitoring data can be usable in the future. Similarly with the availability of a system, the prediction model can become non-usable, and can be restored to a usable state by the introduction of an update prediction model based on new monitoring data (see Figure 4.2).

The average availability of monitoring data for structural performance prediction during a time period t characterized by two mutually exclusive and collectively exhaustive events (i.e., E_1 = prediction model is usable and E_2 = prediction model is not usable) is

$$\overline{A} = \frac{T_L}{t} \cdot P_{ua}(t) + \{1 - P_a(t)\} \qquad 0 < T_L \le t \tag{4.13}$$

where T_L is time to loose usability of prediction model, $P_a(t)$ and $P_{ua}(t)$ are availability and unavailability of the prediction model during t, respectively (see Figure 4.3), and $P_a(t) + P_{ua}(t) = 1.0$. Herein, the criterion for using monitoring data for prediction is associated with the maximum residual between values from prediction model and monitoring. If this residual exceeds the maximum residual during monitoring duration t_{md}, the prediction model cannot be used. According to this criterion, the unavailability of monitoring data $P_{ua}(t)$ can be replaced by the exceedance probability P_{exd} for the six cases of exceedance probabilities (Cases O1,

O2, O3, B1, B2, and B3) indicated in Table 4.1. Cases O1, O2, and O3 correspond, respectively, to at least one, two, and three exceedance(s) considering the largest value. Cases B1, B2, and B3 correspond, respectively, to at least one, two, and three exceedance(s) considering both upcrossing the largest value and downcrossing the smallest value, respectively.

The expected average availability of the monitoring data for prediction can be derived from Equation (4.13) [Ang and Tang 1984] as

$$\begin{aligned} E\left(\overline{A}\right) &= \frac{E\left(T_L\right)}{t}\cdot P_{exd}\left(t\right)+\left\{1-P_{exd}\left(t\right)\right\} \\ &= \frac{1}{t}\left(\frac{1}{P_{exd}\left(t\right)}\int_0^t \frac{\partial P_{exd}\left(x\right)}{\partial x}\cdot x\, dx\right)\cdot P_{exd}\left(t\right)+\left\{1-P_{exd}\left(t\right)\right\} \\ &= 1-\frac{1}{t}\cdot\int_0^t P_{exd}\left(x\right)dx \end{aligned} \tag{4.14}$$

For instance, using Equation (4.14), the expected average availability within prediction duration t of Case O1 in Table 4.1 is computed as [Kim and Frangopol 2011a]

$$\begin{aligned} E\left(\overline{A}\right) &= 1-\frac{1}{t}\cdot\int_0^t P_{exd}\left(x\right)dx \\ &= 1-\frac{1}{t}\cdot\int_0^t 1-exp\left[-x/t_{md}\right]dx \\ &= \frac{t_{md}}{t}\left(1-exp\left[-\frac{t}{t_{md}}\right]\right) \end{aligned} \tag{4.15}$$

The expected average availability is formulated by using the variables t_{md} and t. Figures 4.4(a) and 4.4(b) show the relations between the ratio r_{md} of monitoring duration t_{md} to prediction duration t and expected average availability $E\left(\overline{A}\right)$ for Cases O1, O2, O3, and B1, B2, B3 in Table 4.1, respectively. It can be seen that

higher the expected average availability of the monitoring data for prediction is, longer monitoring duration t_{md} is required relatively to prediction duration t. The expected average availability $E\left(\overline{A}\right)$ of Case O3 has the largest value in Figure 4.4(a), since the prediction model associated with this case is less conservative than those associated with Cases O1 and O2. Similarly, Case B3 is associated with the largest expected average availability in Figure 4.4(b).

4.4 Monitoring Cost and Optimum Balance of Monitoring Time Intervals

4.4.1 Cumulative Monitoring Cost

In general, monitoring cost is the result of the following actions: (a) general preparation and project coordination; (b) sensors, wiring, data acquisition system, and maintenance; (c) analysis of data and preparation of reports; (d) continuous review of data [Frangopol et al. 2008a]. Under the assumption that the total monitoring cost is proportional to the monitoring duration and all actions related to monitoring program are conducted only during the monitoring duration, the cumulative monitoring cost C_{MON} over a prescribed duration is [Kim and Frangopol 2011a]

$$C_{MON} = \left(\frac{t_{md}}{t_{md,o}} \cdot C_{mon,o} \right) \cdot \sum_{i=1}^{n_{mon}} \left(\frac{1}{\left(1 + r_{dis}\right)^{(i-1)(t+t_{md})}} \right) \tag{4.16}$$

where $C_{mon,o}$ = reference monitoring cost during $t_{md,o}$ days, r_{dis} = discount rate of money (%/day), and n_{mon} = total number of monitoring periods over a prescribed duration (days).

4.4.2 Optimum Balance of Availability and Monitoring Cost Using Bi-Objective Optimization Formulation

The potential benefit of SHM can be maximized by reducing the expected failure cost and maintenance cost of structural systems. Through appropriate SHM, structure managers can establish more rational maintenance strategies under uncertainty. A reliable performance prediction model will lead to cost-effective maintenance and repair actions. However, more reliable monitoring data and more frequent monitoring action require higher cost, and, as a result, it may be difficult to obtain the monitoring benefit in financial terms. Therefore, in order to find the optimal balance between the two conflicting criteria, bi-objective optimization should be applied. This approach minimizes the total monitoring cost and maximizes the expected average availability of the monitoring data for performance prediction.

The optimization problem requires (a) design variables, (b) objectives formulated by including the variables, and (c) constraints for the variables and for the objectives. In this chapter, the two conflicting objectives can be defined as: (a) maximize the expected average availability of the monitoring data for prediction $E\left(\overline{A}\right)$ indicated in Equation (4.14); and (b) minimize the cumulative total monitoring cost C_{MON} indicated in Equation (4.16). In order to obtain well-balanced solutions, NSGA-II (Non-Dominated Sorting in Genetic Algorithms) program is used (Deb *et al*., 2002). The two major reasons for using genetic algorithms (GA) for

this optimization problem are: (a) GA does not require continuity or differentiability of the objective function [Arora 2004]; and (b) GA is able to converge to the Pareto optimal set rather than a single Pareto optimal point [Osyczka 2002]. Detailed procedure of NSGA-II is available in Deb et al. (2002).

4.4.3 Optimal Monitoring Plan for a Structural System

The reliability importance factor (RIF) of individual components can be considered for monitoring planning for a structural system. In order to estimate the time-dependent reliability of each component, the state function and the time-dependent function are applied as indicated in Equations (3.16) and (3.13), respectively. For assessment of the structural system performance, a series-parallel system model is used. Total monitoring cost for the structural system is allocated to the components according to their normalized reliability importance factors (NRIF). The allocated monitoring cost of each component determines the monitoring plan (i.e., monitoring duration and prediction duration) by using the Pareto optimal solution set of a bi-objective optimization problem which minimizes the total monitoring cost and maximizes the availability of monitoring data.

The solutions obtained from the bi-objective optimization problem can provide possible monitoring schedules of the monitored structural component. In order to allocate the monitoring cost to each component in a structural system, the time-variant NRIF can be applied. The monitoring cost for the individual component

i, $C_{MON,i}$, is [Kim and Frangopol 2010]

$$C_{MON,i} = C_{MON,system} \times E\left(NRIF_i\right) \tag{4.17}$$

where $C_{MON,system}$ = available total monitoring cost for a structural system during a prescribed period; and $E(NRIF_i)$ = average time-variant normalized reliability importance factor $NRIF_i$ (see Equation (2.19)) during the period. After the monitoring cost $C_{MON,i}$ of component i is assigned according to $E(NRIF_i)$ as indicated in Equation (4.17), the expected average availability and the design variables (i.e., monitoring duration and prediction duration) for the component can be determined from the Pareto solution set of the bi-objective problem. Figure 4.5 shows the schematic of the proposed methodology for establishing optimal monitoring planning for a structural system. The associated detailed flow charts are provided in Appendix (see Figures A.1, A.2 and A.3).

4.4.4 Optimum Balance of Availability and Monitoring Cost Using Decision Analysis

As an alternative method, decision analysis can be used to find the optimal solution. In general, if the decision is expressed in terms of a monetary value, the decision associated with the maximum expected monetary value (EMV) (i.e., minimum monetary loss) is the solution. EMV of the ith alternative is [Ang and Tang 1984]

$$EMV\left(a_i\right) = \sum_j p_{ij} C_{ij} \tag{4.18}$$

where p_{ij} = the probability of the jth consequence associated with alternative a_i, and C_{ij} = the expected monetary of the jth consequence associated with alternative a_i. According to the maximum monetary value criterion, the optimal alternative a_{opt} is determined as the alternative having maximum EMV among n alternatives as:

$$C\left(a_{opt}\right) = max\left\{EMV\left(a_1\right),\ EMV\left(a_2\right),\ ...,\ EMV\left(a_n\right)\right\} \tag{4.19}$$

EMV for cost-effective SHM can be formulated by using the expected average availability of the model and monitoring cost associated with different monitoring durations t_{md} and future non-monitoring durations t. As shown in Figure 4.6, monitoring plan i has two events (j = 1, 2) that are mutually exclusive and collectively exhaustive: the monitoring data are either usable or not during prediction duration t_i. For the usable case over the future non-monitoring period, the probability p_{ij} and the expected cost C_{ij} of monitoring plan i in Equation (4.18) are replaced by the expected average $E_i\left(\overline{A}\right)$ and the monitoring cost $C_{mon,i,u}$, respectively. On the other hand, for non-usable case over the future non-monitoring period, the probability p_{ij} in Equation (4.19) can be computed as $1 - E_i\left(\overline{A}\right)$. The cost associated with the non-usable case $C_{mon,i,nu}$ can include the potential loss occurred from the use of non-usable monitoring data for prediction and the monitoring cost $C_{mon,i,u}$ as well. Therefore, EMV associated with monitoring plan i is [Kim and Frangopol 2011a]

$$EMV\left(Plan\ i\right) = C_{mon,i,u} \cdot E_i\left(\overline{A}\right) + C_{mon,i,nu} \cdot \left(1 - E_i\left(\overline{A}\right)\right) \tag{4.20}$$

If the monitoring cost is proportional to the duration of monitoring, the monitoring cost per day $C_{mon,i,u}$ for the usable case can be calculated based on the reference monitoring cost $C_{mon,o}$ during $t_{md,o}$ days as:

$$C_{mon,i,u} = \left(\frac{C_{mon,o}}{t_{md,o}} \cdot t_{md,i} \right) / \left(t_{md,i} + t_i \right) \tag{4.21}$$

where $t_{md,i}$ = monitoring duration, and t_i = prediction duration for monitoring plan i. Therefore, the monitoring cost per day $C_{mon,i,nu}$ for the non-usable case adding potential loss C_{loss} is

$$C_{mon,i,nu} = \left(\frac{C_{mon,o}}{t_{md,o}} \cdot t_{md,i} \right) / \left(t_{md,i} + t_i \right) + C_{loss} \tag{4.22}$$

As a result, substituting Equations (4.21) and (4.22) into Equation (4.20), EMV for plan i is [Kim and Frangopol 2011a]

$$\begin{aligned} EMV(Plan\ i) = & \left\{ \left(\frac{C_{mon,o}}{t_{md,o}} \cdot r_{md,i} \right) / \left(r_{md,i} + 1 \right) \right\} \cdot E_i\left(\overline{A} \right) \\ & + \left\{ \left(\frac{C_{mon,o}}{t_{md,o}} \cdot r_{md,i} \right) / \left(r_{md,i} + 1 \right) + C_{loss} \right\} \cdot \left(1 - E_i\left(\overline{A} \right) \right) \end{aligned} \tag{4.23}$$

where $r_{md,i}$ is the ratio of the monitoring duration, $t_{md,i}$, to the prediction duration, t_i associated with monitoring plan i

4.5 Application

The methodologies proposed in this study are applied to the long-term monitored data from the strain gage CH4 which was installed on the bottom flange of the

Northbound Bridge I-39 as shown in Figure 3.6. The 80 days monitored data monitored data are used in this example.

4.5.1 Expected Average Availability of Monitoring Extreme Data for Prediction

The linear regression model as a performance prediction model is based on the ten maximum daily stresses during the 80 monitored days as shown in Figure 4.7(a). The residuals between the monitored data and values from the performance prediction model have the mean value of 0.0 MPa and the standard deviation of 4.7 MPa. The probability paper is used as shown in Figure 4.7(b) to check whether the appropriate distribution for these residuals is a normal distribution. For construction of the normal probability paper, 800 residuals are arranged in increasing order, and the *i*th residual value among the 800 data is plotted at the standard normal variate $s_i = \Phi^{-1}(i / (N+1))$, where $N = 800$ and Φ^{-1} is the inverse standard normal CDF. The regression line of these residuals on the normal probability paper can be obtained by the method of least square as shown in Figure 4.7(b). The slope of the regression line and *y*-intercept represent the standard deviation of the residual (4.68 MPa) and the mean value of the residual (0 MPa) respectively. To evaluate how well the estimated regression line fits the data, the coefficient of determination is used [Rosenkrantz 1997]. This coefficient is defined as

$$R^2 = \frac{\sum (y_i - \bar{y})^2}{\sum (f_i - \bar{y})^2} \tag{4.24}$$

where y_i = ith residual value, $\bar{y}$ = mean value of residual values, f_i = value on the regression line associated with s_i. If R^2 is close to 1.0, most of the data can be captured by the linear regression model [Rosenkrantz 1997]. R^2 associated with Figure 4.7(b) is 0.9829. Additionally, the several relative goodness of fit tests (i.e., the Chi-square test, Kolmogorov-Smirnov test, and Anderson-Darling test) were performed with several candidate distributions in order to select the most appropriate distribution which fits the residuals. As a result, the normal distribution was selected as the best-fit distribution for the residuals. Therefore, the maximum and the minimum values have the Type I asymptotic distribution (i.e., the double exponential form). The scale parameters ρ_{max} and ρ_{min} of the maximum and the minimum values are $\sqrt{2 \ln N} / \sigma = \sqrt{2 \ln 800} / 4.68 = 0.78$ and the values of the characteristic maximum, λ_{max}, and minimum, λ_{min}, are assumed to be the maximum and minimum residuals of 14.97MPa and -11.49MPa, respectively, among 800 monitoring data. Therefore, the CDFs of the double exponential asymptotic form for the maximum and the minimum value of the residuals can be formulated (see Equation (4.4)).

$$F_{Ymax}(y) = P(Y_{max} \le y) = exp[-e^{-0.78\,(y\,-14.97)}] \tag{4.25a}$$

$$F_{Ymin}(y) = P(Y_{min} > y) = 1 - exp[-e^{0.78\,(y\,+11.49)}] \tag{4.25b}$$

Figure 4.7(c) shows the histogram from the residual, its appropriate distribution (i.e., normal distribution), and the PDFs of the extreme values of the initial variate (i.e., the residual values).

The expected average availability $E(\overline{A})$ of the monitoring data for prediction can be obtained from Equation (4.14). Therefore, it can be formulated with monitoring duration t_{md} and prediction duration t. The relations between $E(\overline{A})$ for 80 days of monitoring duration t_{md} and the prediction duration t for the six cases in Table 4.1 are plotted in Figures 4.8(a) and 4.8(b). As expected, $E(\overline{A})$ decreases as the prediction duration t increases.

4.5.2 Optimal Monitoring Plan for a Structural Component

The design variables of the bi-objective problem are the monitoring duration t_{md} and the prediction duration t. The variables t_{md} and t are assumed to be between 50 days and 3000 days. The target life is assumed 7,300 days (i.e., about 20 years), and the reference monitoring cost $C_{mon,o}$ during $t_{md,o}$ = 80 days is assumed $10,000. For each case indicated in Table 4.1, 1,000 Pareto solutions are obtained using genetic algorithm after 100 generations as shown in Figures 4.9, 4.10 and 4.11. The values of objectives and design variables for some of these solutions are provided in Tables 4.2 and 4.3.

Figure 4.9(a) represents the 1,000 Pareto solutions for Cases O1, O2 and O3 without considering the discount rate of money (i.e., r_{dis} = 0.0 %/day). In order to provide an expected average availability of the prediction model $E(\overline{A})$ = 0.2 for Case O1 (i.e., Solution A1 in Figures 4.9(b) and 4.9(c)), the required monitoring duration and prediction duration have to be t_{md} = 405 days and t = 2,035 days,

respectively (see design space in Figure 4.9(b)), and the expected total monitoring cost has to be $151,875 (see Figure 4.9(c)). If $E\left(\overline{A}\right)$ has to increase four times (i.e., $E\left(\overline{A}\right)$ = 0.8 for Case O1; see Solution D1 in Figures 4.9(b) and 4.9(c)), the required monitoring duration and prediction duration have to be 1,665 days and 770 days, respectively (see design space in Figure 4.9(b)), and the expected total monitoring cost has to be $624,375 (see Figure 4.9(c)). The Solutions B1 and C1 associated with Case O1, where the expected average availability is 0.4 and 0.6, are also indicated in Figures 4.9(b) and 4.9(c), respectively. Since the allowable number of exceedances is larger for Case O2 than O1, and larger for Case O3 than O2 (see Table 4.1), the total monitoring cost associated with the same expected average availability will be maximum for Case O1 and minimum for Case O3 (see Figures 4.9 and 4.10). Figure 4.9(d) and 4.9(e) indicate three solutions (D1, D2 and D3) associated with the same expected average availability (i.e., $E\left(\overline{A}\right)$ = 0.8) for Cases O1, O2 and O3. If the discount rate of 0.016% per day (6% annual discount rate of money) is considered, the solutions in Figures 4.10(a) to 4.10(e) are obtained for each case and the associated results are indicated in Table 4.3. A substantial reduction in total monitoring cost is observed by comparing results in Table 4.3 with those in Table 4.2. The Solutions E1, F1, G1 and H1 (see Figures 4.10(b) and 4.10(c)) are much less expensive than Solutions A1, B1, C1, and D1 (see Figures 4.9(b) and 4.9(c)), respectively. The same observation is valid for Solutions H1, H2 and H3 (see Figures 4.10(d) and 4.10(e)) as compared to Solutions D1, D2 and D3 (see Figures 4.9(d)

and 4.9(e)). This is due to the fact that both monitoring duration and prediction duration are highly affected by the discount rate (compare results in Figure 4.9(e) with those in Figure 4.10(e)). Figures 4.11(a) and 4.11(b) show the solutions for Cases B1, B2 and B3, without and with discount rate, respectively. It is worth noting that the total monitoring costs associated with Cases B1, B2 and B3 are higher than those associated with Cases O1, O2 and O3, respectively.

4.5.3 Optimal Monitoring Plan for a Structural System

The approach to establish an optimal monitoring plan for a structural system is applied to an existing bridge the Northbound Bridge I-39. In this application, the monitored data from four strain gages (i.e., CH 17, CH 18, CH 19, and CH 20) installed on the top face of the bottom flange of each girder in the second span (see Figure 4.12) were used.

Assessment and prediction of structural performance

The monitored live load strains obtained from four strain gages (CH 17, CH 18, CH 19, and CH 20) are converted into stress data by using Hooke's law. In order to assess the structural performance under uncertainty, the probabilistic distribution type of the maximum live load stress should be determined. Based on this distribution, the reliability with respect to a predefined stress limit can be assessed. Distribution fitting is the procedure of selecting the most appropriate distribution

which fits to monitored data. Among several fitting tests (i.e., the Chi-square test, the Kolmogorov-Smirnov test, and the Anderson-Darling test), the Anderson-Darling test (1952), which assigns more weight to the tail of a specific distribution, was performed using MINITAB (2007). Figures 4.13 and 4.14 show the histograms and the best-fit PDFs of maximum stresses induced by 249 passages of the heavy vehicles on the left lane and 636 passages of the heavy vehicles on the right lane, respectively, during 95 days. The best-fit distributions of maximum stresses from CH 17, CH 18, and CH 19, which were induced by the heavy vehicles passing on the right lane, are Gumbel distributions (see Figures. 4.13(b), 4.13(c), and 4.13(d)). Lognormal distribution is the best-fit distribution for monitored maximum stresses from CH 20 of girder 1 under the right lane loading (see Figure 4.13(a)). The Gumbel distribution is defined as

$$f_X(x) = \rho_{max} \times exp\left[-\rho_{max}\left(x-\lambda_{max}\right)\right] \times exp\left[-exp\left[-\rho_{max}\left(x-\lambda_{max}\right)\right]\right] \tag{4.26}$$

where ρ_{max} = scale parameters; and λ_{max} = characteristic maximum values as indicated in Equation 4.4(a). The lognormal distribution is

$$f_X(x) = \frac{1}{\sigma_{\log} \cdot x\sqrt{2\pi}} \cdot \exp\left[-\frac{1}{2}\left(\frac{\ln x - \mu_{\log}}{\sigma_{\log}}\right)^2\right] \tag{4.27}$$

where μ_{log} = mean of ln(X); and σ_{log} = standard deviation of ln(X). Since the trigger level of CH 17 was set up to be 41.38 MPa (6.00 ksi), there is no maximum stress less than the trigger level, as shown in Figure 4.13(d). The best-fit distributions of monitored maximum stresses from CH 17, CH 18, CH 19, and CH 20 under the left

lane loading are shown in Figures. 4.14(a), 14(b), 14(c), and 14(d), respectively. There is no maximum stress from CH 20 less than 41.38 MPa (6.00 ksi) due to the trigger setup (see Figure 4.14(a)). The best-fit distributions and their associated parameters for the maximum monitored stresses from the four strain gages are summarized in Table 4.4.

The state function for component *i* defined in Equation (3.16) is used to assess and predict the structural performance and RIF. The necessary variables to define the state function of each girder are provided in Tables 4.4. The predefined stress limit $\sigma_{limit,i}$ is assumed to be normally distributed with the mean equal to the maximum stress measured from controlled loading tests, and the coefficient of variation (COV) equal to 0.04. The measurement errors factor C_e is assumed to be normally distributed with the mean value of 1.0 and the COV of 0.02. The deterministic variables in the state function (see Equation (3.16)) are the total number of heavy trucks N_{tt} = 893, total number of heavy trucks passing on right lane N_{rt} = 636, total number of heavy trucks passing on left lane N_{lt} = 249, and total number of heavy trucks passing side by side N_{ss} = 8. The coefficients of correlation among the variables are directly obtained from the monitored data as indicated in Table 4.5. Since the monitored maximum stresses under the left lane loading and the right lane loading are measured independently due to trigger-setup, the coefficients of correlation between monitored maximum stresses induced by heavy vehicles passing on different lanes are 0.0 (see Table 4.5). As the distance between strain gages is

shorter under the same loading condition, the coefficient of correlation has large values. For example, the coefficients of correlation between girders 1 and 2 under the right lane loading is 0.69, and the coefficient of correlation between girders 1 and 4 under the right lane loading is 0.20 (see Table 4.5). For assessment of the system reliability for the predefined stress limit σ_{limit}, series-parallel models are used as shown in Figures 4.15(a), 15(b), and 15(c). For System Model I in Figure 4.15(a) (i.e., the series system), the exceedance probability $P(\sigma_{max} > \sigma_{limit})$ represents the probability that monitored maximum stress of any component exceeds its predefined stress limit. The exceedance probabilities $P(\sigma_{max} > \sigma_{limit})$ for System Models II and III in Figures. 4.15(b) and 4.15(c) represent the probabilities that the predefined stress limits are exceeded by the monitored stresses in any two components, or any three components, respectively.

The exceedance probability can be predicted by using the time-dependent function in Equation (3.13). To predict the expected number of the heavy trucks in the next T years, N_T, based on the initial monitored data during 95 days, the annual number of the heavy vehicles is assumed to be 2,500 on the right lane, 1,000 on the left lane, and 30 side-by-side, respectively. Therefore, in the next T years, the total number of heavy trucks crossing the bridge on the right lane, left lane, and side-by side will be $2{,}500 \times T$, $1{,}000 \times T$, and $30 \times T$, respectively. Figures 4.16(a) and 16(b) show the time-dependent exceedance probabilities $P(\sigma_{max} > \sigma_{limit})$ for the four girders and for the System Models I, II, and III, respectively. It should be noted that the

exceedance probability serves as the reliability measure in this chapter.

Time-dependent normalized importance factor (*NRIF*)

Based on the prediction of the reliability for the predefined stress limit, NRIF can be computed using Equations (2.19) and (2.22). The predefined stress limit for each component σ_{limit} is treated as the independent variable in Equation (2.22), since the predefined limit from controlled tests has no relation to the monitored stresses. Figures 4.17(a), 17(b), and 17(c) show the time-dependent NRIF of each component for System Models I, II, and II, respectively, considering the coefficients of correlation among the variables from monitored data. For model I, the exceedance probability for the system depends mainly on the girder 3 as shown in Figure 4.16(a). Therefore, as expected, the NRIF of the girder 3 has the highest NRIF (see Figure 4.17(a)). However, since the variables associated with the specified component are partially correlated with the variables associated with other components (see Table 4.5), it may be difficult to obtain NRIF of each component directly from comparison between exceedance probabilities of the components and the systems in Figures 4.16(a) and 16(b). For instance, if the variables involved in computing the exceedance probability of girder 4 are independent of the variables associated with other components, the NRIF of girder 4 in a series system will be the smallest since the exceedance probability for girder 4 has the smallest value over time. However, in this case study considering correlations among variables, the NRIF of girder 4 is not

the smallest. This is because the variables associated with girder 4 have relatively high correlation with girder 3 (see Table 4.5) which has the highest NRIF among four girders. From these results, it is clear that the NRIFs of individual components are dependent on the system modeling and the correlations among variables. Thus, it is important to define a realistic system model and to obtain accurate coefficients of correlation.

Pareto optimum solutions

The bi-objective optimization problem consists of two conflicting objective as maximization the expected average availability in Equation (4.15) associated with Case O1 (see Table 4.1) and minimization of the total monitoring cost in Equation (4.16). The design variables are monitoring duration t_{md} and prediction duration t. The design variables t and t_{md} have to be in the interval 30 days and 700 days. It is assumed that monitoring cost is \$10,000 during 80 days. Through the GA process, 1,000 Pareto solutions are obtained as shown in Figure 4.18(a) without considering the discount rate of during the prescribed time period of 730 days (i.e., 2 years). The maximum number of generations used was 100. Table 4.6 provides optimal values of design variables, and optimal total monitoring costs for different values of expected average availability varying from 0.1 to 0.9 for the period of 730 days. The monitoring plan with the expected average availability of 0.2 (Solution A in Figures 4.18(a) and 18(b)) requires a monitoring cost of \$15,625 during 2 years. This

monitoring plan consists of the monitoring period of 125 days and the non-monitoring period of 605 days. For the expected average availability of 0.8 (Solution D in Figures 4.18(a) and 18(b)), the associated total monitoring cost is $62,375 during 2 years. In this case, the monitoring plan has monitoring periods of 499 days and non-monitoring periods of 231 days. According to the importance of the monitored structural member and/or the state of financial resources, the structural managers can select the appropriate monitoring plan among these Pareto solutions.

Effective monitoring plan for structural system

If the total monitoring cost for the system $C_{MON,system}$ = $30,000 is assigned for the first two years, the total monitoring cost $C_{MON,i}$ of each component can be obtained using Equation (4.17). For example, during the first two years, the mean of NRIF of girder 1, $E(NRIF_1)$, of Model II is 0.1871 (see Figure 4.17(b)), and the allocated monitoring cost for girder 1 $C_{MON,1}$ during the first two years becomes 0.187 × $30,000 = $5,610. Using this cost, the associated expected average availability, monitoring duration t_{md} and prediction duration t can be obtained from the Pareto optimal solution set for the prescribed time period of two years as shown in Figure 4.18(a), if the discount rate during this prescribed time is not considered. As a result, during the first two years, the expected average availability is 0.066, and t_{md} and t are 45 days and 685 days, respectively. If the total monitoring cost for the system $C_{MON,system}$ = $30,000 is assigned every two years, the monitoring plans for girder 1

can be obtained until the target time (i.e., 20 years) by using the aforementioned procedure. Figures 4.19(a), 19(b) and 19(c) show monitoring cost, expected average availability, and ratio of t_{md} to t of Model II, respectively. Figures 4.20(a), 20(b) and 20(c) show the monitoring costs, the expected average availability of monitoring data for prediction, and the ratio of t_{md} to t of the four girders in Model II, respectively, when $C_{MON,system}$ = \$60,000 is allocated uniformly every four years and the discount rate is not considered. The mean of NRIF of girder 1, $E(NRIF_1)$, of Model II during the first four years is 0.2208 (see Figure 4.17(b)), and $C_{MON,1}$ becomes 0.2208 × \$60,000 = \$13,250. Based on the Pareto optimal solution set in Figure 4.18(a), the associated monitoring plan of girder 1 during the first four years can be determined as t_{md} = 53 days and t = 677 days. The optimal monitoring plans of four girders are updated every four years as shown in Figures 4.21(a) to 21(e) during the target time of 20 years. The optimal monitoring plan of girder 2 is associated with t_{md} = 84 days and t = 646 days during the first four years (see Figure 4.21(a)) with monitoring cost of \$21,000 (see Figure 4.20(a)) and expected average availability of 0.129 (see Figure 4.20(b)). It should be noted that the NRIFs of individual components are highly dependent on the system modeling. Therefore, the system modeling has a significant effect on the monitoring planning of individual components.

4.5.4 Optimum Solutions from Decision Analysis

The expected monetary value (EMV) associated with various monitoring plans can be obtained by using Equation (4.23) with $C_{mon,o}$ = \$10,000 and $t_{md,o}$ = 80 days. Figures 4.22(a) and 22(b) show the relation between the EMV per day and the ratio r_{md} of the monitoring duration t_{md} to the prediction duration t. From these figures, it is clear that as the potential monitoring loss C_{loss} increases, the optimum monitoring plan requires a larger ratio of monitoring duration to prediction duration. Therefore, structures with very high potential loss need long-term monitoring. In this case, the continuous monitoring program is the optimal plan. If structures have a moderate potential loss (e.g., C_{loss} = \$100/day, see Figure 4.22(b)), the optimal monitoring plan will correspond to the ratio of monitoring duration to prediction duration with the maximum EMV (or minimum monetary loss). For example, \$100/day of the potential loss value yields the optimum design value of r_{md} = 0.63 and the maximum EMV (or minimum monetary loss) = -\$98.2/day as shown in Figure 4.22(b).

4.6 Conclusions

The main objective of SHM is to provide reliable information to structure managers in order to implement cost-effective lifetime maintenance planning. To obtain the maximum benefit from SHM, an optimal monitoring plan is needed by balancing the availability of monitoring and monitoring cost over the service of structures. In this

chapter, this optimization under uncertainty has been formulated as a bi-objective problem: maximization of the availability of monitoring data for structural performance prediction and minimization of the cumulative monitoring cost. Based on this formulation and reliability importance assessment of structural components, the approach for determination of optimal monitoring planning of structural systems was extended. Additionally, as an alternative approach, decision analysis theory has been used based on the minimum monetary loss criterion. The following conclusions can be drawn:

1. The optimum monitoring plan is affected by the discount rate of money and the criterion for using monitoring data for prediction. A higher discount rate of money leads to an optimal monitoring plan with shorter monitoring duration and shorter time intervals between monitorings. The criterion for using monitoring data for prediction is dependent on the number of exceedances allowed for the largest positive and/or negative residual in a prescribed time interval.
2. In order to apply the proposed approach, structural managers have to assign the threshold for the expected average availability of monitoring data according to the importance and state of structural deterioration. In the proposed approach, total monitoring cost for the structural system is allocated to individual components according to the NRIF. These allocated monitoring costs of individual components are used in Pareto optimization to find the monitoring schedules. The NRIF of an individual component can be assessed and predicted

based on SHM data. However, the NRIF is sensitive to the system modeling (e.g., series, parallel, type of series-parallel), and to the correlation among the variables involved in the state functions of a structural system. Therefore, the system should be modeled appropriately, and the correlation structure should be considered based on monitoring data or expert opinion.

3. In order to predict the structural performance, the time-dependent function considering load effects was used. This function is mainly dependent on the initial monitoring data. Therefore, the initial monitoring data should be reliable. Moreover, since the time-dependent function considers only the live load effect, the prediction may be effective only for short time periods.
4. The optimum monitoring planning resulting from the proposed approach may be used as an initial monitoring strategy. This planning has to be updated considering new information obtained after each monitoring. Further research is necessary to develop the updating procedure after each monitoring.
5. As an illustrative example, the proposed approach was applied to an existing bridge. However, it can also be applied to any monitored structure by formulating appropriate time-dependent state functions and developing a representative system model.
6. The potential loss from unavailability of the monitoring for prediction has a significant effect on EMV.

Table 4.1 Exceedance probability P_{exd} with various number of exceedances

Number of exceedances	Case	Exceedance probability P_{exd}
At least one exceedance considering the largest value	O1	$1-exp\left(-\frac{t}{t_{md}}\right)$
At least two exceedances considering the largest value	O2	$1-\frac{(t+t_{md})}{t_{md}}\cdot exp\left(-\frac{t}{t_{md}}\right)$
At least three exceedances considering the largest value	O3	$1-\left[1+\frac{t}{t_{md}}+\frac{1}{2}\left(\frac{t}{t_{md}}\right)^2\right]\cdot exp\left(-\frac{t}{t_{md}}\right)$
At least one exceedance considering both the largest and the smallest values	B1	$1-exp\left(-\frac{2t}{t_{md}}\right)$
At least two exceedances considering both the largest and the smallest values	B2	$1-\left(\frac{t+t_{md}}{t_{md}}\right)^2\cdot exp\left(-\frac{2t}{t_{md}}\right)$
At least three exceedances considering both the largest and the smallest values	B3	$exp\left(-\frac{2t}{t_{md}}\right)\cdot\left[\frac{t^4}{4t_{md}^4}+\frac{t^3}{t_{md}^3}+\frac{2t^2}{t_{md}^2}+\frac{2t}{t_{md}}+\left(exp\left(\frac{2t}{t_{md}}\right)-1\right)\right]$

Table 4.2 Objective and design variable values associated with various cases as indicated in Table 4.1: discount rate of money = 0%/day

Case	Objectives		Design variables	
	$E(\bar{A})$	C_{MON} (\$)	t (days)	t_{md} (days)
O1	0.2	151,875	2,035	405
	0.4	283,125	1,680	755
	0.6	431,250	1,285	1,150
	0.8	624,375	770	1,665
O2	0.2	82,500	2,215	220
	0.4	155,625	2,020	415
	0.6	236,250	1,805	630
	0.8	354,375	1,490	945
O3	0.2	58,125	2,285	155
	0.4	108,750	2,155	290
	0.6	163,125	2,000	435
	0.8	240,000	1,795	640
B1	0.2	264,375	1,735	705
	0.4	431,250	1,285	1,150
	0.6	583,125	880	1,555
	0.8	740,625	460	1,975
B2	0.2	125,625	2,100	335
	0.4	223,125	1,840	595
	0.6	320,625	1,580	855
	0.8	448,125	1,240	1,195
B3	0.2	80,625	2,220	215
	0.4	148,125	2,040	395
	0.6	215,625	1,860	575
	0.8	301,875	1,630	805

Table 4.3 Objective and design variable values associated with various cases as indicated in Table 4.1: discount rate of money = 0.016 %/day

Case	Objectives		Design variables	
	$E(\overline{A})$	C_{MON} (\$)	t (days)	t_{md} (days)
O1	0.2	93,813	320	65
	0.4	170,044	145	65
	0.6	256,969	90	80
	0.8	376,889	60	130
O2	0.2	52,553	500	50
	0.4	93,912	245	50
	0.6	143,645	170	60
	0.8	213,591	110	70
O3	0.2	37,422	890	60
	0.4	67,049	405	55
	0.6	98,874	255	55
	0.8	146,158	180	65
B1	0.2	159,743	160	65
	0.4	258,588	130	115
	0.6	350,900	65	115
	0.8	449,895	50	215
B2	0.2	77,387	375	60
	0.4	135,823	230	75
	0.6	194,741	185	100
	0.8	271,646	155	150
B3	0.2	49,985	515	50
	0.4	90,547	310	60
	0.6	130,143	195	60
	0.8	181,097	205	100

Table 4.4 Random variables for the state functions associated with CH17, CH18, CH19, and CH20

	Description	Random Variable	Type of distribution	Parameters for distribution	
	Measurement error factor	C_e	Normal distribution	$\mu = 1.0$	$\sigma = 0.02$
CH 20 (girder 1)	Predefined limit stress	$\sigma_{limit,1}$ (MPa)	Normal distribution	$\mu = 42.03$	$\sigma = 1.68$
	Monitored stress from right lane loading	$\sigma_{mon,1,r}$ (MPa)	Lognormal distribution	$\mu_{log} = 2.66$	$\sigma_{log} = 0.45$
	Monitored stress from left lane loading	$\sigma_{mon,1,l}$ (MPa)	Gumbel distribution	$\rho_{max} = 0.47$	$\lambda_{max} = 44.52$
	Monitored stress from side-by-side	$\sigma_{mon,1,ss}$ (MPa)	Gumbel distribution	$\rho_{max} = 0.12$	$\lambda_{max} = 40.05$
CH 19 (girder 2)	Predefined limit stress	$\sigma_{limit,2}$ (MPa)	Normal distribution	$\mu = 40.65$	$\sigma = 1.63$
	Monitored stress from right lane loading	$\sigma_{mon,2,r}$ (MPa)	Gumbel distribution	$\rho_{max} = 0.30$	$\lambda_{max} = 22.03$
	Monitored stress from left lane loading	$\sigma_{mon,2,l}$ (MPa)	Gumbel distribution	$\rho_{max} = 0.25$	$\lambda_{max} = 30.05$
	Monitored stress from side-by-side	$\sigma_{mon,2,ss}$ (MPa)	Gumbel distribution	$\rho_{max} = 0.14$	$\lambda_{max} = 31.48$
CH 18 (girder 3)	Predefined limit stress	$\sigma_{limit,3}$ (MPa)	Normal distribution	$\mu = 37.90$	$\sigma = 1.52$
	Monitored stress from right lane loading	$\sigma_{mon,3,r}$ (MPa)	Gumbel distribution	$\rho_{max} = 0.34$	$\lambda_{max} = 28.08$
	Monitored stress from left lane loading	$\sigma_{mon,3,l}$ (MPa)	Gumbel distribution	$\rho_{max} = 0.26$	$\lambda_{max} = 21.53$
	Monitored stress from side-by-side	$\sigma_{mon,3,ss}$ (MPa)	Gumbel distribution	$\rho_{max} = 0.20$	$\lambda_{max} = 33.83$
CH 17 (girder 4)	Predefined limit stress	$\sigma_{limit,4}$ (MPa)	Normal distribution	$\mu = 61.32$	$\sigma = 2.45$
	Monitored stress from right lane loading	$\sigma_{mon,4,r}$ (MPa)	Gumbel distribution	$\rho_{max} = 0.40$	$\lambda_{max} = 46.09$
	Monitored stress from left lane loading	$\sigma_{mon,4,l}$ (MPa)	Lognormal distribution	$\mu_{log} = 2.81$	$\sigma_{log} = 0.68$
	Monitored stress from side-by-side	$\sigma_{mon,4,ss}$ (MPa)	Gumbel distribution	$\rho_{max} = 0.21$	$\lambda_{max} =$ 40.07

Table 4.5 Coefficients of correlation among the monitored data

Girder (Channel)		1 (CH20)			2 (CH19)			3 (CH18)			4 (CH17)		
	Traffic	Right lane	Left lane	Side by side	Right lane	Left lane	Side by side	Right lane	Left lane	Side by side	Right lane	Left lane	Side by side
1	Right lane	1.00	0.00	0.00	0.69	0.00	0.00	0.56	0.00	0.00	0.20	0.00	0.00
	Left lane	0.00	1.00	0.00	0.00	0.54	0.00	0.00	0.37	0.00	0.00	0.11	0.00
	Side by side	0.00	0.00	1.00	0.00	0.00	0.69	0.00	0.00	0.47	0.00	0.00	0.01
2	Right lane	0.69	0.00	0.00	1.00	0.00	0.00	0.80	0.00	0.00	0.60	0.00	0.00
	Left lane	0.00	0.54	0.00	0.00	1.00	0.00	0.00	0.67	0.00	0.00	0.51	0.00
	Side by side	0.00	0.00	0.69	0.00	0.00	1.00	0.00	0.00	0.46	0.00	0.00	0.39
3	Right lane	0.56	0.00	0.00	0.80	0.00	0.00	1.00	0.00	0.00	0.61	0.00	0.00
	Left lane	0.00	0.37	0.00	0.00	0.67	0.00	0.00	1.00	0.00	0.00	0.74	0.00
	Side by side	0.00	0.00	0.47	0.00	0.00	0.46	0.00	0.00	1.00	0.00	0.00	0.67
4	Right lane	0.20	0.00	0.00	0.60	0.00	0.00	0.61	0.00	0.00	1.00	0.00	0.00
	Left lane	0.00	0.11	0.00	0.00	0.51	0.00	0.00	0.74	0.00	0.00	1.00	0.00
	Side by side	0.00	0.00	0.01	0.00	0.00	0.39	0.00	0.00	0.67	0.00	0.00	1.00

Table 4.6 Pareto optimal solutions for prescribed time period of two years without discount rate

Expected average availability E(Ā)	Monitoring duration t_{md} (days)	Prediction duration t (days)	Total monitoring cost C_{MON} ($)
0.1	66	664	8,250
0.2	125	605	15,625
0.3	173	557	21,625
0.4	226	504	28,250
0.5	281	449	35,125
0.6	344	386	43,000
0.7	415	315	51,875
0.8	499	231	62,375
0.9	601	129	72,125

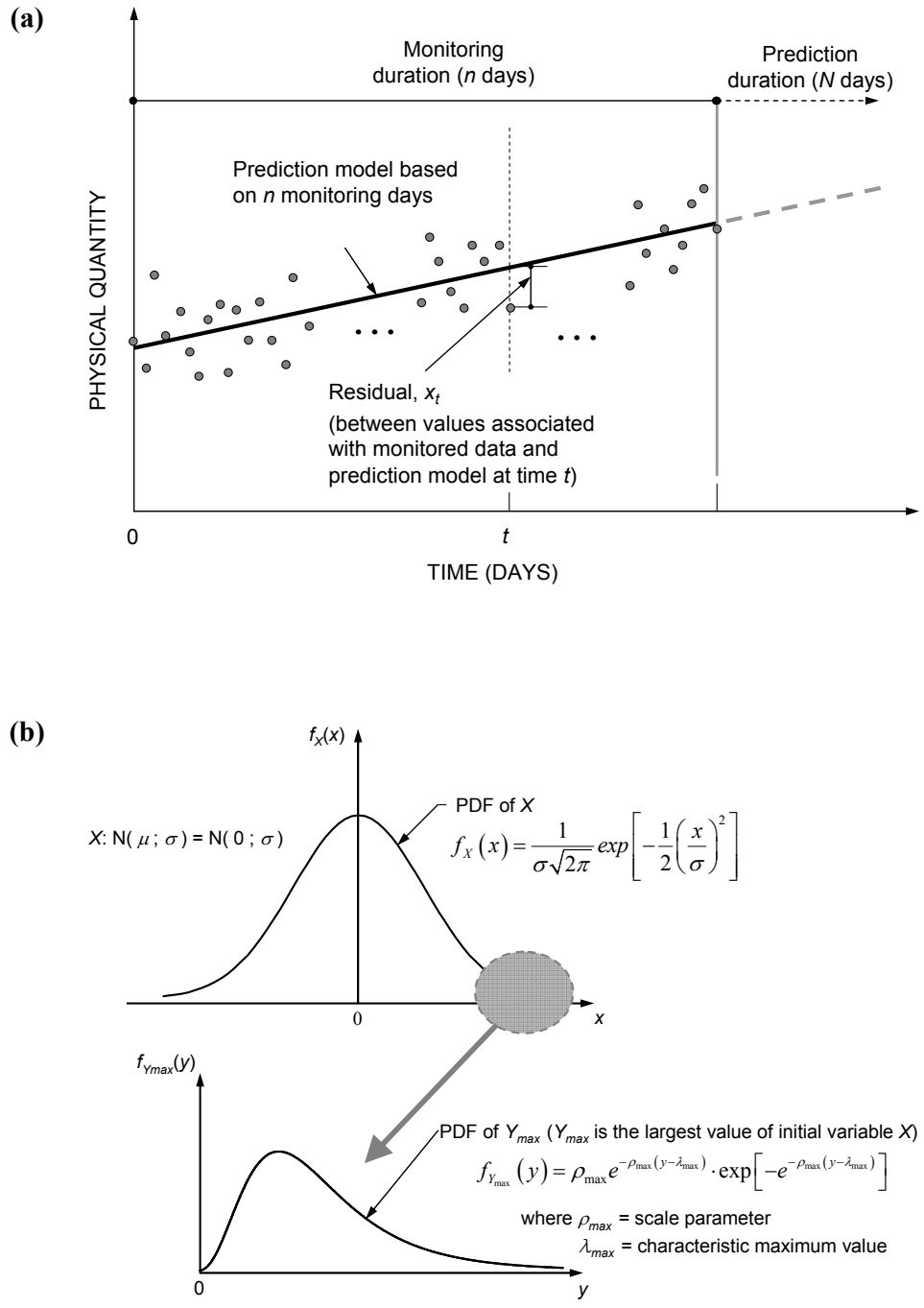

Figure 4.1 (a) Residuals between values from prediction model and monitoring data; and **(b)** the PDF of the residuals, X, and the PDF of the maximum residual, Y_{max}

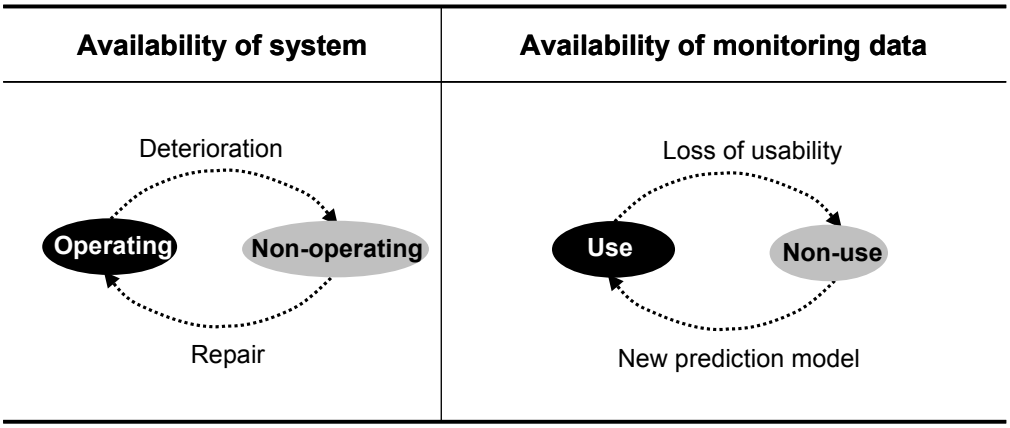

Figure 4.2 Comparison between availability of system and availability of monitoring data

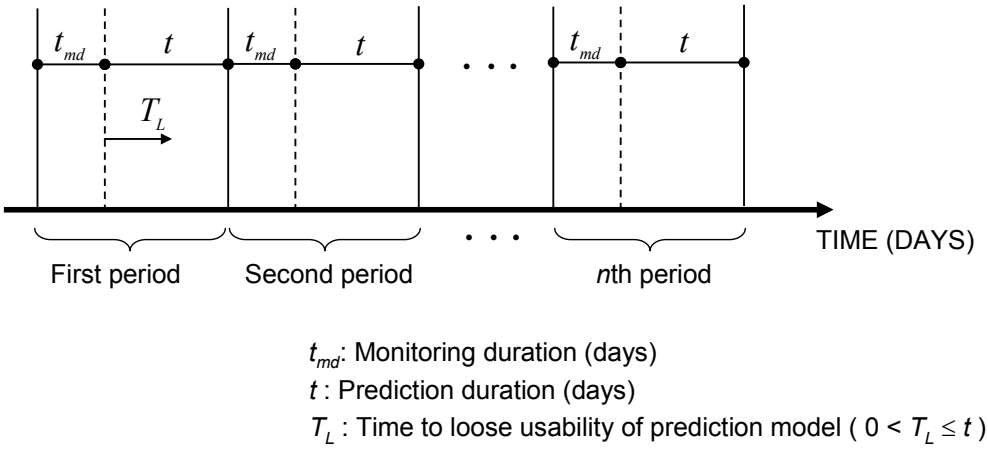

t_{md}: Monitoring duration (days)
t : Prediction duration (days)
T_L : Time to loose usability of prediction model ($0 < T_L \leq t$)

Figure 4.3 Timeline of monitoring and prediction at regular time intervals

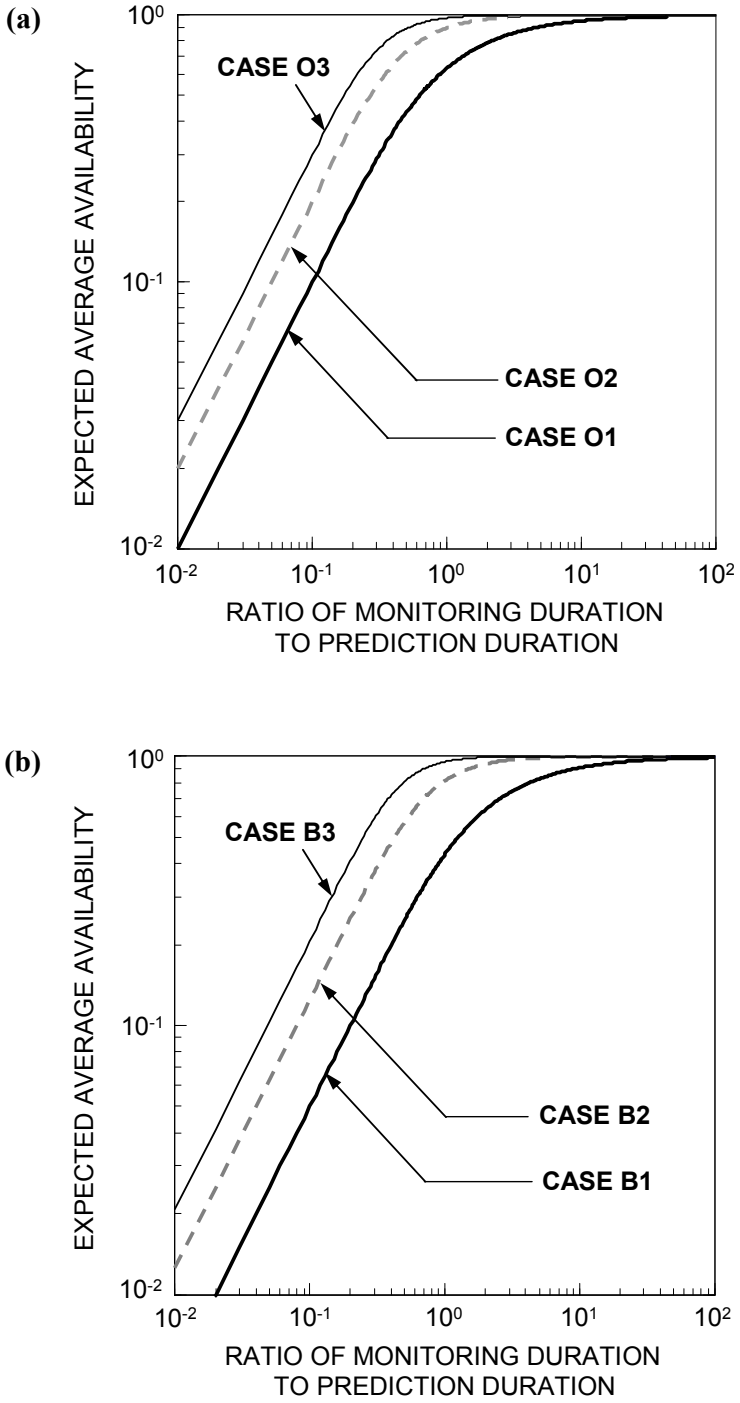

Figure 4.4 The relation between the ratio of monitoring duration to prediction duration and the expected average availability of monitoring data; **(a)** Cases O1, O2 and O3; and **(b)** Cases B1, B2 and B3

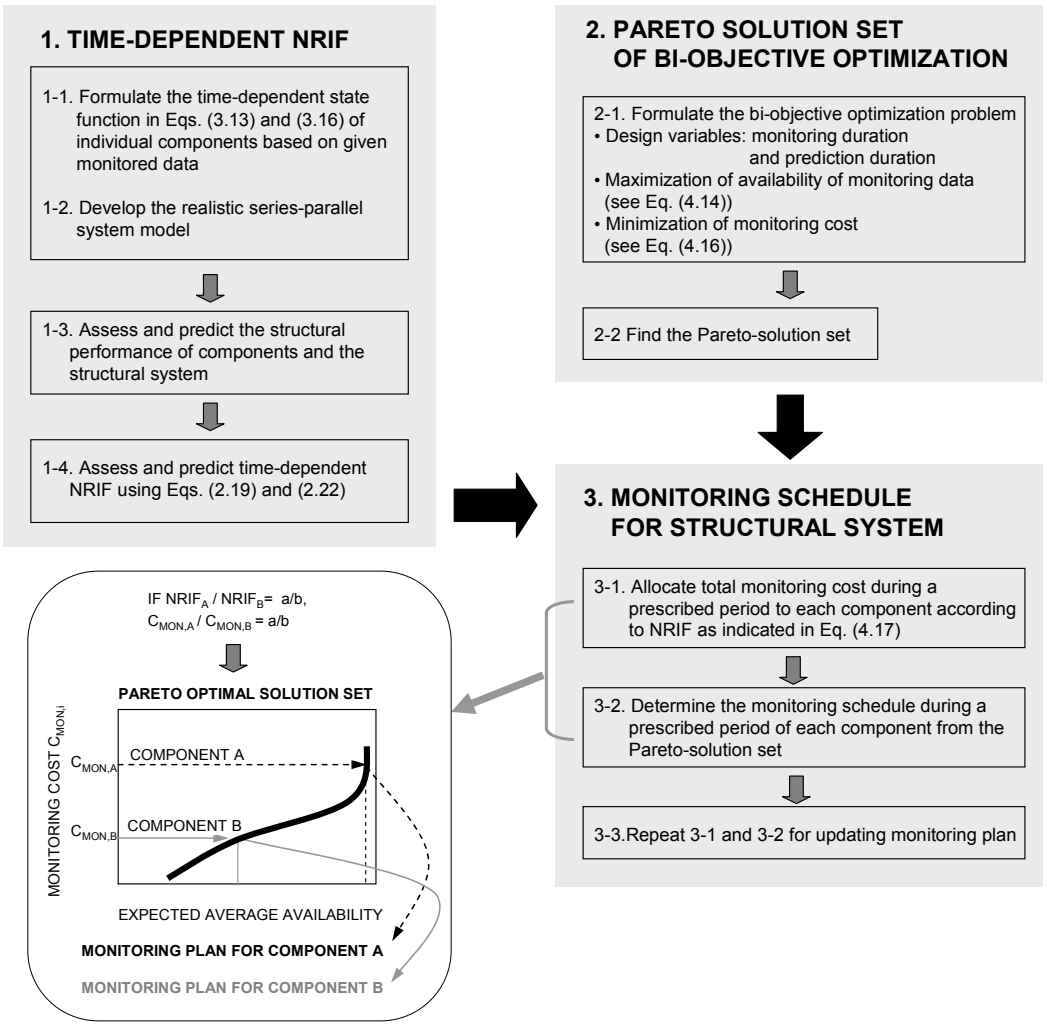

Figure 4.5 Schematic representation for establishing effective monitoring planning of a structural system.

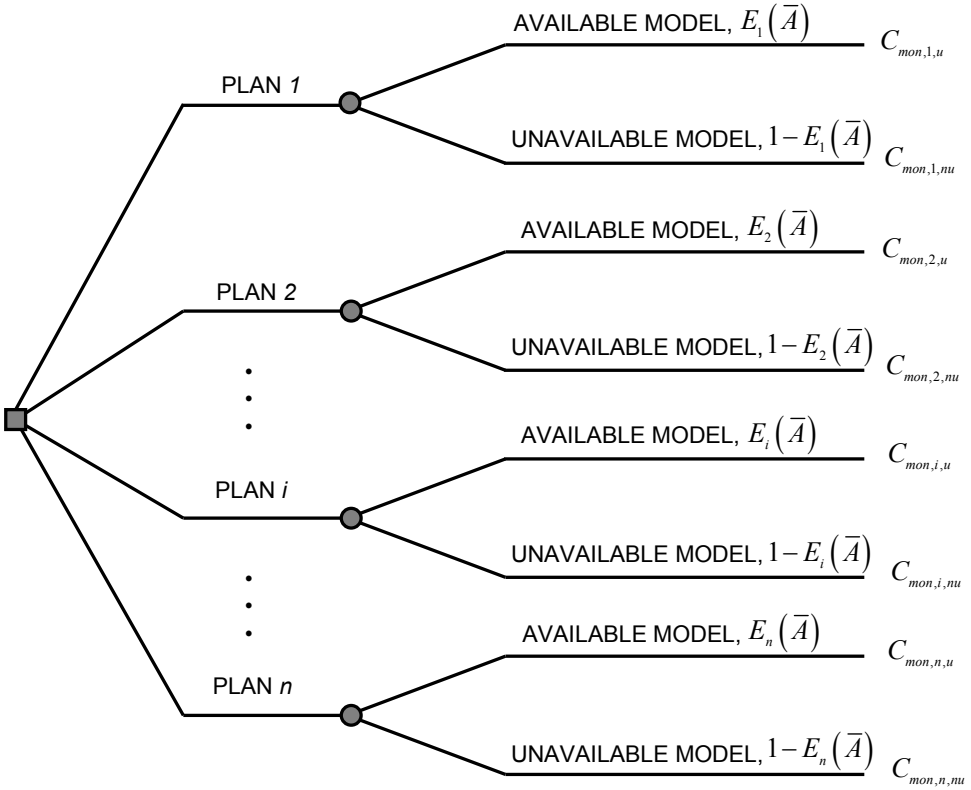

Figure 4.6 Decision tree for monitoring plan

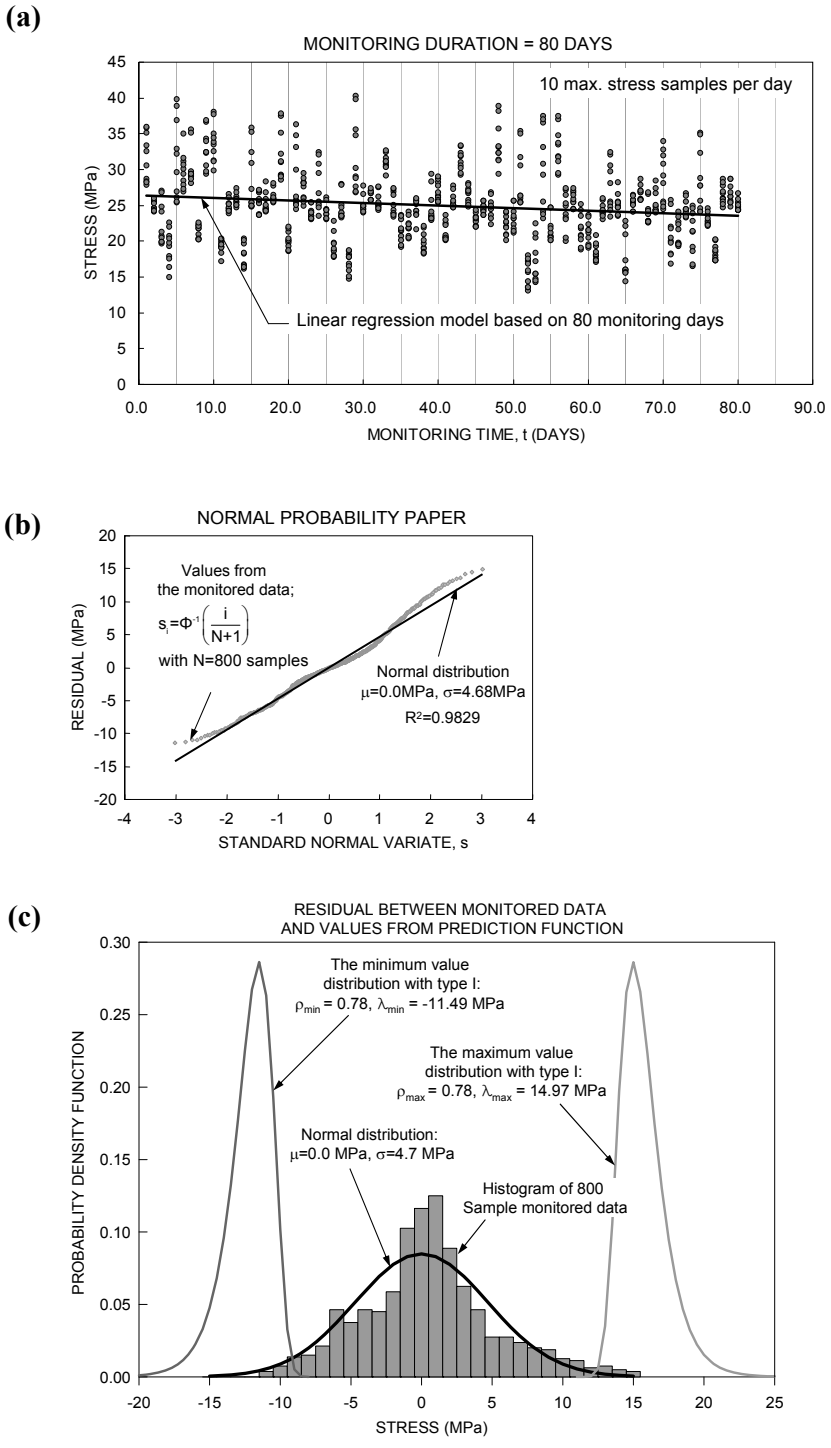

Figure 4.7 (a) Linear regression model based using 800 monitored data from the sensor CH 4; **(b)** normal probability paper for the residuals; and **(c)** PDF of the residuals and its extremal asymptotic distributions

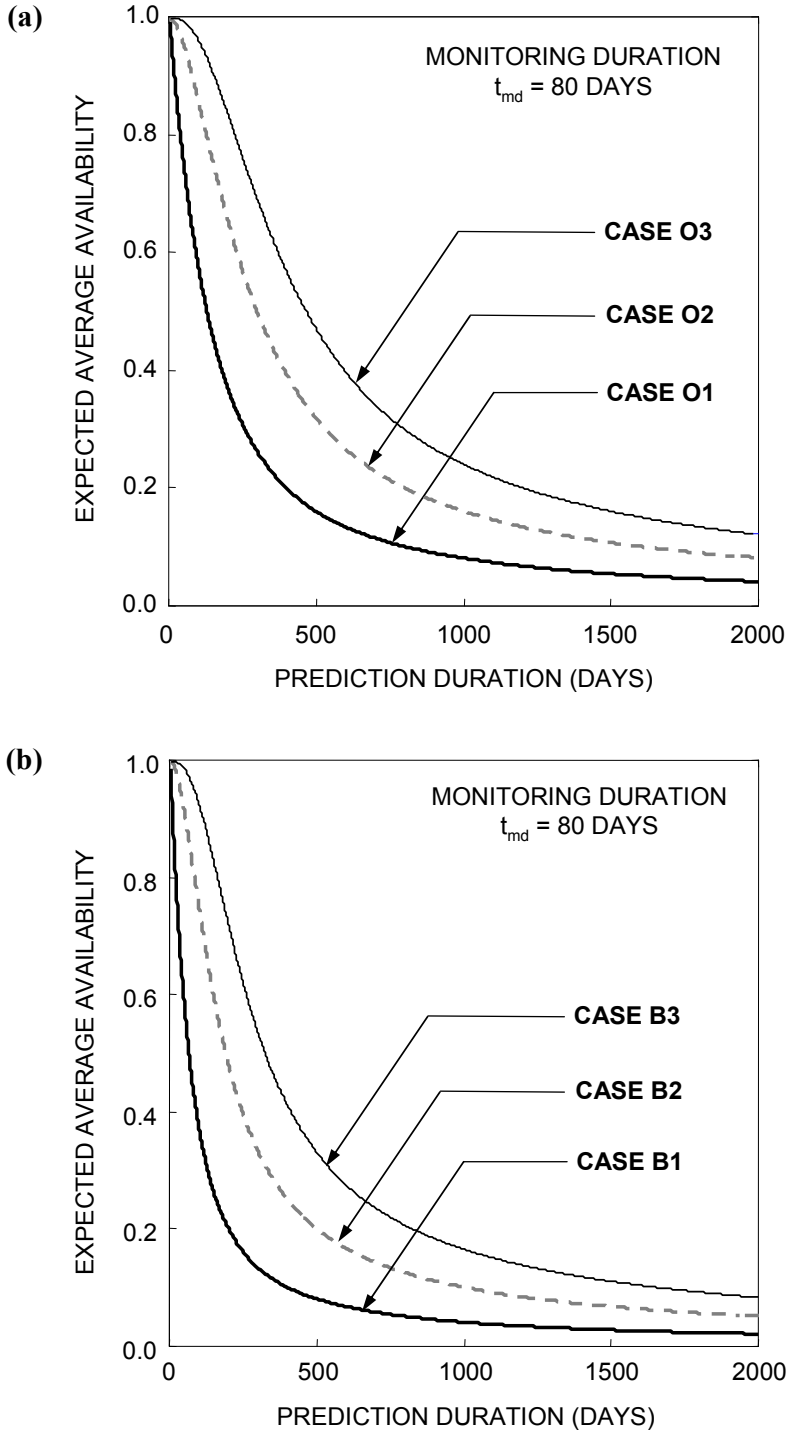

Figure 4.8 Prediction duration versus expected average availability of monitoring data for 80 monitoring days: **(a)** Cases O1, O2, and O3; and **(b)** Cases B1, B2, and B3

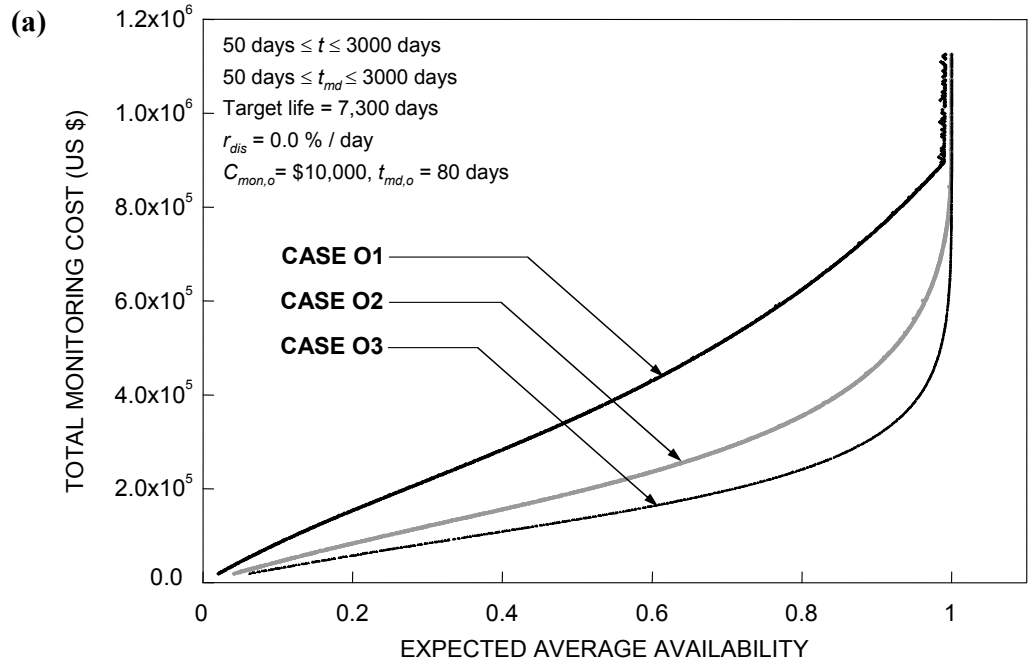

Figure 4.9 (a) Pareto solution sets of the bi-objective problem without discount rate for Cases O1, O2 and O3; **(b)** design space with Solutions A1, B1, C1 and D1; **(c)** monitoring plans of Solutions A1, B1, C1 and D1; **(d)** design space with Solutions D1, D2 and D3; and **(e)** monitoring plans for Solutions D1, D2 and D3

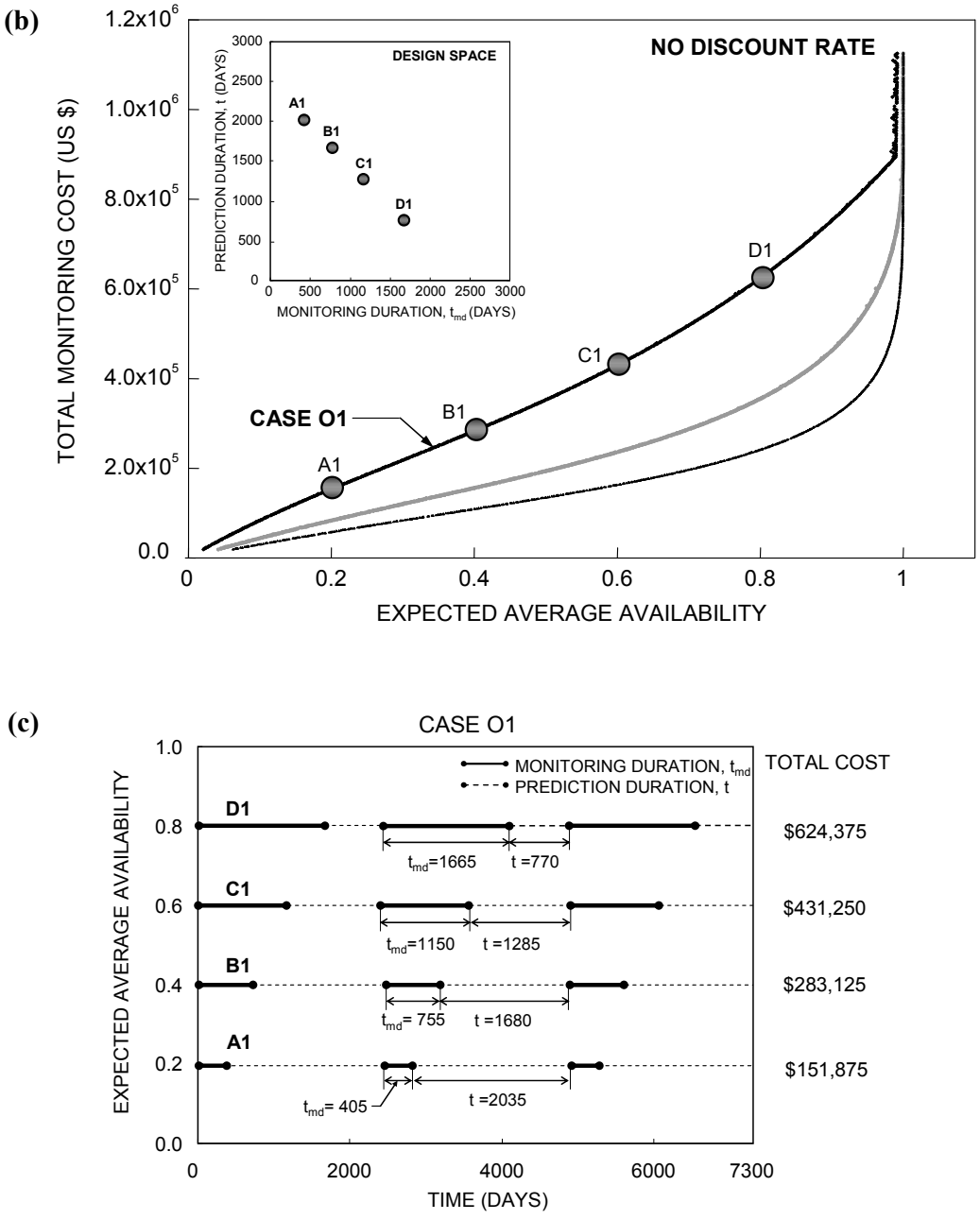

Figure 4.9 Pareto solution sets of the bi-objective problem without discount rate for Cases O1, O2 and O3; **(b)** design space with Solutions A1, B1, C1 and D1; **(c)** monitoring plans of Solutions A1, B1, C1 and D1; **(d)** design space with Solutions D1, D2 and D3; and **(e)** monitoring plans for Solutions D1, D2 and D3 (continued)

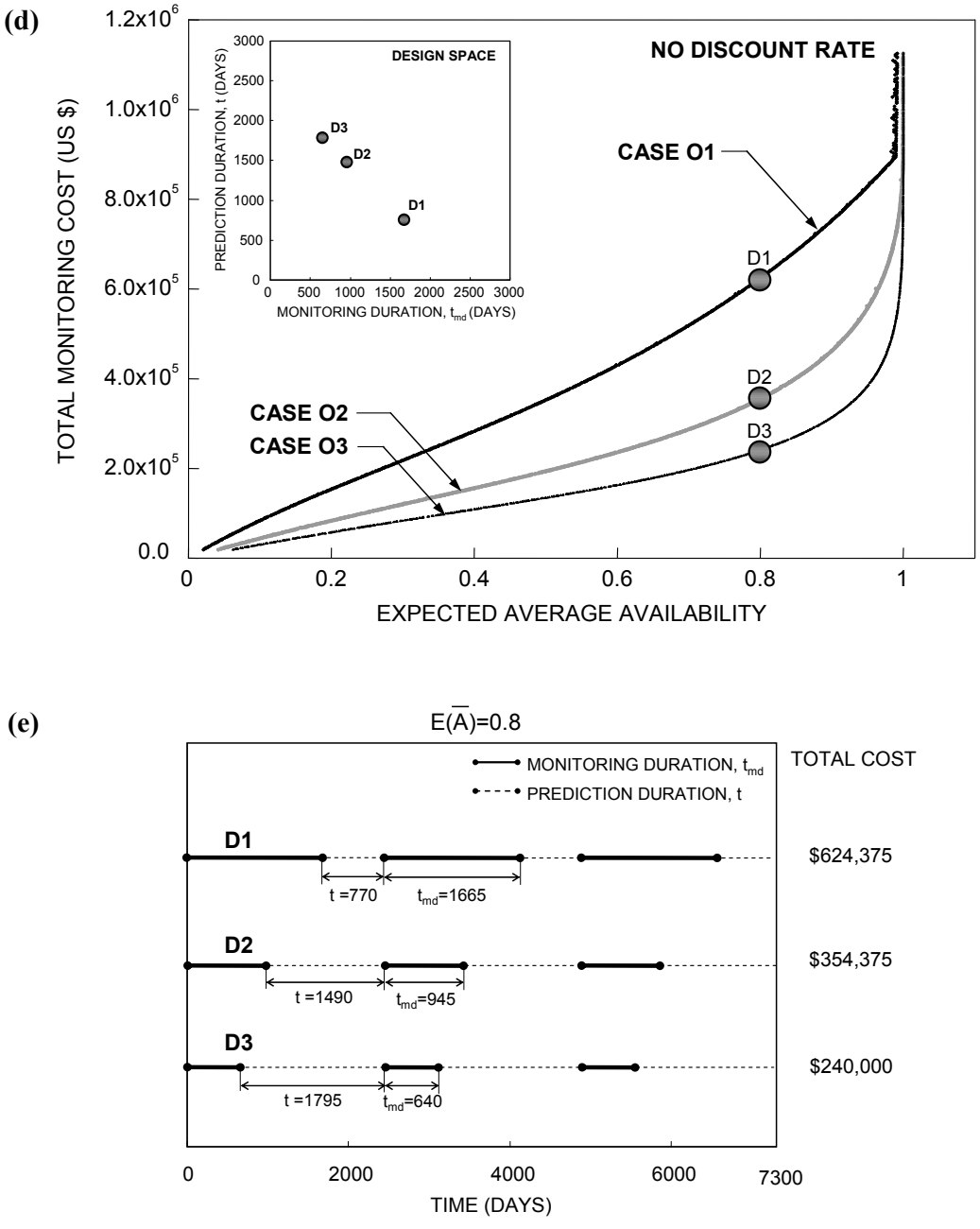

Figure 4.9 Pareto solution sets of the bi-objective problem without discount rate for Cases O1, O2 and O3; **(b)** design space with Solutions A1, B1, C1 and D1; **(c)** monitoring plans of Solutions A1, B1, C1 and D1; **(d)** design space with Solutions D1, D2 and D3; and **(e)** monitoring plans for Solutions D1, D2 and D3 (continued)

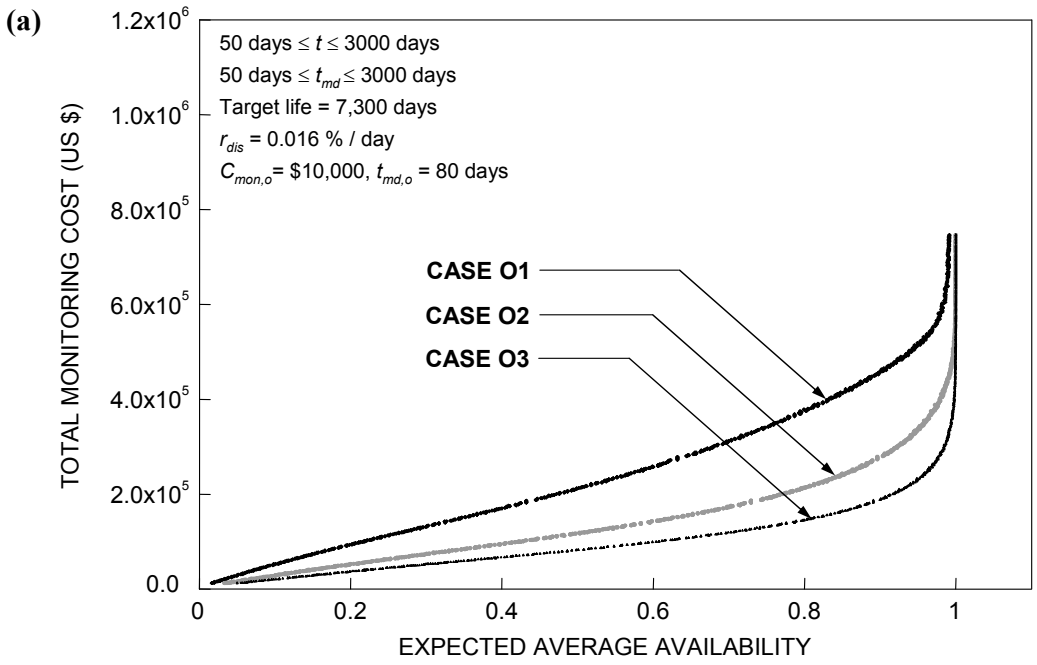

Figure 4.10 (a) Pareto solution sets of the bi-objective problem with discount rate r_{dis} = 0.016%/day for Cases O1, O2 and O3; **(b)** design space with Solutions E1, F1, G1 and H1; **(c)** monitoring plans for Solutions E1, F1, G1 and H1; **(d)** design space with Solutions H1, H2 and H3; and **(e)** monitoring plans for Solutions H1, H2 and H3

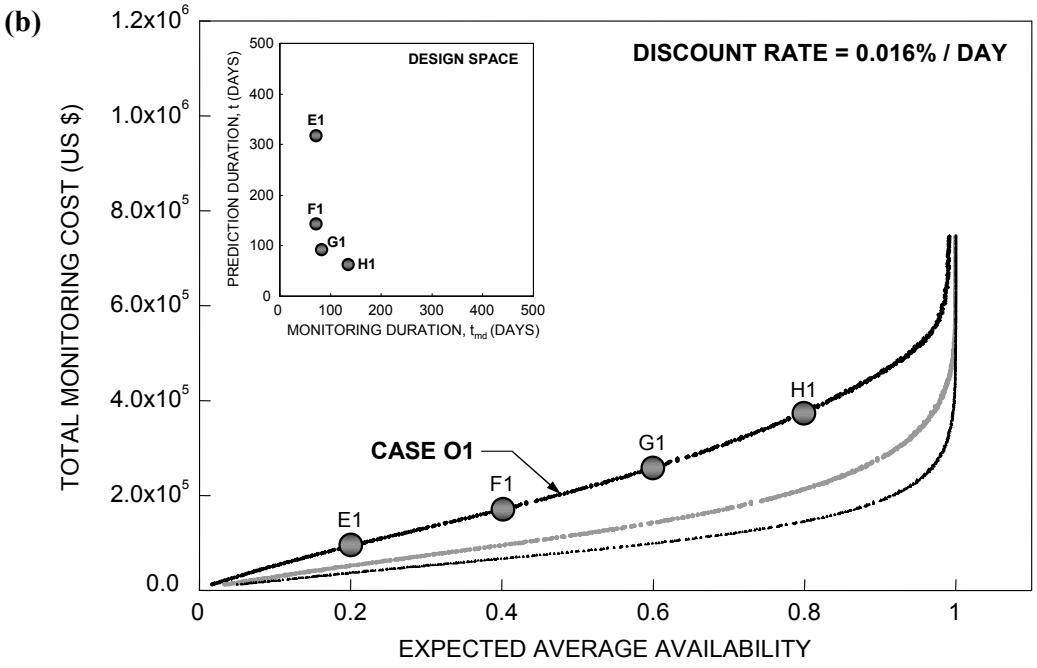

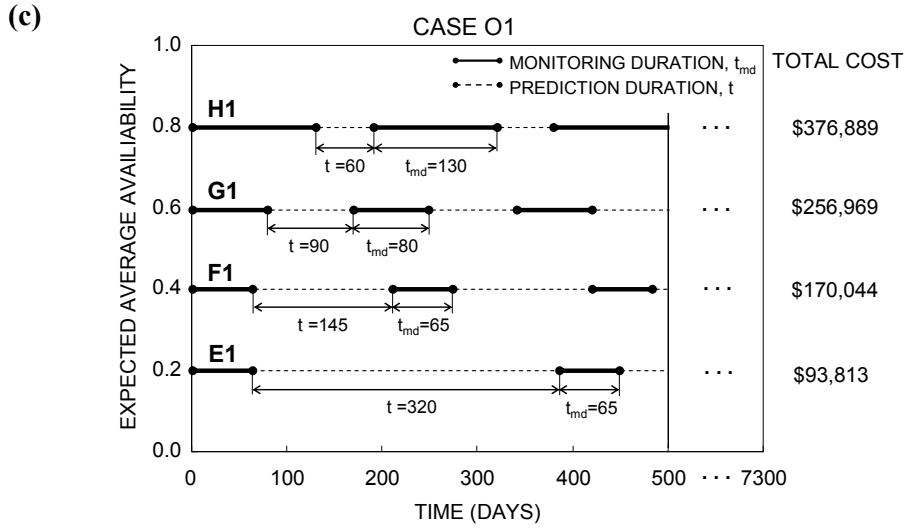

Figure 4.10 (a) Pareto solution sets of the bi-objective problem with discount rate r_{dis} = 0.016%/day for Cases O1, O2 and O3; **(b)** design space with Solutions E1, F1, G1 and H1; **(c)** monitoring plans for Solutions E1, F1, G1 and H1; **(d)** design space with Solutions H1, H2 and H3; and **(e)** monitoring plans for Solutions H1, H2 and H3 (continued)

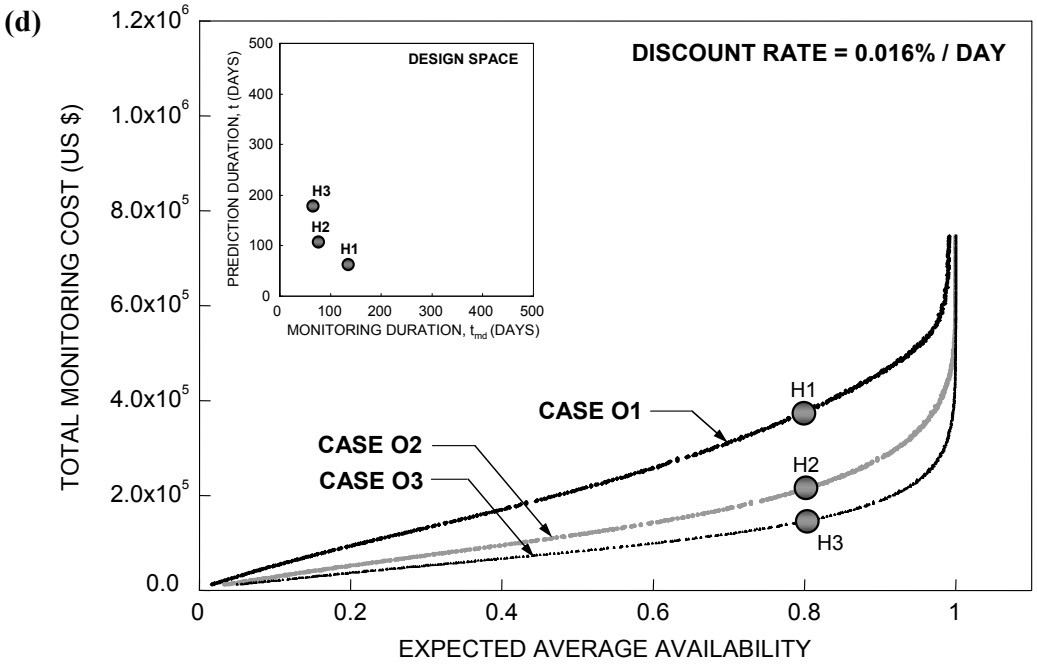

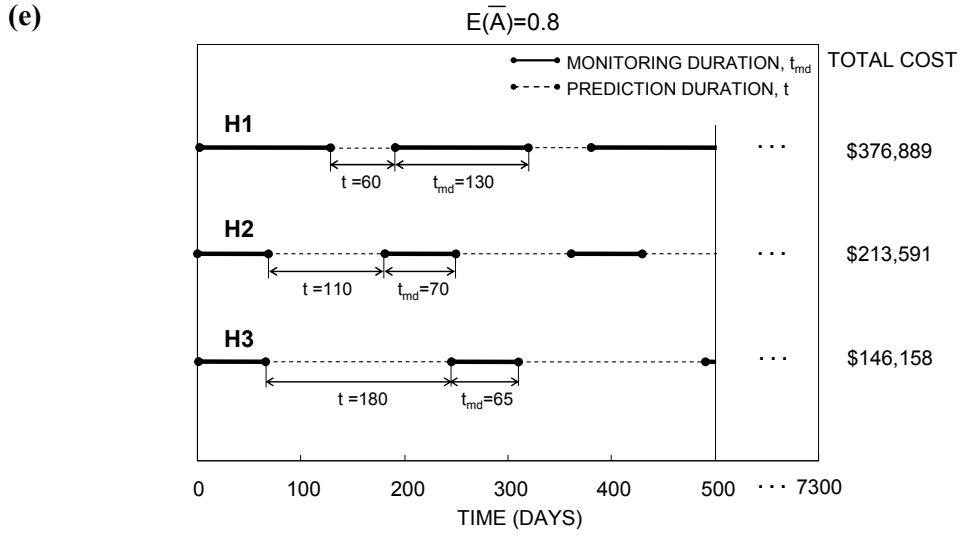

Figure 4.10 (a) Pareto solution sets of the bi-objective problem with discount rate r_{dis} = 0.016%/day for Cases O1, O2 and O3; **(b)** design space with Solutions E1, F1, G1 and H1; **(c)** monitoring plans for Solutions E1, F1, G1 and H1; **(d)** design space with Solutions H1, H2 and H3; and **(e)** monitoring plans for Solutions H1, H2 and H3 (continued)

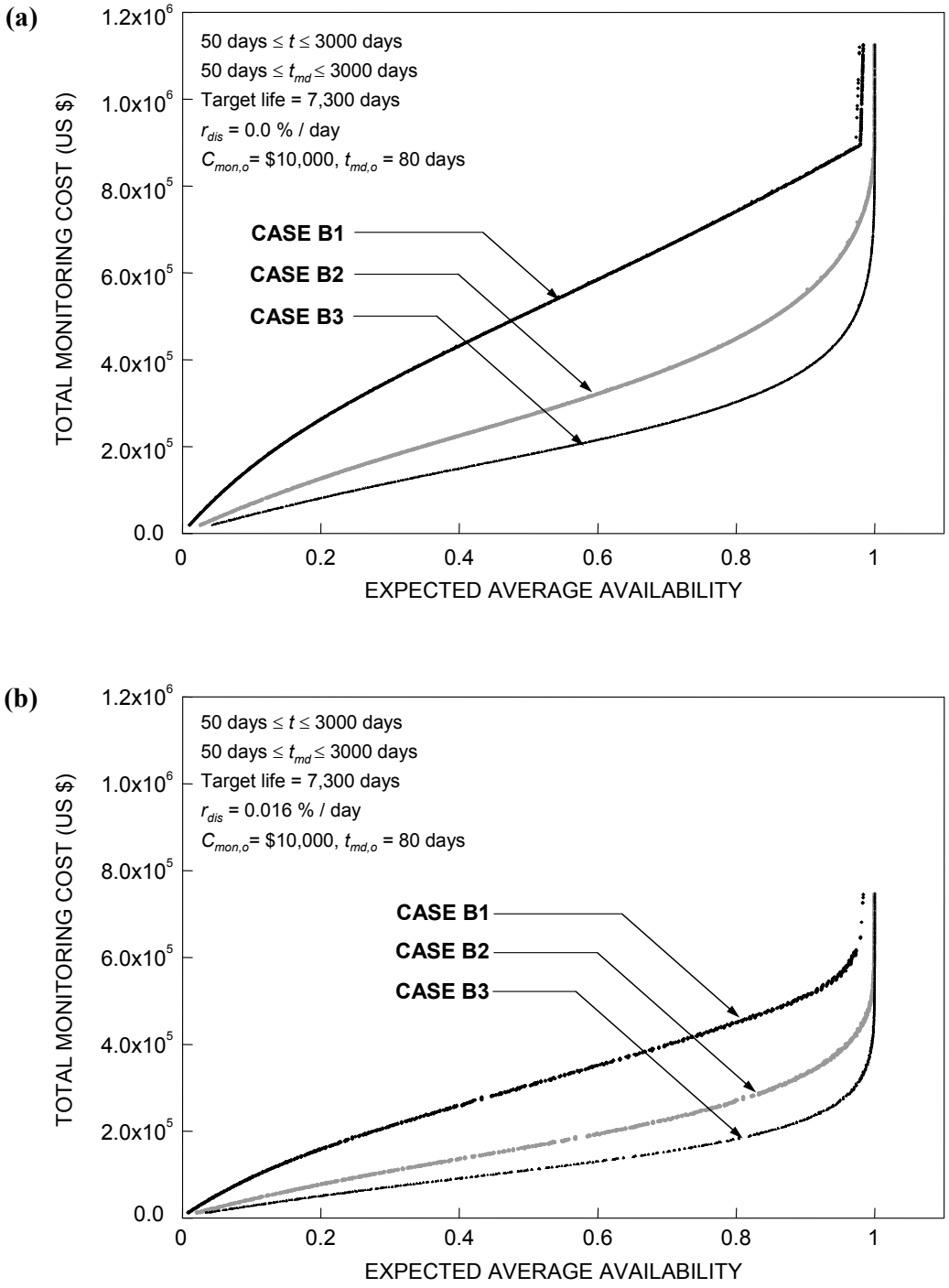

Figure 4.11 Pareto solution sets of multi-objective problem for Case B1, B2 and B3; **(a)** without discount rate of money; and **(b)** with discount rate of money r_{dis} = 0.016% / day

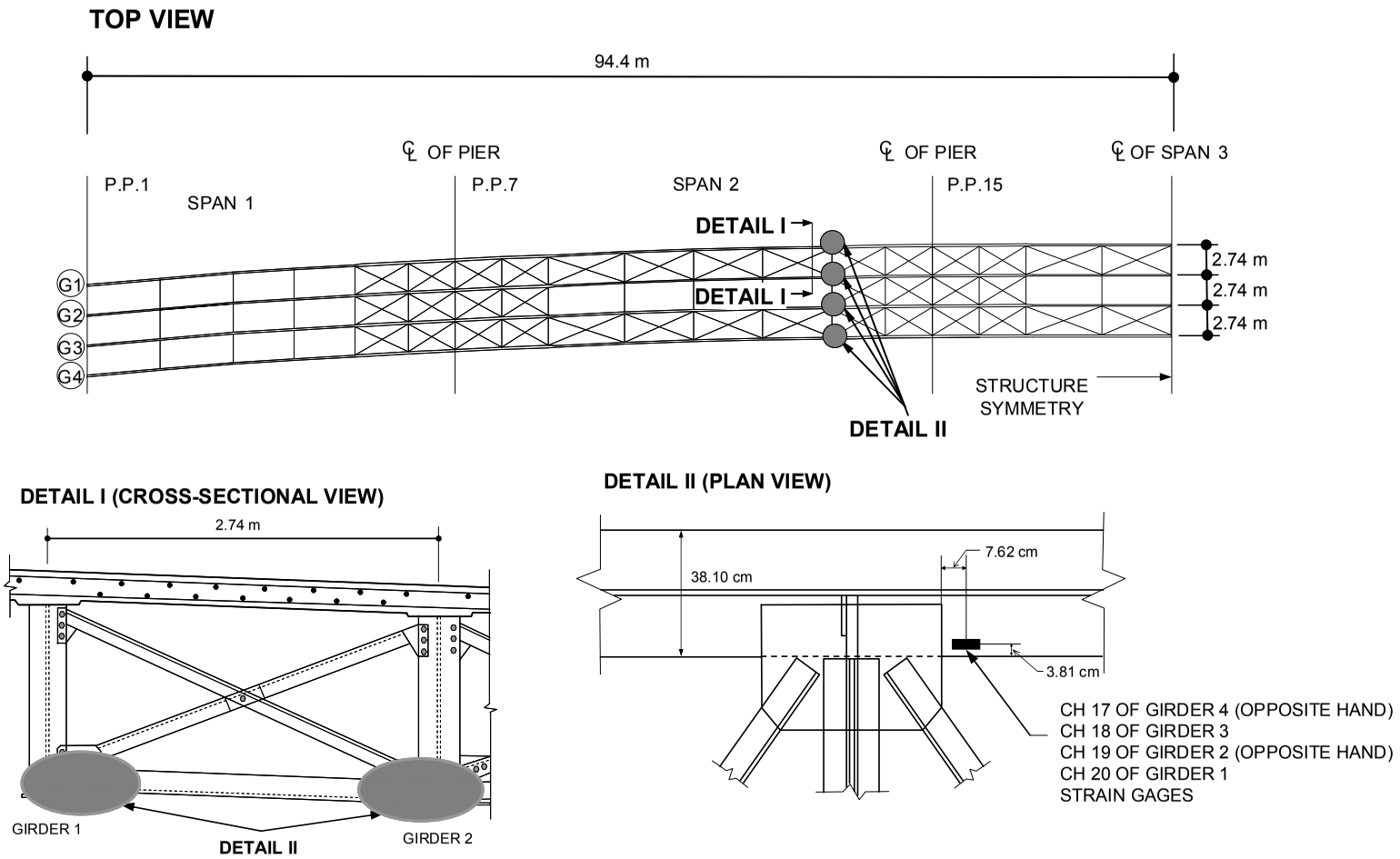

Figure 4.12 I-39 North Bound Bridge: Instrumentation plan of CH17, CH18, CH19 and CH20 (adapted from Mahmoud et al. (2005))

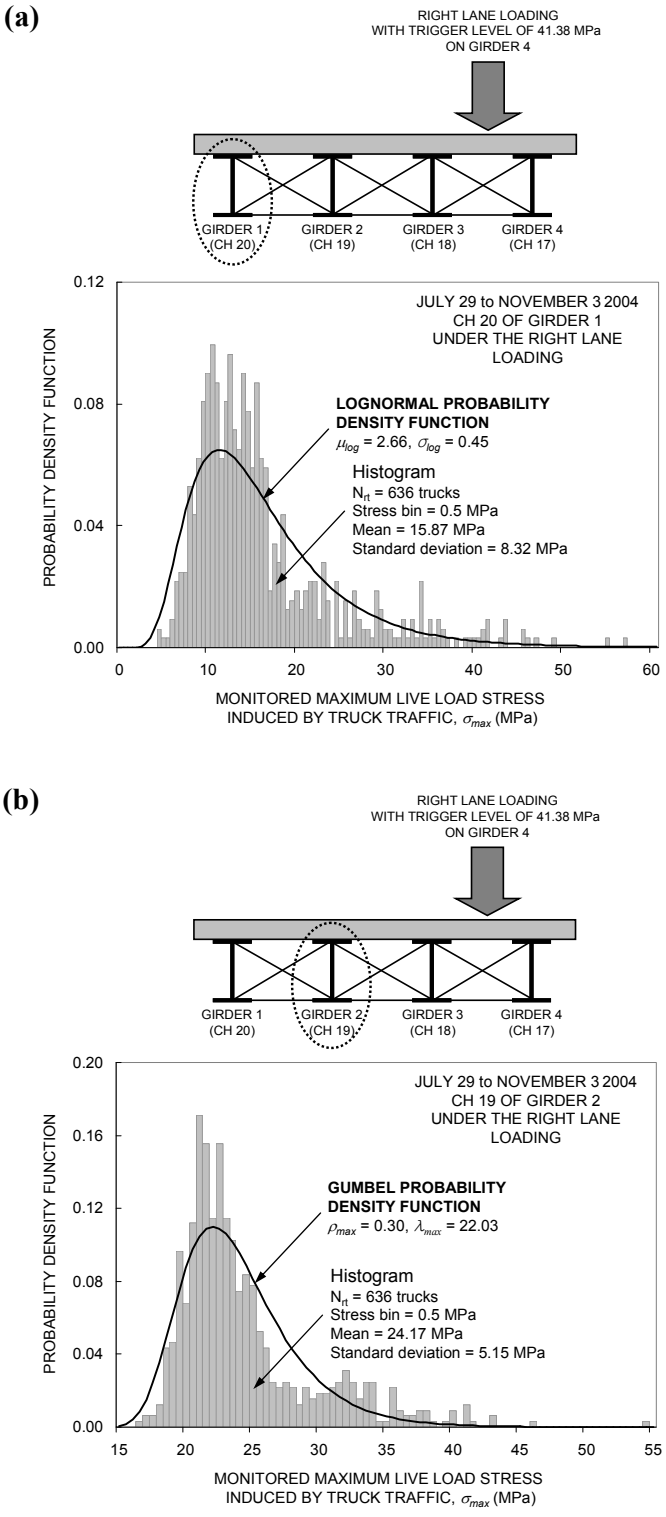

Figure 4.13 Histograms and the best-fit PDFs of monitored data from **(a)** CH 20; **(b)** CH 19; **(c)** CH 18; and **(d)** CH 17 under the right lane loading

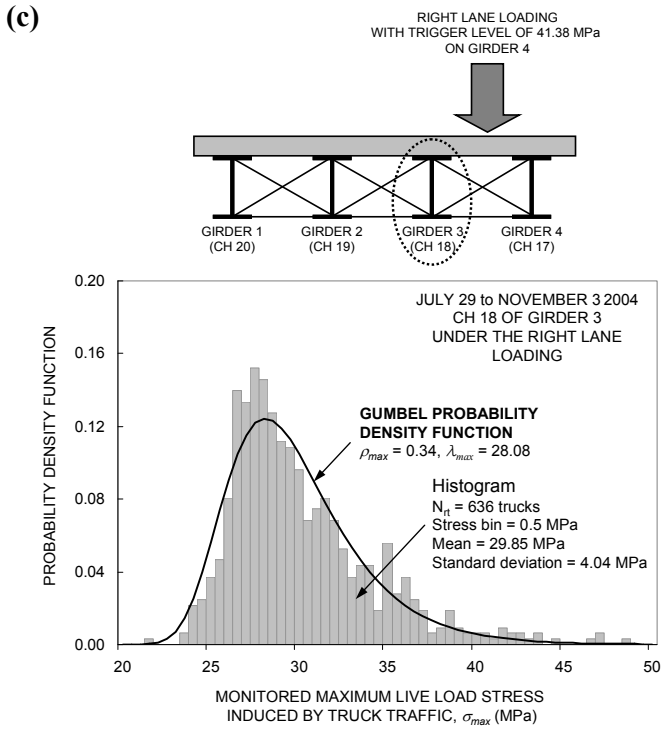

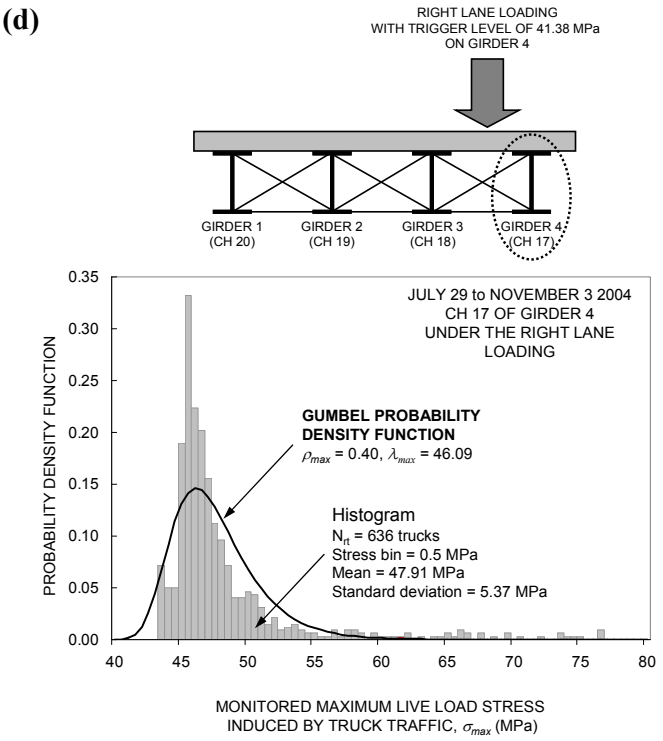

Figure 4.13 Histograms and the best-fit PDFs of monitored data from **(a)** CH 20; **(b)** CH 19; **(c)** CH 18; and **(d)** CH 17 under the right lane loading (continued)

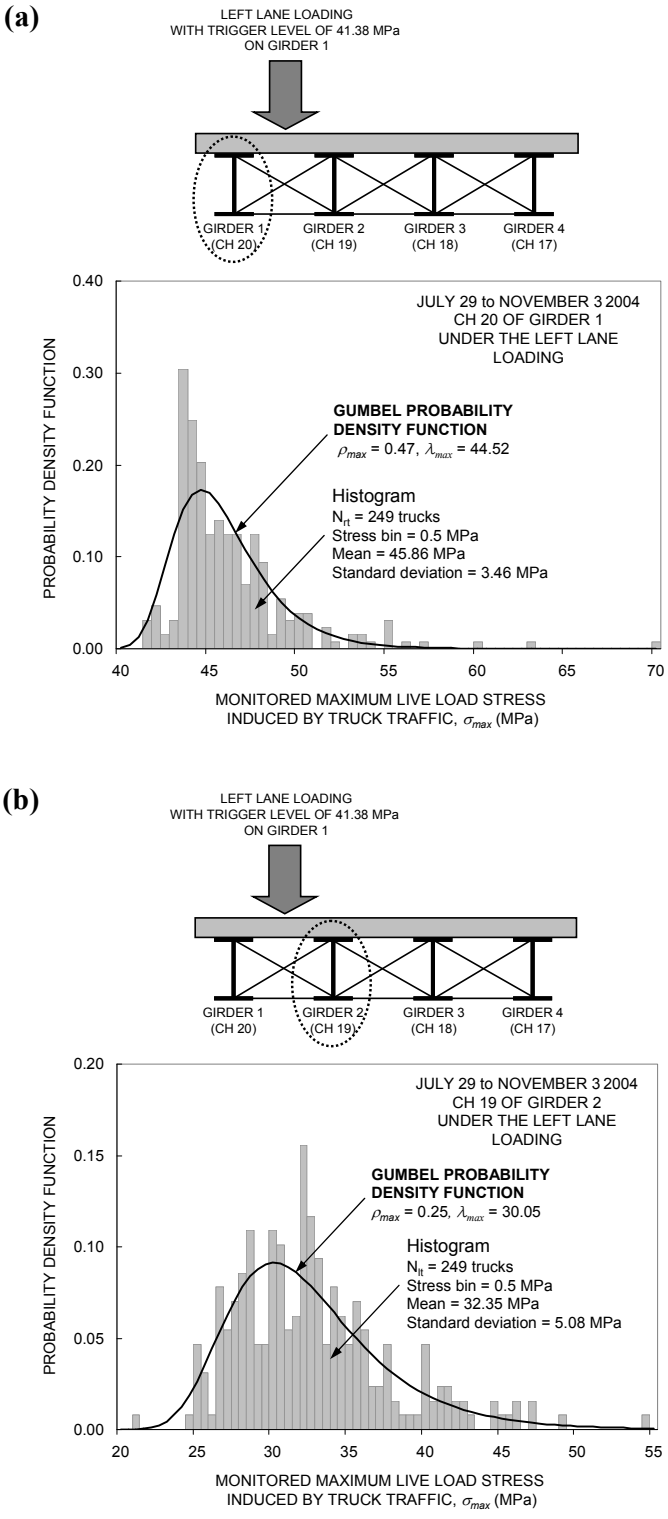

Figure 4.14 Histograms and the best-fit PDFs of monitored data from **(a)** CH 20; **(b)** CH 19; **(c)** CH 18; and **(d)** CH 17 under the left lane loading

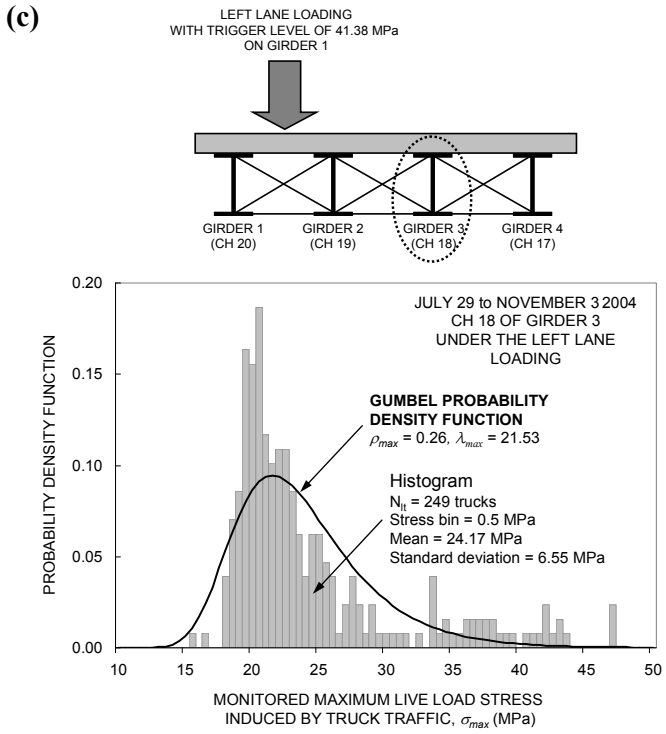

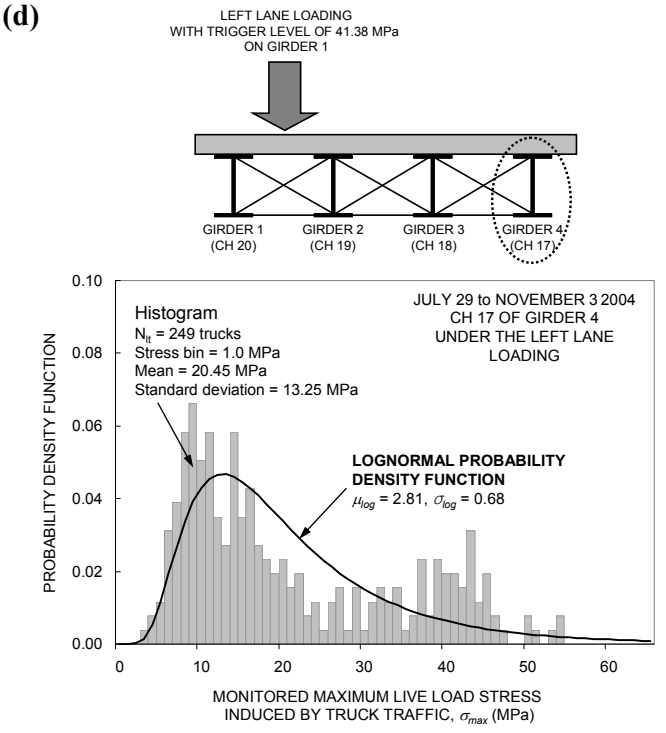

Figure 4.14 Histograms and the best-fit PDFs of monitored data from **(a)** CH 20; **(b)** CH 19; **(c)** CH 18; and **(d)** CH 17 under the left lane loading (continued)

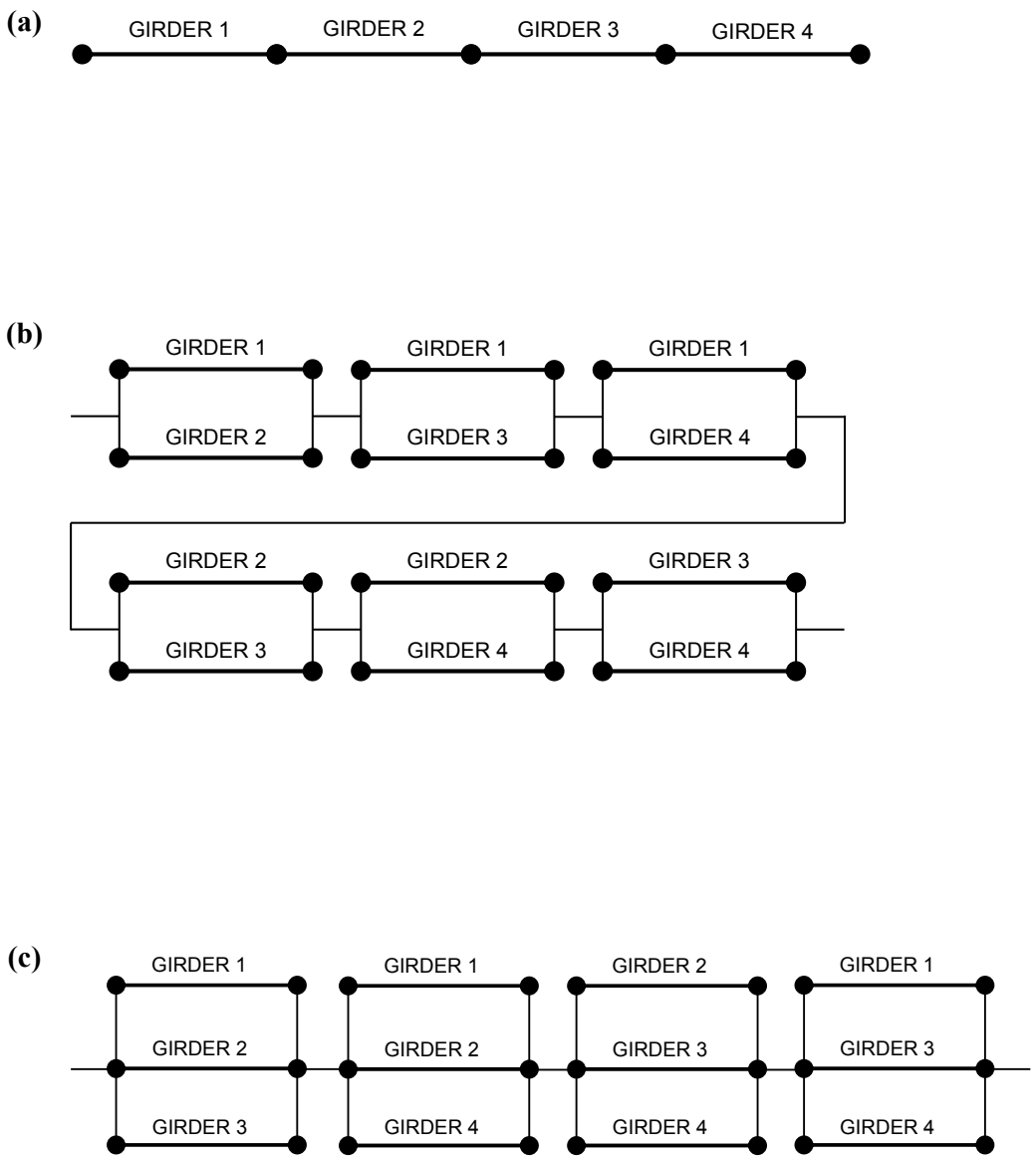

Figure 4.15 (a) System model I; **(b)** System Model II; and **(c)** System Model III

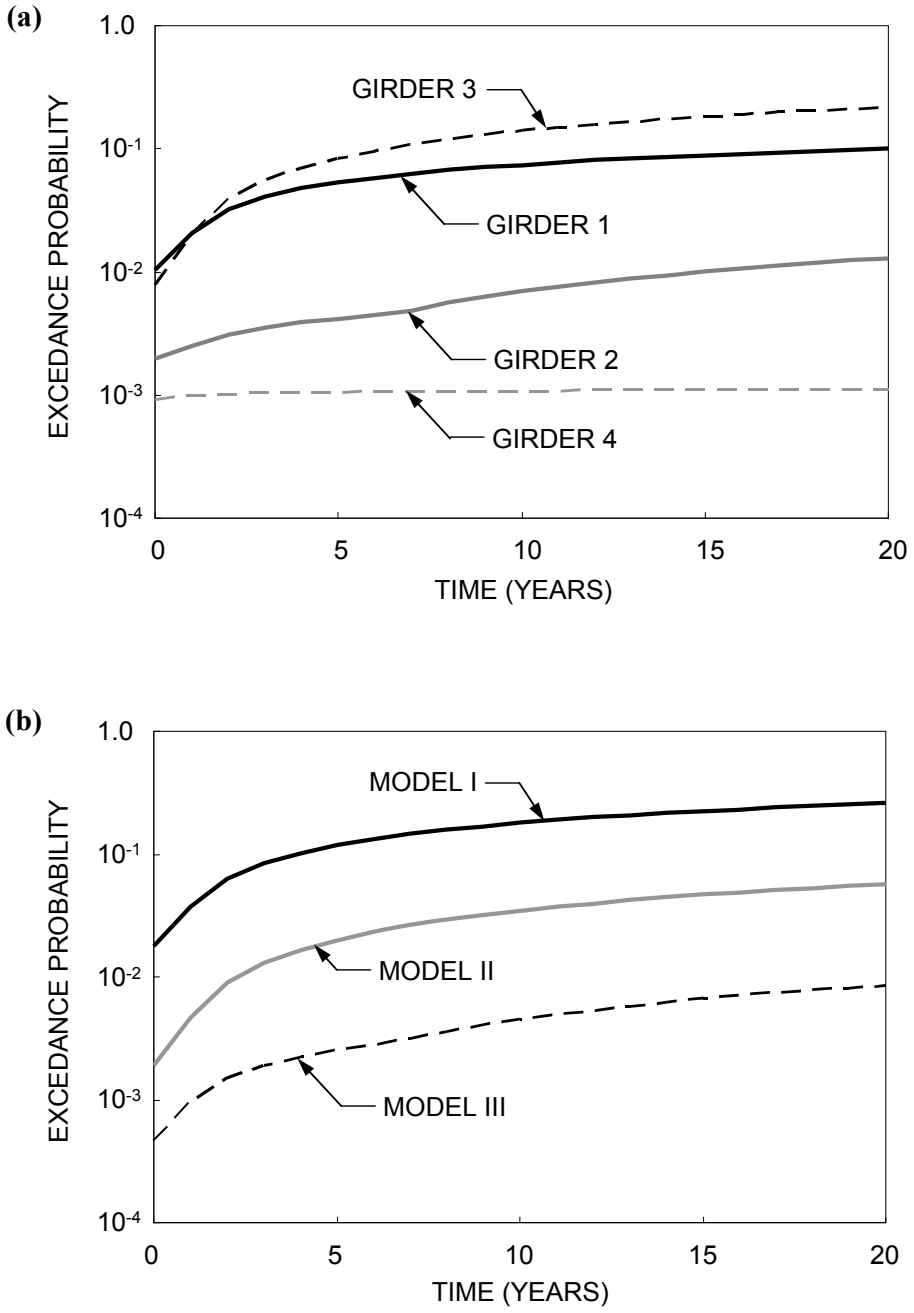

Figure 4.16 Exceedance probabilities associated with **(a)** girders 1, 2, 3, and 4; and **(b)** System Models I, II, and III over time

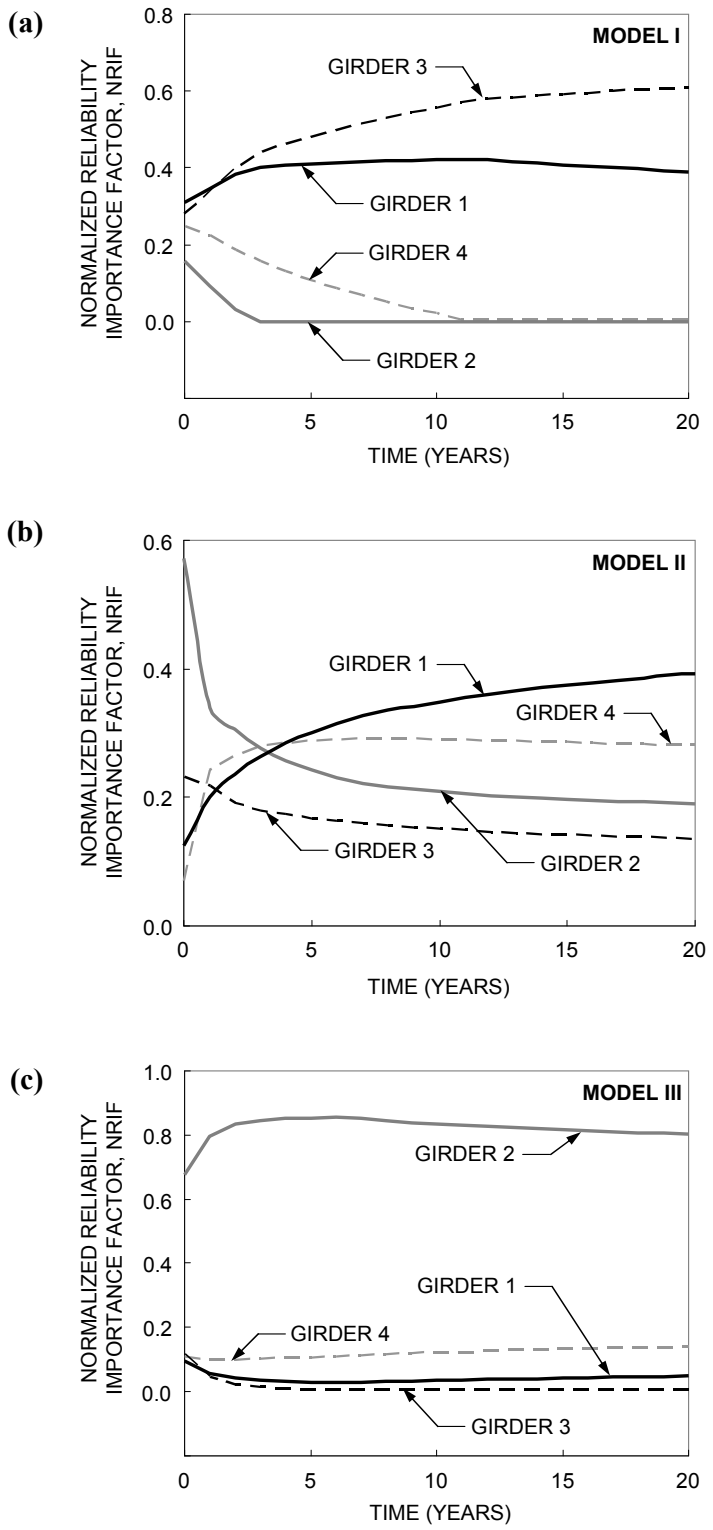

Figure 4.17 Normalized reliability importance factors (NRIFs) of girders 1 to 4 associated with **(a)** System Model I; **(b)** System Model II; and **(c)** System Model III

over time

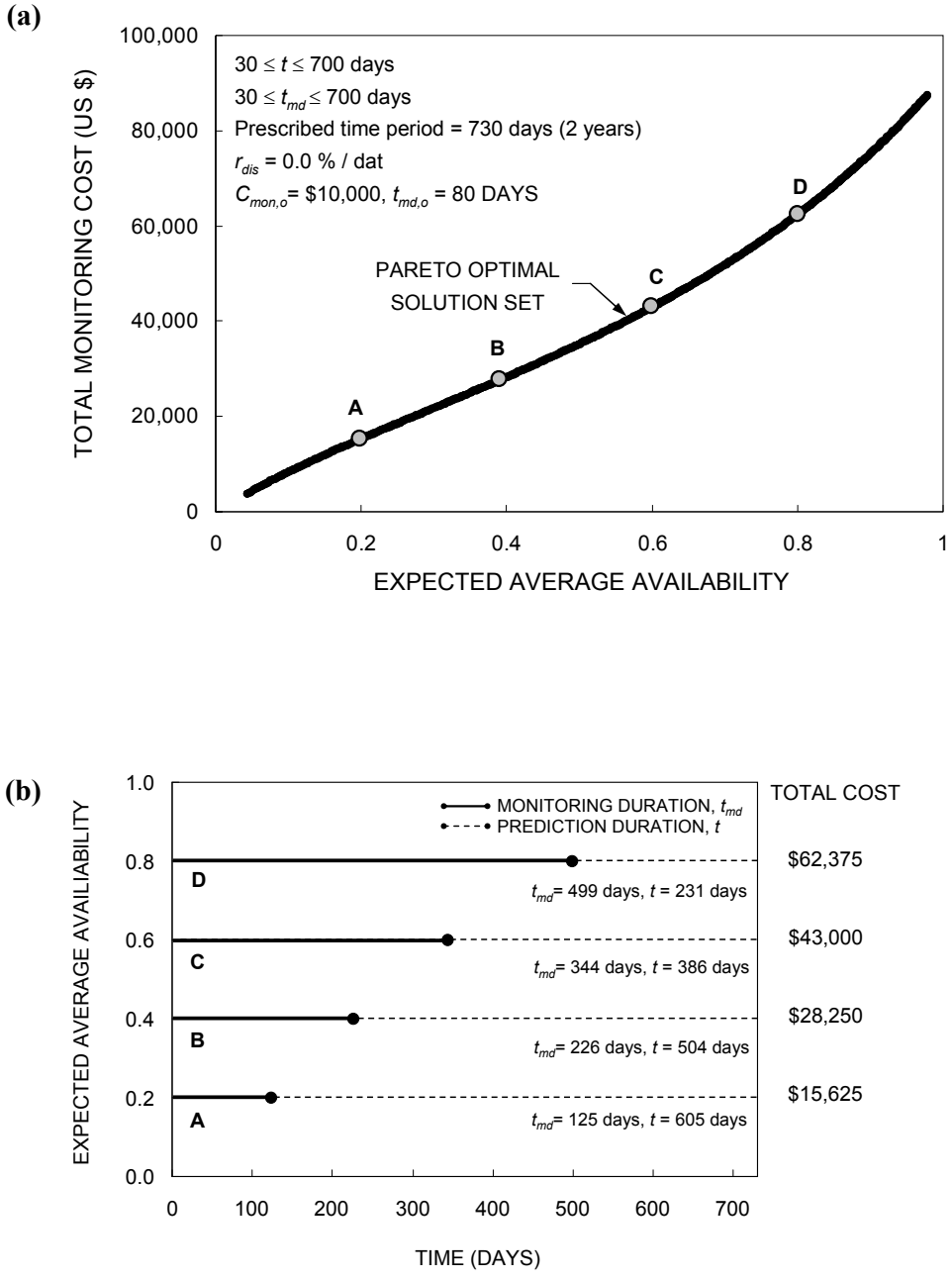

Figure 4.18 (a) Pareto solution set associated with a prescribed time period of two years without considering the discount rate; and **(b)** monitoring plan associated with Solutions A, B, C, and D in (a)

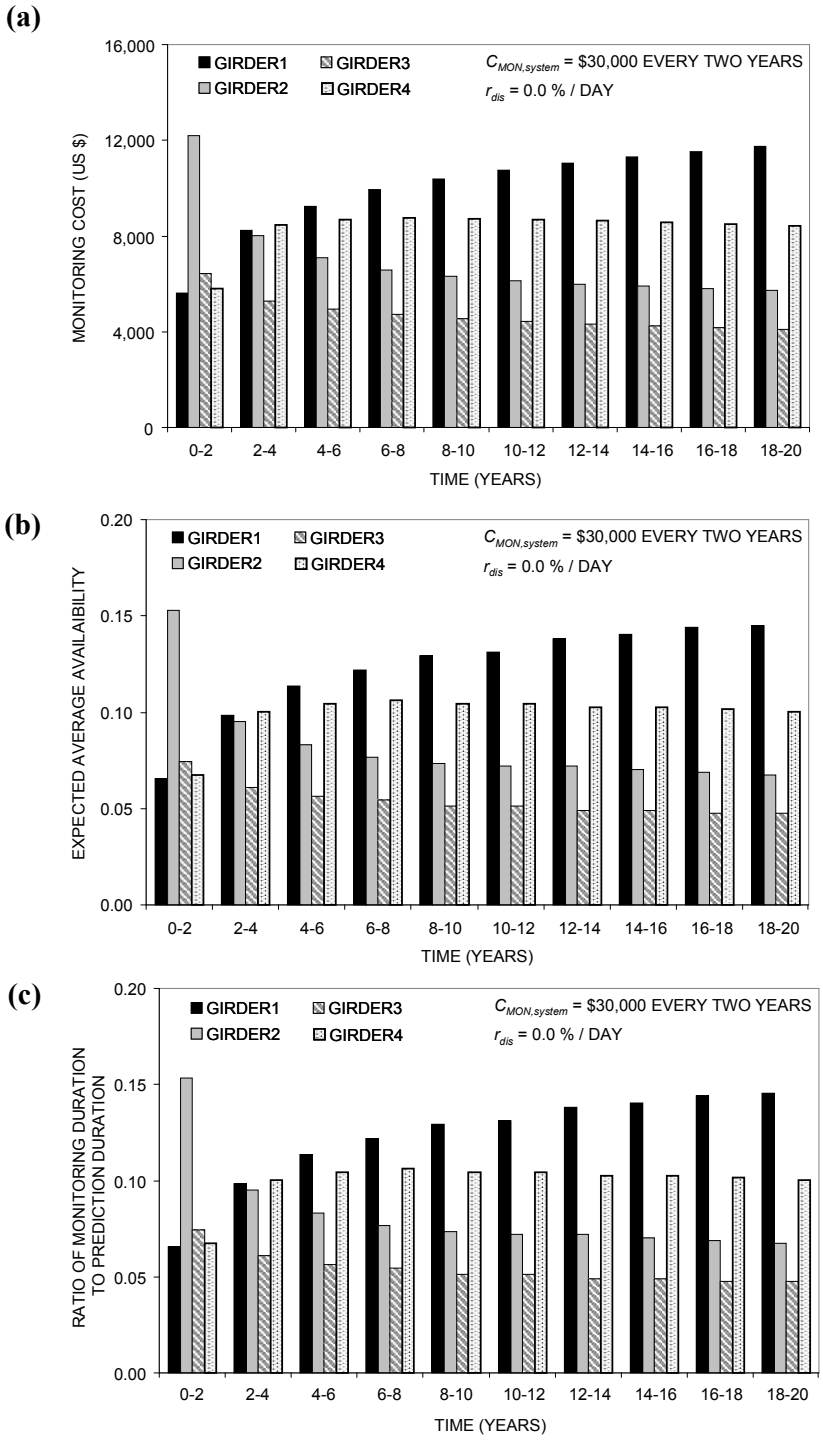

Figure 4.19 Monitoring cost of $ 30,000 allocated every two years for system model II: **(a)** monitoring cost; **(b)** expected average availability; and **(c)** ratio of the monitoring duration to the prediction duration of girders 1, 2, 3, and 4

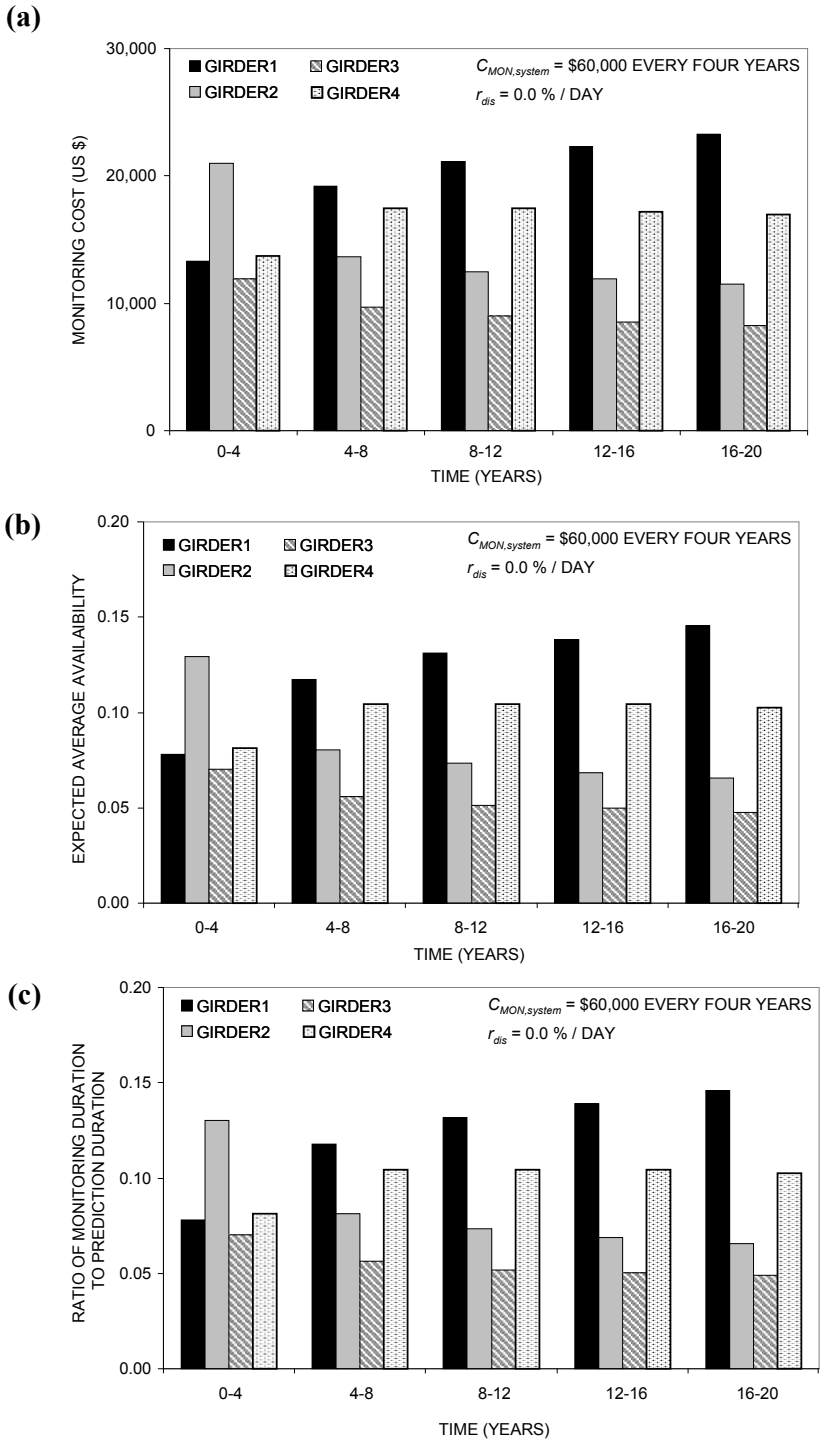

Figure 4.20 Monitoring cost of $ 60,000 allocated every four years for system model II: **(a)** monitoring cost; **(b)** expected average availability; and **(c)** ratio of the monitoring duration to the prediction duration of girders 1, 2, 3, and 4

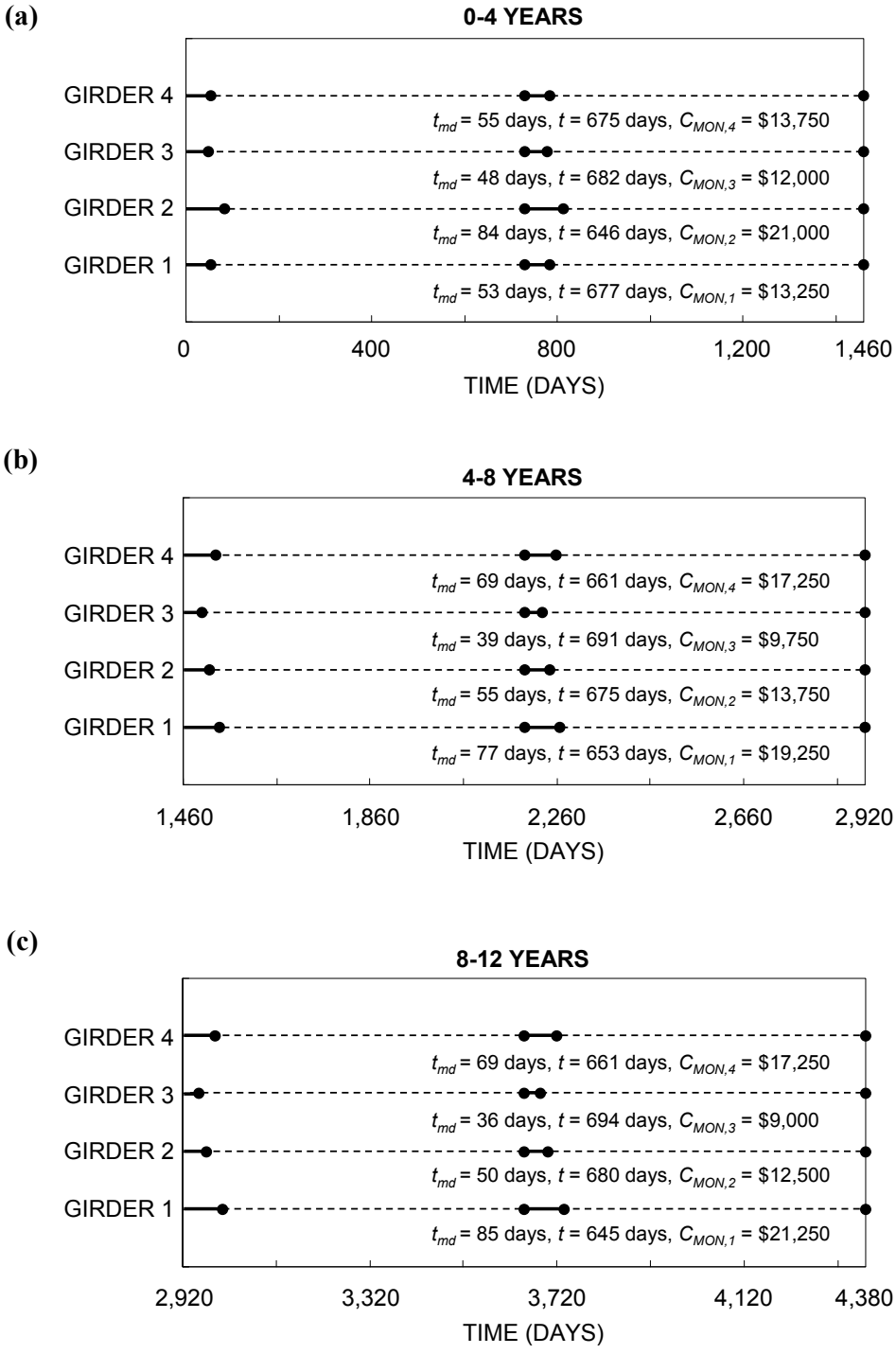

Figure 4.21 Optimum monitoring planning associated with Figure 4.20: **(a)** 0–4 years; **(b)** 4–8 years; **(c)** 8–12 years; **(d)** 12–16 years; and **(e)** 16–20 years with a four-year updating period

(d)

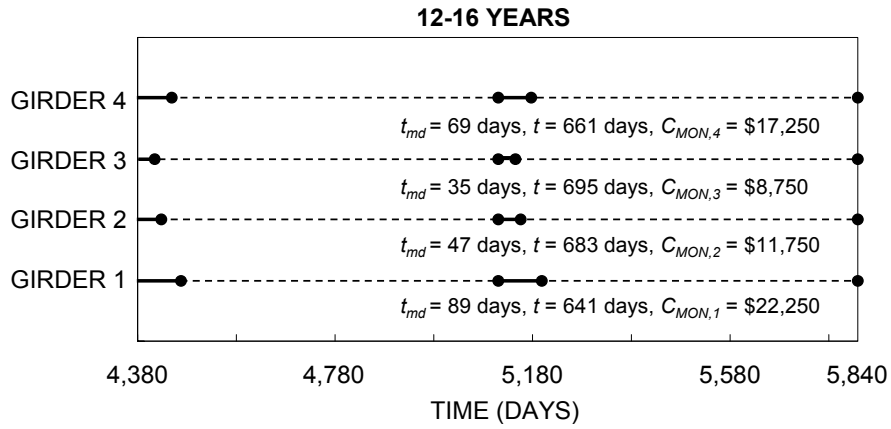

(e)

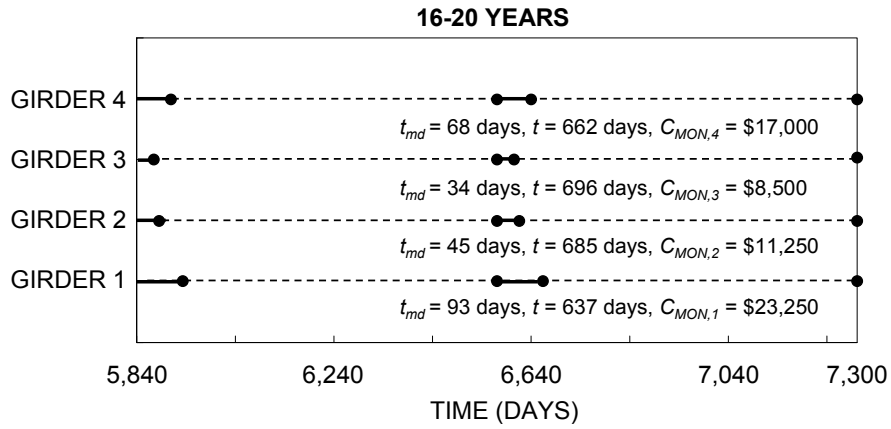

Figure 4.21 Optimum monitoring planning associated with Figure 4.20: **(a)** 0–4 years; **(b)** 4–8 years; **(c)** 8–12 years; **(d)** 12–16 years; and **(e)** 16–20 years with a four-year updating period (continued)

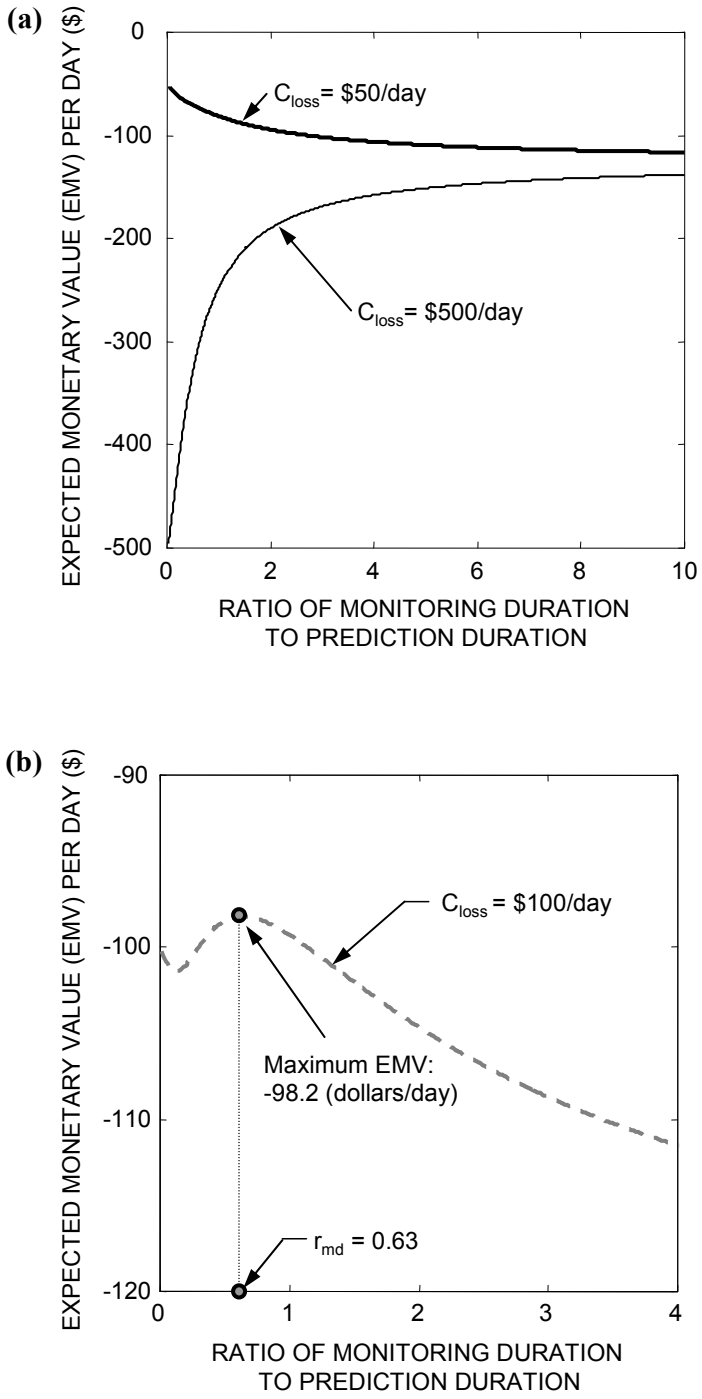

Figure 4.22 Expected monetary value per day versus ratio of the monitoring duration to the prediction duration; **(a)** for C_{loss} = \$50 / day, and C_{loss} = \$500 / day; and **(b)** for C_{loss} = \$100 / day

CHAPTER 5

INSPECTION AND MONITORING PLANNING FOR MINIMIZING DAMAGE DETECTION DELAY

5.1 Introduction

The performance of engineering structures including reinforced concrete (RC) structures and steel structures over their service life can deteriorate under various mechanical and/or environmental processes. Among the processes to induce deterioration of RC structures, corrosion of reinforcement in concrete was considered as predominant [Chaker 1992, NCHRP 2005]. A significant amount of effort has been made to predict the propagation of corrosion damage. However, since the mechanism of RC degradation is highly dependent on the environment and concrete material properties are uncertain, it is still not possible to accurately predict structural performance of deteriorating RC structures. One of main deterioration processes of steel structures is fatigue defined as the process of initiation and growth of cracks under repetitive loads. The fatigue evolution process is generally affected by uncertainties associated with the location and size of initial crack, stress range near the initial crack, number of cycles, and material and geometric properties [Fisher *et al.* 1998]. For this reason, a probabilistic approach is necessary to predict damage occurrence/propagation due to corrosion or fatigue for inspection and monitoring planning. [Madsen and Sørensen 1990, Madsen et al. 1991, Soares and Garbatov 1996a and 1996b, Ayyub et al. 2002, Moan 2005, Kwon and Frangopol

2010]

Several studies focusing on effects of corrosion [Frangopol et al. 1997a, Enright and Frangopol 1998a and 1998b, Stewart 2004, Li et al. 2005] have been conducted on service-life prediction of deteriorating concrete bridges under uncertainty. Based on these studies, lifetime optimization methodologies for planning repair strategies of corroded RC structures were developed [Frangopol et al. 1998b, Enright and Frangopol 1999b, Estes and Frangopol 1999 and 2001]. For steel structures including ship and bridge structures subjected to fatigue, several probabilistic approaches have also been developed and applied [Madsen and Sørensen 1990, Madsen et al. 1991, Ayyub et al. 2002, Moan 2005, Kwon and Frangopol 2010]. These studies were extended into cost-effective inspection and maintenance planning considering probability of fatigue damage detection [Garbatov and Soares 2001, Chung et al. 2006].

In general, maintenance actions will follow inspection if structural damage is detected [Farhey 2005]. If the damage is not detected, no maintenance will be applied. Higher quality of inspection can lead to effective and timely maintenance actions which will prevent unserviceability or collapse and extend the service life of a structure cost-effectively. For this reason, research towards technical development of inspection methods has been performed actively. However, even though high quality inspection methods can be applied, damage cannot be always detected on time. This is due to the fact that there are still uncertainties related to damage

occurrence/propagation and inspection methods are not perfect. Therefore, in order to detect damage on time, inspection timing and number and quality of inspections should be considered simultaneously in a rational probabilistic framework.

In this chapter, such a framework is proposed to establish an optimum inspection and monitoring plan. The objective of this optimization is to minimize the expected damage detection delay defined as the expected time-lapse since a structure has been damaged until the damage is detected by inspection. In this formulation, uncertainties associated with prediction of damage occurrence / propagation in an engineering structure are considered, and the detectability function is used to quantify the quality of inspection method according to the degree of damage (e.g., corroded reinforcement area, crack size). This proposed approach is further used for optimum monitoring planning. The effect of additional information on optimal solutions is studied using Bayesian updating. Furthermore, increase of number of inspections and improvement of inspection quality can lead to reduction of damage detection delay, but additional cost is required. In order to consider the conflicting criteria of minimization of both expected damage detection delay and inspection cost, a bi-objective optimization problem was solved. The well-balanced inspection planning from this bi-objective optimization problem provides optimum inspection types and times considering a single-type or multi-types of inspections. This bi-objective optimization formulation is extended to establish an optimum combined inspection / monitoring planning. The solution provides the sequence of inspections

and monitorings (e.g., inspection followed by monitoring, monitoring followed by inspection) as well as inspection and/or monitoring times, and inspection quality, and monitoring durations. The proposed approach in this chapter is applied to existing highway bridges subjected to corrosion or fatigue, and ship hull structures subjected to fatigue.

5.2 Damage Occurrence and Propagation

The most common causes of resistance reduction of concrete and steel structures are corrosion and fatigue. Among the factors affecting the deterioration of concrete structures, corrosion is the main factor which may develop into crack and spalling as well as loss of bond between concrete and reinforcing steel, and loss of steel section. [Zhang and Lounis 2006]. The general deterioration process due to corrosion has six steps [Thoft-Christensen 2003]: (a) penetration of chloride ions into the concrete structure; (b) corrosion initiation in the reinforcement; (c) evolution of corrosion of the reinforcement; (d) crack initiation in the concrete; (e) crack propagation in the concrete; and (f) spalling. Spalling may cause additional cracks in the concrete through which reinforcement of the concrete structure is exposed directly to aggressive environments [Bertolini et al. 2004]. The causes of steel corrosion process in concrete are mainly related to chloride penetration into concrete and concrete carbonation [Roberge 1999]. This study considers the penetration of chloride ions into concrete as the primary cause of corrosion process.

Fatigue in metals can be defined as the process of initiation and growth of cracks under repetitive stresses. If crack growth is allowed to develop, failure of the steel member can occur and this process can take place at stress levels that are less than levels at which failure occurs under static loading condition. In general, the fatigue life of a fabricated steel structure may be determined by three factors as (a) number of loading cycles; (b) stress range at the location of a steel member; and (c) type of detail of a steel member [Fisher et al. 1998].

5.2.1 Corrosion Damage Occurrence and Propagation

The deterioration process due to corrosion generally consists of the following two steps: corrosion initiation/propagation [Tuutti 1982, Al-Tayyib et al. 1988, Dhir et al. 1989, Stewart and Rosowsky 1998].

Corrosion initiation

The time for the concentration of chloride at the rebar surface to exceed a threshold limit can be referred to as the corrosion initiation time [Arora et al. 1997, Zhang and Lounis 2006]. In order to predict time-dependent chloride concentration $C_{ch}(x, t)$ (g/mm^3) at depth x (mm) from the concrete surface and time t (years), Fick's second law can be used as

$$\frac{\partial C_{ch}(x,t)}{\partial t} = \frac{\partial}{\partial x}\left[D_{ch} \frac{\partial C_{ch}(x,t)}{\partial x} \right] \tag{5.1}$$

where D_{ch} (mm^2/year) is the effective chloride diffusion coefficient. If D_{ch} and the surface chloride concentration $C_{ch,o}$ (g/mm^3) are constant over time, and C_{ch} = 0 for time t = 0, the solution of Equation (5.1) is [Crank 1975]

$$C_{ch}(x,t) = C_{ch,o}\left[1 - erf\left(\frac{x}{2\sqrt{D_{ch} \cdot t}}\right)\right] \tag{5.2}$$

where *erf* denotes the standard error function. Assuming that corrosion of reinforcement starts when the concentration of chloride reaches the threshold limit $C_{ch,th}$ (g/mm^3) of reinforcement, the time to corrosion initiation T_{corr} (years) is [Rafiq 2005]

$$T_{corr} = \frac{x^2}{4D_{ch}\left[erfc^{-1}\left(\frac{C_{ch,th}}{C_{ch,o}}\right)\right]^2} \tag{5.3}$$

where *erfc* = complementary error function. It should be noted that the effective chloride diffusion coefficient D_{ch} and the surface chloride concentration $C_{ch,o}$ can be time-dependent parameters, and initial chloride concentration C_{ch} at time t = 0 may not be equal to 0 [Maage et al. 1996 and 1999, NCHRP 2006].

Corrosion propagation

The evolution of corrosion of the reinforcement can be represented by using the general (also called uniform) and pitting corrosion models [Val and Melchers 1997, Jemajtis 1998, Marsh and Frangopol 2008]. The general corrosion model is based on the assumption that the entire cross-sectional area of reinforcement is reduced

uniformly. The total reinforcement area $A_{st}(t)$ at time t (years) is [Enright and Frangopol 1998a, Marsh and Frangopol 2008]

$$A_{st}(t) = \begin{cases} \dfrac{n_s \pi \ d_{st0}{}^2}{4} & for \quad 0 \le t \le T_{corr} \\ \dfrac{n_s \pi \left[d_{st0} - r_{corr}\left(t - T_{corr}\right) \right]^2}{4} & for \quad t > T_{corr} \end{cases} \tag{5.4}$$

where n_s = number of steel bars experiencing active corrosion, d_{st0} = initial diameter of reinforcement (mm), and r_{corr} = rate of corrosion (mm/year).

The rate of corrosion r_{corr} is generally obtained by considering the overall reinforcement surface. However, corrosion can be highly localized, and the maximum pit depth is larger than the average pit depth based on uniform corrosion model [Gonzalez et al. 1995]. Stewart (2004) showed that pitting corrosion can lead to a larger probability of failure than uniform corrosion. The maximum penetration of pitting $PT(t)$ at time t is expressed by [Val and Melchers 1997]

$$PT(t) = r_{corr} R_{pit} (t - T_{corr}) \qquad \text{for } t > T_{corr} \tag{5.5}$$

where R_{pit} = ratio of maximum pit depth to average pit depth. R_{pit} generally lies in the interval between 4 and 8 [Gonzalez et al. 1995]. Based on a hemispherical form of pits, the remaining cross sectional area $A_{st}(t)$ of reinforcement can be estimated as [Val and Melchers 1997]

$$A_{st}\left(t\right) = \frac{n_s \pi d_{st0}{}^2}{4} - A_1 - A_2 \qquad \text{for} \quad PT\left(t\right) \le \frac{\sqrt{2}\ d_{st0}}{2} \tag{5.6a}$$

$$A_{st}\left(t\right) = A_1 - A_2 \qquad \text{for} \quad \frac{\sqrt{2}\ d_{st0}}{2} < PT\left(t\right) \le d_{st0} \tag{5.6b}$$

$$A_{st}(t) = 0 \qquad \text{for} \quad PT(t) > d_{st0} \tag{5.6c}$$

where

$$A_1 = \frac{n_s}{2}\left[\theta_1\left(\frac{d_{st0}}{2}\right)^2 - a\left|\frac{d_{st0}}{2} - \frac{PT(t)^2}{d_{st0}}\right|\right] \quad \text{and} \quad A_2 = \frac{n_s}{2}\left[\theta_2 PT(t)^2 - a\frac{PT(t)^2}{d_{st0}}\right] \tag{5.7a}$$

$$a = 2PT(t)\left[1 - \left(\frac{PT(t)}{d_{st0}}\right)^2\right]^{0.5} \tag{5.7b}$$

$$\theta_1 = 2\,arcsin\left(\frac{a}{d_{st0}}\right) \quad \text{and} \quad \theta_2 = 2\,arcsin\left(\frac{a}{2PT(t)}\right) \tag{5.7c}$$

where n_s = number of steel bars experiencing active corrosion, and d_{st0} = initial diameter of reinforcement (mm).

5.2.2 Fatigue Damage Occurrence and Propagation

Fatigue is the process of initiation and growth of cracks under repetitive loads. The crack may be pre-existing from fabrication, and be initiated by fatigue and/or corrosion. The crack growth can be affected by the location and length of initial crack, stress range near the initial crack, number of cycles associated with the stress range, material and geometric properties of a structure with crack damage [Fisher et al. 1998]. All these factors have complex relation to each other. Due to this complexity of the fatigue fracture process, it is difficult to predict crack length accurately. So far several empirical and phenomenological-based crack propagation models have been proposed to predict fatigue life [Fatemi and Yang 1998, Schijve 2003, Mohanty et al. 2009]. In order to predict crack length, Paris' equation based on linear elastic fracture

mechanics has been generally used. The ratio of the crack size increment to stress cycle increment is described by the following equation [Paris and Erdogan 1963]

$$\frac{da}{dN_{cycle}} = C\,(\Delta K)^m \qquad \text{for } \Delta K > \Delta K_{thr} \tag{5.8}$$

where a = crack size; N_{cycle} = cumulative number of cycles; ΔK = stress intensity factor; and ΔK_{thr} = threshold of stress intensity factor. C and m are material parameters. The stress intensity factor ΔK is [Irwin 1958]

$$\Delta K = S_{sr} \cdot Y(a) \sqrt{\pi a} \tag{5.9}$$

where S_{sr} = stress range, and $Y(a)$ = geometry function. From Equation (5.8) and (5.9), the cumulative number of cycles N_{cycle} associated with crack size a_N is obtained as [Fisher 1984]

$$N_{cycle} = \frac{1}{C \cdot {S_{sr}}^m} \cdot \int_{a_o}^{a_N} \frac{1}{(Y(a)\sqrt{\pi \cdot a})^m}\, da \tag{5.10}$$

where a_o= initial crack size. Furthermore, the time t (years) associated with the occurrence of the crack size a_N is predicted by considering the annual number of cycles N_{an} and annual increase rate of number of cycles r_{cycle} as [Madsen et al. 1985 and 1987]

$$t = \frac{ln[1 + \frac{1}{N_{an} \cdot C \cdot {S_{sr}}^m} \cdot ln(1 + r_{cycle}) \cdot \int_{a_o}^{a_N} \frac{1}{(Y(a)\sqrt{\pi \cdot a})^m}\, da]}{ln(1 + r_{cycle})} \qquad \text{for } r_{cycle} > 0 \tag{5.11a}$$

$$t = \frac{1}{N_{an} \cdot C \cdot {S_{re}}^m} \cdot \int_{a_o}^{a_N} \frac{1}{(Y(a)\sqrt{\pi \cdot a})^m}\, da \qquad \text{for } r_{cycle} = 0 \tag{5.11b}$$

If the geometry function is constant (*i.e.*, $Y(a) = Y$), the crack length after N cycles a_N

can be obtained as

$$a_N = [a_o^{(2-m)/2} + (\frac{2-m}{2}) \cdot C \cdot S_{sr}^m \cdot Y^m \cdot \pi^{m/2} \cdot N_{cycle}]^{(\frac{2}{2-m})} \quad \text{for } m \neq 2 \quad (5.12a)$$

$$a_N = a_o \cdot exp[C \cdot S_{sr}^m \cdot Y^m \cdot \pi \cdot N_{cycle}] \quad \text{for } m = 2 \quad (5.12b)$$

5.3 Uncertainty Associated with Inspection

Damage detection using a particular inspection method and interpretation of inspection data are associated with large uncertainties [Mori and Ellingwood 1994b, Frangopol et al. 1997b, Enright and Frangopol 1999a]. These uncertainties include the randomness of damage occurrence/propagation and the imperfection of inspection method. There are two events when inspection result is "no damage": (a) no damage occurrence; (b) damage occurred but is not detected. The later event is associated with uncertainties in the inspection method. In order to treat the uncertainty of inspection in a rational way, uncertainties associated with both damage prediction and quality of inspection should be considered.

5.3.1 Probability of corrosion damage detection

Variables associated with prediction of structural performance are affected by uncertainties and, therefore, they should be treated as random variables. For example, in order to predict the corrosion initiation time under uncertainty, randomness of the associated four coefficients in Equation (5.3) (i.e., effective chloride diffusion

coefficient D_{ch}, surface chloride concentration $C_{ch,o}$, depth x from the concrete surface, and threshold limit $C_{ch,th}$) should be considered. Enright and Frangopol (1998a) studied the relationship between the corrosion initiation time and these four parameters under uncertainty using parametric studies. They concluded that both the mean and standard deviation of the corrosion initiation time increase with an increase in the coefficients of variation (COVs) of these four parameters.

The quality of inspection technique being used, the degree of damage, and the number and timing of inspections have an effect on the ability to detect damage. In order to quantify the quality of inspection method considering the degree of damage, a detectability function can be used. The detectability function $P_{insp}(\delta_c)$ is defined as the probability that corrosion damage is detected when the corrosion damage intensity at time t is δ_c. This time-dependent corrosion damage intensity δ_c for the uniform (or general) model indicated in Equation (5.4) is defined as [Frangopol et al. 1997b]

$$\delta_c(t) = \begin{cases} 0 & for \quad 0 \le t \le T_{corr} \\ \dfrac{r_{corr}(t - T_{corr})}{d_{st0}} & for \quad t > T_{corr} \end{cases} \tag{5.13}$$

The localized corrosion damage intensity δ_c at time t can be expressed as [Kim et al. 2011]

$$\delta_c(t) = \frac{PT(t)}{d_{st0}} \tag{5.14}$$

Once corrosion initiates and propagates, damage intensity δ_c increases from zero (i.e.,

no damage) to one (full damage). The probability of corrosion damage detection $P_{insp,c}(\delta_c)$ is [Frangopol et al. 1997b]

$$P_{insp,c} = \Phi\left(\frac{\delta_c - \delta_{c,0.5}}{\sigma_{c,\delta}}\right) \tag{5.15}$$

where $\Phi(\cdot)$ = standard normal CDF; $\delta_{c,0.5}$ = corrosion damage intensity at which the inspection method has a 50% probability of damage detection; and $\sigma_{c,\delta}$ = standard deviation of the damage intensity $\delta_{c,0.5}$. An inspection method with a lower value of $\delta_{c,0.5}$ has a higher probability of detection. For instance, suppose that two inspection methods are used to detect the corrosion in a reinforcement with the degree of damage δ_c = 0.03; the associated damage intensities at which the inspection method has a 50% probability of detection are 0.03 and 0.05, respectively, and $\sigma_{c,\delta} = 0.1\,\delta_{c,0.5}$. The detectability (i.e., probability of detection) of the inspection method associated with $\delta_{c,0.5}$ = 0.03 will be $1 - 2.06 \times 10^{-11}$, and the probability of detection with $\delta_{c,0.5}$ = 0.05 will be 0.5. The relation between the corrosion damage intensity δ_c and the probability of corrosion damage detection is shown in Figure 5.1(a). Therefore, $\delta_{c,0.5}$ can be used to quantify the quality of inspection.

5.3.2 Probability of fatigue damage detection

Probability of fatigue damage detection is defined as the conditional probability that the crack is detected by an inspection method, when the crack exists with a specific size [Chung et al. 2006]. The probability of fatigue damage detection depends on the

degree of fatigue damage (*i.e.*, crack length or defect size) and quality of inspection. Packman et al. (1969), Berens and Hovey (1981), Madsen et al. (1991), Mori and Ellingwood (1994a), and Chung et al. (2006) investigated the relation between probability of detection and crack length (or defect size). The representative relations between probability of fatigue damage detection $P_{insp,f}$ and crack size a are:

(a) Shifted exponential form [Packman et al. 1969]

$$P_{insp,f} = 1 - exp\left(-\frac{a - a_{min}}{\lambda_{insp}}\right) \qquad \text{for } a > a_{min} \tag{5.16}$$

where a_{min} = smallest detectable crack size, λ_{insp} = characteristic parameter for inspection quality. The value of this parameter ranges from 0 to ∞, and λ_{insp} decreases with increasing the quality of inspection.

(b) Log-logistic form [Berens and Hovey 1981]

$$P_{insp,f} = \frac{exp[\chi_{insp} + \kappa_{insp}\, ln(a)]}{1 + exp[\chi_{insp} + \kappa_{insp}\, ln(a)]} \tag{5.17}$$

where χ_{insp} and κ_{insp} are statistical parameters. These parameters can be estimated using the maximum likelihood method for a specific inspection method [Chung et al. 2006].

(c) Normal cumulative distribution function (CDF) form [Frangopol et al. 1997b]

$$P_{insp,f} = \Phi\left(\frac{\delta_f - \delta_{f,0.5}}{\sigma_{f,\delta}}\right) \tag{5.18}$$

where $\Phi(\cdot)$ = standard normal CDF; δ_f = fatigue damage intensity; $\delta_{f,0.5}$ = fatigue damage intensity at which the inspection method has a probability of

detection of 0.5; and $\sigma_{f,\delta}$ = standard deviation of $\delta_{f,0.5}$. In this study, the normal CDF form in Equation (5.18) is used, and the coefficient of variation of $\delta_{f,0.5}$ is assumed 0.1 (i.e., $\sigma_{f,\delta} = 0.1 \times \delta_{f,0.5}$). The fatigue damage intensity δ_f is defined as [Kim and Frangopol 2011c]

$$\delta_f = 0 \qquad \text{for } a < a_{min} \tag{5.19a}$$

$$\delta_f = \frac{a - a_{min}}{a_{max} - a_{min}} \qquad \text{for } a_{min} \le a < a_{max} \tag{5.19b}$$

$$\delta_f = 1 \qquad \text{for } a \ge a_{max} \tag{5.19c}$$

where a_{min} and a_{max} are the minimum and maximum detectable crack sizes when the result of the detection is uncertain (i.e., if $a < a_{min}$ and $a \ge a_{max}$, the probability of detection is 0 and 1, respectively). For example, in case the minimum and maximum crack lengths for damage intensity are 1 *mm* and 50 *mm*, respectively (*i.e.,* a_{min} = 1 *mm*, and a_{max} = 50 *mm*), the relations between the crack length a and probability of fatigue damage detection $P_{insp,f}$ for three inspections with $\delta_{f,0.5}$= 0.01, 0.03, and 0.05 is shown in Figure 5.1(b). For the inspection method with $\delta_{f,0.5}$ = 0.05, the probability of detection is 0.5 when the fatigue damage intensity is 0.05, and the associated crack length can be obtained as 3.45 *mm*, using Equation (5.19b); the crack length associated with probability of detection 0.999 is 4.21 *mm* as shown in Figure 5.1(b). If the inspection method with $\delta_{f,0.5}$ = 0.01 is used to detect the damage, the probability of damage detection will be 0.999, when the crack length is 1.64 *mm*.

5.4 Expected Damage Detection Delay

5.4.1 Expected Damage Detection Delay when Inspection is Used

Damage detection delay can be defined as the time-lapse since the structure has been damaged until the damage is identified by inspection [Huang and Chiu 1995]. If the time t for damage to occur is deterministic, and the probability of detection is certain, the damage detection delay t_{delay} will be

$$t_{delay} = t_{insp} - t \tag{5.20}$$

where t_{insp} denotes inspection time. However, inspection methods are not perfect. In order to formulate the damage detection delay considering probability of damage detection and number of inspections, an event tree model can be used. This model represents all the possible events having a particular consequence. There is a chance node associated with detection and no detection at every inspection. For instance, assuming that damage occurs in the time interval t_s to t_e, and three inspections to detect damage are used, formulation of damage detection delay is based on the four cases according to damage occurrence time t as follows: (a) case 1: $t_s \le t < t_{insp,1}$; (b) case 2: $t_{insp,1} \le t < t_{insp,2}$; (c) case 3: $t_{insp,2} \le t < t_{insp,3}$; and (d) case 4: $t_{insp,3} \le t \le t_e$, where t_s and t_e are the times representing the lower and upper bounds of damage occurrence, respectively, and $t_{insp,i}$ is ith inspection time. Figure 5.2 illustrates event trees and damage detection delays associated with possible branches for these four cases. The gray circle node in Figure 5.2 indicates a chance node at every inspection

where there are two events (*i.e.*, detection and no detection). For case 1 (see Figure 5.2(a)), there are four branches. Branch 1 represents the event of damage detection at the first inspection. The associated damage detection delay and probability are $t_{insp,1} - t$ and $P_{insp,1}$, respectively. If the damage is not detected until the third inspection, and is detected at time $t_{insp,e}$, the associated damage detection delay and probability will be $t_{insp,e} - t$ and $(1 - P_{insp,1}) \times (1 - P_{insp,2}) \times (1 - P_{insp,3})$, respectively (see branch 4 in Figure 5.2(a)). Therefore, considering the damage detection delays and their probabilities associated with four possible branches, the expected damage detection delays for cases 1, 2, 3, and 4 are

$$\begin{aligned} E(t_{delay})_{case,1} = {} & (t_{insp,1} - t) \cdot P_{insp,1} \\ & + (t_{insp,2} - t)[(1 - P_{insp,1}) \cdot P_{insp,2}] \\ & + (t_{insp,3} - t)[(1 - P_{insp,1})(1 - P_{insp,2}) \cdot P_{insp,3}] \\ & + (t_{insp,e} - t)[(1 - P_{insp,1})(1 - P_{insp,2})(1 - P_{insp,3})] \end{aligned} \quad \text{for } t_s \le t < t_{insp,1} \qquad (5.21a)$$

$$\begin{aligned} E(t_{delay})_{case,2} = {} & (t_{insp,2} - t) \cdot P_{insp,2} \\ & + (t_{insp,3} - t)[(1 - P_{insp,2}) \cdot P_{insp,3}] \\ & + (t_{insp,e} - t)\left[(1 - P_{insp,2})(1 - P_{insp,3})\right] \end{aligned} \quad \text{for } t_{insp,1} \le t < t_{insp,2} \qquad (5.21b)$$

$$E(t_{delay})_{case,3} = (t_{insp,3} - t) \cdot P_{insp,3} + (t_{insp,e} - t)(1 - P_{insp,3}) \quad \text{for } t_{insp,2} \le t < t_{insp,3} \qquad (5.21c)$$

$$E(t_{delay})_{case,4} = (t_{insp,e} - t)(1 - P_{insp,3}) \quad \text{for } t_{insp,3} \le t \le t_e \qquad (5.21d)$$

In Equation (5.21), the expected damage detection delay for case i is denoted as $E(t_{delay})_{case,i}$.

When the time t for damage to occur is a continuous random variable described by the probability density function (PDF) $f_T(t)$ as shown in Figure 5.2, the expected

damage detection delay $E(t_{delay})$ for n_{insp} inspections is [Kim and Frangopol 2011b and 2011c]

$$E(t_{delay}) = \sum_{i=1}^{n_{insp}+1} \{ \int_{t_{insp,i-1}}^{t_{insp,i}} [E(t_{delay})_{case,i} \cdot f_T(t)] dt \} \tag{5.22}$$

where $E(t_{delay})_{case,i}$ = expected damage detection delay when $t_{insp,i-1} \le t < t_{insp,i}$. The time $t_{insp,0}$ for $i = 1$ and $t_{insp,n+1}$ for $i = n_{insp}+1$ in Equation (5.22) are t_s and t_e, respectively. Based on the PDF of damage occurrence time $f_T(t)$, t_s and t_e (i.e., lower and upper bounds of damage occurrence, respectively) are defined as [Kim and Frangopol 2011b]

$$t_s = F_T^{-1}(\Phi(-u)) \tag{5.23a}$$

$$t_e = F_T^{-1}(\Phi(u)) \tag{5.23b}$$

where $F_T^{-1}(\cdot)$ = the inverse CDF of the damage occurrence time t, and $u > 0$. If, for example, the time t for damage to occur is assumed lognormally distributed with the mean of 10 years and the standard deviation of 2 years, and u is assumed to be 3.0, t_s and t_e are 5.41 and 17.76 years, respectively, using Equation (5.23). The probability that the damage will occur before 5.41 and 17.76 years is 0.0013 and 0.9987, respectively. The value of u is fixed at 3.0 herein.

5.4.2 Expected Damage Detection Delay when Monitoring is Used

A properly installed structural health monitoring (SHM) system can provide more accurate information about the actual performance of a structure. The quality of the

information to assess and predict the structural performance can vary widely according to the monitoring duration, the type of data collected, the location of sensors, and the number of sensors installed. Under assumptions that the detectability during monitoring duration t_{md} is perfect, and only one monitoring is applied, the expected detection delay $E\left(t_{delay}\right)$ can be formulated based on Equation (5.22) as [Kim and Frangopol 2011b]

$$E\left(t_{delay}\right)=\int_{t_s}^{t_{mon,1}}\left(t_{mon,1}-t\right)\cdot f_T\left(t\right)dt+\int_{t_{mon,1}+t_{md}}^{t_e}\left(t_{insp,e}-t\right)\cdot f_T\left(t\right)dt \tag{5.24}$$

If the damage occurs before monitoring starting time $t_{mon,1}$, the detection delay will be $t_{mon,1} - t$. It is assumed that there will be no detection delay, if the damage occurs during monitoring period (*i.e.*, from $t_{mon,1}$ to $t_{mon,1} + t_{md}$). In addition, if the damage occurs after monitoring period (*i.e.*, $t_{mon,1} + t_{md} \leq t \leq t_e$), damage detection will be delayed until the time $t_{insp,e}$. If monitoring is applied n_{mon} times with the same duration t_{md}, the expected damage detection delay is [Kim and Frangopol 2011b]

$$E(t_{delay})=\sum_{i=1}^{n_{mon}}\left(\int_{t_{mon,i-1}+t_{md}}^{t_{mon,i}}(t_{mon,i}-t)\cdot f_T(t)dt\right)+\int_{t_{mon,n_{mon}}+t_{md}}^{t_e}(t_{insp,e}-t)\cdot f_T(t)dt \tag{5.25}$$

where $t_{mon,i}$ = the ith monitoring starting time. $t_{mon,0} + t_{md}$ for $i = 1$ is associated with the lower bound of damage occurrence time t_s of Equation (5.23a).

5.4.3 Expected Damage Detection Delay when Combined Inspection / Monitoring is Used

When combined inspection / monitoring is used to detect damage, the expected

damage detection delay E (t_{delay}) can be formulated using Equations (5.22) and (5.25). For instance, if one-time inspection and monitoring are used, and the inspection is applied before monitoring (*i.e.*, $t_{mon,1} > t_{insp,1}$) as shown in Figure 5.3, there will be four possible cases according to damage occurrence time: (a) case1: $t_s \le t < t_{insp,1}$; (b) case 2: $t_{insp,1} \le t < t_{mon,1}$; (c) case 3: $t_{mon,1} \le t < t_{mon,1} + t_{md}$; (d) case 4: $t_{mon,1} + t_{md} \le t \le t_e$. The associated expected damage detection delay is formulated as [Kim and Frangopol 2011d]

$$\begin{aligned} E(t_{delay}) = & \int_{t_s}^{t_{insp,1}} [P_{insp,1} \cdot (t_{insp,1} - t) + (1 - P_{insp,1}) \cdot (t_{mon,1} - t)] \cdot f_T(t) dt \\ & + \int_{t_{insp,1}}^{t_{mon,1}} (t_{mon,1} - t) \cdot f_T(t) dt + \int_{t_{mon,1}+t_{md}}^{t_e} (t_{p,e} - t) \cdot f_T(t) dt \end{aligned} \tag{5.26}$$

It should be noted that case 3 is not considered in Equation (5.26), because it is assumed that there is no detection delay during monitoring duration t_{md}. On the contrary, when the inspection is used to detect damage after monitoring (i.e., $t_{mon,1} + t_{md} < t_{insp,1}$), the expected damage detection is [Kim and Frangopol 2011d]

$$\begin{aligned} E\left(t_{delay}\right) = & \int_{t_s}^{t_{mon,1}} \left(t_{mon,1} - t\right) \cdot f_T\left(t\right) dt \\ & + \int_{t_{mon,1}+t_{md}}^{t_{ins,1}} \left[P_{insp,1} \cdot \left(t_{insp,1} - t\right) + \left(1 - P_{insp,1}\right) \cdot \left(t_{insp,e} - t\right)\right] \cdot f_T\left(t\right) dt \\ & + \int_{t_{insp,1}}^{t_e} \left(t_{insp,e} - t\right) \cdot f_T\left(t\right) dt \end{aligned} \tag{5.27}$$

5.5 Inspection and Monitoring Cost

The inspection cost is related to the quality of an inspection method. In general, inspection methods associated with a higher quality are more expensive [Frangopol

et al., 1997b]. In this study, the cost C_{ins} associated with an inspection method is expressed using $\delta_{0.5}$ in Equations (5.15) and (5.18) (i.e., damage intensity at which the inspection method has a probability of detection of 0.5) as [Mori and Ellingwood 1994b]

$$C_{ins} = \alpha_{ins}(1-0.7\delta_{0.5})^{20} \tag{5.28}$$

where α_{ins} is a constant. The total inspection cost C_{INS} for n_{insp} inspections is computed as

$$C_{INS} = \sum_{i=1}^{n_{insp}} \frac{C_{ins}}{(1+r_{dis})^{t_{insp,i}}} \tag{5.29}$$

where r_{dis} = discount rate of money, where $t_{insp,i}$ = the ith inspection time.

The monitoring cost includes initial design, installation, operation and repair cost of the monitoring system [Frangopol and Messervey 2009a and 2009b]. The monitoring cost C_{mon} can be estimated as

$$C_{mon} = C_{mon,ini} + t_{md} \times C_{mon,an} \tag{5.30}$$

where t_{md} = monitoring duration (years); $C_{mon,ini}$ = initial cost of monitoring system consisting of design and installation cost of the monitoring system; $C_{mon,an}$ = annual cost related to operation and repair of the monitoring system. Furthermore, when a structure is monitored n_{mon} times with the same monitoring duration t_{md}, the total monitoring cost is

$$C_{MON} = C_{mon,ini} + \sum_{i=1}^{n_{mon}} \frac{t_{md} \cdot C_{mon,an}}{(1+r_{dis})^{t_{mon,i}}} \tag{5.31}$$

where $t_{mon,i}$ = the ith monitoring starting time.

5.6 Bayesian Updating

When the observed data are limited, inspection results can be used to update systematically an existing information or judgment by using Bayesian techniques, and furthermore the updated results can provide the better prediction. If the parameter υ is a random variable with the PDF $f'(\upsilon)$ and the inspection results provide the likelihood $L(\upsilon)$ of observing the experimental outcome assuming that the value of parameter is υ, the updated (*i.e.*, posterior) PDF $f''(\upsilon)$ of the parameter υ can be obtained as [Ang and Tang 2007]

$$f''(\upsilon) = \frac{L(\upsilon) f'(\upsilon)}{\int_{-\infty}^{\infty} L(\upsilon) f'(\upsilon) d\upsilon} \tag{5.32}$$

Furthermore, the updated mean μ_{υ}'' and standard deviation σ_{υ}'' of a random variable υ are

$$\mu''_{\upsilon} = \int_{-\infty}^{\infty} \upsilon f''(\upsilon) d\upsilon \tag{5.33a}$$

$$\sigma''_{\upsilon} = [\int_{-\infty}^{\infty} (\upsilon - \mu''_{\upsilon})^2 f''(\upsilon) d\upsilon]^{0.5} \tag{5.33b}$$

Enright and Frangopol (1999a and 1999b) investigated the effects of updating corrosion initiation time and rate on time-dependent reliability and optimal lifetime maintenance planning. Based on the procedure provided in Enright and Frangopol (1999a), Bayesian technique is used to consider the effect of updating a parameter associated with prediction of corrosion initiation time on inspection and monitoring planning associated with minimization of the expected corrosion damage detection

delay.

5.7 Application to Existing RC Bridge under Corrosion

5.7.1 Description of E-17-HS

The proposed approach is applied to the existing RC bridge E-17-HS. According to Akgül (2002), E-17-HS is a four span two-lane bridge located over Interstate Highway 25 on 160th Avenue between 144th Avenue and State Highway 7 in Adams County, Colorado. Figure 5.4 shows the cross-sectional view of this bridge. The concrete deck of this bridge is 177.8 mm thick with 38.1 mm thick asphalt pavement. The deck is supported by four RC beams at end spans and four steel plate girders at intermediate spans. The concrete deck at the end spans is 11.28 m long and 10.36 m wide. The space between RC girders at end spans is 2.64m, and each girder has a width of 40.64 cm and a depth of 66.04 cm. More detailed information is given in Akgül (2002), and Marsh and Frangopol (2008). This application focuses on corrosion of top transverse reinforcement bars of the interface between the slab and girders at end spans where the maximum negative moment can occur as shown in Figure 5.4.

5.7.2 Prediction of Reinforcement Area Loss

Corrosion initiation and loss of reinforcement area over time are calculated using Equation (5.3) and Equation (5.4) associated with uniform corrosion model,

respectively. All the variables in Equation (5.3) and (5.4) are assumed to be lognormally distributed. These random variables are summarized in Table 5.1. Monte Carlo simulation (*i.e.*, a sample size of 100,000) is used to predict time-dependent slab reinforcement area as shown in Figure 5.5. PDFs of reinforcement area A_{st} at every 10 years are shown in Figure 5.5(a). PDFs of corrosion initiation time and time for $A_{st} = 0.95A_{init}$, $0.90A_{init}$, $0.85A_{init}$, $0.80A_{init}$ are shown in Figure 5.5(b). From Figure 5.5, it can be seen that the dispersion of reinforcement area A_{st} increases over time. Early detection of corrosion is important to structure managers in order to update the maintenance strategy. Figure 5.6 shows the PDF of lognormal distribution associated with corrosion initiation time. Mean and standard deviation of corrosion initiation time are 3.35 years and 1.61 years (see Figure 5.6), respectively. In this application, corrosion initiation serves as the damage criterion. The PDF in Figure 5.6 is used to formulate the expected damage detection $E(t_{delay})$ of Equations (5.22) and (5.25), and to define the lower-bound t_s and the upper-bound t_e in Equation (23).

5.7.3 Optimum Inspection Plans

In order to establish a cost-effective maintenance strategy for a deteriorating RC structure, the degree of corrosion damage should be predicted as accurately as possible. However, since there are uncertainties related to the prediction of structural performance, inspection should be applied according to an optimized schedule

considering uncertainties associated with damage occurrence/propagation and quality of inspection. The quality of inspection depends on the inspection methods and the number of inspection readings. In order to measure the damage intensity of a deteriorating RC deck, visual inspection, non-destructive testing including half-cell potential, radiographic, and ultrasonic tests can be applied.

As the damage detection delay increases, the probability of damage detection increases due to the increase of damage propagation during the delay. For example, if the damage (e.g., corrosion) has occurred at time t ($T_{corr} = t < t_{insp,1} < t_{insp,2}$), the degree of corrosion damage $\delta_c(t_{insp,1})$ at the time of first inspection $t_{insp,1}$ will be less than the degree of damage $\delta_c(t_{insp,2})$ at the time of second inspection $t_{insp,2}$. Therefore, according to Equations (5.13) and (5.15), the probability of detection $P_{insp,c,1}$ at time $t_{insp,1}$ is less than the probability of detection $P_{insp,c,2}$ at time $t_{insp,2}$. For this reason, the detectability function $P_{insp,c,i}(\delta)$ for the ith inspection at time $t_{insp,i}$ in Equation (5.15) is applied for formulation of the expected damage detection delay $E(t_{delay})$ in Equation (5.22), considering the effect of corrosion damage propagation between time for damage to occur and time to detect corrosion. The standard deviation $\sigma_{c,\delta}$ in Equation (5.15) is assumed to be $0.1\,\delta_{c,0.5}$ [Frangopol et al. 1997b].

In this application, inspection planning is formulated as an optimization problem by minimizing the expected damage detection delay $E(t_{delay})$ as follows

$$\text{Find} \qquad \mathbf{t_{insp}} = \{t_{insp,1}, t_{insp,2}, \ldots, t_{insp,i}, \ldots, t_{insp,nisnp}\} \tag{5.34}$$

to minimize $E(t_{delay})$ (5.35)

such that $t_s < t_{insp,1} < t_{insp,2} < \cdots < t_{insp,i} < \cdots < t_{insp,n_{insp}} < t_e$ (5.36a)

$t_{insp,i} - t_{insp,i-1} \geq 1$ year (5.36b)

given n_{insp}, $\delta_{c,0.5}$ and $f_T(t)$ (5.37)

where $\mathbf{t_{insp}}$ = vector of design variables (*i.e*, inspection times), t_s = lower-bound of damage occurrence time (years), t_e = upper-bound of damage occurrence time (years), $t_{insp,i}$ = *i*th inspection time (years) among n_{insp} inspections, and $\delta_{c,0.5}$ = corrosion damage intensity at which the given inspection method has 50% probability of detection as indicated in Equation (5.15). With the given PDF of the damage occurrence time $f_T(t)$ (see Figure 5.6), t_s and t_e in Equation (5.36a) are obtained from Equation (5.23). Based on Equation (5.22), $E(t_{delay})$ associated with a given number n_{insp} of inspections is the objective function of this optimization problem. In this application, $t_{insp,e}$ in Equation (5.21) is assumed to be equal to t_e. In order to solve the optimization problem, the toolbox (*i.e.*, constrained nonlinear minimization) provided in MATLAB® version R2009a [MathWorks Inc. 2009] was used. The objective is to minimize the expected delay $E(t_{delay})$ from the corrosion initiation time to time for corrosion to be detected by inspections. The design variables are the inspection times $t_{insp,1}$, $t_{insp,2}$,…, $t_{insp,ninsp}$ in Equation (5.34), and the constraints are indicated in Equation (5.36). The PDF of the corrosion initiation time in Figure 5.6 is used as the given PDF $f_T(t)$ in Equation (5.37). The time interval between inspections is assumed to be at least one year as indicated in Equation

(5.36b).

The effects of number of inspections and inspection quality on the minimum expected corrosion damage detection delay are plotted in Figure 5.7(a). The relation between minimum expected damage detection delay $E(t_{delay})$ and the total inspection cost C_{INS} is shown in Figure 5.7(b), and the total inspection cost C_{INS} is computed using Equation (5.29) without considering discount rate of money. α_{ins} in Equation (5.28) is assumed 7. Figures 5.8(a) and 5.8(b) show the optimal plans for inspection method associated with $\delta_{c,0.5}$ = 0.01 and 0.05. The values of design variables objectives, and the cost associated with each optimum inspection plan are provided in Tables 5.2.

If two inspections with $\delta_{c,0.5}$ = 0.05 is used to detect corrosion, the inspections should be performed at 4.46 and 6.71 years as shown in Figure 5.8(b). The associated expected damage detection delay $E(t_{delay})$ and cost C_{INS} are 2.51 years and 6.87 (see Figures 5.7(a), 5.8(b) and Table 5.2). If the number of inspection increases twice (i.e., four inspections), the inspections have to be applied at 3.61 years, 4.64 years, 5.90 years, and 7.81 years, and $E(t_{delay})$ is 1.89 years (see Figures 5.7(a), 5.8(b) and Table 5.2). Furthermore, if a three-time inspection with higher probability of damage detection (i.e., $\delta_{c,0.5}$ = 0.01) is applied, the inspections should be performed at 3.05 years, 4.50 years and 6.68 years as shown in Figure 5.8(a). In this case, as indicated in Table 5.2, the associated $E(t_{delay})$ and C_{INS} are 1.25 years and 18.25, respectively.

From these results, it can be seen that an increase in the number of inspections leads to reduction of the minimum $E(t_{delay})$ and increase of the total inspection cost C_{INS}. Also, the minimum $E(t_{delay})$ decreases with improving the quality of inspection. It is noted that the values of the lower and upper bounds t_s and t_e, respectively, depend on the PDF of the corrosion initiation time (see Figure 5.6) as indicated in Equation (5.23) rather than the number of inspections or quality of inspection.

5.7.4 Optimum Monitoring Plans

The optimum design process of corrosion monitoring includes decisions on (a) types of sensors, (b) location and number of sensors, and (c) operating duration of sensors. In order to detect corrosion, a special macrocell system (*i.e.*, anode-ladder-system) can be used, which indicate the critical depth of the reinforcement of a concrete deck with respect to corrosion [Raupach and Schießl 2001]. Furthermore, measurement of the corrosion rate of the reinforcement is useful to estimate and predict the area of the reinforcement. The most extensively used method for determining corrosion rates of the deteriorating reinforcement is the linear polarization resistance (LPR) measurement [Qian, 2005]. This chapter focuses on the optimum monitoring planning under assumptions that sensors are properly installed to detect the corrosion damage and, as mentioned previously, the probability of corrosion damage detection during monitoring duration is perfect.

The formulation of the optimization problem to minimize the expected damage

detection delay $E(t_{delay})$ in Equation (5.25) is as follows

$$\text{Find} \quad \mathbf{t_{mon}} = \{t_{mon,1}, t_{mon,2}, \ldots, t_{mon,i}, \ldots, t_{mon,nmon}\} \tag{5.38}$$

$$\text{to minimize} \quad E(t_{delay}) \tag{5.39}$$

$$\text{such that} \quad t_{mon,i+1} - t_{mon,i} > t_{md} \tag{5.40a}$$

$$t_s < t_{mon,1}; \;\; t_e - t_{mon,m} > t_{md} \tag{5.40b}$$

$$\text{given} \quad n_{mon}, \;\; t_{md} \;\; \text{and} \; f_T(t) \tag{5.41}$$

where $\mathbf{t_{mon}}$ = vector of design variables (*i.e.*, monitoring starting times), $t_{mon,i}$ = ith monitoring starting time (years) (i = 1, 2, ..., n_{mon}), t_{md} = given monitoring duration (years), and n_{mon} = given total number of monitoring actions. t_s and t_e are the lower and upper bounds of damage occurrence time t (years), respectively, and are obtained from the given PDF $f_T(t)$ (see Equation 5.23), where the PDF of corrosion initiation time $f_T(t)$ is defined in Figure 5.6. The objective function $E(t_{delay})$ with a given number n_{mon} of monitoring actions can be formulated using Equation (5.25).

Optimal monitoring plans to detect the corrosion with the minimum expected detection delay $E(t_{delay})$ are provided in Figures 5.9 and 5.10 and Table 5.3. Figure 5.9(a) shows the effects of monitoring duration and number of monitorings on the minimum $E(t_{delay})$. Figure 5.9(b) shows the effects of monitoring durations on the interaction between the total monitoring cost C_{MON} and the minimum $E(t_{delay})$. C_{MON} is estimated using Equations (5.30) and (5.31). The discount rate of money r_{dis} in Equation (5.31) is not considered in this application. $C_{mon,ini}$ and $C_{mon,an}$ in Equation

(5.30) are assumed to be 10. The optimal monitoring plans associated with the monitoring durations t_{md} = 0.1 year and t_{md} = 1.0 year are shown in Figures 5.10(a) and 5.10(b), respectively. If two monitorings with the same monitoring duration t_{md} = 0.1 year are performed, the starting times of the first and second monitoring actions, in order to minimize the expected delay from the corrosion initiation time to the time for the corrosion to be detected, has to be 3.31 years and 5.74 years, respectively (see Figure 5.10(a) and Table 5.3). It means that the first monitoring should be conducted from 3.31 to 3.41 years, and the second monitoring from 5.74 to 5.84 years. The associated $E(t_{delay})$ and C_{MON} are 1.37 years and 12, respectively (see Figures 5.9(a) and 5.9(b), and Table 5.3). It can be seen that increases of number of monitoring actions and monitoring duration result in reduction of the minimum $E(t_{delay})$ and increase of C_{MON}.

5.7.5 Effect of Inspection Updating

If the additional information on the surface chloride concentration $C_{ch,o}$ in Equation (5.2) is available, the corrosion initiation time of reinforcement can be predicted more accurately by incorporating the additional information into the existing information. For illustrative purposes, suppose that an inspection is performed before making monitoring planning, and the surface chloride concentration $C_{ch,o}$ measured from this inspection is lognormally distributed with a mean of $\mu_{Cch,o}$ of 0.20 g/mm^3 and the standard deviation of $\sigma_{Cch,o}$ of 0.020 g/mm^3. This additional information

can be used for updating by Bayesian techniques. The PDF of the updated chloride concentration in Figure 5.11(a) is computed by using Equation (5.32). Based on the prior, inspected and updated chloride concentration, the corrosion initiation time of reinforcement area of the RC deck can be predicted as shown in Figure 5.11(b).

The optimal inspection and monitoring plans to minimize the expected detection delay, from the corrosion initiation time to time for corrosion to be detected, can be computed using the PDFs in Figure 5.11(b). The effects of updating surface chloride concentration $C_{ch,o}$ and number of inspections on the minimum expected detection delay $E(t_{delay})$ are shown in Figure 5.12(a). The optimum inspection plans associated with the prior, inspection, and updated PDFs in Figure 5.11(b) are presented in Figure 5.12(b) for the three-time inspection with $\delta_{c,0.5} = 0.03$. For the optimum monitoring planning for corrosion detection, the effects of updating surface chloride concentration on the minimum $E(t_{delay})$ are shown in Figure 5.13(a). The optimal monitoring plans are illustrated in Figure 5.13(b), when the three-time monitoring with the duration $t_{md} = 0.5$ year are applied. It is interesting to note that the standard deviation of corrosion initiation time has a dominant effect on the minimum $E(t_{delay})$.

5.7.6 Optimum Balance of the Expected Damage Detection Delay and Cost

The increase of number of inspections as well as the increase of inspection quality is necessary to reduce the expected damage detection delay. However, this increase

needs additional financial resources. In order to deal with these two conflicting criteria, a bi-objective optimization is applied by simultaneously minimizing both the inspection cost and the expected damage detection delay. The bi-objective optimization problem for optimum inspection planning is formulated as

Find $\mathbf{t_{insp}} = \{t_{insp,1}, t_{insp,2}, \dots, t_{insp,i}, \dots, t_{insp,ninsp}\}$, (5.42)

n_{insp}, and $\delta_{c,0.5}$

to minimize both $E(t_{delay})$ and C_{INS} (5.43)

such that $t_s < t_{insp,1} < t_{insp,2} < \cdots < t_{insp,i} < \cdots < t_{insp,n_{insp}} < t_e$ (5.44a)

$t_{insp,i} - t_{insp,i-1} \geq 1$ year ; $n_{insp} = 1, 2, ..., 5$ (5.44b)

$0.01 \leq \delta_{c,0.5} \leq 0.1$ (5.44c)

given $f_T(t)$ (5.45)

In the bi-objective optimization problem, the design variables are the inspection times $t_{insp,1}$, $t_{insp,2}$,…, $t_{insp,ninsp}$, the number of inspections n_{insp}, and $\delta_{c,0.5}$ as indicated in Equation (5.42). The constraints are provided in Equation (5.44). The total inspection cost C_{INS} is computed using Equation (5.29), as indicated previously. The PDF of corrosion initiation time $f_T(t)$ in Figure 5.6 is used as given in Equation (5.45). In order to find the Pareto optimal solution set of this bi-objective optimization problem, NSGA-II (Non-Dominated Sorting Genetic Algorithms) program developed by Deb et al. (2002) is used. An initial population of 1000 is considered, and the maximum number of generations is fixed at 200. Crossover and mutation operations are used with respective probabilities of 80% and 20%,

respectively.

The Pareto optimal solution set associated with minimization of both $E(t_{delay})$ and C_{INS} is shown in Figure 5.14(a). Optimum values of design variables and the associated $E(t_{delay})$ and C_{INS} for solutions $A_{c,1}$, $A_{c,2}$, $A_{c,3}$, and $A_{c,4}$ in Figure 5.14(a) are provided in Figure 5.14(b) and Table 5.4. For solution $A_{c,4}$ in Figure 5.14(a), the associated $E(t_{delay})$ and C_{INS} are 2.96 years and 5, respectively. The inspection plan for solution $A_{c,4}$ requires two-time inspection with $\delta_{c,0.5} = 0.072$. If solution $A_{c,1}$ instead of solution $A_{c,4}$ is selected as an inspection plan, $E(t_{delay})$ is reduced by 70% (*i.e.*, from 2.96 to 0.89), but the cost has to increase six times (*i.e.*, from 5 to 30) (see Table 5.4).

5.8 Application to Ship Hull Structures Subjected to Fatigue

5.8.1 Description of a Ship Hull Structure

The proposed approach is applied to ship hull as shown in Figure 5.15. In this application, the joint between bottom plate and longitudinal plate is considered as a critical location subjected to fatigue. Under longitudinal loading and unloading, the crack in the plate can initiate on the edge connected to the stiffener and propagate away from the stiffener in the transverse direction as shown in Figure 5.15.

5.8.2 Time-Dependent Crack Growth

Crack length over time and time for a given crack length are calculated using

Equations (5.11) and (5.12), respectively. Initial crack length a_o, annual stress cycles N_{an}, and material crack growth parameter C are assumed lognormally distributed random variables. The stress range S_{sr} is treated as a random variable with a Weibull PDF [Madsen et al. 1991]. Herein mean value of material parameter C is assumed to be 3.54×10^{-11}, and m is assumed 2.54 for high yield steel (HY80) [Dobson et al. 1983]. Descriptors of variables in Equations (5.11) and (5.12) are given in Table 5.5. In this application, the geometry function $Y(a)$ is assumed to be one [Madsen et al. 1991, Akpan et al., 2002]. Monte Carlo simulation with sample size of 100,000 is used to predict the crack length over time. Figure 5.16(a) shows the mean and standard deviation of time t associated with crack length a, and PDFs of time for a = 10, 20, 30, and 40 *mm*. From this figure, it can be seen that after the crack size of around 1 *mm*, the crack size increases at a very high rate. In this application, the crack size of 1.0 *mm* serves as the crack damage criterion. It means that if the crack size is larger than 1 *mm*, the target structural component for inspection is in damaged state, and therefore the minimum crack length a_{min} for fatigue damage intensity of Equation (5.19) becomes 1.0 *mm*. The maximum crack length a_{max} in Equation (5.19) is assumed to be 50 *mm* herein. Figure 5.16(b) shows the PDF of fatigue damage occurrence time (*i.e.*, time for crack length to reach 1.0 *mm*) obtained from Monte Carlo simulation and the best fitted PDF (i.e., Generalized Extreme Value (GEV) PDF defined in Equation (3.14)). The associated values of parameters ξ_{par}, ρ_{par} and λ_{par} are 0.15, 1.65 and 3.21, respectively, as shown in Figure 5.16(b). This GEV PDF

is used to formulate the expected damage detection delay in Equation (5.22). Based on this PDF, t_s and t_e are obtained as 0.51 and 21.95 years, respectively (see Equation (5.23)).

5.8.3 Optimum Inspection Plans

After fatigue damage has been occurred, the crack length grows so that the probability of detection will increase. In other words, as the damage detection delay increases, the probability of detection increases. Since the variables associated with the crack growth model are not deterministic, the probability of detection in terms of crack length a at time t is random. In order to formulate the expected damage detection delay $E(t_{delay})$ in Equation (5.22), the expected probability of detection using Equation (5.18) is applied herein. Figure 5.17 shows the expected probability of detection over time after crack damage occurrence (i.e., time for crack length a to be larger than a_{min}) for three inspections with $\delta_{f,0.5}$ = 0.01, 0.03, and 0.05. As indicated in Equation (5.21) and Figure 5.2, $t_{insp,e}$ is associated with the time when the damage can be detected with perfect detectability. In this application, $t_{insp,e}$ is defined as

$$t_{insp,e} = t_e + t_p \tag{5.46}$$

where t_e = upper-bound of damage occurrence time as indicated in Equation 5.23(b), and t_p = time associated with the expected probability of detection of 0.999 after damage occurrence. When the inspection method with $\delta_{f,0.5} = 0.01$ is used, t_p will be

9.74 years when the damage is detected with the expected probability of detection of 0.999 as shown in Figure 5.17. Therefore, $t_{insp,e}$ for $\delta_{f,0.5} = 0.01$ is 31.69 years, since the upper-bound of damage occurrence time t_e is 21.95 years as mentioned previously.

In this chapter, inspection planning is formulated as an optimization problem by minimizing the expected fatigue damage detection delay $E(t_{delay})$ in Equation (5.22) with a given number n_{insp} of inspections as follows

$$\text{Find} \qquad \mathbf{t_{insp}} = \{t_{insp,1}, t_{insp,2}, \ldots, t_{insp,i}, \ldots, t_{insp,ninsp}\} \tag{5.47}$$

$$\text{to minimize} \qquad E(t_{delay}) \tag{5.48}$$

$$\text{such that} \qquad t_{insp,i} - t_{insp,i-1} \geq 1 \text{ year} \tag{5.49}$$

$$\text{given} \qquad n_{insp},\ \delta_{f,0.5},\ f_T(t) \tag{5.50}$$

where $\mathbf{t_{insp}}$ = vector consisting of n_{insp} design variables of inspection times; $t_{insp,i}$ = ith inspection time (years); and $\delta_{f,0.5}$ = fatigue damage intensity at which the given inspection method has 50% probability of detection. The objective is to minimize the expected time delay $E(t_{delay})$ from the crack damage initiation to time for the crack to be detected by inspections. The time interval between inspections is assumed to be at least one year (see Equation (5.49)). The times $t_{insp,0}$ (for i = 1) and $t_{insp,n+1}$ (for i = n_{insp} + 1) are t_s and $t_{insp,e}$, respectively, as indicated in Equation (5.22). The number of inspections, $\delta_{f,0.5}$ representing the quality of inspection, and PDF of the fatigue damage occurrence time $f_T(t)$ in Figure 5.16(b) are given (see Equation (5.50)).

The optimization toolbox (*i.e.*, constrained nonlinear minimization) provided in MATLAB® version R2009a [MathWorks Inc. 2009] was used to solve this problem.

Figure 5.18 shows the effects of (a) number of inspections and (b) total inspection costs on minimum expected damage detection delay $E(t_{delay})$ for $\delta_{f,0.5} = 0.01$, $\delta_{f,0.5} = 0.03$, and $\delta_{f,0.5} = 0.05$. The total inspection cost C_{INS} is computed using Equations (5.28) and (5.29), where α_{ins} is assumed 5, and the discount rate of money r_{dis} is not considered in this application. It should be noted that the inspection associated with time $t_{insp,e}$ in Equation (5.46) is not accounted in the number of inspections.

The optimal inspection plans associated with the number of inspections $n_{insp} = 1$, 3, and 5 are shown in Figure 5.19. If one time inspection with $\delta_{f,0.5} = 0.03$ is used to detect fatigue crack damage, the inspection has to be performed at 11.90 years as shown in Figure 5.19(a). The associated $E(t_{delay})$ and C_{INS} are 9.74 years and 3.27, respectively (see Figure 5.18(b)). If the number of inspection increases three times (i.e., the number of inspection $n_{insp} = 3$), the inspections should be applied at 7.66, 10.62, and 16.67 years, and $E(t_{delay})$ will be 5.66 years (see Figure 5.19(b)). Furthermore, if three inspections with $\delta_{f,0.5} = 0.01$ instead of $\delta_{f,0.5} = 0.03$ is used, $E(t_{delay})$ will be reduced by 36% (i.e., from 5.66 to 3.62 years), but the total inspection cost C_{INS} will increase by 33% (i.e., from 9.81 to 13.03), as shown in Figure 5.18(b). The associated optimum inspection times will be 5.64, 8.35, and 13.51 years (see Figure 5.19(b)). From these results, it can be seen that reduction of

the minimum $E(t_{delay})$ results from increase in the number and/or the quality of inspections. Through comparison among the optimum inspection times associated with $\delta_{f,0.5}$ = 0.01, 0.03 and 0.05, it can also be seen that the inspection with higher quality (i.e., smaller value of $\delta_{f,0.5}$) can be applied earlier than the inspection with lower quality (i.e., larger value of $\delta_{f,0.5}$), in order to minimize $E(t_{delay})$.

5.8.4 Optimum Balance of the Expected Damage Detection Delay and Cost

Well-balanced inspection planning should be considered as a solution of a two conflicting criteria optimization problem by simultaneously minimizing both the expected damage detection delay and/or the total inspection cost. In this application, optimum balanced inspection planning is obtained, when (a) same type and (b) different types of inspections are used. NSGA-II [Deb et al. 2002] is used, in order to find the Pareto optimal solution set of this bi-objective optimization problem.

Optimum balance when same type of inspection is applied

When same type of inspection (i.e., constant $\delta_{f,0.5}$) is applied n_{insp} time, the bi-objective optimization problem for inspection planning is formulated as

Find $\mathbf{t_{insp}} = \{t_{insp,1}, t_{insp,2}, \ldots, t_{insp,i}, \ldots, t_{insp,,ninsp}\}$, (5.51)

and $\delta_{f,0.5}$

to minimize both $E(t_{delay})$ and C_{INS} (5.52)

such that $t_{insp,i} - t_{insp,i-1} \geq 1$ year (5.53a)

$$t_{insp,1} \leq \text{ 20 years} \tag{5.53b}$$

$$0.01 \leq \delta_{f,0.5} \leq 0.1 \tag{5.53c}$$

given n_{insp}, $f_T(t)$ (5.54)

In this bi-objective optimization problem, the objectives are minimization of both the expected damage detection delay $E(t_{delay})$ and the total inspection cost C_{INS}. The design variables are the vector of inspection times $\mathbf{t_{insp}}$, and $\delta_{f,0.5}$. As indicated in Equation (5.53), time interval between inspections should be at least one year, and application of the first inspection is required within 20 years. The value of $\delta_{f,0.5}$ has to be in the interval 0.01 to 0.1. $f_T(t)$ in Figure 5.16(b) and number of inspections n_{insp} are used as given as indicated in Equation (5.54).

Through the generic algorithm (GA) process with 200 generations, a Pareto set of 100 solutions for n_{insp} = 1 is obtained as shown in Figure 5.20(a). The relations between design variables (i.e., first inspection time $t_{insp,1}$ and $\delta_{f,0.5}$) for solutions $A_{f,1}$, $A_{f,2}$, $A_{f,3}$,$A_{f,4}$ and $A_{f,5}$ are also illustrated in Figure 5.20(a). The expected damage detection delay $E(t_{delay})$ of solutions $A_{f,1}$ to $A_{f,5}$ decreases from 13.21 to 7.09 years with decrease of both $\delta_{f,0.5}$ (from 0.1 to 0.01) and $t_{insp,1}$ (from 15.27 to 9.35), respectively. Accordingly, the associated total inspection cost C_{INS} increases from 1.17 to 4.35. Figure 5.20(b) shows Pareto optimum solution sets for n_{insp} = 1, 2, 3, 4 and 5.

In order to find the final Pareto front considering the number of inspections n_{insp} as a design variable, ε-constraint approach, based on the Pareto solution sets for n_{insp}

= 1 to 5 in Figure 5.20(b), can be used. In this approach, multi-criteria optimization problem is transformed into a single objective optimization problem by selecting one of the objectives to be minimized and treating other objective functions as constraints [Haimes et al. 1971]. The general formulation of ε-constraint approach is [Arora 2004]

$$\text{Minimize} \qquad f_i \tag{5.55}$$

$$\text{subject to} \qquad f_j \le \varepsilon_j \text{ for all } j = 1, 2, \ldots, k; \quad j \ne i \tag{5.56}$$

where $i \in \{1, 2, \ldots, k\}$. The number of objective functions k is equal to 2, and $f_i = f_1$ is the expected damage detection delay $E(t_{delay})$, and $f_j = f_2$ is the total inspection cost C_{INS}. By changing the value of ε_j from the minimum value of f_2 (i.e., 1.17) to the maximum value of f_2 (i.e., 21.72), the final Pareto front of the Pareto solution sets for n_{insp} = 1 to 5 in Figure 5.20(b) is obtained as shown in Figure 5.20(c). The optimum inspection times for solution $B_{f,1}$, $B_{f,2}$, $B_{f,4}$, and $B_{f,6}$ in Figure 5.20(c) are provided in Table 5.6 and Figure 5.20(d). For Pareto point $B_{f,4}$, the associated $E(t_{delay})$ and C_{INS} are 4.55 years and 8.69, respectively (see Table 5.6). The inspection plan for solution $B_{f,4}$ requires two inspections with $\delta_{f,0.5}$ = 0.01 as shown in Figure 5.20(d). If Pareto solution $B_{f,6}$ instead of solution $B_{f,4}$ is selected as an inspection plan, the number of inspections has to increase twice (i.e., from 2 to 4), C_{INS} should also increase twice, but $E(t_{delay})$ will be reduced from 4.55 to 3.15 years (see Table 5.6). It should be noted that solutions $B_{f,3}$, $B_{f,5}$ and $B_{f,7}$ in Figure 5.20(c) are the same as the solutions associated with n_{insp} = 1; $\delta_{f,0.5}$ = 0.01 in Figure 5.19(a), n_{insp} = 3; $\delta_{f,0.5}$ = 0.01 in

Figure 5.19(b), and $n_{insp} = 5$; $\delta_{f,0.5} = 0.01$ in Figure 5.19(c), respectively.

Optimum balance when different inspection types are applied

When different inspection types are applied (i.e., $\delta_{f,0.5}$ is not the same), the formulation of the bi-objective optimization problem is

Find $\mathbf{t_{insp}} = \{t_{insp,1}, t_{insp,2}, \ldots, t_{insp,i}, \ldots, t_{insp,,ninsp}\}$, (5.57)

and $\boldsymbol{\delta_{f,0.5}} = \{\delta_{f,0.5,1}, \delta_{f,0.5,2}, \ldots, \delta_{f,0.5,i}, \ldots, \delta_{f,0.5,ninsp}\}$

to minimize both $E(t_{delay})$ and C_{INS} (5.58)

As indicated, the constraints and given condition of this problem are identical with those in Equations (5.53) and (5.54). A Pareto set of 100 solutions is obtained after 500 generations. Figure 5.21 shows Pareto solution sets based on both same type (i.e., case 1 in Figure 5.21(a) and case 3 in Figure 5.21(b)) and different types (i.e., case 2 in Figure 5.21(a) and case 4 in Figure 5.21(b)) of inspections. Optimum values of design variables and the associated $E(t_{delay})$ and C_{INS} for Pareto solutions in Figure 5.21 are provided in Table 5.7. Solutions $C_{f,1}$, $C_{f,4}$, and $D_{f,5}$ in Figure 5.21 are the same as $B_{f,2}$, $B_{f,4}$, and $B_{f,5}$ in Figure 5.20(c), respectively. As shown in Table 5.7 and Figures 5.21(a) associated with number of inspections $n_{insp} = 2$, solutions $C'_{f,2}$ of case 1 and $C_{f,2}$ of case 2 have the same $E(t_{delay})$ (i.e., 7.92 years), but if solution $C_{f,2}$ instead of $C'_{f,2}$ is selected as an inspection plan, the total inspection cost can be reduced by 19% (*i.e.*, from 4.93 to 4.13). Similarly, in Figure 5.21(b) associated with $n_{insp} = 3$, solutions $D_{f,2}$ (of case 4) and $D'_{f,2}$ (of case 3) have the same $E(t_{delay})$, but

$D_{f,2}$ requires less cost than $D'_{f,2}$. From these comparisons between Pareto solution sets of cases 1 and 2 (or cases 3 and 4), it can be seen that the inspection plan based on different inspection types will require less cost than the inspection plan based on the same type of inspection for given expected damage detection delay. As indicated in Table 5.7, Pareto solutions $C_{f,1}$ and $C_{f,3}$ have $\delta_{f,0.5,1}$ = 0.10 and 0.01, respectively, while having the same $\delta_{f,0.5,2}$ = 0.10. The values of $\delta_{f,0.5,1}$ for solutions $C_{f,3}$ and $C_{f,4}$ are the same (i.e., 0.01), but $\delta_{f,0.5,2}$ for $C_{f,3}$ and $C_{f,4}$ are 0.10 and 0.01, respectively.

Furthermore, the Pareto solution sets of the bi-objective optimization problem for n_{insp} = 1, 4, 5 are obtained. The ε-constraint approach (see Equations (55) and (56)) based on Pareto solution sets for n_{insp} = 1 to 5 provides the final Pareto front as shown Figure 5.22(a). Values of objective functions and design variables for solutions $E_{f,1}$ to $E_{f,7}$ are provided in Table 5.8. As indicated in this table, values of objective functions and design variables for solutions $E_{f,1}$, $E_{f,3}$ and $E_{f,5}$ in Figure 5.22(a) are identical to those of solutions $B_{f,1}$, $B_{f,2}$ and $B_{f,4}$ in Figure 5.20(c), respectively. In the final Pareto front , solution $E_{f,1}$ needs the lowest total inspection cost C_{INS} of 1.17, but leads to the largest expected damage detection delay $E(t_{delay})$ of 13.21 years. In contrast, solution $E_{f,7}$ requires the highest inspection cost C_{INS} of 17.38, while results in the least expected damage detection delay $E(t_{delay})$ of 3.15 years. It should be noted that there is no solution associated with n_{insp} = 5. When the discount rate of money r_{dis} = 3 %/year for the total inspection cost in Equation (5.29) is applied, the final Pareto front is presented in Figure 5.22(b). Table 5.8 provides

values of objective functions and design variables for solutions $F_{f,1}$ to $F_{f,5}$. Solution $F_{f,4}$ in Figure 5.22(b) has the same expected damage detection delay (i.e., $E(t_{delay})$ = 4.55 years) as that of solution $E_{f,5}$ in Figure 5.22(a). However, the total inspection cost C_{INS} associated with solution $F_{f,4}$ is less than that of solution $E_{f,5}$ as indicated in Table 5.8 and Figure 5.22. It can be seen that for given expected damage detection delay, the inspection plan considering discount rate of money requires less cost than that without consideration of discount rate. Among the final Pareto solution set with r_{dis} = 3 %/year, solution $F_{f,5}$ requires the highest inspection cost C_{INS} of 11.53, leading to the least expected damage detection delay $E(t_{delay})$ of 3.63 years.

5.9 Combined Inspection / Monitoring Planning

5.9.1 Bi-Objective Optimization Formulation for Combined Inspection / Monitoring Planning

If both inspection and monitoring are used to detect damage, and the available number N of inspection n_{insp} and/or monitorings n_{mon} is equal to 2 (*i.e.*, $N = n_{insp} + n_{mon} = 2$), then there will be four possible cases (inspection followed by inspection, inspection followed by monitoring, monitoring followed by inspection, and monitoring followed by monitoring) as shown in Figure 5.23(a). The event tree in Figure 5.23(a) is used to consider all possible cases (I, II, III, and IV) associated with inspection or monitoring. Every case has its own bi-objective optimization problem. Each bi-objective optimization problem consists of its own design variables, and

produces a Pareto solution set. For example, the design variables of case I in Figure 5.23(a) are inspection times (i.e., $t_{insp,1}$ and $t_{insp,2}$), and inspection quality represented by $\delta_{0.5}$ as indicated in Table 5.9. The objective functions associated with this case are the expected damage detection delay $E(t_{delay})$ of Equation (5.22) and the total inspection cost C_{INS} of Equation (5.29), when the number of inspections $n_{insp} = 2$. For this case, the total cost C_{COM} (i.e., $C_{INS} + C_{MON}$) is equal to C_{INS}, since there is no monitoring (i.e., $C_{COM} = 0$). For case IV in Figure 5.23(a), the bi-objective optimization problem is formulated by selecting the design variables as monitoring times (i.e., $t_{mon,1}$ and $t_{mon,2}$) and monitoring duration t_{md} (see Table 5.9). The associated objective functions are indicated in Equations (5.25) and (5.31) for $n_{mon} = 2$. Pareto fronts corresponding to the four cases can be obtained after solving bi-objective optimization problems as shown in Figure 5.23(b). Based on these four Pareto solution sets, the final Pareto solution set can be determined. This Pareto solution set $\boldsymbol{PS}_N$ for $N = 2$ will provide the sequence of inspections and monitorings (i.e., inspection followed by inspection, inspection followed by monitoring, monitoring followed by inspection, or monitoring followed by monitoring) as well as inspection and/or monitoring times, and inspection quality, and monitoring durations. This procedure to determine the Pareto solution set $\boldsymbol{PS}_N$ for a given number of inspections and/or monitorings N can be extended to find the final Pareto solution set $\boldsymbol{PS}$ when the available number of inspections and/or monitorings N ranges from 1 to N_{max}. Figure 5.24 and Figure A.4 in Appendix provides such flowchart to find the

final Pareto solution set ***PS***. The final Pareto solution set ***PS*** will provide the number of inspections and/or monitorings, the sequence of inspections and monitorings, the inspection and/or monitoring times, inspection quality, and monitoring duration.

5.9.2 Application to a Naval Ship Hull Structure Subjected to Fatigue

The proposed approach is applied to a naval ship hull structure. As shown in Figure 5.15, a critical location subjected to fatigue is assumed to be the joint between longitudinal plate and bottom plate. The variables associated with the prediction of crack size (see Equations (5.11) and (5.12)) are provided in Table 5.10. Figure 5.25 shows the PDF of fatigue damage initiation (i.e., a_{min} = 1.0 *mm*) time obtained from Monte Carlo simulation with 100,000 samples and its best fitted PDF (i.e., GEV PDF defined in Equation (3.14)). The lower and upper bounds of damage occurrence time (i.e., t_s and t_e in Equation (5.23)) are 0.41 and 17.56 years, respectively.

When the available number of inspections and/or monitorings is N = 2, there will be four cases. Each case has its own bi-objective optimization formulation as mentioned previously (see Figure 5.23 and Table 5.9). The bi-objective optimization formulations of these four cases are formulated as

Find $t_{insp,1}$, $t_{insp,2}$, and $\delta_{f,0.5}$ for case I (5.59a)

$t_{insp,1}$, $t_{mon,1}$, $\delta_{f,0.5}$, and t_{md} for cases II and III (5.59b)

$t_{mon,1}$, $t_{mon,2}$, and t_{md} for case IV (5.59c)

to minimize both $E(t_{delay})$ and C_{COM} (5.60)

such that $t_{insp,2} - t_{insp,1} \geq 1$ year; and for case I (5.61a)

$0.01 \leq \delta_{f,0.5} \leq 0.1$

$t_{mon,1} - t_{insp,1} \geq 1$ year; for case II (5.61b)

$0.01 \leq \delta_{f,0.5} \leq 0.1$; and

$0.3 \leq t_{md} \leq 1.0$ year

$t_{insp,1} - t_{mon,1} \geq 1$ year; for case III (5.61c)

$0.01 \leq \delta_{f,0.5} \leq 0.1$;and

$0.3 \leq t_{md} \leq 1.0$ year

$t_{mon,2} - t_{mon,1} \geq 1$ year, and for case IV (5.61d)

$0.3 \leq t_{md} \leq 1.0$ year

given $N = n_{insp} + n_{mon} = 2$, and $f_T(t)$ (5.62)

The design variables and constraints of the bi-objective optimization formulations for cases I, II, III, and IV are indicated in Equations (5.59) and (5.61), respectively. The objectives are to minimize both $E(t_{delay})$ and C_{COM}. The GEV PDF $f_T(t)$ in Figure 5.25 indicated in Equation (5.26) is used to formulate $E(t_{delay})$. NSGA-II program [Deb et al. 2002] is used to find the Pareto optimal solution set of the bi-objective optimization formulations in Equations (5.59) to (5.62). In order to estimate the inspection and/or monitoring cost, Equations (5.29) and (5.31) are used with the assumptions that α_{ins} in Equation (5.28) is 5, $C_{mon,ini}$ and $C_{mon,an}$ in Equation (5.30) are assumed 10 and 20, respectively.

The GA process with 500 generations provides Pareto solutions sets for cases I,

II, III, and IV as shown in Figure 5.26(a). $\boldsymbol{PS_{N,n}}$ denotes a Pareto set of nth case when available number of inspections and/or monitorings is N. For example, $\boldsymbol{PS_{2,I}}$ in Figure 5.26(a) is the Pareto solution set of case I (INS $\rightarrow$ INS case in Figure 5.23 and Table 5.9). A Pareto set $\boldsymbol{PS_{N,n}}$ consists of 100 populations. The final Pareto solution set $\boldsymbol{PS_2}$, based on the Pareto solution sets for n = I to IV in Figure 5.26(a), is obtained using the ε-constraint approach in Equations (5.55) and (5.56).

The final Pareto solution set $\boldsymbol{PS_2}$ is shown in Figure 5.26(b). Combined inspection / monitoring plans of the three representative solutions $A_{s,1}$, $A_{s,2}$ and $A_{s,3}$ in Figure 5.26(b) are illustrated in Figure 5.26(c). The inspection and monitoring plan for solution $A_{s,1}$ requires two-time inspection (case I) applied at time $t_{insp,1}$ = 5.34 years and $t_{insp,2}$ = 9.48 years with $\delta_{f,0.5}$ = 0.01, and the associated $E(t_{delay})$ and C_{COM} are 3.64 years and 8.69, respectively. If Pareto solution $A_{s,2}$ is selected instead of $A_{s,1}$, the expected damage detection delay $E(t_{delay})$ will be reduced from 3.64 years to 2.42 years, but an additional cost of 12.66 (*i.e.*, 21.35 – 8.69) is needed as shown in Figure 5.26(b). The inspection and monitoring plan associated with $A_{s,2}$ (case II) consists of the inspection at time $t_{insp,1}$ = 4.07 years with $\delta_{f,0.5}$ = 0.01 and the monitoring starting time $t_{mon,1}$ = 10.02 years with monitoring duration t_{md} = 0.3 year (see Figure 5.26(c)). It should be noted that the discount rate of money r_{dis} is not considered, the value of $\delta_{f,0.5}$ is assumed to be the same for the first and second inspections associated with case I, and also the same monitoring duration t_{md} is used for the first and second monitoring associated with case IV.

In a similar way, the Pareto sets $\boldsymbol{PS}_N$ for N = 1 to 5 are obtained as shown in Figures 5.27(a) to 5.27(e). The final Pareto set ***PS*** considering N as a design variable is also found by using the ε-constraint approach based on the Pareto solution sets $\boldsymbol{PS}_N$. The detailed procedure to find the final Pareto set ***PS*** is provided in Figure 5.24. Figure 5.27(f) shows the Pareto set ***PS***. The optimum values of design variables and objective functions of the seven representative solutions $B_{s,1}$ to $B_{s,7}$ in Figure 5.27 are provided in Table 5.11. Combined inspection / monitoring plans for solutions $B_{S,1}$ to $B_{S,7}$ are illustrated in Figure 5.28. Solutions $B_{s,3}$ and $B_{s,5}$ in Figure 5.27(f) are found in the Pareto solution set $\boldsymbol{PS}_3$ in Figure 5.27(c). Solutions $B_{s,4}$ and $B_{s,6}$ in Figure 5.27(f) are associated with the Pareto set $\boldsymbol{PS}_4$ in Figure 5.27(d). Solution $B_{s,6}$ requires three-time monitoring with monitoring duration t_{md} = 0.33 year, and one-time inspection with $\delta_{f,0.5}$ = 0.01, and the corresponding $E(t_{delay})$ and C_{COM} are 0.99 year and 33.90, respectively (see Table 5.11). Monitoring times $t_{mon,1}$, $t_{mon,2}$, $t_{mon,3}$ are 2.58, 4.21, 6.68 years, and inspection time $t_{insp,1}$ is 12.59 years as shown in Figure 5.28. In order to reduce the total cost C_{COM}, solution $B_{s,4}$ consisting of four inspections with $\delta_{f,0.5}$ = 0.01 can be selected. As a result, C_{COM} can be reduced from 33.90 to 17.38, but $E(t_{delay})$ will increase from 0.99 to 2.49.

5.9.3 Application to an Existing Highway Bridge Subjected to Fatigue

The proposed approach is applied to an existing highway bridge, the Yellow Mill Pond Bridge located in Bridgeport, Connecticut, USA. In this application, critical

location is assumed to be the end of the cover plate weld. Detailed information is available in Fisher (1984). In order to predict the time for the occurrence of a given crack size at this critical location, Equation (5.11) is used. The geometry function $Y(a)$ in Equation (5.11) is defined as [Fisher 1984]

$$Y(a) = Y_e(a) \cdot Y_s(a) \cdot Y_w(a) \cdot Y_g(a) \tag{5.63}$$

where $Y_e(a)$ = crack shape factor = 0.952; $Y_s(a)$ = front face factor = 1.211 – $0.186 \cdot \sqrt{a/c}$; $Y_w(a)$ = finite width factor = 1.0; and $Y_g(a)$ = stress gradient factor = $K_{tm} \cdot \left[1 + 6.79 \cdot (a/t_f)^{0.435}\right]^{-1}$ where a = depth crack size; c = width crack size; t_f = flange thickness; K_{tm} = stress concentration factor = –3.54 $ln(Z / t_f)$ + 1.98 $ln(t_{cp} / t_f)$ + 5.80; Z = weld size; t_{cp} = cover plate thickness. The relation between depth crack size a and width crack size c is assumed as $c = 5.462 \times a^{1.133}$. All necessary data to predict crack growth of this critical location are provided in Table 5.12. Material crack growth parameter C is assumed lognormally distributed random variable with mean value = 2.024×10^{-13} and coefficient of variation (COV) = 0.25, and material parameter m is assumed deterministic m = 3.0 [Shetty and Baker 1990]. The annual increase rate of number of cycles r_{cycle} is treated as a random variable with lognormal PDF.

Figure 5.29(a) shows PDF of time for the crack size a_{min} = 1.0 *mm* assumed as the fatigue crack damage criterion. Through comparison with Monte Carlo simulation with 100,000 samples, best fitting PDF (i.e., GEV PDF) with ξ_{par} = 0.14, ρ_{par} = 1.33 and λ_{par} = 2.69 (see Equation (3.14)) is obtained as shown in Figure

5.29(a). If the maximum crack size a_{max} for damage intensity defined in Equation (5.19) is assumed to be 25 *mm*, the time for damage intensity to be 1.0 will have the mean value of 30.29 years and the standard deviation of 11.00 years as shown in Figure 5.29(b). Furthermore, frequency diagram associated with the time interval between damage occurrence (i.e., crack size $a = a_{min}$) and full damage (i.e., crack size $a = a_{max}$) is shown in Figure 5.29(b). In general, damage should be detected and repaired before the time when the crack size reaches a_{max}. Since crack size will increase from a_{min} to a during the damage detection delay, the damage detection delay has to be less than the time associated with $a_{max} - a_{min}$. Therefore, the time interval between damage occurrence and full damage in Figure 5.29(b) can provide an upper limit of the damage detection delay.

The general formulation of the bi-objective optimization problem for the available number of inspection and/or monitorings N is

Find $\mathbf{t_{insp}} = \{t_{ins,1}, t_{ins,2}, \ldots, t_{ins,,ninsp}\}$; (5.64)

$\mathbf{t_{mon}} = \{t_{mon,1}, t_{mon,2}, \ldots, t_{mon,,nmon}\}$;

$\mathbf{t_{md}} = \{t_{md,1}, \delta_{md,2}, \ldots, \delta_{md,nmon}\}$; and

$\boldsymbol{\delta}_{\mathbf{f,0.5}} = \{\delta_{0.5,1}, \delta_{0.5,2}, \ldots, \delta_{0.5,ninsp}\}$

to minimize both $E(t_{delay})$ and C_{COM} (5.65)

such that $t_{insp,i} - t_{insp,i-1} \geq 1$ year, $0.01 \leq \delta_{f,0.5,i} \leq 0.1$; (5.66)

$t_{mon,i} - t_{mon,i-1} \geq 1$ year; 0.3 year $\leq t_{md,i} \leq$ 1.0 year;

and $\left|\mathbf{t_{mon}} - \mathbf{t_{insp}}\right| \geq 1$ year

given $N = n_{insp} + n_{mon}$; and $f_T(t)$ (5.67)

The design variables are the vectors of inspection times $\mathbf{t_{insp}}$, monitoring times $\mathbf{t_{mon}}$, monitoring duration $\mathbf{t_{md}}$, and quality of inspections $\boldsymbol{\delta}_{\mathbf{f,0.5}}$. The GEV PDF $f_T(t)$ in Figure 5.29(a) is used to formulate $E(t_{delay})$. For given N, the total number 2^N of Pareto sets $\boldsymbol{PS}_{N,n}$ can be obtained by solving the bi-objective optimization problems in Equations. (5.64) to (5.67). Finally, the Pareto solution set $\boldsymbol{PS}$ can be obtained through the procedure given in Figure 5.24. Figure 5.30(a) shows this final Pareto set $\boldsymbol{PS}$, and six representative solutions $A_{b,1}$ to $A_{b,6}$. Values of design variables (i.e., N, $\mathbf{t_{insp}}$, $\mathbf{t_{mon}}$, $\mathbf{t_{md}}$, and $\boldsymbol{\delta}_{\mathbf{f,0.5}}$) and objective functions (i.e., $E(t_{delay})$ and C_{COM}) are given in Table 5.13. It should be noted that annual discount rate of money r_{dis} is considered 3%. The combined inspection / monitoring plans corresponding to solutions $A_{b,1}$ to $A_{b,6}$ are illustrated in Figure 5.30(b).

5.10 Conclusions

An approach to establish an optimum inspection and/or monitoring plan considering uncertainties associated with damage occurrence/propagation and inspection methods, and monitoring duration was proposed in this chapter. The optimization problem was formulated with the objective to minimize the expected damage detection delay. The effects of the quality of inspection method, number of inspections or monitorings, monitoring duration, and dispersion associated with damage occurrence on the minimization of the expected damage detection delay

were investigated. A well-balanced inspection and/or monitoring plan was considered as the solution of a bi-objective optimization problem by simultaneously minimizing both the expected damage detection delay and the total inspection and/or monitoring cost. A comparison of the cost-effective inspection plans based on same type and different types of inspections was carried out. For a given number of inspections and monitorings, all possible combinations of inspection and monitoring were considered to establish an optimum combined inspection / monitoring planning. The proposed approach is applied to existing highway bridges subjected to corrosion or fatigue, and ship hull structures subjected to fatigue. The following conclusions can be drawn:

1. Uncertainties associated with damage occurrence/propagation and inspection methods are taken into account to formulate the damage detection delay. In order to consider damage propagation during the interval between damage occurrence time and time to detect damage, the time-dependent damage intensity was used to define the probability of damage detection.
2. In the formulation of the expected damage detection delay, the lower and upper bounds for damage occurrence time were assumed as the limits based on the PDF of damage occurrence time. From the results presented in this chapter, it can be concluded that the time interval between the lower and upper bounds is directly affected by the dispersion of the damage occurrence time and has a significant influence on the expected damage detection delay.

3. Increase in the number of inspections and/or inspection quality (or number of monitorings and/or monitoring duration) may lead to reduction of the expected damage detection delay. However, this increase requires additional financial resources. Therefore, in order to establish cost-effective inspection and/or monitoring planning, an optimization problem based on minimization of both expected damage detection delay and inspection cost has to be solved. The result of this optimization problem provides the Pareto solution set. Based on this set, structure managers can select the appropriate inspection and/or monitoring plan considering also the importance of the structural component or system inspected.
4. For a predefined expected damage detection delay, an optimum inspection plan based on different inspection types is more economical than that based on the same type of inspection.
5. In general, damage may be detected with less delay by using monitoring than inspection. However, monitoring is usually more expensive than inspection. Therefore, combined inspection / monitoring planning provides an optimal-balanced solution.
6. Damage detection delay leads to repair delay. This delay increases the probability of failure. The probability of failure based on the damage detection delay is formulated and extended for the optimum inspection or monitoring planning in Chapter 6.
7. Several assumptions in this chapter need to be further investigated. For example,

the formulation of the expected damage detection delay for optimum monitoring planning is based on the assumption that the probability of damage detection during monitoring period is perfect, when the sensors are installed properly. However, there are uncertainties associated with the monitored data to identify the damage. Further studies need to consider these uncertainties.

8. For deteriorating RC structure, concrete carbonation, time-dependent effects on both the chloride diffusion coefficient and the initial chloride concentration, and loss of bond between concrete and reinforcing bars have to be considered.
9. The fatigue damage occurrence and propagation are random processes involving intermittent growths and dormant periods among others. In order to consider these evolutionary features, Markov chains, jump process models and stochastic differential equations have been developed [Sobczyk 1987]. The scheduling of inspection and monitoring can be affected by the time evolution model of fatigue cracks. Therefore, further studies are needed to incorporate such advanced stochastic modelings into the approach proposed in this chapter.
10. Even though the damage is not detected by inspection or monitoring, each inspection or monitoring provides additional information to update the prior deterioration model and parameters [Zhang and Mahadevan 2000]. Therefore, further studies are necessary to establish the inspection and/or monitoring planning considering updating.
11. The probabilistic approach proposed in this chapter does not include the effects

of maintenance to improve structural performance. Further studies are needed to develop cost-effective lifetime maintenance strategies considering both effects of maintenance on structural performance and minimization of expected damage detection delay.

Table 5.1 Random variables for corrosion initiation and loss of reinforcement (based on information provided in Akgül 2002; Marsh and Frangopol 2008)

Random variables	Units	Mean	COV	Type of distribution
Depth from the concrete surface	x (mm)	30.2	0.2	Lognormal
Surface chloride concentration	$C_{ch,o}$ (g/mm^3)	0.15	0.1	Lognormal
Effective chloride diffusion coefficient	D_{ch} (mm^2/year)	109.68	0.1	Lognormal
Threshold chloride concentration	$C_{ch,th}$ (g/mm^3)	0.04	0.14	Lognormal
Initial diameter of reinforcement	d_{st0} (mm)	15.88	0.02	Lognormal
Rate of corrosion	r_{corr} (mm/year)	0.0582	0.3	Lognormal

Table 5.2 Optimum inspection times, expected detection delay, and the associated inspection cost

$\delta_{c,0.5}$	n_{insp}	Optimum inspection times (years)							$E(t_{delay})$ (years)	C_{INS}
		t_s	$t_{insp,1}$	$t_{insp,2}$	$t_{insp,3}$	$t_{insp,4}$	$t_{insp,5}$	t_e		
0.01	1	0.77	4.89	-	-	-	-	11.87	2.73	6.08
	2	0.77	3.61	6.00	-	-	-	11.87	1.67	12.17
	3	0.77	3.05	4.50	6.68	-	-	11.87	1.25	18.25
	4	0.77	2.73	3.80	5.11	7.17	-	11.87	1.01	24.33
	5	0.77	2.48	3.48	4.48	5.72	7.65	11.87	0.87	30.41
0.03	1	0.77	5.28	-	-	-	-	11.87	3.10	4.58
	2	0.77	4.03	6.36	-	-	-	11.87	2.09	9.16
	3	0.77	3.49	4.91	7.02	-	-	11.87	1.68	13.74
	4	0.77	3.17	4.22	5.51	7.49	-	11.87	1.45	18.32
	5	0.77	2.91	3.91	4.91	6.11	7.97	11.87	1.31	22.89
0.05	1	0.77	5.66	-	-	-	-	11.87	3.48	3.43
	2	0.77	4.46	6.71	-	-	-	11.87	2.51	6.87
	3	0.77	3.92	5.31	7.35	-	-	11.87	2.11	10.30
	4	0.77	3.61	4.64	5.90	7.81	-	11.87	1.89	13.73
	5	0.77	3.35	4.35	5.35	6.51	8.28	11.87	1.76	17.16

Note: Inspection at time t_e is not accounted in the number of inspections and total inspection cost

Table 5.3 Optimum monitoring times, expected detection delay, and the associated total monitoring cost

t_{md} (years)	n_{mon}	Optimum monitoring starting times (years)							$E(t_{delay})$ (years)	C_{MON}
		t_s	$t_{mon,1}$	$t_{mon,2}$	$t_{mon,3}$	$t_{mon,4}$	$t_{mon,5}$	t_e		
0.1	1	0.77	4.61	-	-	-	-	11.87	2.45	11
	2	0.77	3.31	5.74	-	-	-	11.87	1.37	12
	3	0.77	2.74	4.21	6.44	-	-	11.87	0.94	13
	4	0.77	2.42	3.49	4.83	6.94	-	11.87	0.70	14
	5	0.77	2.20	3.07	4.03	5.31	7.33	11.87	0.55	15
0.5	1	0.77	4.28	-	-	-	-	11.87	2.13	15
	2	0.77	2.96	5.46	-	-	-	11.87	1.04	20
	3	0.77	2.39	3.91	6.21	-	-	11.87	0.61	25
	4	0.77	2.07	3.20	4.59	6.76	-	11.87	0.39	30
	5	0.77	1.85	2.78	3.82	5.14	7.21	11.87	0.26	35
1.0	1	0.77	3.89	-	-	-	-	11.87	1.76	20
	2	0.77	2.58	5.17	-	-	-	11.87	0.70	30
	3	0.77	2.01	3.66	6.05	-	-	11.87	0.32	40
	4	0.77	1.68	2.99	4.52	6.76	-	11.87	0.16	50
	5	0.77	1.44	2.61	3.84	5.30	7.41	11.87	0.08	60

Table 5.4 Design variable and objective function values for Pareto solutions $A_{c,1}$, $A_{c,2}$, $A_{c,3}$, and $A_{c,4}$ in Figures 5.14(a) and (b)

Pareto optimum solution			$A_{c,1}$	$A_{c,2}$	$A_{c,3}$	$A_{c,4}$
Objective function values	C_{INS}		30	15	10	5
	$E(t_{delay})$ (years)		0.89	1.55	1.96	2.96
Design variables	n_{insp}		5	3	2	2
	$\delta_{c,0.5}$		0.11	0.024	0.024	0.072
	Optimum inspection times (years)	t_s	0.77	0.77	0.77	0.77
		$t_{insp,1}$	2.50	3.40	3.92	4.94
		$t_{insp,2}$	3.50	4.82	6.24	7.12
		$t_{insp,3}$	4.50	6.95	-	-
		$t_{insp,4}$	5.72	-	-	-
		$t_{insp,5}$	7.67	-	-	-
		t_e	11.87	11.87	11.87	11.87

Note: Inspection at time t_e is not accounted in the number of inspections and total inspection cost

Table 5.5 Variables for crack growth model

Random variables	Units	Mean	*COV	Type of distribution
Initial crack size, a_o	*mm* (*in*)	0.5 (0.02)	0.2	Lognormal
Annual number of cycles, N_{an}	*cycles*/*year*	0.8×10^6	0.2	Lognormal
Stress range, S_{sr}	*MPa* (*ksi*)	40 (5.81)	0.1	Weibull
Material crack growth parameter, C		3.54×10^{-11} ($^{\dagger}1.77 \times 10^{-9}$)	0.3	Lognormal
Deterministic variable			Value	
Material crack growth parameter, m			2.54	

*COV: coefficient of variation

$^{\dagger}1.77 \times 10^{-9}$: material parameter for da/dN and ΔK in units of *in*/*cycles* and $ksi\sqrt{in}$, respectively (see Equations (5.9) and (5.10))

Table 5.6 Design variable and objective function values associated with Pareto optimum solutions in Figures 5.20(c)

Pareto optimum solution			$B_{f,1}$	$B_{f,2}$	$B_{f,3}$	$B_{f,4}$	$B_{f,5}$	$B_{f,6}$	$B_{f,7}$
Objective function values		C_{INS}	1.17	2.34	4.35	8.69	13.03	17.38	21.72
		$E(t_{delay})$ (years)	13.21	9.66	7.09	4.55	3.62	3.15	2.86
Design variables		n_{insp}	1	2	1	2	3	4	4
		$\delta_{f,0.5}$	0.10	0.10	0.01	0.01	0.01	0.01	0.01
	$\mathbf{t_{insp}}$ (years)	$t_{insp,1}$	15.27	11.73	9.35	6.67	5.64	5.07	4.71
		$t_{insp,2}$	-	18.50	-	11.85	8.35	6.94	6.15
		$t_{insp,3}$	-	-	-	-	13.51	9.60	7.93
		$t_{insp,4}$	-	-	-	-	-	14.76	10.60
		$t_{insp,5}$	-	-	-	-	-	-	-

Table 5.7 Design variable and objective function values associated with Pareto optimum solutions in Figure 5.21

Pareto optimum solution	Objective function values		Design variables						
	$E(t_{delay})$ (years)	C_{INS}	n_{insp}	$\mathbf{t_{insp}}$ (years)			$\boldsymbol{\delta_{f,\,0.5}}$		
				$t_{insp,1}$	$t_{insp,2}$	$t_{insp,3}$	$\delta_{f,\,0.5,1}$	$\delta_{f,\,0.5,2}$	$\delta_{f,\,0.5,3}$
$C_{f,1}$	9.66	2.34	2	11.73	18.50	-	0.10	0.10	-
$C_{f,2}$	7.92	4.13		9.78	18.80	-	0.37	0.10	-
$C'_{f,2}$	7.92	4.93		10.00	16.34	-	0.05	0.05	-
$C_{f,3}$	6.07	5.49		8.42	19.74	-	0.01	0.10	-
$C_{f,4}$	4.55	8.69		6.67	11.85	-	0.01	0.01	-
$D_{f,1}$	8.46	3.51	3	10.44	13.68	20.70	0.10	0.10	0.10
$D_{f,2}$	7.17	5.17		9.13	14.21	22.32	0.04	0.10	0.10
$D'_{f,2}$	7.17	6.58		9.18	12.28	18.91	0.06	0.06	0.06
$D_{f,3}$	5.24	6.68		8.15	15.40	18.75	0.01	0.10	0.10
$D_{f,4}$	4.32	9.87		6.59	11.13	21.47	0.01	0.01	0.10
$D_{f,5}$	3.62	13.03		5.64	8.35	13.51	0.01	0.01	0.01

Table 5.8 Design variable and objective function values associated with Pareto optimum solutions in Figure 5.22

Pareto optimum solution	Objective function values		Design variables							
	$E(t_{delay})$ (years)	C_{INS}	n_{insp}	$\mathbf{t_{insp}}$ (years)				$\boldsymbol{\delta_{f,\,0.5}}$			
				$t_{insp,1}$	$t_{insp,2}$	$t_{insp,3}$	$t_{insp,4}$	$\delta_{f,\,0.5,1}$	$\delta_{f,\,0.5,2}$	$\delta_{f,\,0.5,3}$	$\delta_{f,\,0.5,4}$
$E_{f,1}$	13.21	1.17	1	15.27	-	-	-	0.10	-	-	-
$E_{f,2}$	11.22	2.34	1	13.33	-	-	-	0.05	-	-	-
$E_{f,3}$	9.66	2.34	2	11.73	18.50	-	-	0.10	0.10	-	-
$E_{f,4}$	7.09	4.35	1	9.35	-	-	-	0.01	-	-	-
$E_{f,5}$	4.55	8.69	2	6.67	11.85	-	-	0.01	0.01	-	-
$E_{f,6}$	3.62	13.03	3	5.64	8.35	13.51	-	0.01	0.01	0.01	-
$E_{f,7}$	3.15	17.38	4	5.07	6.94	9.60	14.76	0.01	0.01	0.01	0.01
$F_{f,1}$	13.88	0.70	1	17.28	-	-	-	0.10	-	-	-
$F_{f,2}$	11.77	1.18	2	14.96	34.78	-	-	0.10	0.10	-	-
$F_{f,3}$	6.08	4.05	2	8.05	20.27	-	-	0.01	0.10	-	-
$F_{f,4}$	4.55	6.63	2	6.67	11.85	-	-	0.01	0.01	-	-
$F_{f,5}$	3.63	11.53	4	5.64	7.24	8.36	13.51	0.01	0.07	0.01	0.01

Table 5.9 Objectives and design variables of cases for number of inspections and/or monitorings $N = n_{insp} + n_{mon} = 2$

Case	1 INS → INS	2 INS → MON	3 MON → INS	4 MON → MON
Number of inspections n_{insp}	2	1	1	0
Number of monitorings n_{mon}	0	1	1	2
Objective function	$E(t_{delay})$ and $C_{COM} = C_{INS} + C_{MON}$			
Design variables	$t_{insp,1}$	$t_{insp,1}$	$t_{insp,1}$	$t_{mon,1}$
	$t_{insp,2}$	$t_{mon,1}$	$t_{mon,1}$	$t_{mon,2}$
	$\delta_{f,0.5}$	$\delta_{f,0.5}$	$\delta_{f,0.5}$	t_{md}
	-	t_{md}	t_{md}	-

Table 5.10 Variables for crack growth model of a joint between bottom plate and longitudinal plate

Random variables	Units	Mean	*COV	Type of distribution
Initial crack size, a_o	*mm* (*in*)	0.5 (0.02)	0.2	Lognormal
Annual number of cycles, N_{an}	*cycles*/*year*	1.0×10^{6}	0.2	Lognormal
Stress range, S_{sr}	*MPa* (*ksi*)	40 (5.81)	0.1	Weibull
Material crack growth parameter, C		3.54×10^{-11} ($^{\dagger}1.77 \times 10^{-9}$)	0.3	Lognormal
Deterministic variable			Value	
Material crack growth parameter, m			2.54	

*COV: coefficient of variation

$^{\dagger}1.77 \times 10^{-9}$: material parameter for da/dN and ΔK in units of *in*/*cycles* and *ksi*$\sqrt{in}$, respectively (see Equations (5.9) and (5.10))

Table 5.11 Design variable and objective function values associated with Pareto optimum solutions in Figure 5.27

Pareto optimum solution	Objective values		Values of design variables						
	$E(t_{delay})$ (years)	C_{COM}	N	Optimum inspection and/or monitoring times (years)					$\delta_{f,0.5}$	t_{md} (years)
$B_{s,1}$	5.67	4.35	1	$t_{insp,1}$					0.01	-
				7.47						
$B_{s,2}$	3.64	8.69	2	$t_{insp,1}$	$t_{insp,2}$				0.01	-
				5.34	9.48					
$B_{s,3}$	2.90	13.03	3	$t_{insp,1}$	$t_{insp,2}$	$t_{insp,3}$			0.01	-
				4.51	6.82	10.82				
$B_{s,4}$	2.49	17.38	4	$t_{insp,1}$	$t_{insp,2}$	$t_{insp,3}$	$t_{insp,4}$		0.01	-
				4.11	5.61	7.73	11.81			
$B_{s,5}$	1.45	27.69	3	$t_{mon,1}$	$t_{mon,2}$	$t_{insp,1}$			0.01	0.33
				3.03	5.68	11.49				
$B_{s,6}$	0.99	33.90	4	$t_{mon,1}$	$t_{mon,2}$	$t_{mon,3}$	$t_{insp,1}$		0.01	0.33
				2.58	4.21	6.68	12.59			
$B_{s,7}$	0.74	39.44	5	$t_{mon,1}$	$t_{mon,2}$	$t_{mon,3}$	$t_{mon,4}$	$t_{ins,1}$	0.01	0.31
				2.19	3.50	5.10	7.79	13.46		

Table 5.12 Variables for crack growth model of a cover plate

Deterministic variable	Notation (Units)	Value
Material crack growth parameter	M	3.0
Flange thickness	t_f (mm)	32.0
Cover plate thickness	t_{cp} (mm)	31.8

Random variables	Notation (Units)	Mean	*COV	Type of distribution
Initial crack size	c_o (mm)	0.5	0.2	Lognormal
Annual number of cycles	N_{an} (cycles/year)	1.62×10^6	0.2	Lognormal
Annual increase rate of number of cycles	r_{cycle} (%)	2	0.1	Lognormal
Stress range	S_{sr} (MPa)	13.78	0.1	Weibull
Material crack growth parameter	C	2.024×10^{-13}	0.25	Lognormal
Weld size	Z (mm)	16	0.1	Lognormal

*COV : coefficient of variation

Table 5.13 Design variable and objective function values associated with Pareto optimum solutions in Figure 5.30(a)

Pareto optimum solution	Objective values		Values of design variables										
	$E(t_{delay})$ (years)	C_{COM}	N	$\mathbf{t_{insp}}$ and/or $\mathbf{t_{mon}}$ (years)					$\boldsymbol{\delta_{f,0.5}}$ and/or $\mathbf{t_{md}}$ (years)				
$A_{b,1}$	2.40	10.41	3	$t_{insp,1}$	$t_{insp,2}$	$t_{insp,3}$	-	-	$\delta_{f,0.5,1}$	$\delta_{f,0.5,2}$	$\delta_{f,0.5,3}$	-	-
				4.42	7.01	10.97	-	-	0.01	0.01	0.01	-	-
$A_{b,2}$	2.00	17.95	5	$t_{insp,1}$	$t_{insp,2}$	$t_{insp,3}$	$t_{insp,4}$	$t_{insp,5}$	$\delta_{f,0.5,1}$	$\delta_{f,0.5,2}$	$\delta_{f,0.5,3}$	$\delta_{f,0.5,4}$	$\delta_{f,0.5,5}$
				3.73	5.17	7.31	11.40	16.81	0.01	0.01	0.01	0.02	0.10
$A_{b,3}$	1.64	21.61	3	$t_{mon,1}$	$t_{mon,2}$	$t_{insp,1}$	-	-	$t_{md,1}$	$t_{md,2}$	$\delta_{f,0.5,1}$	-	-
				3.45	6.56	14.83	-	-	0.32	0.30	0.08	-	-
$A_{b,4}$	1.22	26.02	4	$t_{mon,1}$	$t_{mon,2}$	$t_{insp,1}$	$t_{insp,2}$	-	$t_{md,1}$	$t_{md,2}$	$\delta_{f,0.5,1}$	$\delta_{f,0.5,2}$	-
				3.03	5.23	9.31	16.09	-	0.36	0.30	0.01	0.07	-
$A_{b,5}$	0.60	17.95	5	$t_{mon,1}$	$t_{mon,2}$	$t_{mon,3}$	$t_{mon,4}$	$t_{mon,5}$	$t_{md,1}$	$t_{md,2}$	$t_{md,3}$	$t_{md,4}$	$t_{md,5}$
				2.14	3.65	4.99	6.90	10.78	0.51	0.30	0.30	0.30	0.30
$A_{b,6}$	0.40	68.70	5	$t_{mon,1}$	$t_{mon,2}$	$t_{mon,3}$	$t_{mon,4}$	$t_{mon,5}$	$t_{md,1}$	$t_{md,2}$	$t_{md,3}$	$t_{md,4}$	$t_{md,5}$
				1.93	3.93	6.02	7.98	11.60	1.00	0.98	0.34	0.30	0.31

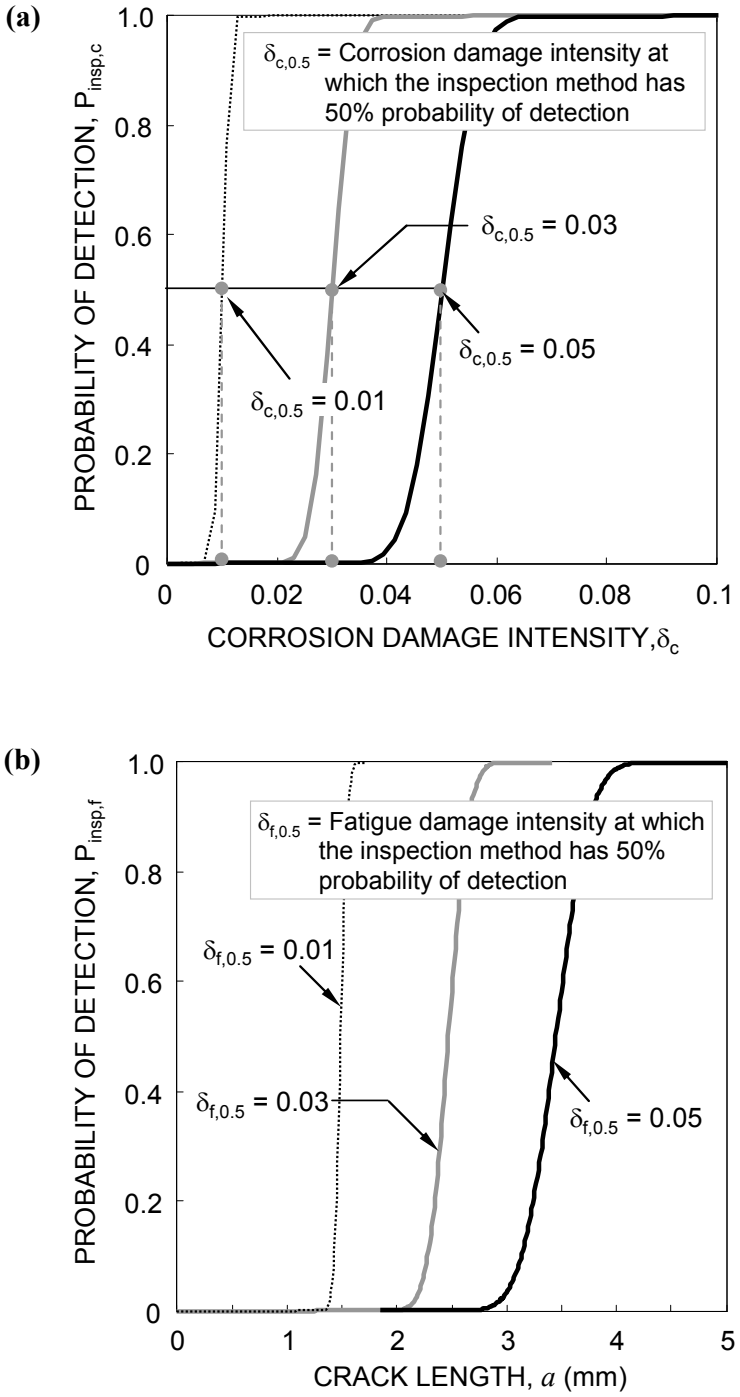

Figure 5.1 (a) Relation between the corrosion damage intensity and the probability of corrosion damage detection ; and **(b)** relation between the crack length and the probability of fatigue damage detection

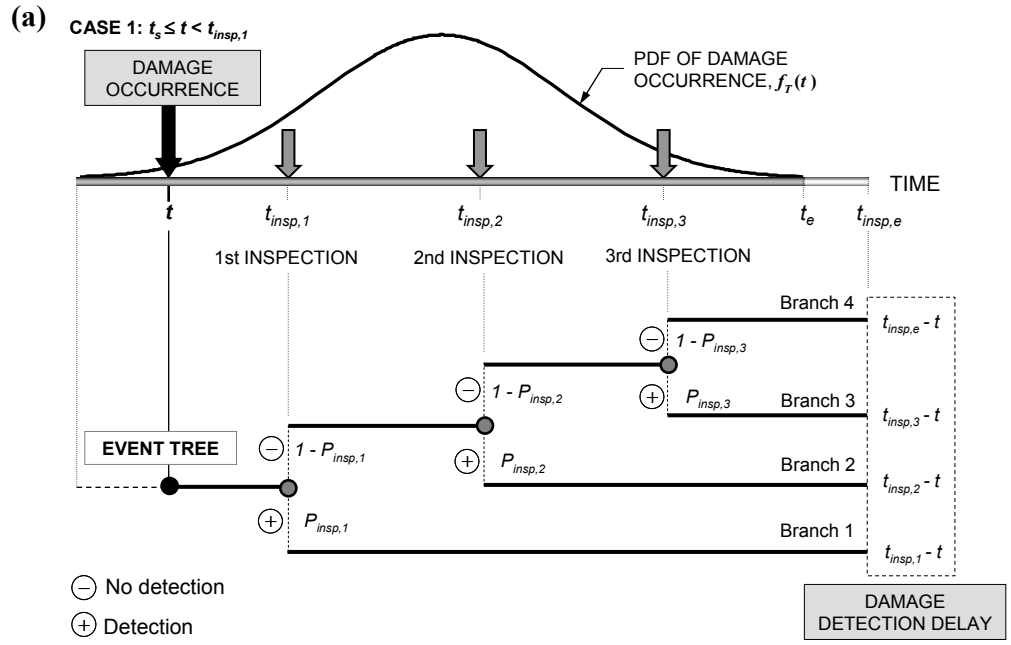

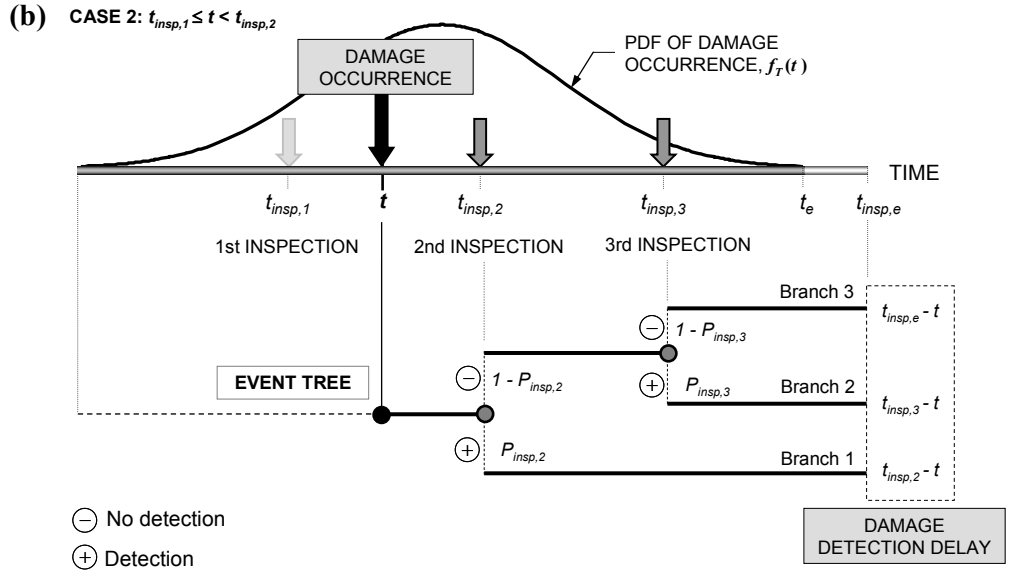

Figure 5.2 Damage detection delay for **(a)** case 1: $t_s \le t < t_{insp,1}$; **(b)** case 2: $t_{insp,1} \le t < t_{insp,2}$; **(c)** case 3: $t_{insp,2} \le t < t_{insp,3}$; and **(d)** case 4: $t_{insp,3} \le t \le t_{insp,e}$

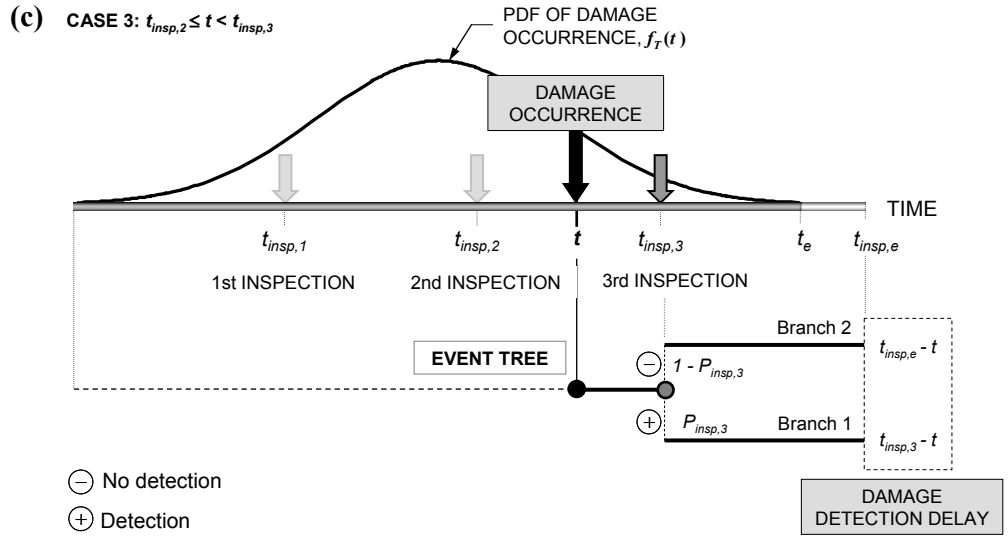

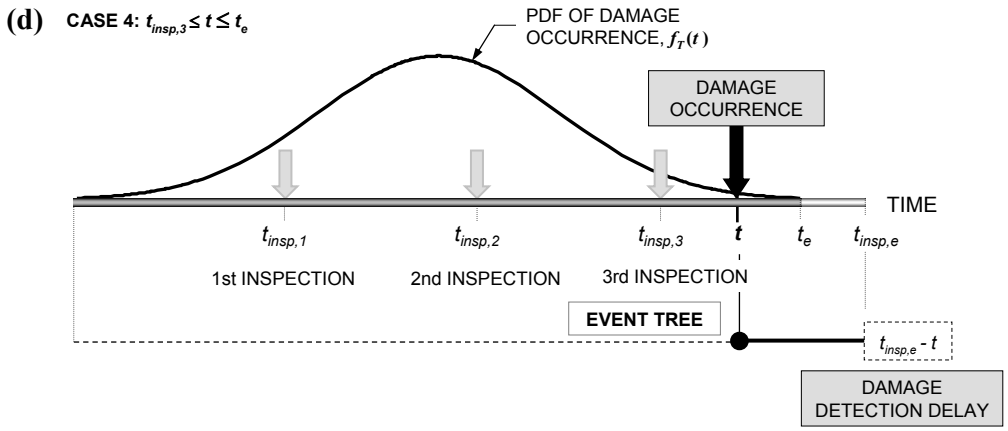

Figure 5.2 Damage detection delay for **(a)** case 1: $t_s \le t < t_{insp,1}$; **(b)** case 2: $t_{insp,1} \le t < t_{insp,2}$; **(c)** case 3: $t_{insp,2} \le t < t_{insp,3}$; and **(d)** case 4: $t_{insp,3} \le t \le t_{insp,e}$ (continued)

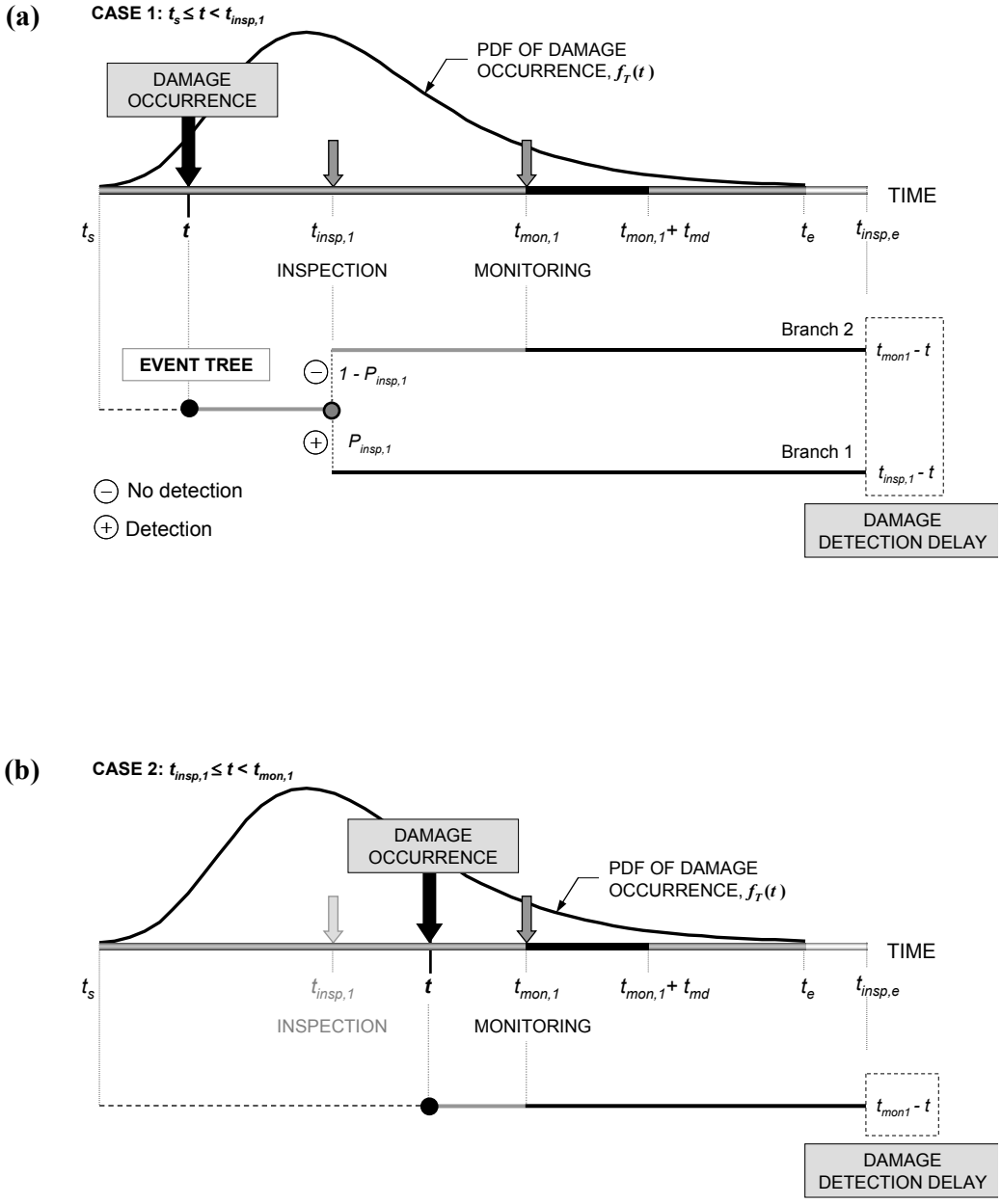

Figure 5.3 Damage detection delay when inspection and monitoring are used **(a)** case 1: $t_s \le t < t_{insp,1}$; **(b)** case 2: $t_{insp,1} \le t < t_{mon,1}$; (c) case 3: $t_{mon,1} \le t < t_{mon,1} + t_{md}$; and (d) case 4: $t_{mon,1} + t_{md} \le t < t_e$

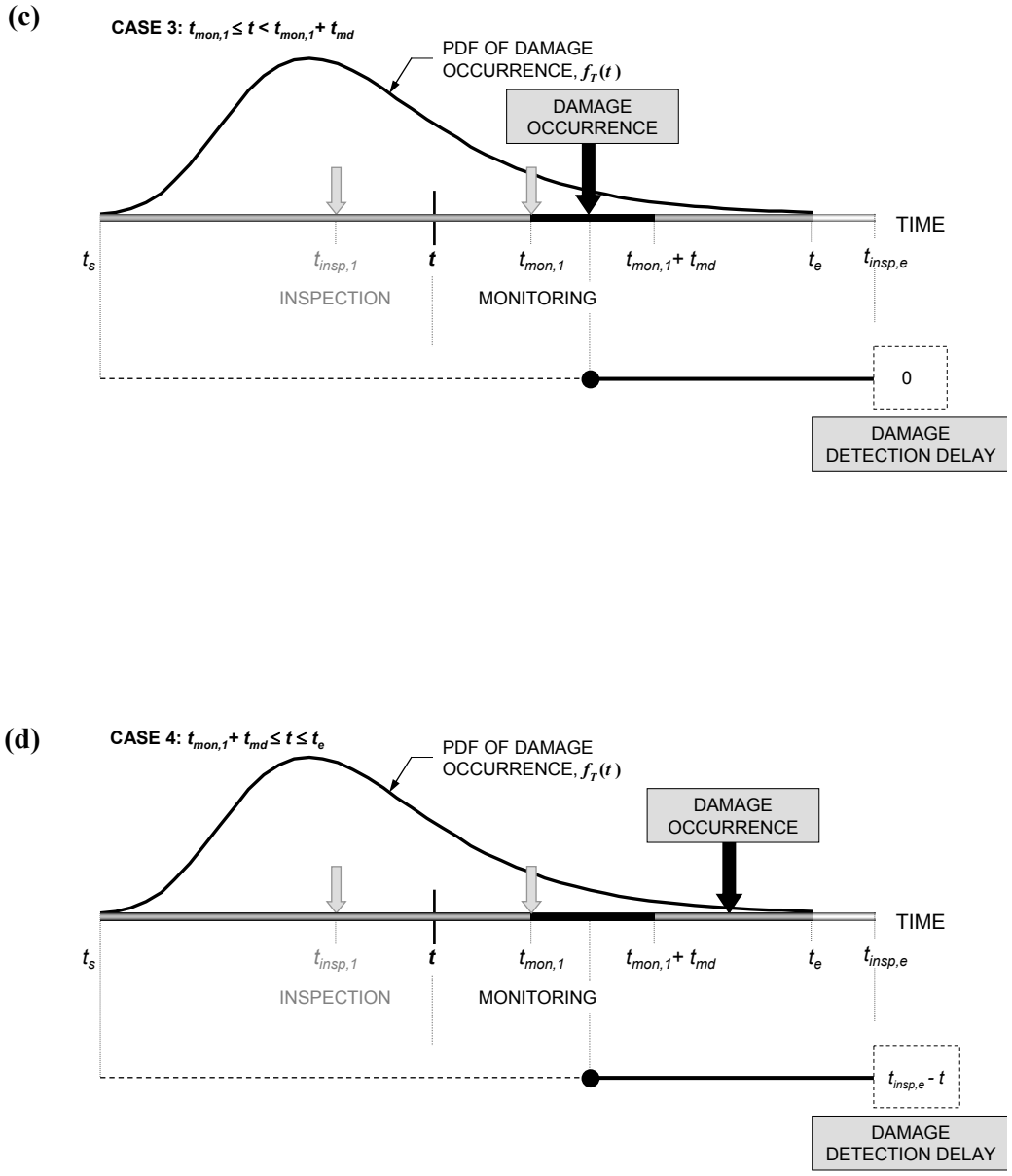

Figure 5.3 Damage detection delay when inspection and monitoring are used **(a)** case 1: $t_s \le t < t_{insp,1}$; **(b)** case 2: $t_{insp,1} \le t < t_{mon,1}$; (c) case 3: $t_{mon,1} \le t < t_{mon,1} + t_{md}$; and (d) case 4: $t_{mon,1} + t_{md} \le t < t_e$ (continued)

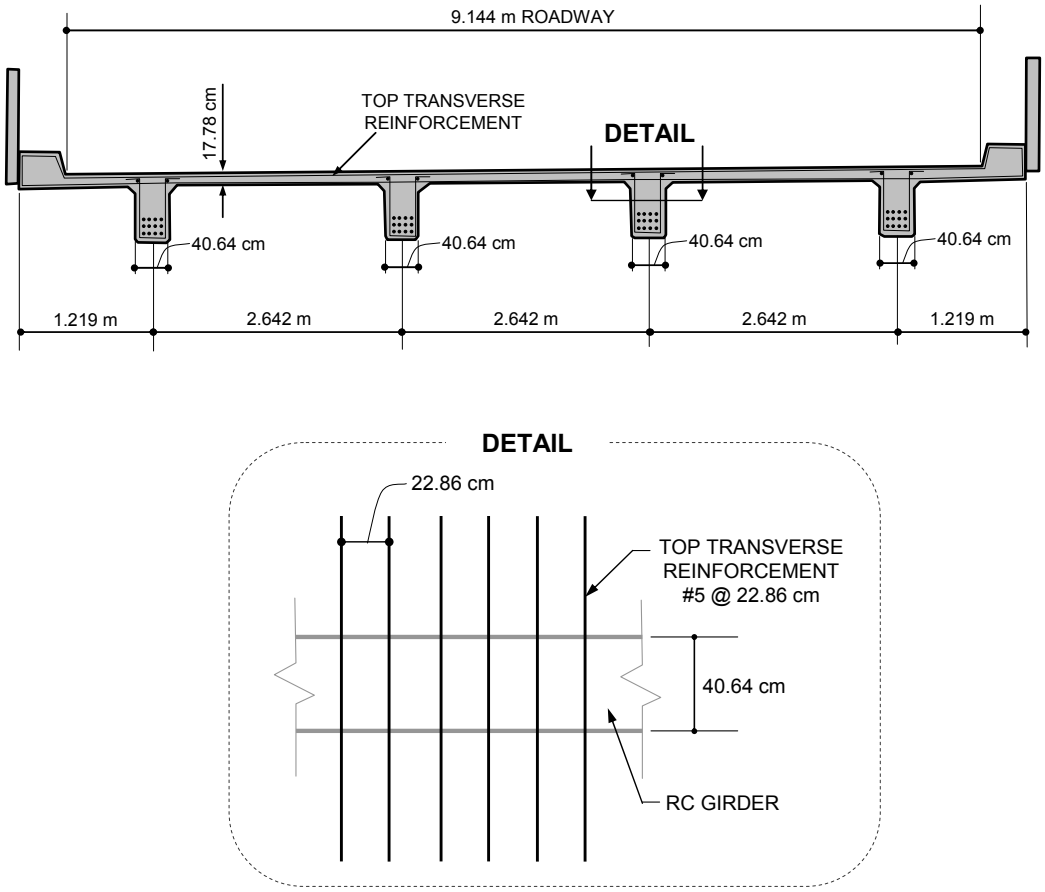

Figure 5.4 Cross-sectional view and layout of top transverse reinforcement bars at end spans of E-17-HS (adapted from Akgül 2002)

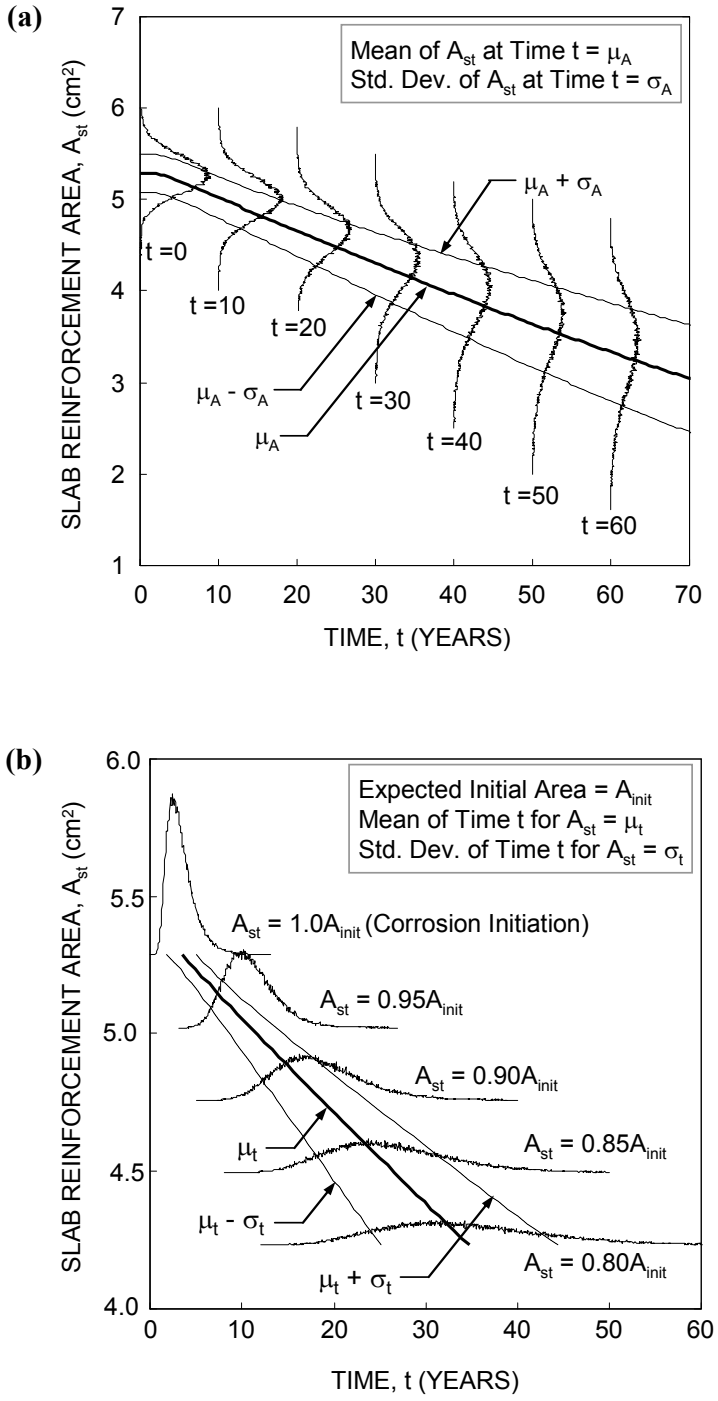

Figure 5.5 Time-dependent reinforcement area of RC slab deck with **(a)** PDFs of reinforcement area A_{st} at every 10 years; **(b)** PDFs of corrosion initiation time and times when $A_{st} = 0.95A_{init}$, $0.90A_{init}$, $0.85A_{init}$, and $0.80A_{init}$

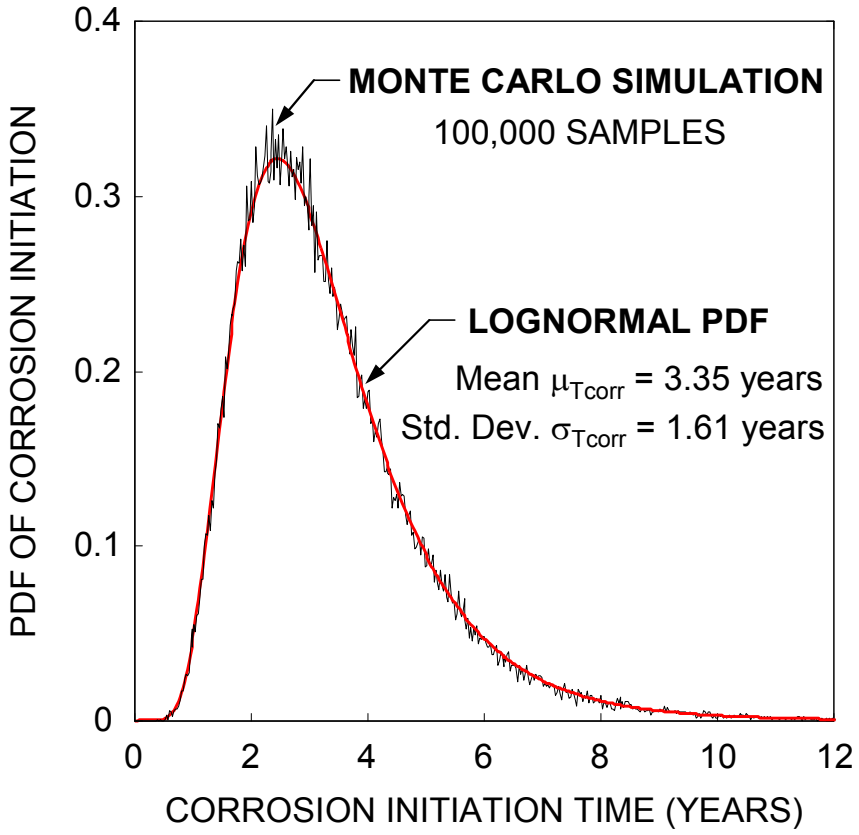

Figure 5.6 Lognormal PDF of corrosion initiation time

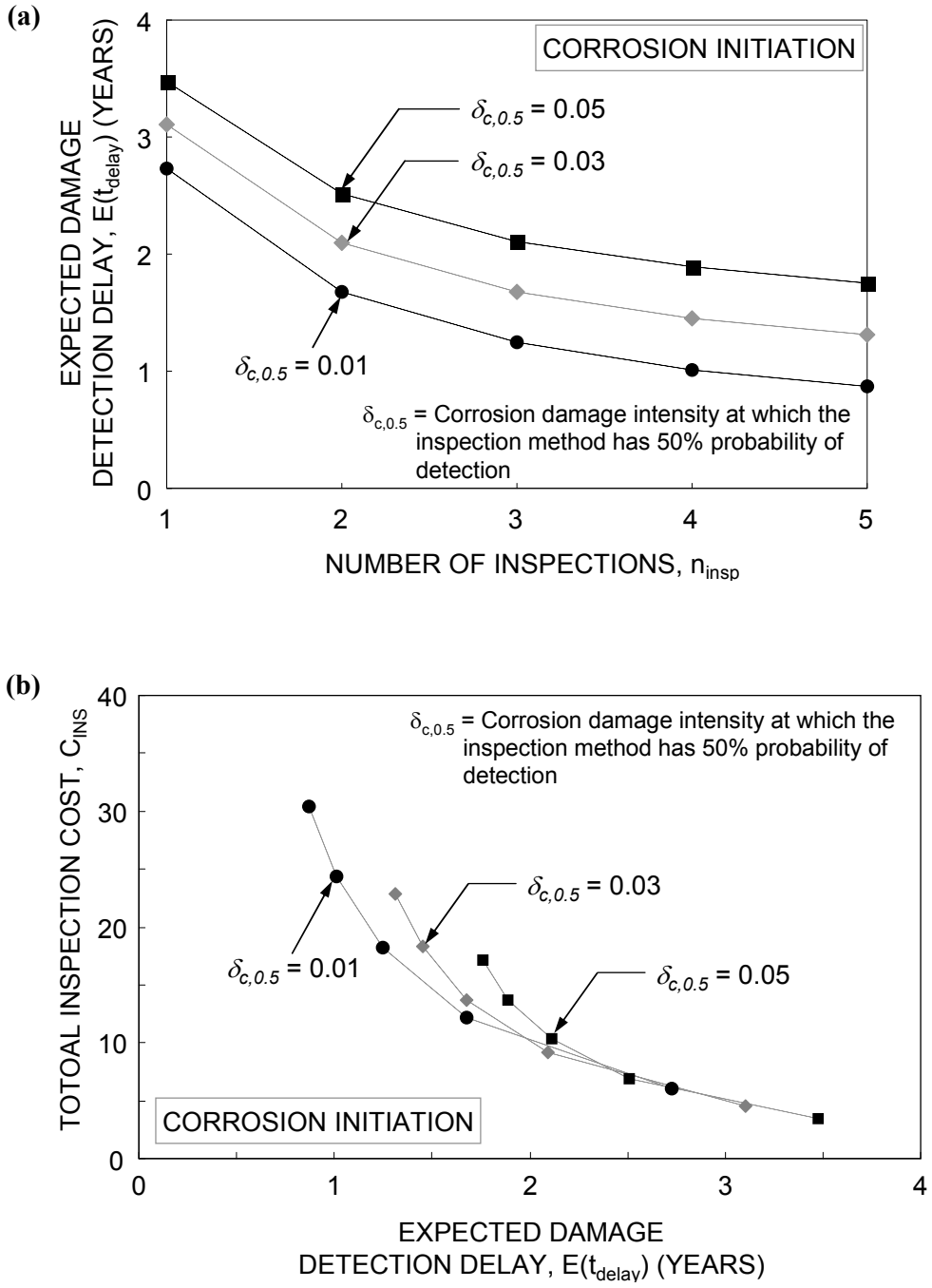

Figure 5.7 Inspection: **(a)** effects of number of inspections and inspection quality on minimum expected corrosion damage detection delay; and **(b)** relation between minimum expected damage detection delay and total inspection cost

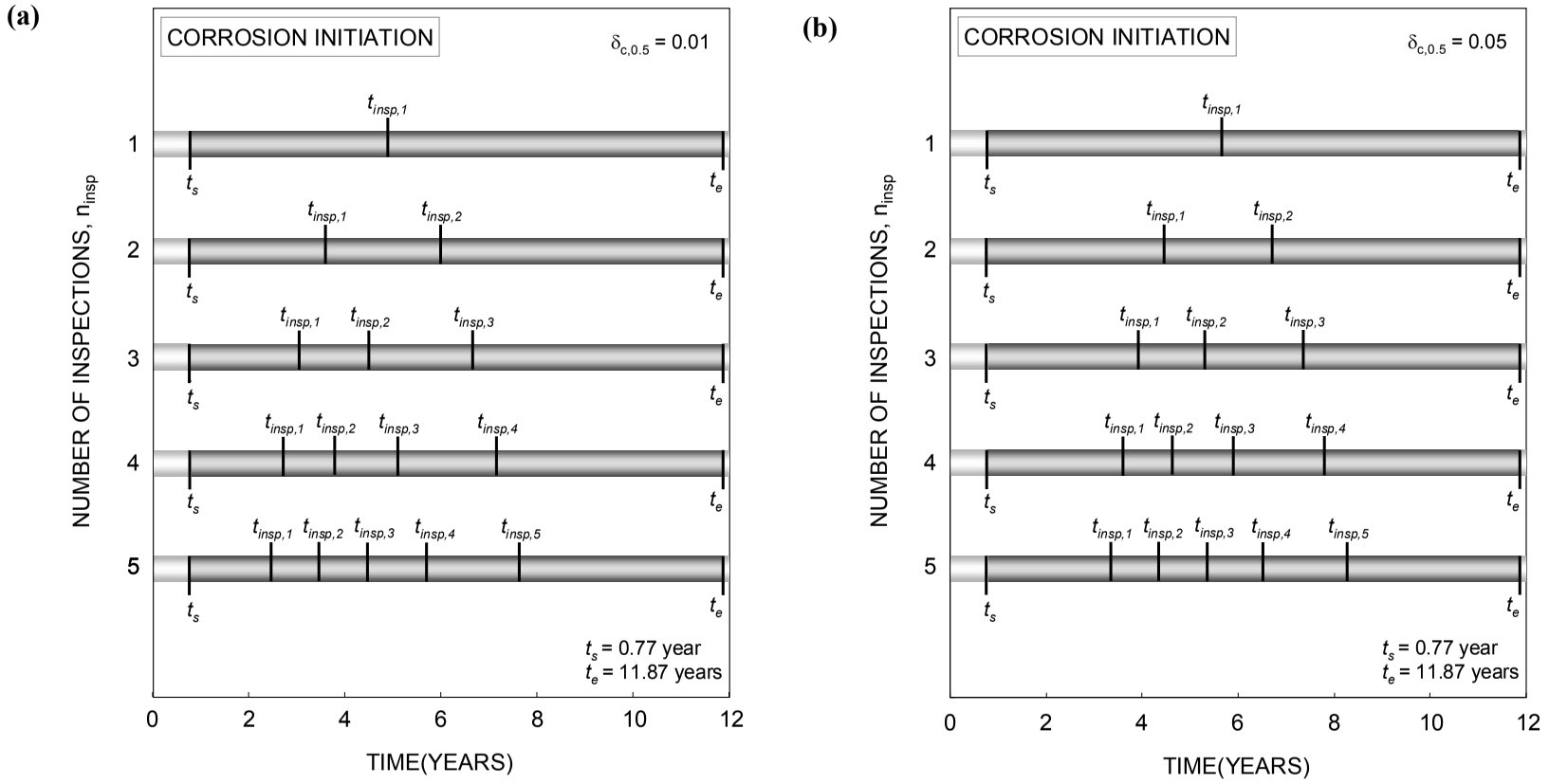

Figure 5.8 Optimum inspection plans for **(a)** $\delta_{c,0.5} = 0.01$; and **(b)** $\delta_{c,0.5} = 0.05$

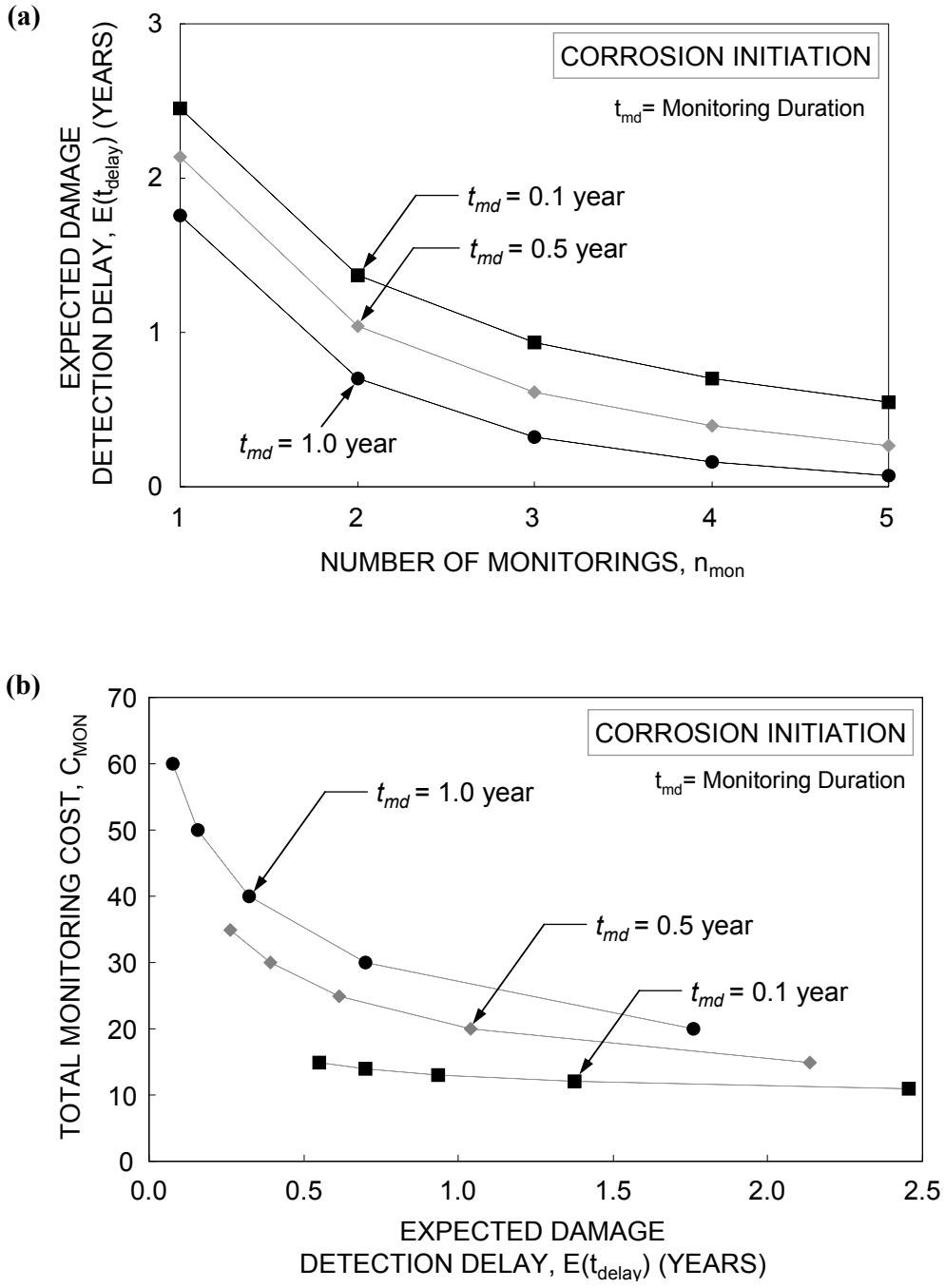

Figure 5.9 Monitoring: **(a)** effects of number of monitorings and monitoring duration on minimum expected corrosion damage detection delay; and **(b)** relation between minimum expected damage detection delay and total monitoring cost

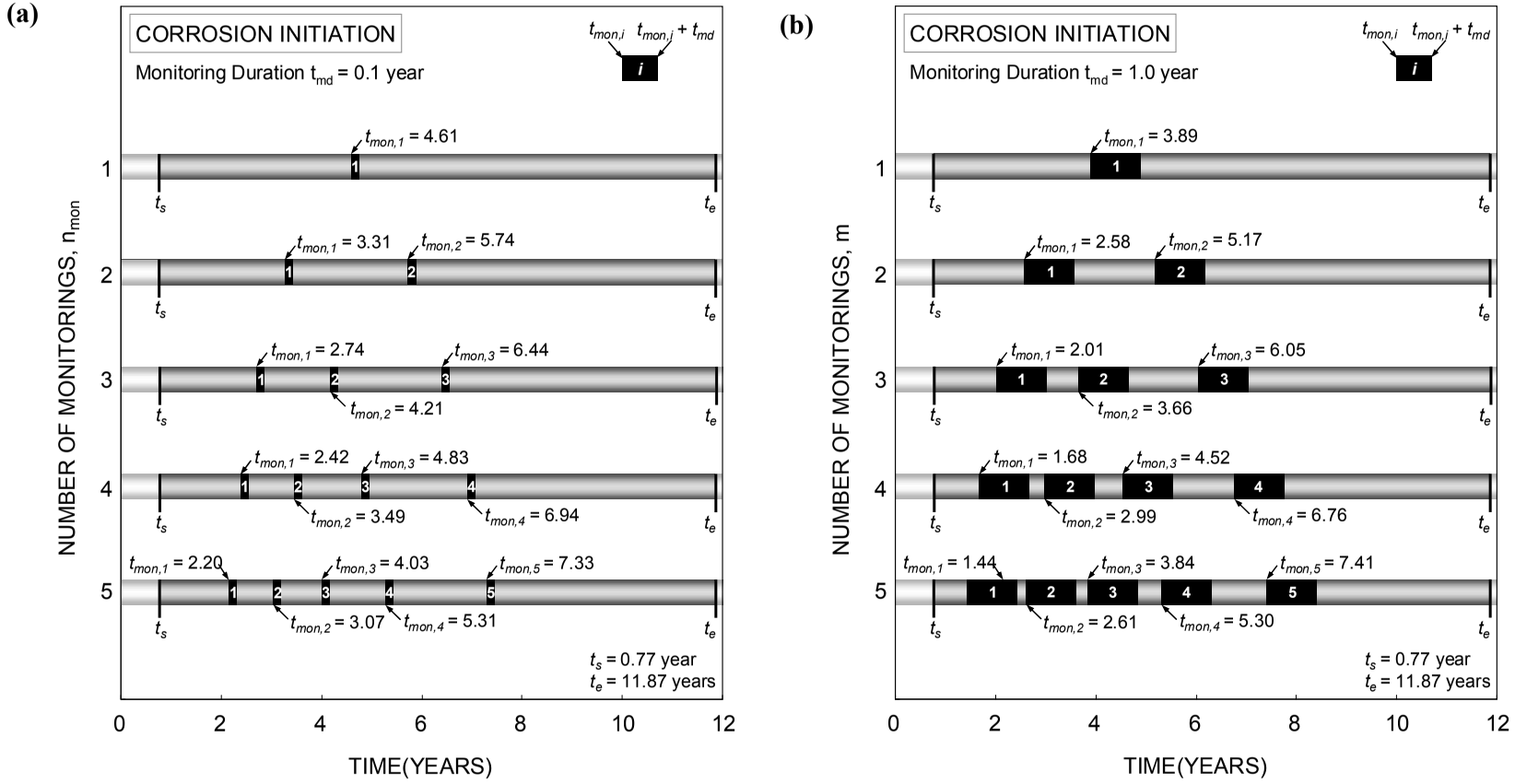

Figure 5.10 Optimum monitoring plans for monitoring duration **(a)** t_{md} = 0.1 year; and **(b)** t_{md} = 1.0 year

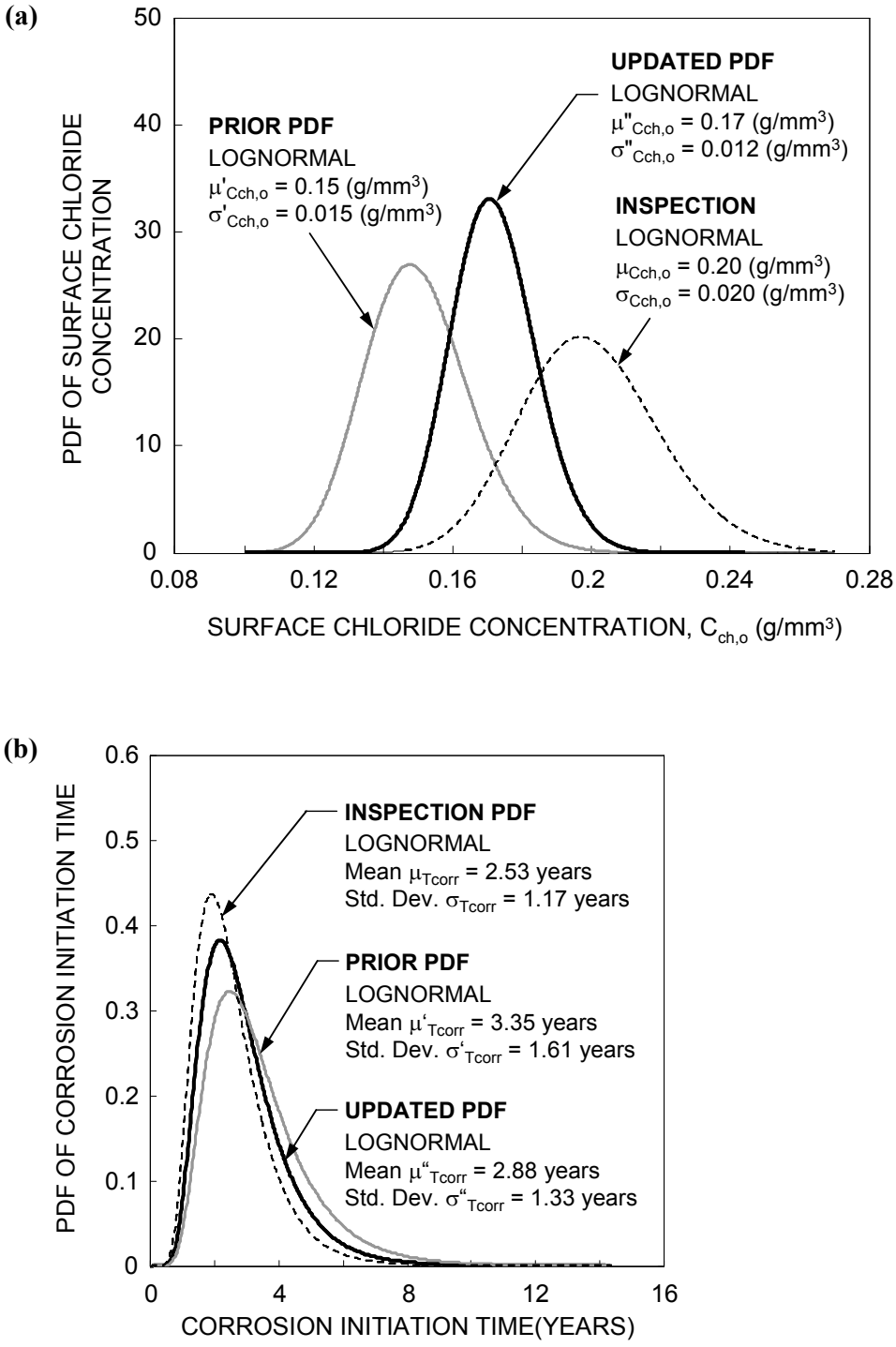

Figure 5.11 (a) Bayesian updating of surface chloride concentration; and **(b)** corrosion initiation time based on updating of surface chloride concentration

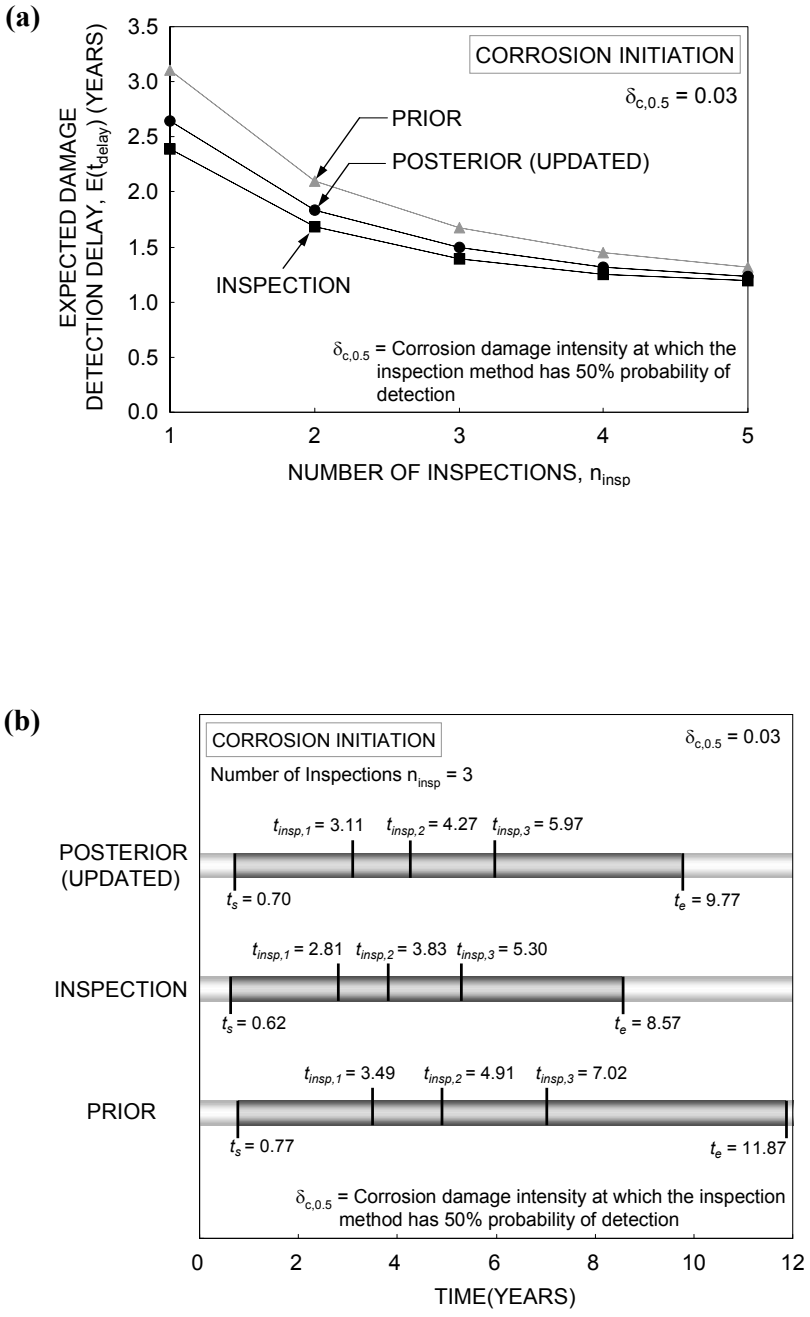

Figure 5.12 Inspection: effects of updating of surface chloride concentration on **(a)** minimum expected corrosoin damage detection delay associated with $\delta_{c,0.5}$ = 0.03; and **(b)** optimum inspection plan for the number of inspections n_{insp} = 3 and $\delta_{c,0.5}$ = 0.03

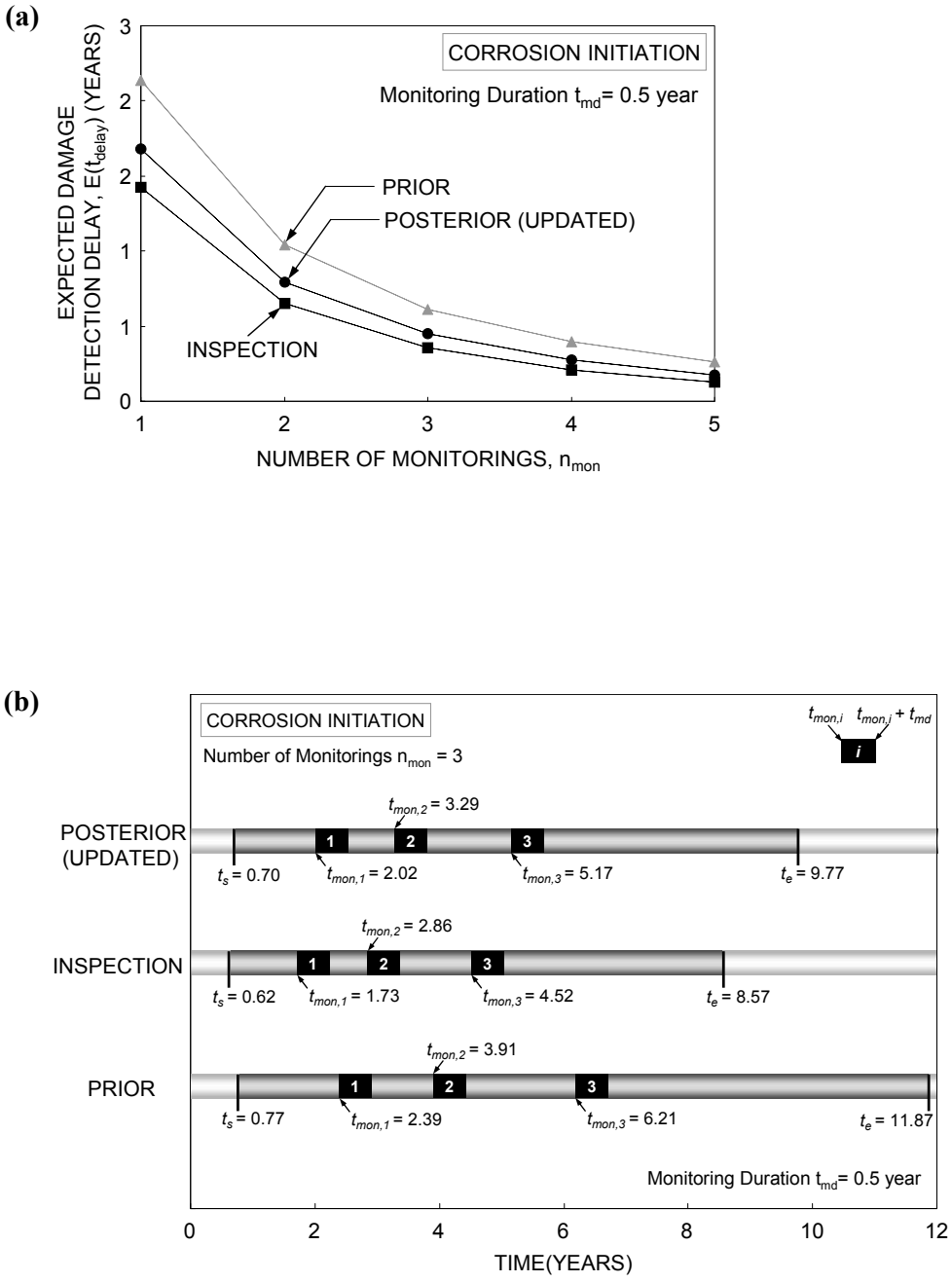

Figure 5.13 Monitoring: effects of updating of surface chloride concentration on **(a)** minimum expected corrosion damage detection delay associated with monitoring duration t_{md} = 0.5 year; **(b)** optimum inspection plan for the number of monitorings n_{mon} = 3 and t_{md} = 0.5 year

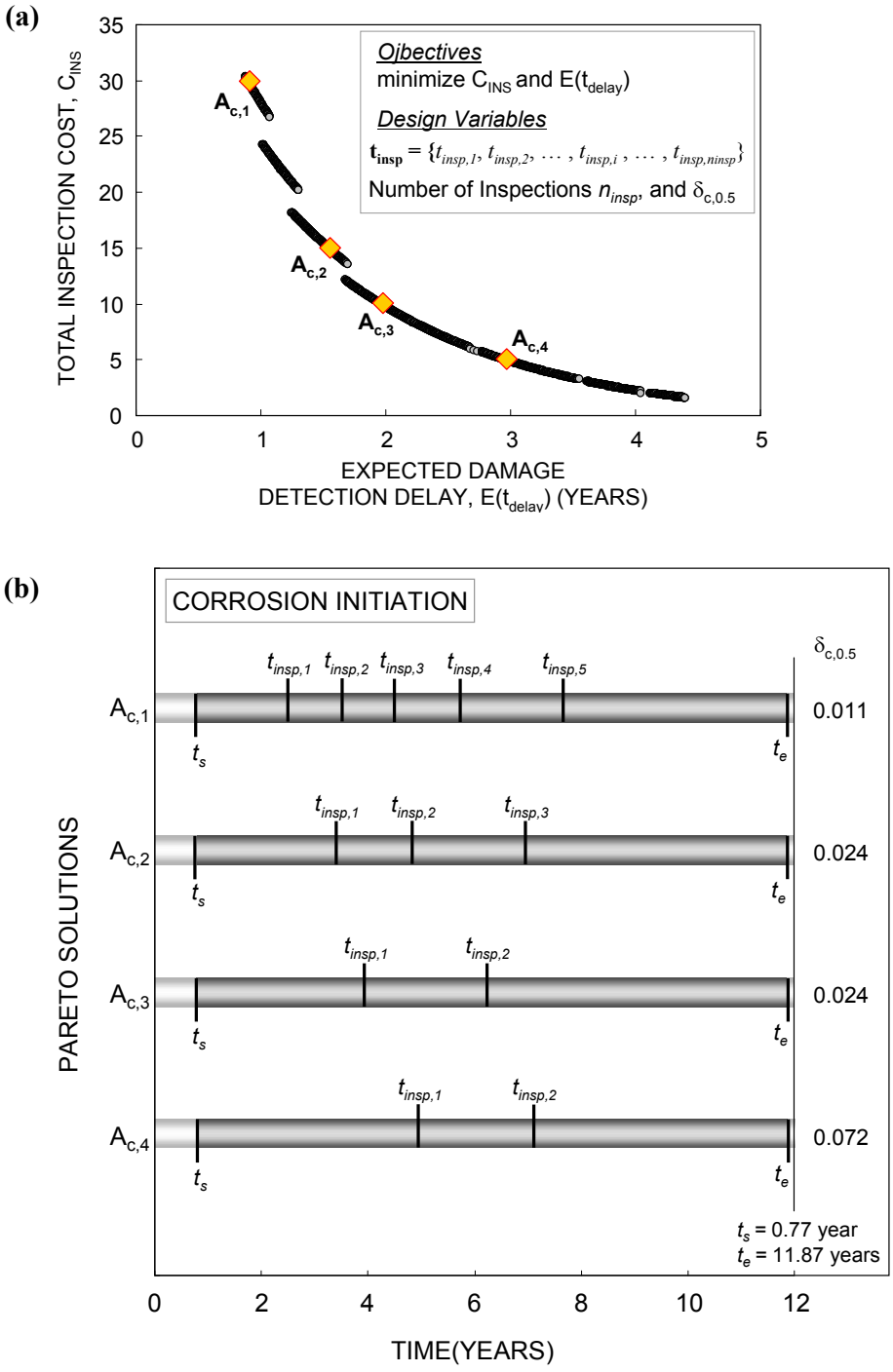

Figure 5.14 (a) Pareto solution set of bi-objective optimization problem; and **(b)** inspection plans for solutions $A_{c,1}$, $A_{c,2}$, $A_{c,3}$, and $A_{c,4}$ in (a)

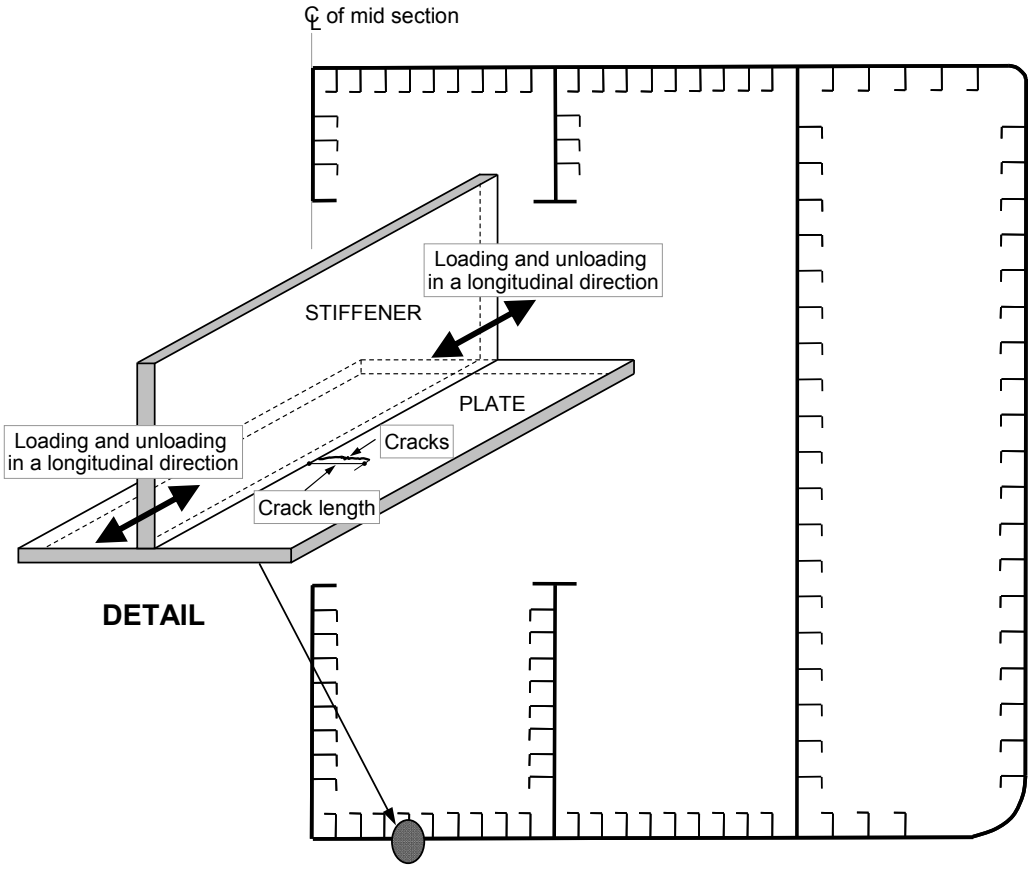

Figure 5.15 Schematic diagrams of the mid-ship section of a ship and the assumed location of cracks

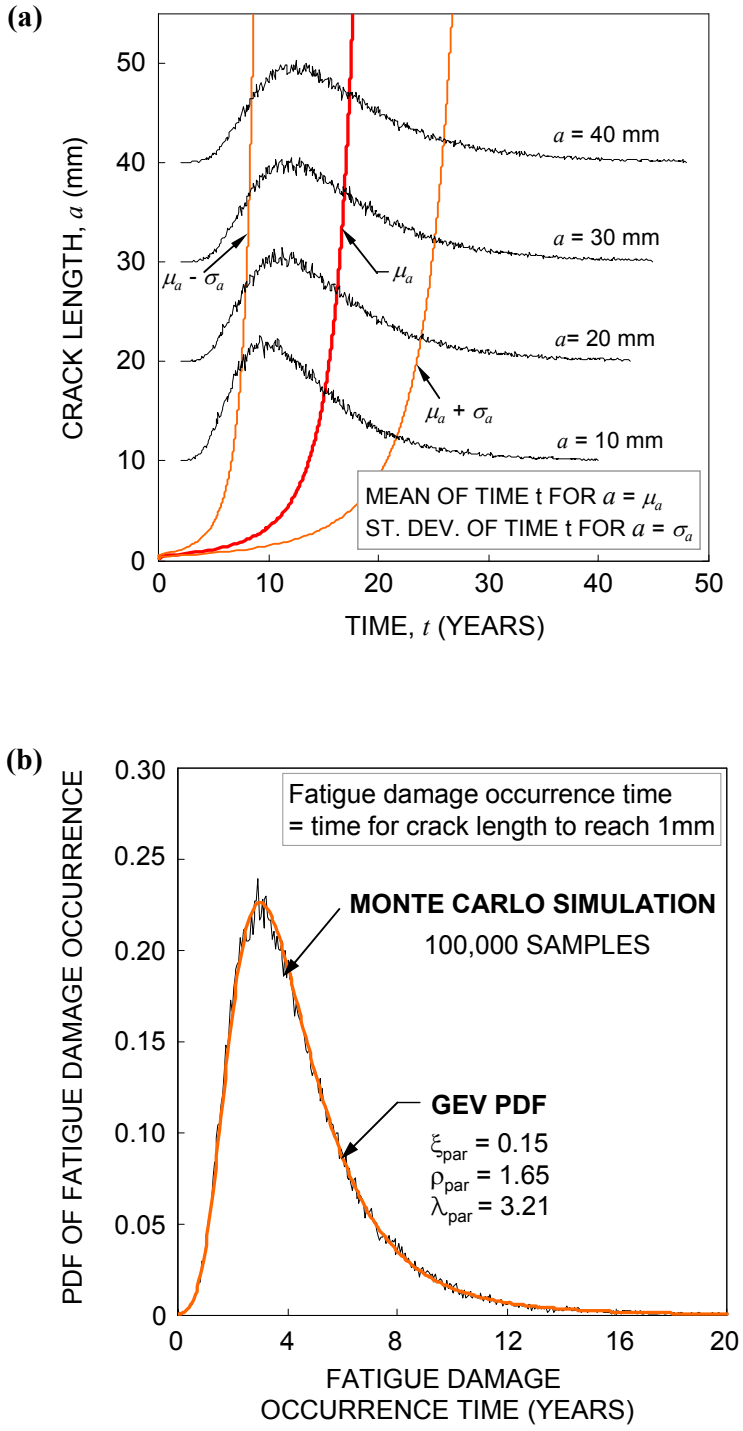

Figure 5.16 (a) Time-variant crack length with PDFs of times when $a = 10mm$, $20mm$, $30mm$, and $40mm$; and **(b)** GEV PDF of fatigue damage occurrence time

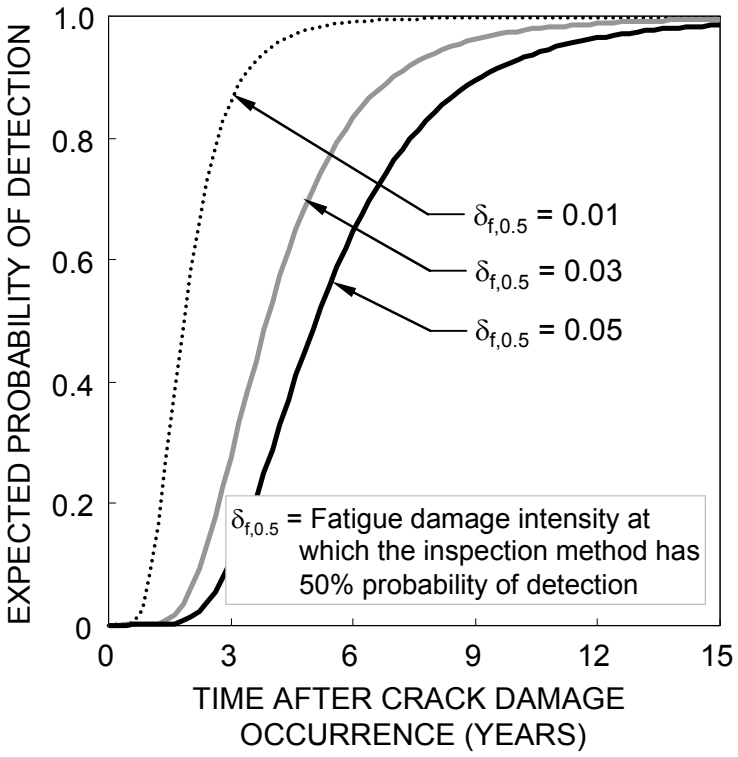

Figure 5.17 Expected probability of detection versus time after fatigue crack damage occurrence for $\delta_{f,0.5} = 0.01$, $\delta_{f,0.5} = 0.03$, and $\delta_{f,0.5} = 0.05$

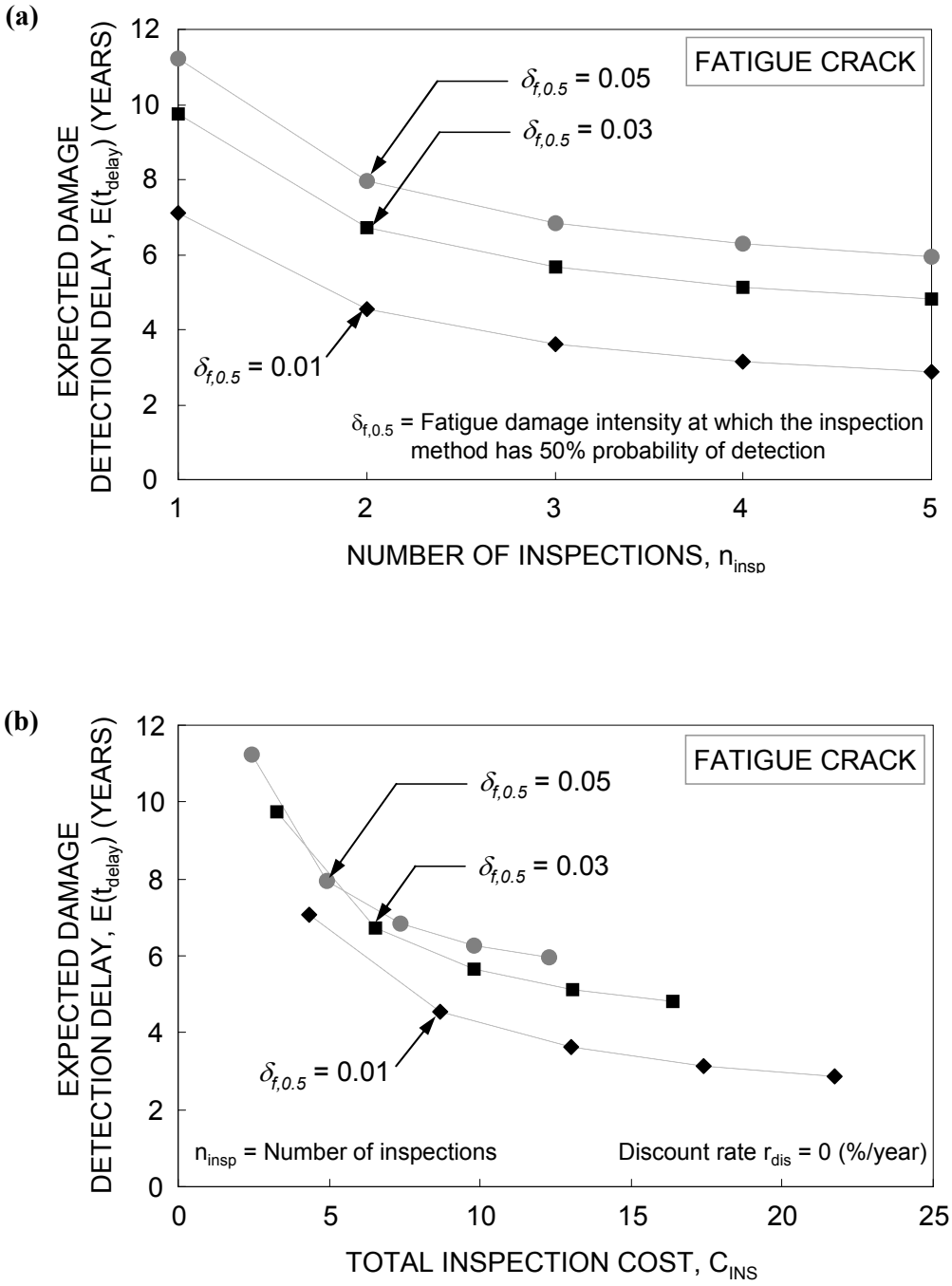

Figure 5.18 Effects of **(a)** number of inspections and **(b)** total inspection costs on minimum expected fatigue damage detection delay for $\delta_{f,0.5} = 0.01$, $\delta_{f,0.5} = 0.03$, and $\delta_{f,0.5} = 0.05$

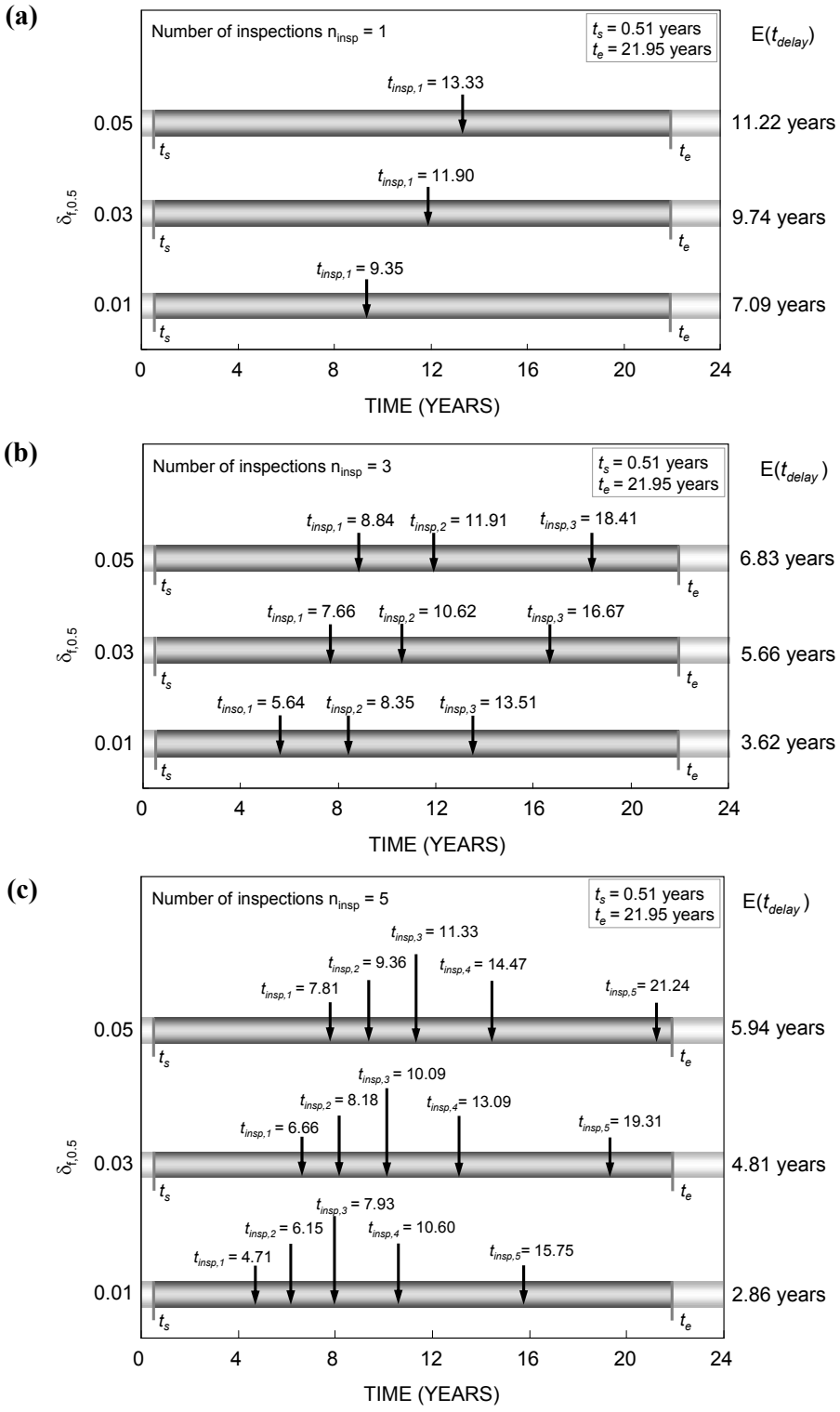

Figure 5.19 Optimum inspection plans for number of inspections **(a)** $n_{insp} = 1$; **(b)** $n_{insp} = 3$; **(c)** $n_{insp} = 5$

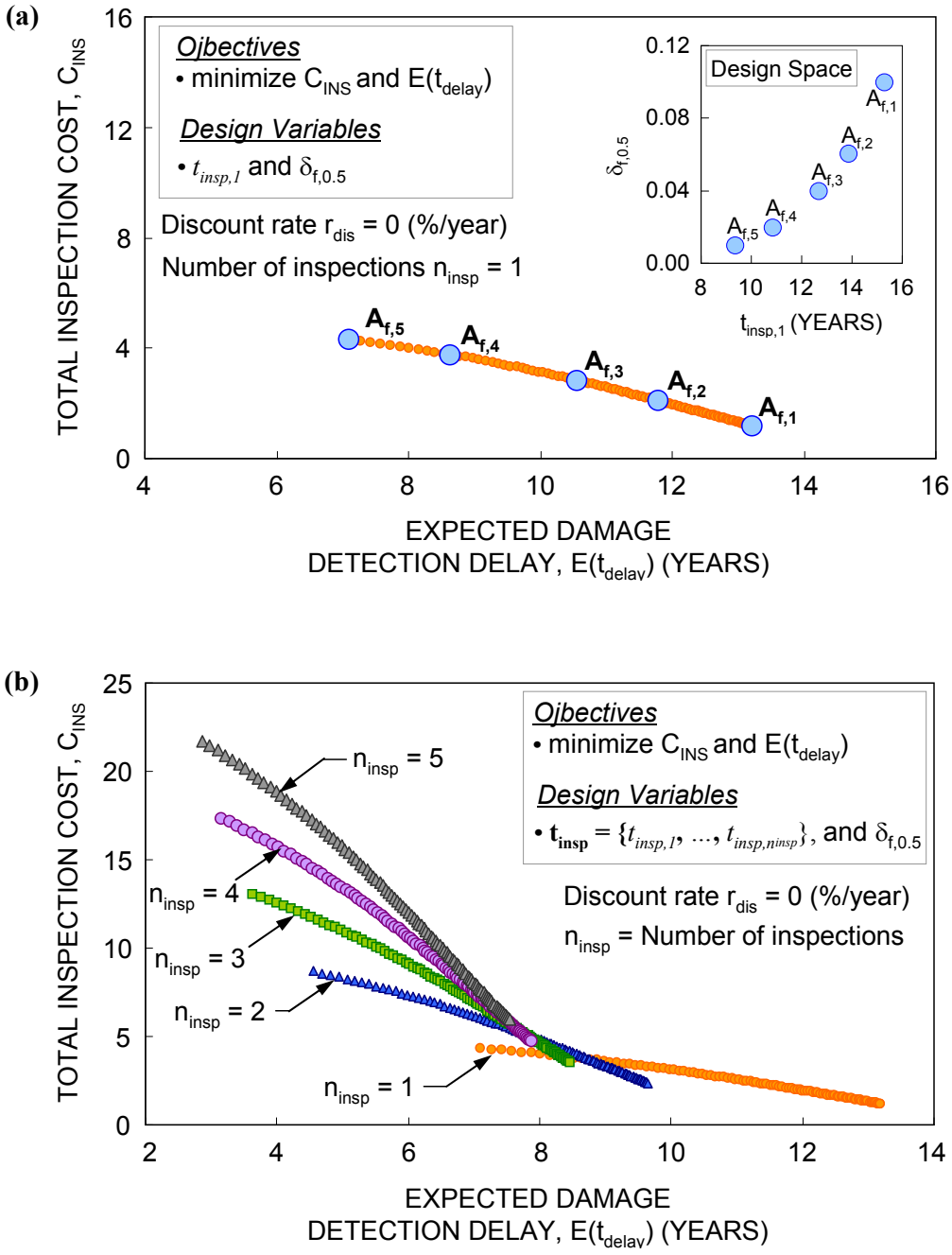

Figure 5.20 (a) Pareto solution set and design space of $t_{insp,1}$ and $\delta_{f,0.5}$, for given n_{insp} = 1; **(b)** Pareto solution sets for design variables $\mathbf{t_{insp}}$ and $\delta_{f,0.5}$, and given n_{insp} = 1, 2, 3, 4, and 5; **(c)** final Pareto solution set; and **(d)** optimum inspection plans for solutions $B_{f,1}$, $B_{f,2}$, $B_{f,4}$, and $B_{f,6}$ in (c)

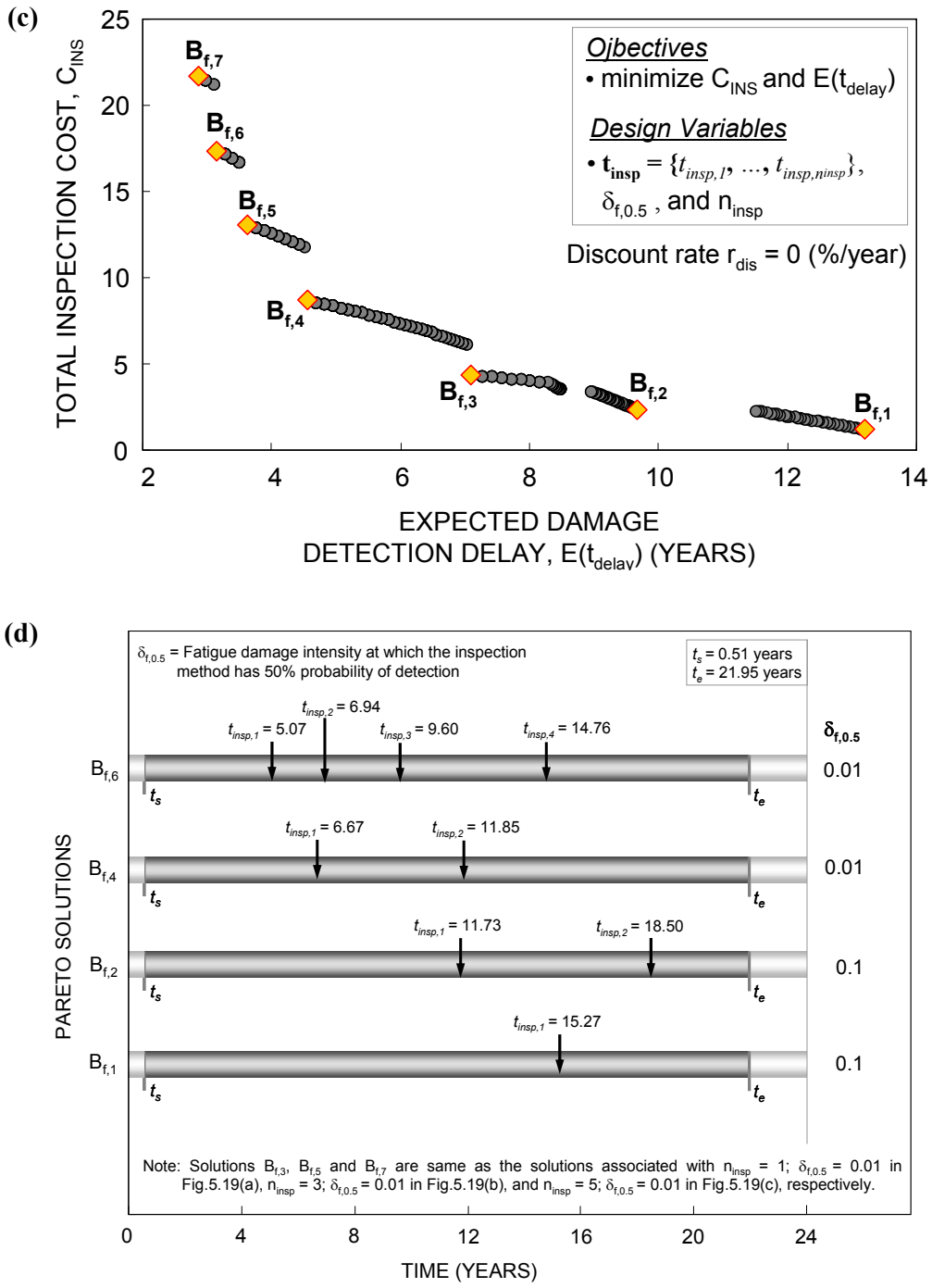

Figure 5.20 (a) Pareto solution set and design space of $t_{insp,1}$ and $\delta_{f,0.5}$, for given n_{insp} = 1; **(b)** Pareto solution sets for design variables $\mathbf{t_{insp}}$ and $\delta_{f,0.5}$, and given n_{insp} = 1, 2, 3, 4, and 5; **(c)** final Pareto solution set; and **(d)** optimum inspection plans for solutions $B_{f,1}$, $B_{f,2}$, $B_{f,4}$, and $B_{f,6}$ in (c) (continued)

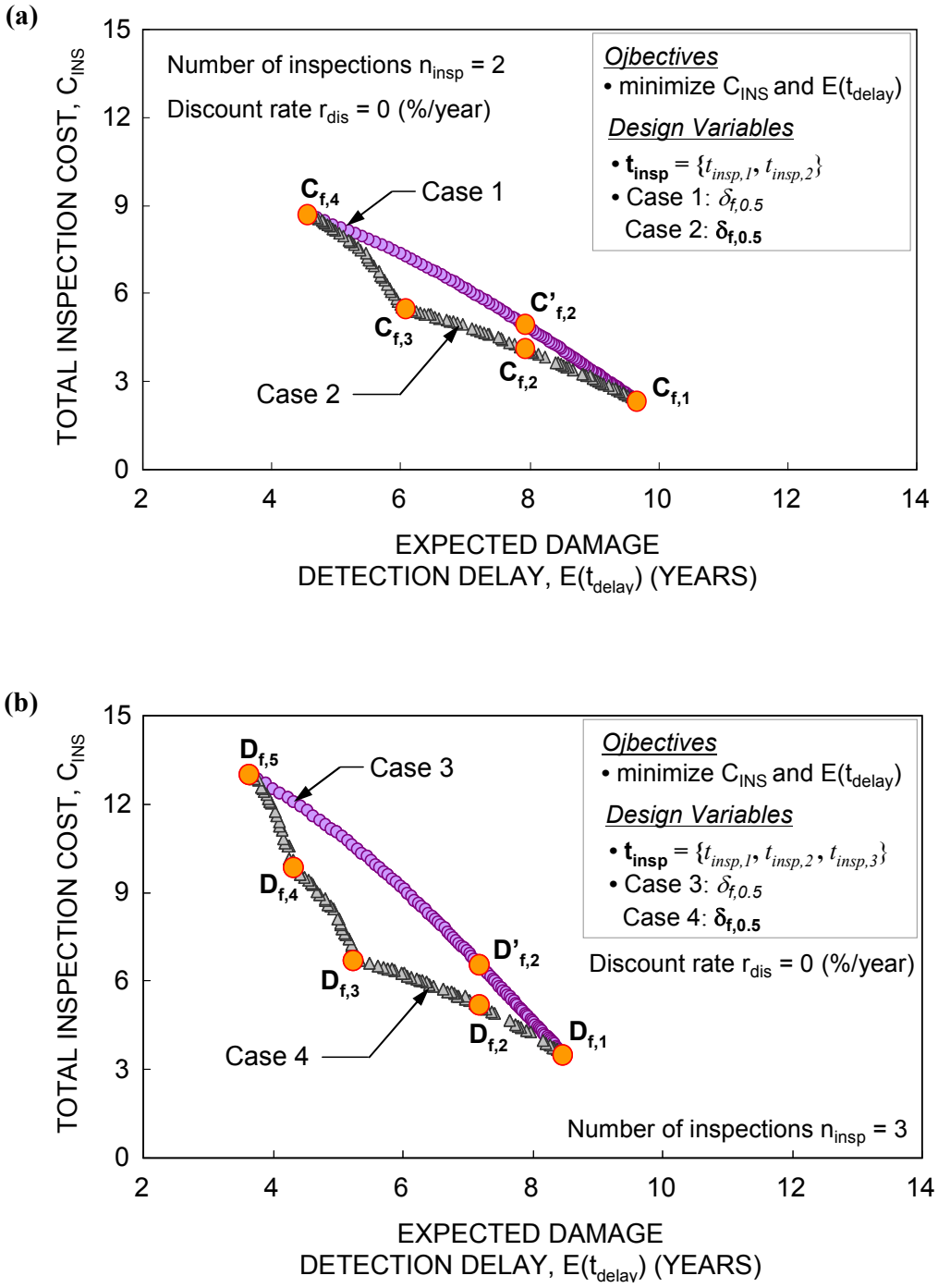

Figure 5.21 Comparison between Pareto solution sets based on same type and different types of inspections for number of inspections **(a)** $n_{insp} = 2$; **(b)** $n_{insp} = 3$

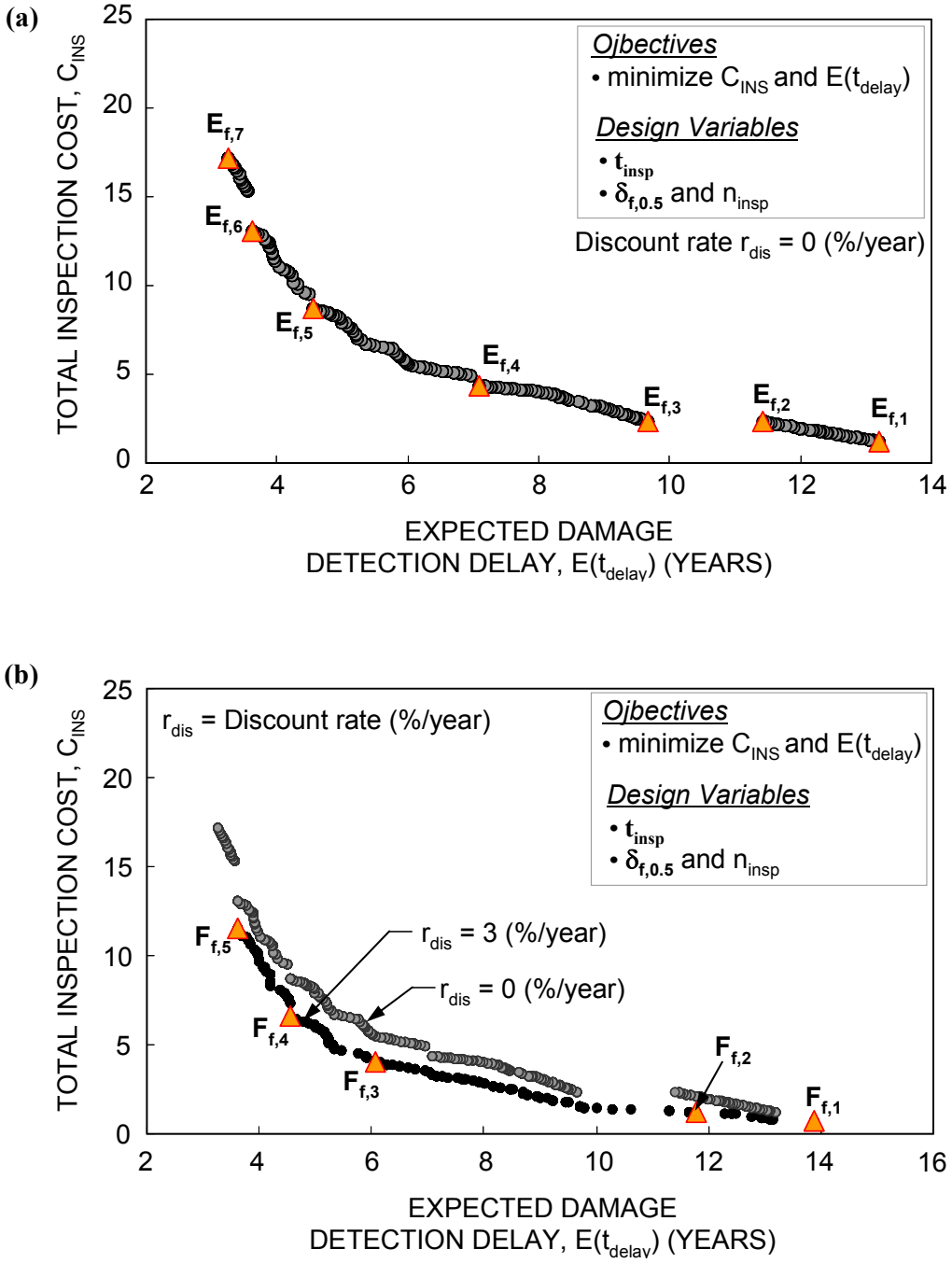

Figure 5.22 Pareto solution set of bi-objective optimization problem with design variables $\mathbf{t_{insp}}$, $\boldsymbol{\delta_{f,0.5}}$, and $\boldsymbol{n_{insp}}$ **(a)** without discount rate of money; **(b)** with discount rate of money r_{dis} = 3 %/year.

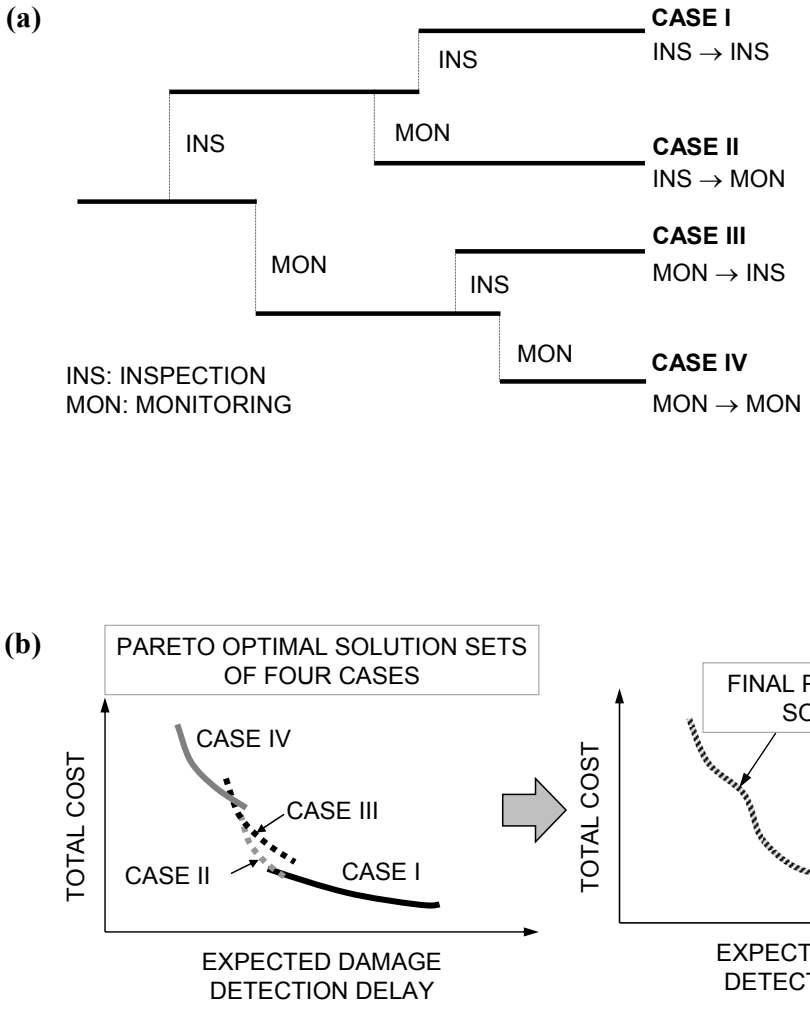

Figure 5.23 (a) Four possible cases for number of inspections and/or monitorings $n_{com} = 2$; and **(b)** Pareto optimal solution sets associated with four possible cases, and final Pareto solution sets for $n_{com} = 2$

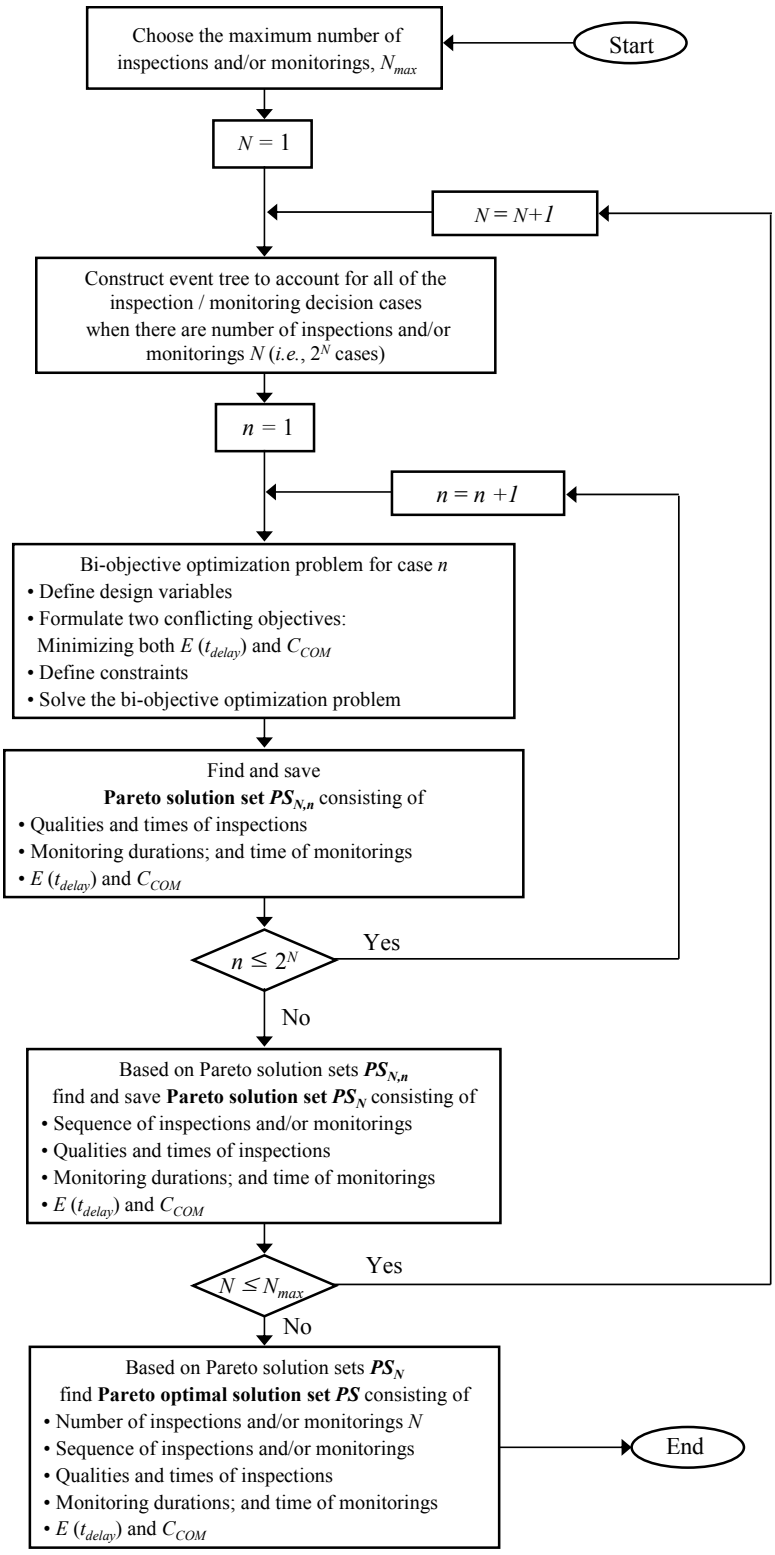

Figure 5.24 Flowchart to find the final Pareto optimal solution set ***PS***

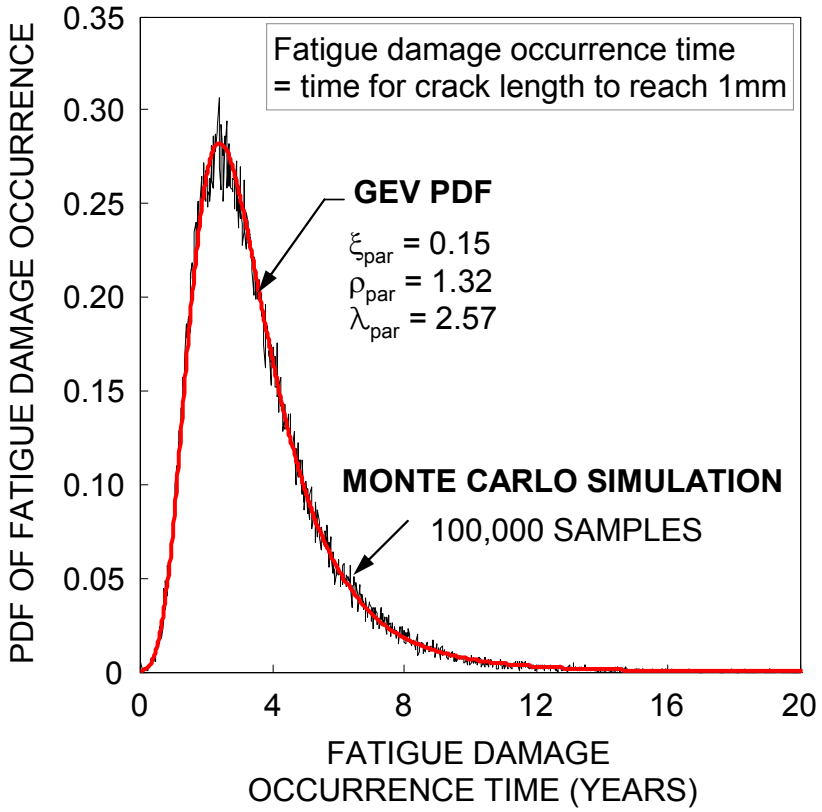

Figure 5.25 GEV PDF of fatigue damage occurrence time

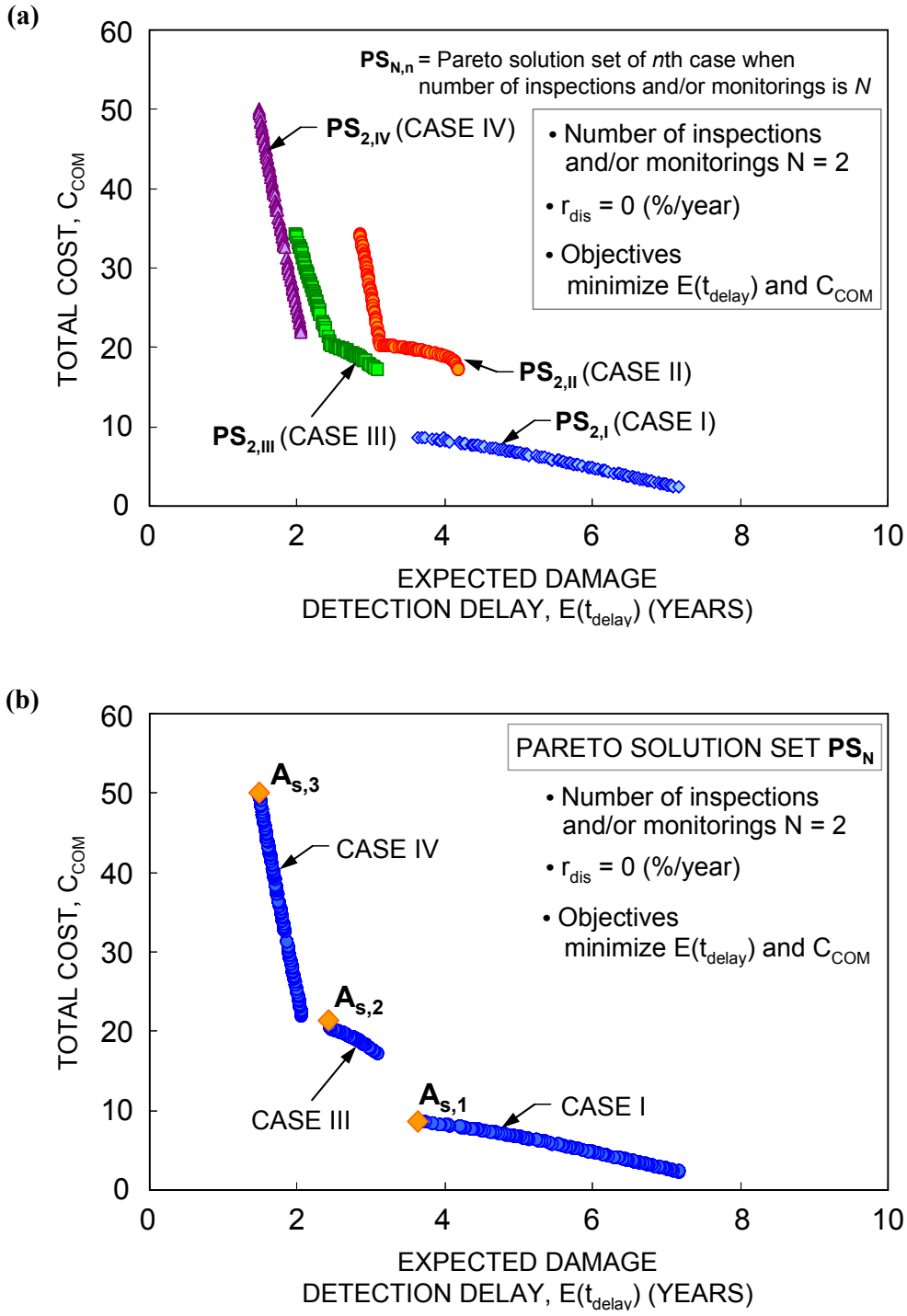

Figure 5.26 Number of inspections and/or monitorings $N = 2$, **(a)** Pareto solution sets $\boldsymbol{PS_{N,n}}$ for cases I, II, III, and IV; **(b)** Pareto solution set $\boldsymbol{PS_N}$; **(c)** combined inspection / monitoring plans for solutions $A_{s,1}$, $A_{s,2}$ and $A_{s,3}$ in **(b)**

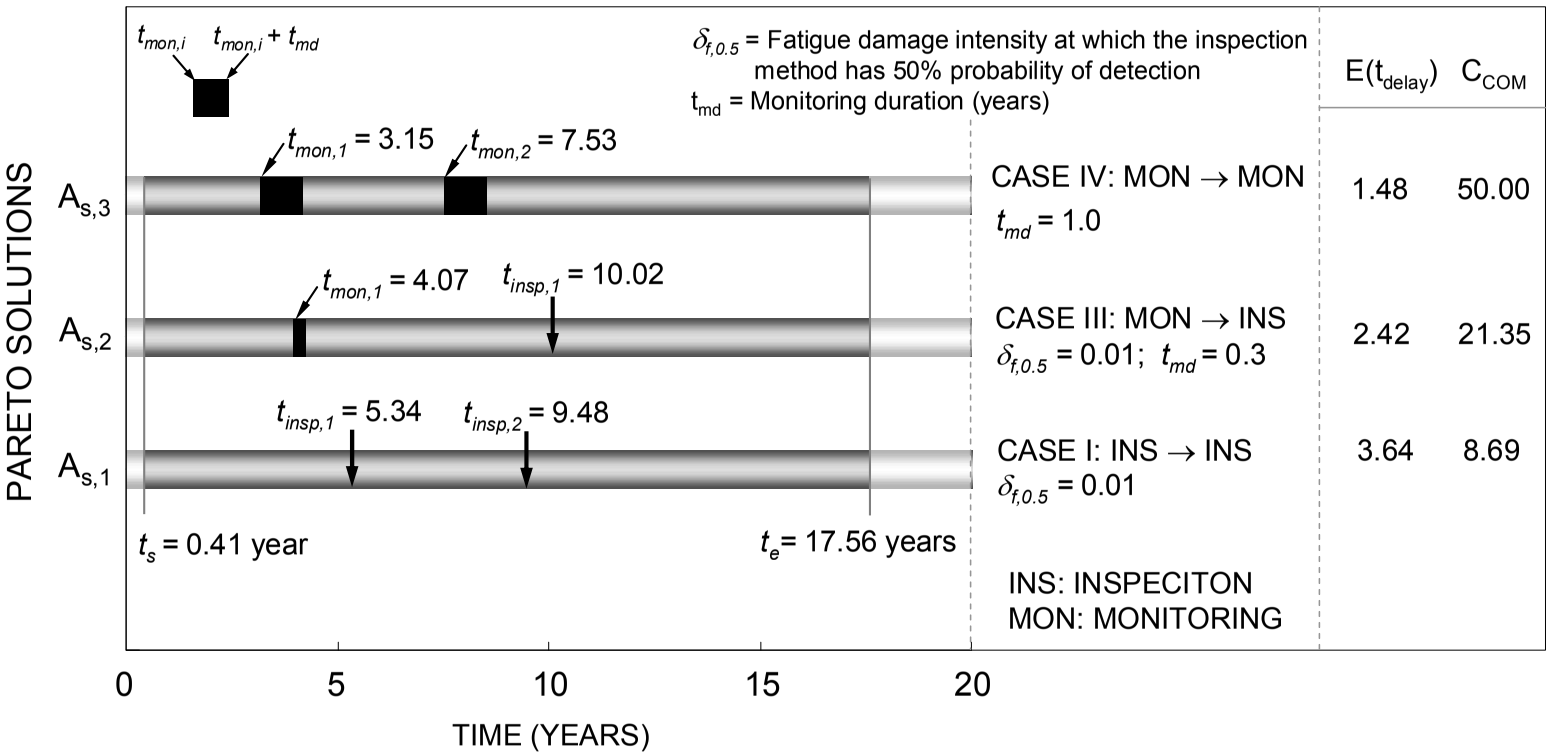

Figure 5.26 Number of inspections and/or monitorings N = 2, **(a)** Pareto solution sets $\boldsymbol{PS_{N,n}}$ for cases I, II, III, and IV; **(b)** Pareto solution set $\boldsymbol{PS_N}$; **(c)** combined inspection / monitoring plans for solutions $A_{s,1}$, $A_{s,2}$ and $A_{s,3}$ in **(b)** (continued)

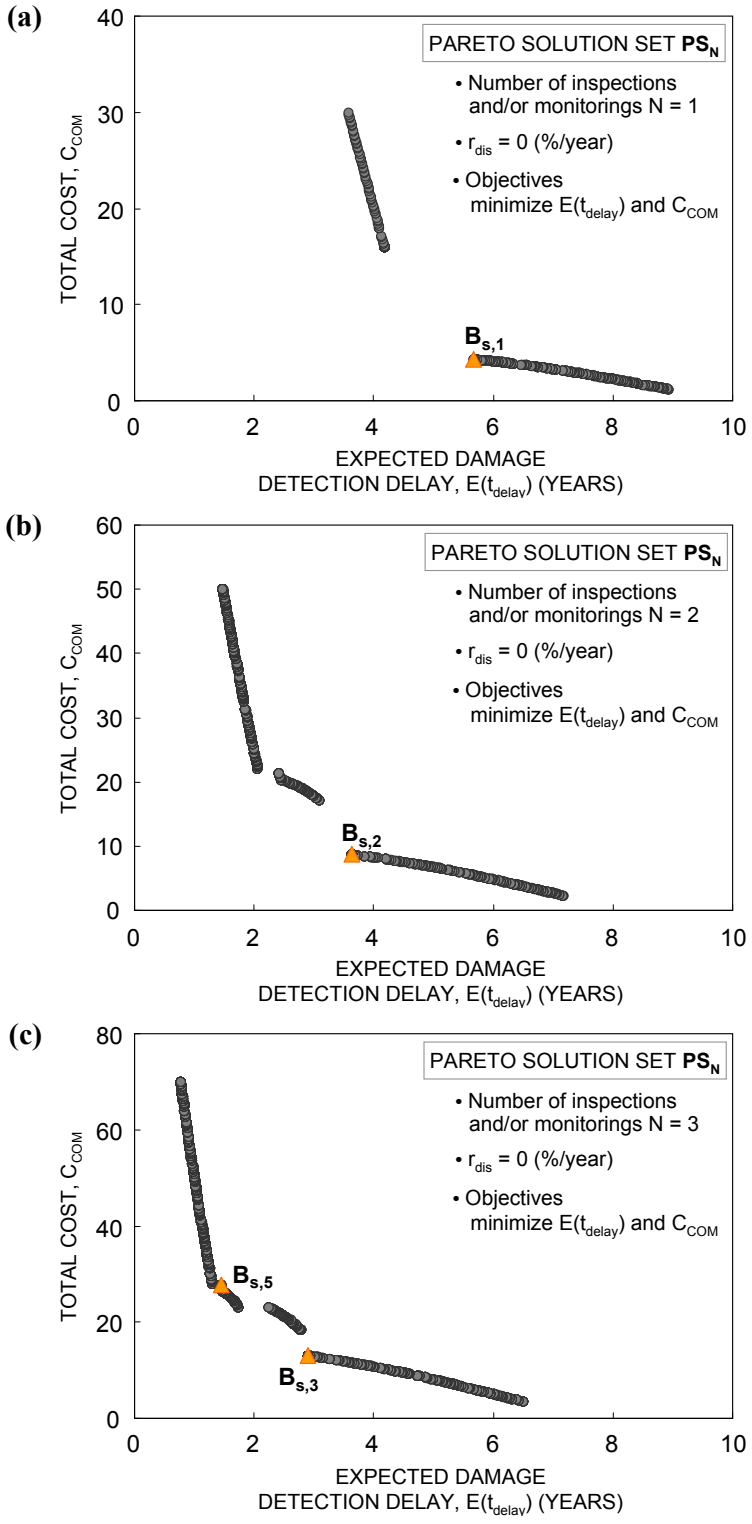

Figure 5.27 Pareto solution set $\boldsymbol{PS_N}$ for **(a)** $N = 1$; **(b)** $N = 2$; **(c)** $N = 3$; **(d)** $N = 4$; and **(e)** $N = 5$, and **(f)** final Pareto solution set ***PS***

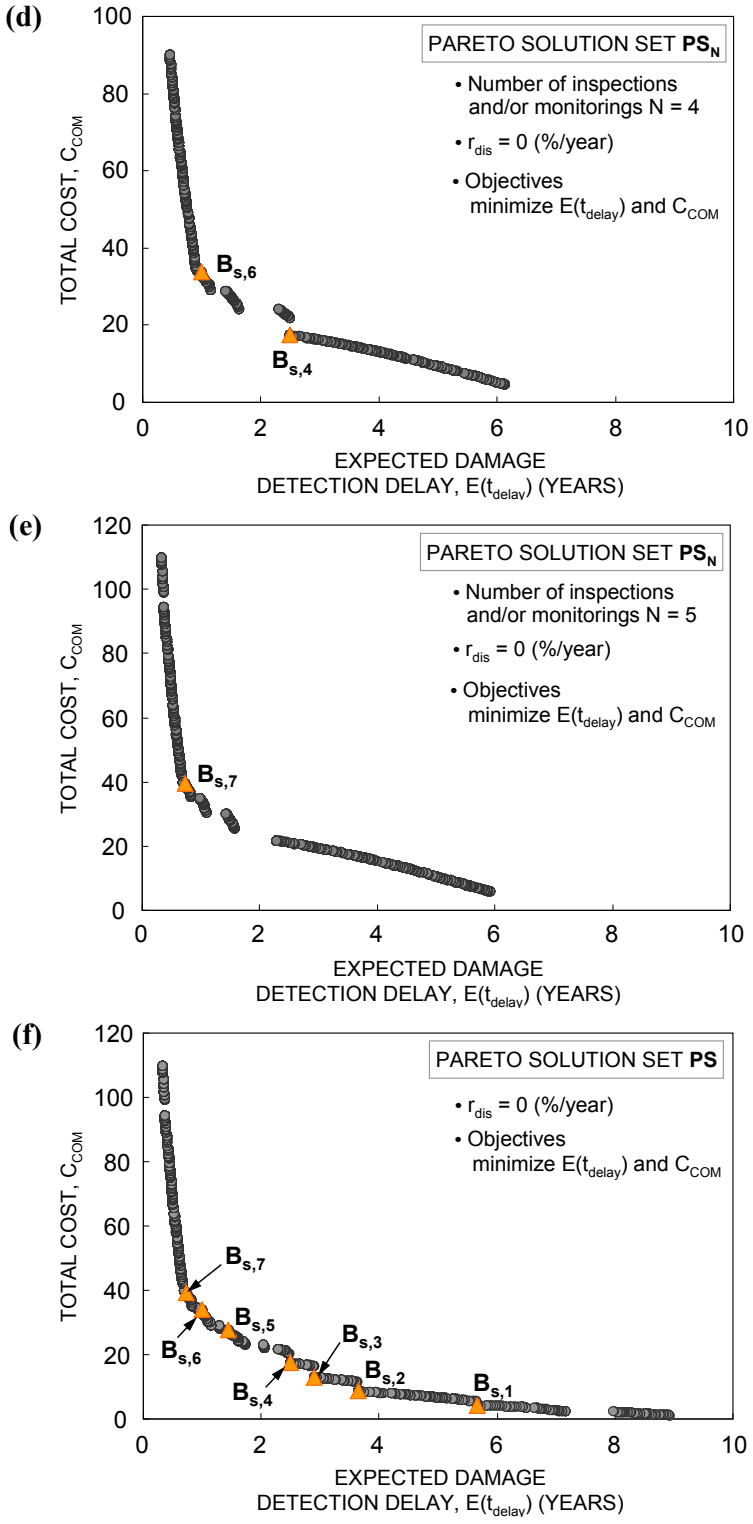

Figure 5.27 Pareto solution set $\boldsymbol{PS}_N$ for **(a)** $N = 1$; **(b)** $N = 2$; **(c)** $N = 3$; **(d)** $N = 4$; and **(e)** $N = 5$, and **(f)** final Pareto solution set ***PS*** (continued)

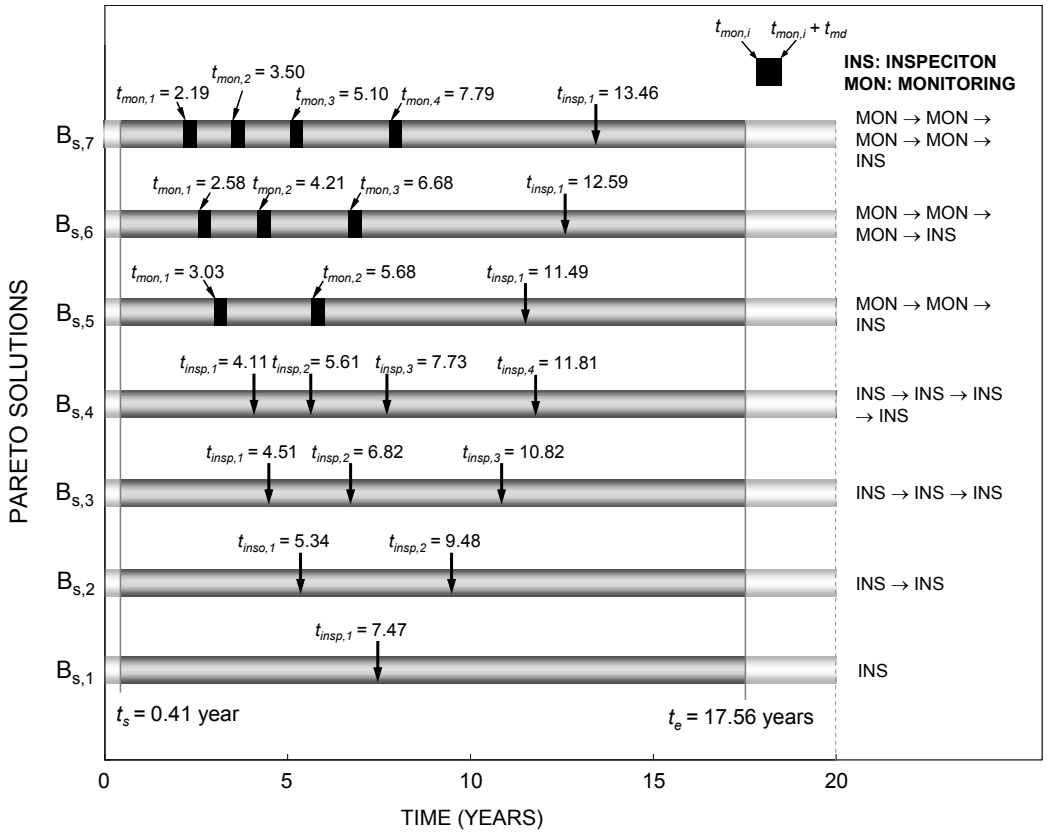

Figure 5.28 Combined inspection / monitoring plans for solutions $B_{s,1}$ to $B_{s,7}$ in Figure 5.27(f)

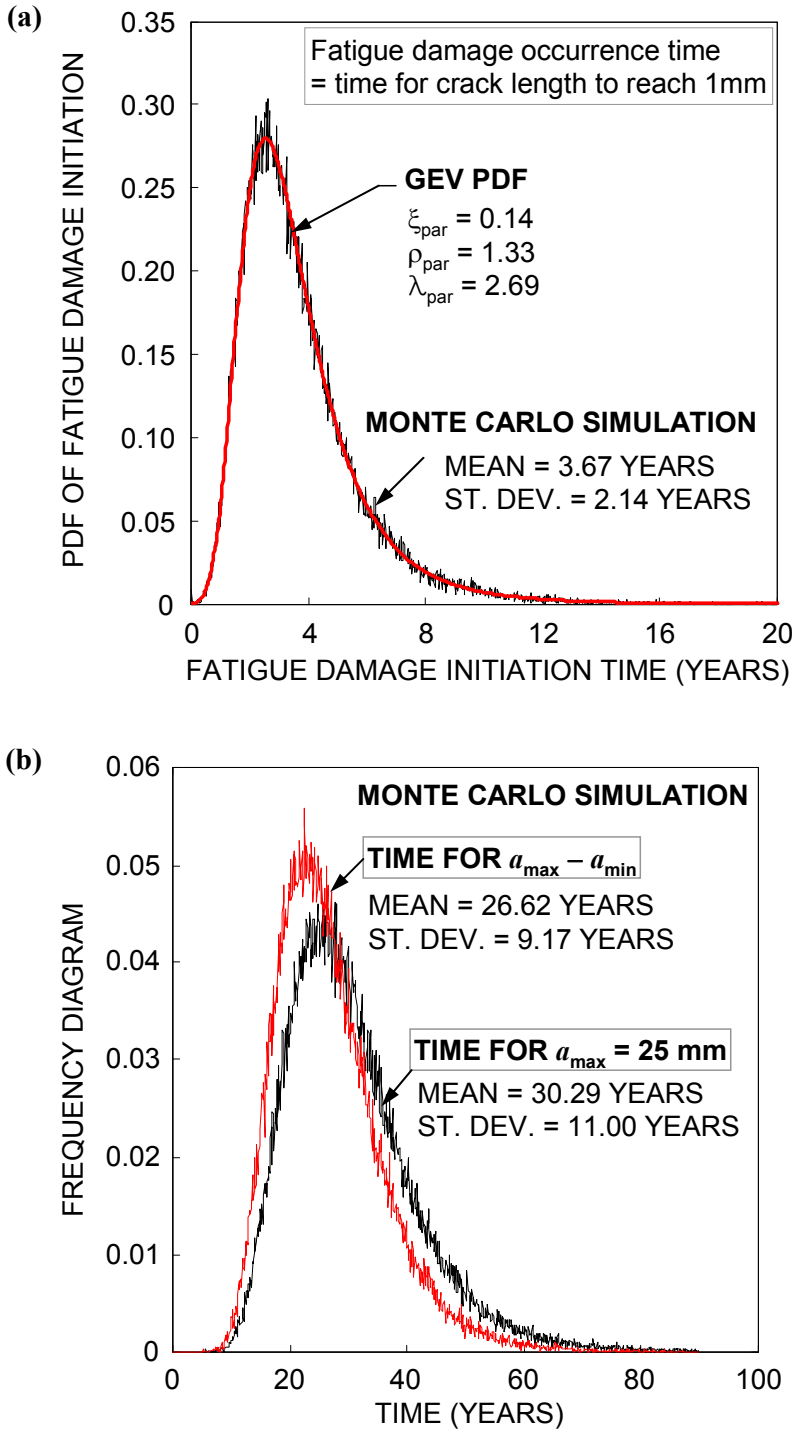

Figure 5.29 PDFs of time for reaching **(a)** crack size a_{min}; and **(b)** crack sizes a_{max} and a_{max} - a_{min}

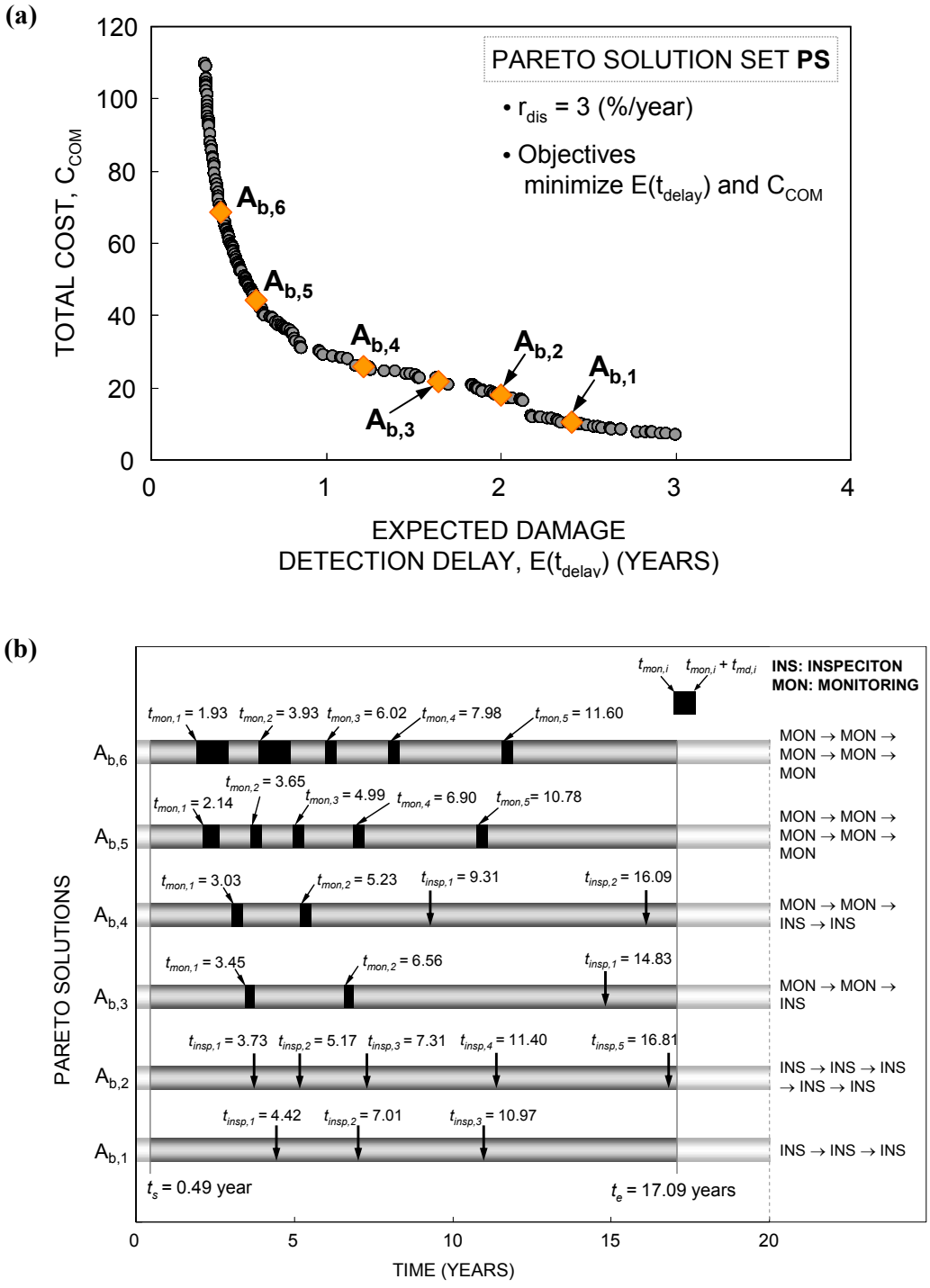

Figure 5.30 (a) Final Pareto solution set ***PS***; and **(b)** combined inspection / monitoring plans for solutions $A_{b,1}$ to $A_{b,6}$ in (a)

CHAPTER 6

COST-BASED OPTIMUM INSPECTION AND MONITORING PLANNING

6.1 Introduction

Inspection and monitoring are essential to detect the defects and predict the remaining life of deteriorating structures [Chang et al. 2003, Moan 2005, Ellingwood 2005]. Inspection is performed at uniform or non-uniform time intervals in order to find the location and extent of damage and apply a timely maintenance [Cramer et al. 1992]. Effective and timely inspection and maintenance can extend the lifetime of a structural system while preventing unexpected costly failure. For this reason, studies for developing methodologies to establish optimum inspection and repair strategies have been performed [Madsen et al. 1991, Mori and Ellingwood 1994b, Frangopol et al. 1997b, Estes and Frangopol 1999, Enright and Frangopol 1999, Estes and Frangopol 2001, Garbatov et al. 2001].

This chapter proposes a probabilistic approach for cost-based optimum inspection and monitoring scheduling. The proposed approach is illustrated by using a fatigue sensitive ship hull structure. The inspection schedule is the solution of an optimization problem to minimize the expected total cost including the costs of inspections or monitorings and the expected failure cost. The solution of this problem provides optimum inspection times and quality of inspections. Optimum

monitoring starting times and monitoring durations are obtained by solving the optimization for monitoring scheduling. The time-based failure criterion is defined using time-based safety margin defined as the difference between the time for damage to reach the critical fatigue crack size and the damage detection time. This criterion is based on the assumption that appropriate repair and retrofit methods are applied immediately after the crack is detected. Uncertainties associated with prediction of damage occurrence time and time to reach the critical fatigue crack size are considered by using Monte Carlo simulation. Damage detection time and damage detection delay are formulated using the event tree model. This formulation considers the uncertainties associated with fatigue crack damage occurrence / propagation and damage detection. Effects of the failure cost on inspection and monitoring scheduling are also studied.

6.2 Inspection and Monitoring of Steel Structures

Steel structures are usually inspected at uniform or non-uniform time periods to detect damage and apply a timely maintenance. The quality of inspection method affects optimum inspection and repair strategy to minimize the expected life-cycle cost [Frangopol et al. 1997b]. The quality of inspection method to detect fatigue crack is generally represented by the probability of detecting an existing defect size [Madsen et al. 1991, Mori and Ellingwood 1994a and 1994b, Chung et al. 2006]. The probability of detection considering crack size and inspection quality has been

studied by Packman et al. (1969), Berens and Hovey (1981), and Cramer et al. (1992).

During the past two decades, powerful damage detection techniques including structural health monitoring (SHM) have been developed and applied. The following inspection methods are commonly used to detect fatigue crack: visual inspection, dye penetrant testing, magnetic particle testing, ultrasonic testing, acoustic emission testing and X-radiographic testing. Appropriate inspection methods should be selected by considering the type of defect (e.g., surface crack, embedded crack), probability of detection, and inspection cost. For example, magnetic particle testing provides reliable outcomes for surface crack but not for embedded crack [Cartz 1995]. Ultrasonic testing has higher probability of detection than other inspection methods for embedded crack. However, this type of testing is considerably expensive [Fisher et al. 1998, Miki 2007].

SHM has been treated as an efficient tool to assess structural integrity and the nature of damage in a structure [Chang et al. 2003, Kulkarni and Achenbach 2008]. The main advantages of SHM are: (a) lead to timely damage detection through continuous and automating inspection process [Boller and Buderath 2007], (b) provide additional information to reliably assess and predict the structural performance [Kwon and Frangopol 2010]. For monitoring fatigue crack growth in steel structures, surface mountable eddy-current sensor, surface acoustic wave sensor, and electrochemical fatigue sensor can be useful [Papazian et al. 2007].

6.3 Cost-Based Optimum Inspection and Monitoring Planning For Steel Structures Subjected to Fatigue

Fatigue cracks may not threaten structural integrity of steel structures with high degree of structural redundancy [White and Ayyub 1987, Rolfe et al. 1993, Clark 1991]. However, any crack should be detected as early as possible, and appropriate repair and retrofit methods have to be applied immediately, in order to prevent unexpected structural failure [Fisher et al. 1998, Glen et al. 2000]. For this reason, fatigue cracks must be detected and repaired before the time for cracks to reach critical sizes [Glen et al. 2000, Dexter et al. 2003].

6.3.1 Crack Size-Based and Time-Based Safety Margins

A fatigue sensitive structure has a safety margin during a fatigue damage process. This safety margin depends on the resistance to fatigue crack growth. Increase of the fatigue crack growth resistance leads to larger safety margin during a fatigue damage process. This safety margin can be expressed using crack-size and time. A crack size-based safety margin a_{mar} during a fatigue damage process is [Kim and Frangopol 2011e]

$$a_{mar} = a_{max} - a_{min} \tag{6.1}$$

where a_{min} = minimum detectable crack size, and a_{max} = maximum crack size. The critical state of fatigue damage is referred to as the state when the crack size reaches

a_{max}, as mentioned in Equation (5.19). A time-based safety margin t_{mar} is defined herein as [Kim and Frangopol 2011e]

$$t_{mar} = t_{cr} - t_{ini} \tag{6.2}$$

where t_{ini} = fatigue damage initiation time, and t_{cr} = time when fatigue damage reaches the critical state. Figure 6.1 illustrates both crack size-based and time-based safety margins, and the relation between them. The minimum detectable crack size a_{min} and maximum crack size a_{max} are associated with fatigue damage initiation time (i.e., t_{ini}) and time for crack to reach the maximum crack size a_{max} (i.e., t_{cr}), respectively. If damage occurs at time t_{ini} and is detected at time t_{det}, the damage detection delay t_{delay} is $t_{det} - t_{ini}$ (see Figure 6.1). In order to apply the appropriate maintenance action, damage should be detected before time t_{cr}. In other words, the damage detection delay t_{delay} has to be less than the time-based safety margin t_{mar}.

Fatigue crack growth over time is uncertain. Therefore, crack size-based and time-based safety margins are uncertain. Figure 6.2(a) shows the PDFs of the minimum crack size a_{min} at time t_{ini}, maximum crack size a_{max} at time t_{cr} , and crack size a_{det} at time t_{det} when the damage is detected. The PDF of crack size-based safety margin a_{mar} during a fatigue damage process can be obtained using the PDFs of crack sizes a_{min} and a_{max}. The PDFs of time (i.e., t_{ini}, t_{det}, t_{cr}) for fatigue crack to reach a specific crack size are illustrated in Figure 6.2(b). The time-based safety margin t_{mar} can be represented by its PDF considering uncertainites associated with times t_{ini} and t_{cr}. In this study, the time-based safety margin is used to formulate the failure

criterion.

6.3.2 Expected Damage Detection Time and Damage Detection Delay

Inspection methods are not perfect. In order to consider the probability of detection of an inspection method, the event tree model can be used as shown in Figure 5.2. Based on this model, expected damage detection time and delay can be formulated. When n_{insp} inspections are used to detect the damage, and damage occurs in the time interval $t_{insp,i-1} \le t_{ini} < t_{insp,i}$, the expected damage detection delay $\overline{t}_{delay}$ is

$$\overline{t}_{delay} = \sum_{k=i}^{n_{insp}+1} \left\{ \left(\prod_{j=1}^{k} \left(1 - P_{insp,j-1}\right) \right) \cdot P_{insp,k} \cdot t_{insp,k} \right\} - t_{ini} \qquad \text{for } t_{insp,i-1} \le t_{ini} < t_{insp,i} \tag{6.3}$$

where $P_{insp,k}$ = probability of detection of kth inspection, $t_{insp,k}$ = kth inspection time. Furthermore, based on Equation (6.3) and the relation between damage detection time t_{det} and delay t_{delay} (i.e., $t_{delay} = t_{det} - t_{ini}$) in Figure 6.1, the expected damage detection time $\overline{t}_{det}$ becomes

$$\overline{t}_{det} = \overline{t}_{delay} + t_{ini} \tag{6.4}$$

Under the assumption of no damage detection delay during monitoring, the expected damage detection time $\overline{t}_{det}$ is formulated based on Equation (6.4) as

$$\overline{t}_{det} = t_{mon,i} \qquad \text{for } t_{mon,i-1} + t_{md} \le t_{ini} < t_{mon,i} \tag{6.5a}$$

$$\overline{t}_{det} = t_{ini} \qquad \text{for } t_{mon,i} \le t_{ini} < t_{mon,i} + t_{md} \tag{6.5b}$$

where $t_{mon,i}$ = ith monitoring starting time. If the damage occurs before $t_{mon,i}$, $\overline{t}_{det}$ = $t_{mon,i}$. When the damage occurs during monitoring, $\overline{t}_{det}$ = t_{ini}. Furthermore, the

relation between $\overline{t}_{det}$ and $\overline{t}_{delay}$ is $\overline{t}_{det} = \overline{t}_{delay} + t_{ini}$.

6.3.3 Time-Based Probability of Failure

If appropriate repair and/or retrofit methods are applied immediately after the damage is detected, the time-based failure criterion can be defined as

$$t_{cr} - \overline{t}_{det} < 0 \tag{6.6}$$

where t_{cr} = time when fatigue damage reaches the critical state (see Figure 6.1 and and Equation (6.2)), and $\overline{t}_{det}$ = expected damage detection time. This failure criterion is also expressed in terms of the time-based safety margin t_{mar} and the expected damage detection delay $\overline{t}_{delay}$ as

$$t_{mar} - \overline{t}_{delay} < 0 \tag{6.7}$$

Considering the uncertainties associated with damage occurrence, propagation, and detection, t_{cr}, $\overline{t}_{det}$, t_{mar}, and $\overline{t}_{delay}$ in Equations (6.6) and (6.7) are treated as random variables. Therefore, the time-based probability of failure just before damage detection is

$$p_F = P\,[t_{cr} - \overline{t}_{det} < 0] = P\,[t_{mar} - \overline{t}_{delay} < 0] \tag{6.8}$$

6.3.4 Expected Total Cost

The expected total cost $E(C_{total})$ includes the initial cost, the inspection (or monitoring) cost, the expected maintenance cost, and the expected failure cost [Frangopol et al. 1997b]. The failure cost represents the monetary loss due to a

structural failure, and the expected failure cost $E(C_{FAIL})$ is [Frangopol et al. 1997b]

$$E(C_{FAIL}) = p_F \times C_{FAIL} \tag{6.9}$$

where p_F = time-based probability of failure, and C_{FAIL} = expected monetary loss due to structural failure. Estimation of C_{FAIL} should consider in a rational way the cost of design and construction of a new structure, expected cost of human injuries, and user costs, among others [Estes and Frangopol 2005]. In this study, p_F defined in Equation (6.8) is used for estimating the expected failure cost $E(C_{FAIL})$. An approach to establish an optimum inspection or monitoring schedule is based on a formulation with the objective of minimizing the expected total cost $E(C_{total})$. In this study, $E(C_{total})$ is estimated as

$$E(C_{total}) = C_{INS} + E(C_{FAIL}) \quad \text{for inspection} \tag{6.10a}$$

$$E(C_{total}) = C_{MON} + E(C_{FAIL}) \quad \text{for monitoring} \tag{6.10b}$$

where C_{INS} = total inspection cost (see Equation (5.29)), and C_{MON} = total inspection cost (see Equation (5.31)). In this chapter, α_{ins} , $C_{mon,ini}$ and $C_{mon,an}$ in Equation (5.28) and (5.30) are assumed 5, 10 and 20, respectively. The detail computational procedure associated with the approach proposed in this chapter is provided in Figure A.5.

6.4 Application to Ship Hull Structures Subjected to Fatigue

The proposed approach is applied to a ship hull structure subjected to fatigue. The intersection of longitudinal stiffeners with transverse web frames (see Figure 6.3(a)) is

in general the critical location with the highest priority for inspection and repair [Dexter et al. 2003]. As shown in Figure 6.3(b), the fatigue crack in the bottom hull plate can initiate in the fillet weld between hull plating and transverse frame, and the crack growth model is based on semi-elliptical shape.

6.4.1 Time-Dependent Crack Growth

In order to predict the crack size in the critical location in Figure 6.3, Equation (5.11) is used. The geometry function $Y(a)$ (see Equation (5.9)) for a semi-elliptical shape is expressed as [Madsen et al. 1991]

$$Y(a) = Y_e(a) \cdot Y_s(a) \cdot Y_t(a) \cdot Y_w(a) \cdot Y_g(a) \tag{6.11}$$

where $Y_e(a)$ = crack shape factor = $\left[1.0 + 4.59\left(a/2c\right)^{1.65}\right]^{-0.5}$ where a = depth crack size, c = length crack size, $Y_s(a)$ = front face factor = $0.98 - 0.16\left(a/2c\right)$, $Y_t(a)$ = finite thickness correction factor = $1.0 + 0.21\left(a/t_{hp}\right) + 0.14\left(a/t_{hp}\right)^2$, $Y_w(a)$ = finite width correction factor = 1.0, $Y_g(a)$ = stress gradient factor = $K_{tm}\left[1 + 1/0.36\left(a/t_{hp}\right)^{0.249}\right]^{-1}$ where t_{hp} = hull plating thickness = 30 *mm*, K_{tm} = stress concentration factor = 3.475. The relation between a and c is assumed as $2c = 2.59 \cdot a^{0.946}$. All necessary data to predict depth crack size a are provided in Table 6.1. In this application, the initial depth crack size a_o is assumed lognormally distributed with mean value = 0.5 *mm* [Chung et al. 2006] and coefficient of variation (COV) = 0.2. Material crack growth parameter C is considered to be lognormally distributed with mean value = 2.3×10^{-12} [BS7910 2005], and COV =

0.3. The stress range S_{sr} is treated as a random variable with a Weibull PDF, and the parameter m in Equation (5.8) is assumed to be deterministic $m = 3.0$ [Madsen et al. 1991]. Increase rate of number of cycles r_{cycle} in Equation (5.11) is not considered in this application.

Figure 6.4(a) shows the PDF of the damage initiation time t_{ini}, defined as the time when the fatigue crack depth size reaches $1mm$. The mean and standard deviation of t_{ini} are 4.25 and 2.79 years, respectively. The PDF of time t_{cr} for the depth crack size to reach 20 *mm* is shown in Figure 6.4(b). Figures 6.4(a) and 6.4(b) are obtained by Monte Carlo simulation with 100,000 samples. In this chapter, the fatigue depth crack size of 1.0 *mm* serves as the crack damage criterion (i.e., $a_{min} = 1$ *mm* in Equation (5.19)), and the critical depth crack size a_{max} in Equation (5.19) is assumed 20 *mm*. Based on the PDFs in Figures 6.4(a) and 6.4(b), the PDF of time-based safety margin $t_{mar} = t_{cr} - t_{ini}$ is obtained as shown in Figure 6.5. In order to find the probability of time to failure as indicated in Equation (6.8), the PDF of t_{cr} (or t_{mar}) is used. The inspection times, number of inspections, and detectability of an inspection method affect the uncertainties associated with $\overline{t}_{det}$ (or $\overline{t}_{delay}$) in Equations (6.3) and (6.4).

6.4.2 Optimum Inspection Schedules to Minimize Expected Total Cost

Inspection scheduling is the solution of an optimization problem with the objective of minimizing the expected total cost $E(C_{total})$ as follows:

Find $\mathbf{t_{insp}} = \{t_{insp,1}, t_{insp,2}, \ldots, t_{insp,ninsp}\}$ (6.12)

to minimize $E(C_{total})$ (6.13)

such that $t_{insp,i} - t_{insp,i-1} \geq 1$ year (6.14)

given n_{insp}, $\delta_{f,0.5}$, C_{FAIL}, and PDFs of t_{ini} and t_{cr} (6.15)

where $\mathbf{t_{insp}}$ = vector consisting of design variables of inspection times, and $t_{insp,i}$ = ith inspection time (years). As indicated in Equation (6.14), the time interval between inspections should be at least one year. The number of inspections n_{insp}, $\delta_{f,0.5}$, and monetary loss due to structural failure C_{FAIL} are given (see Equation (6.15)). The PDFs of t_{ini} and t_{cr} are provided in Figures 6.4(a) and 6.4(b), respectively. The optimization toolbox provided in MATLAB® version R2009a [MathWorks Inc. 2009] was used to solve this problem. In order to check if the solution from the optimization toolbox of MATLAB® is a global minimum, NSGA-II [Deb et al. 2002] was used. It should be noted that the discount rate of money is not considered to estimate the expected total cost $E(C_{total})$ in this application.

Effect of inspection quality on optimum inspection scheduling

As mentioned previously in chapter 5, $\delta_{f,0.5}$ is the fatigue damage intensity at which the inspection method has a 50% probability of detection, and represents the quality of inspection. The optimum inspection schedules associated with $\delta_{f,0.5}$ = 0.01, 0.03, and 0.05 are provided in Table 6.2, when n_{insp} = 2, and C_{FAIL} = 1,000. If

two inspections with $\delta_{f,0.5}$ = 0.05 are used to detect fatigue crack damage, the inspections should be performed at 7.23 and 15.32 years. In this case, the associated time-based probability of failure p_F and expected total cost $E(C_{total})$ are 0.0272 and 32.10, respectively. If the inspection method with $\delta_{f,0.5}$ = 0.01 is used instead of $\delta_{f,0.5}$ = 0.05, the time-based probability of failure p_F will decrease from 0.0272 to 0.001, and the expected total cost $E(C_{total})$ will be reduced by 70% (i.e., from 32.10 to 9.69), even though the inspection cost for $\delta_{f,0.5}$ = 0.01 is larger than $\delta_{f,0.5}$ = 0.05 (see Equation (5.28)).

Figure 6.6 shows the PDFs of the expected damage detection delay $\overline{t}_{delay}$, time-based safety margin t_{mar} (i.e., $t_{cr} - t_{ini}$), and difference between t_{mar} and $\overline{t}_{delay}$ for the optimum inspection schedule $t_{insp,1}$ = 4.66 years and $t_{insp,2}$ = 12.49 years as indicated in Table 6.2. p_F is defined herein as the probability that $t_{mar} - \overline{t}_{delay}$ is less than 0 as indicated in Equation (6.7). The area under the PDF of $t_{mar} - \overline{t}_{delay}$ below 0 in Figure 6.6 is 0.001. Figure 6.7(a) shows the PDFs of $\overline{t}_{delay}$ associated with $\delta_{f,0.5}$ = 0.01 and 0.05. The mean values of $\overline{t}_{delay}$ for $\delta_{f,0.5}$ = 0.01 and 0.05 are 6.12 and 9.83 years, respectively, as shown in Table 6.2. The mean of the expected damage detection time $\overline{t}_{det}$ for $\delta_{f,0.5}$ = 0.01 and 0.05 is 10.31 and 14.02 years, respectively (see Table 6.2). Figure 6.7(a) indicates that the PDF of $\overline{t}_{delay}$ shifts to the right as $\delta_{f,0.5}$ increases from 0.01 to 0.05. The PDF of t_{mar} in Figure 6.6 is independent of $\delta_{f,0.5}$. Therefore, the area under the PDF of $t_{mar} - \overline{t}_{delay}$ below 0 for $\delta_{f,0.5}$ = 0.01 is less than the area associated with $\delta_{f,0.5}$ = 0.05 (see Figure 6.7(b)). From these

results, it can be quantified how the quality of inspection affects the time-based probability of failure by changing the expected damage detection delay.

Effect of number of inspections on optimum inspection scheduling

Table 6.3 provides the optimum inspection schedules for number of inspections n_{insp} = 1, 3 and 5, when C_{FAIL} = 1,000 and $\delta_{f,0.5}$ = 0.03. For one inspection, the optimum inspection time is 10.82 years. If five-time inspection is available to detect damage, the inspections should be applied at 3.28, 7.47, 11.39, 14.89 and 18.07 years (see Table 6.3). The PDFs of $\overline{t}_{delay}$ and $t_{mar} - \overline{t}_{delay}$ associated with the optimum solutions for n_{insp} = 1 and 5 are shown in Figure 6.8. As the number of inspections n_{insp} increases from 1 to 5, the PDF of $\overline{t}_{delay}$ shifts to the left, and both the mean and standard deviation are reduced as shown in Figure 6.8(a). Since the time-based safety margin t_{mar} is not affected by the number of inspections, the increase of n_{insp} from 1 to 5 shifts the PDF of $t_{mar} - \overline{t}_{delay}$ to the right, and reduces the dispersion of the PDF of $t_{mar} - \overline{t}_{delay}$. As a result, the increase of n_{insp} leads to the reduction of area under the PDF of $t_{mar} - \overline{t}_{delay}$ below 0 (i.e., reduction of P_{fail}) as shown in Table 6.3 and Figure 6.8(b).

Optimum number of inspections and inspection quality

From Tables 6.2 and 6.3, and Figures 6.7 and 6.8, it can be seen that reduction of p_F results from the increase of number of inspections and/or inspection quality. This

increase requires additional inspection cost C_{INS}. Therefore, the number of inspections and inspection quality should be considered as design variables of an optimization problem for minimizing the expected total cost $E(C_{total})$.

Table 6.4 provides the expected total costs $E(C_{total})$ consisting of the inspection cost C_{INS} and the expected failure cost $E(C_{FAIL})$ for different number of inspections n_{insp} = 1 to 5, when $\delta_{f,0.5}$ = 0.01 and C_{FAIL} = 1,000. Increase of the number of inspection n_{insp} leads to both reduction of $E(C_{FAIL})$ and increase of C_{INS}. The optimum inspection schedule with the minimum expected total cost $E(C_{total})$ has two-time inspection with $\delta_{f,0.5}$ = 0.01 (see Table 6.4). The associated inspection schedule is provided in Table 6.2. If the three inspection methods associated with $\delta_{f,0.5}$ = 0.01, 0.03 and 0.05 are used to detect fatigue crack damage, the optimum number of inspections for different values of $\delta_{f,0.5}$ are presented in Figure 6.9. The optimum inspection schedules of solutions I_1, I_2 and I_3 (for C_{FAIL} = 100 in Figure 6.9(a)), II_1, II_2 and II_3 (for C_{FAIL} = 1,000 in Figure 6.9(b)), and III_1, III_2 and III_3 (for C_{FAIL} = 10,000 in Figure 6.9(c)) are provided in Table 6.5. For instance, when C_{FAIL} = 1,000, optimum solution II_2 associated with $\delta_{f,0.5}$ = 0.03 requires inspections at 3.74, 8.29 and 17.34 years, and its associated minimum expected total cost is 9.95 as shown in Table 6.5 and Figure 6.9(b). Among II_1, II_2 and II_3, II_3 has the smallest expected total cost $E(C_{total})$ = 8.04 and smallest time-based probability of failure $p_F = 6.82 \times 10^{-4}$. It means that solution II_3 is the optimum solution for C_{FAIL} = 1,000. Furthermore, the optimum cost-based solutions for C_{FAIL} = 100 and 10,000 are I_2 in Figure 6.9(a) and

III_3 in Figure 6.9(c), respectively.

6.4.3 Optimum Monitoring Schedules to Minimize Expected Total Cost

The formulation of an optimization problem for monitoring scheduling is as follows:

$$\text{Find} \quad \mathbf{t_{mon}} = \{t_{mon,1}, t_{mon,2}, \ldots, t_{mon,nmon}\} \tag{6.16}$$

$$\text{to minimize} \quad E(C_{total}) \tag{6.17}$$

$$\text{such that} \quad t_{mon,i} - \left(t_{mon,i-1} + t_{md}\right) \geq 1 \text{ year} \tag{6.18}$$

$$\text{Given} \quad n_{mon}, t_{md}, C_{FAIL}, \text{ and PDFs of } t_{ini} \text{ and } t_{cr} \tag{6.19}$$

where $\mathbf{t_{mon}}$ = vector of design variables of monitoring starting times, $t_{mon,i}$ = ith monitoring starting time (years), and t_{md} = monitoring duration (years). In this optimization problem, the objective is minimization of the expected total cost $E(C_{total})$ defined in Equation (6.10b). The time interval between monitoring starting time of ith monitoring (i.e., $t_{mon,i}$) and monitoring ending time of (i –1)th monitoring (i.e., $t_{mon,i-1} + t_{md}$) is assumed to be at least 1 year as a constraint (see Equation (6.18)). Similarly to the formulation of optimum inspection scheduling, the number of monitorings n_{mon}, and monitoring duration t_{md}, failure cost C_{FAIL} and the PDFs of t_{ini} and t_{cr} are given.

The result of the optimization problem to minimize $E(C_{total})$ for different number of monitorings n_{mon} = 1 to 5 and C_{FAIL} = 1,000 is shown in Figure 6.10(a).

Monitoring scheduling of optimum solutions IV_1, IV_2 and IV_3 associated with monitoring duration t_{md} = 0.1, 0.3 and 0.5 year, respectively are illustrated in Figure 6.10(b). Solution IV_3 requires the minimum $E(C_{total})$ for given monitoring duration t_{md} = 0.5 year, and needs two monitorings at $t_{mon,1}$ = 3.28 and $t_{mon,2}$ = 11.58 years. Among optimum solutions IV_1, IV_2 and IV_3, p_F associated with solution IV_3 is the smallest (i.e., 3.01×10^{-5}), but has the highest $E(C_{total})$ of 30.03 (see Figure 6.10(b)). This is because increasing the monitoring duration t_{md} leads to reduction of the expected failure cost $E(C_{FAIL})$, but requires higher monitoring cost. As a result, the optimum solution for C_{FAIL} = 1,000 is solution IV_1 with t_{md} = 0.1 year. The results of the optimizations for given C_{FAIL} = 10,000 are presented in Figure 6.11(a). The solutions V_1, V_2 and V_3 are associated with monitoring durations t_{md} = 0.1, 0.3 and 0.5 year, respectively. The monitoring schedules of solutions V_1, V_2 and V_3 are provided in Figure 6.11(b). Figure 6.11 indicates that solution V_1 has the minimum expected total cost of 18.01, and the associated optimum monitoring duration and number of monitorings are 0.1 year and 3, respectively.

6.5 Conclusions

A probabilistic approach to establish an optimum cost-based inspection and monitoring scheduling of deteriorating structures has been proposed. This approach is applied to a fatigue sensitive structure. The total expected cost includes the costs of inspection and failure. Under the assumption that repair and retrofit methods are

applied immediately after damage is detected, the failure criterion is formulated using damage detection time and time for damage to reach the critical state. The optimum scheduling provides the optimum inspection times and quality of inspection for a given cost of failure. The optimum monitoring starting times and monitoring durations are also obtained by the optimization process. The following conclusions are drawn:

1. Increasing the number of inspections and/or inspection quality leads to (a) reductions of both the expected damage detection delay and time-based probability of failure, and (b) increase of inspection cost.
2. The failure cost affects significantly the optimum scheduling of inspections and monitorings. A higher failure cost leads to an optimum solution requiring more inspections and monitorings. Therefore, for practical use of the proposed approach, rational estimation of the failure cost is needed considering various factors such as loss of life, reconstruction, and users' inconvenience.
3. The failure criterion is associated with the time-based safety margin. This safety margin considers uncertainty associated with the time for damage to reach a critical level. Alternatively, the failure criterion can be associated with the crack size-based safety margin. Further studies are necessary to compare the effects of these two approaches on inspection and monitoring planning.
4. For use of the proposed approach to other deteriorating processes such as corrosion, fatigue-induced corrosion, and fracture, future effort is needed to

establish a methodology to consistently deal with lack of knowledge and data associated with deterioration mechanisms, inspection and monitoring methods, and time-dependent performance prediction. Furthermore, for more reliable planning, the Bayesian updating process after each inspection or monitoring should be considered in future studies.

Table 6.1 Variables for crack size prediction

Random variables	Notation (Units)	Mean	COV	Type of distribution
Initial crack size	a_o (mm)	0.5	0.2	Lognormal
Annual number of cycles	N_{an} (cycles/year)	5×10^5	0.2	Lognormal
Stress range	S_{sr} (MPa)	20	0.1	Weibull
Material crack growth parameter	C	2.3×10^{-12}	0.3	Lognormal
Deterministic variable	Notation (Units)		Value	
Material crack growth parameter	m		3.0	

Table 6.2 Design variable and objective values associated with optimum solutions for $\delta_{f,0.5}$ = 0.01, 0.03, and 0.05

$\delta_{f,0.5}$		0.01	0.03	0.05
Values of design variables $\mathbf{t_{insp}}$ (years)		4.66	5.99	7.23
		12.49	14.02	15.32
Given	C_{FAIL}	1,000	1,000	1,000

Table 6.3 Design variable and objective function values associated with optimum solutions for number of inspections n_{insp} = 1, 3 and 5

Number of inspections n_{insp}		1	3	5
Values of design variables $\mathbf{t_{insp}}$ (years)	$t_{insp,1}$	10.82	3.74	3.28
	$t_{insp,2}$	-	8.29	7.47
	$t_{insp,3}$	-	17.34	11.39
	$t_{insp,4}$	-	-	14.89
	$t_{insp,5}$	-	-	18.07
Given				
	C_{FAIL}	1,000	1,000	1,000

Table 6.4 Costs as function of number of inspections n_{insp} = 1 to 5

Number of inspections n_{insp}	Total expected cost $E(C_{total})$	Inspection cost C_{INS}	Expected failure cost $E(C_{FAIL})$	Given	
				$\delta_{f,0.5}$	C_{FAIL}
1	110.45	4.35	106.10	0.01	1,000
2	9.69	8.69	0.9999	0.01	1,000
3	13.05	13.03	0.01991	0.01	1,000
4	17.39	17.38	0.009807	0.01	1,000
5	21.73	21.72	0.009786	0.01	1,000

Table 6.5 Design variable and objective function values associated with optimum solutions in Figure 6.9

Optimum solution	Given values		Values of design variables					Value of objective	Probability of failure, p_F	Mean of $\bar{t}_{delay}$ (years)	Mean of $\bar{t}_{det}$ (years)
				Inspection times (years)							
	C_{FAIL}	$\delta_{f,0.5}$	Number of inspections, n_{insp}	$t_{insp,1}$	$t_{insp,2}$	$t_{insp,3}$	$t_{insp,4}$	$E(C_{total})$			
I_1		0.01	2	4.66	12.49	-	-	8.79	1.20×10^{-3}	6.12	10.32
I_2	100	0.03	2	5.99	14.02	-	-	7.33	7.90×10^{-3}	8.38	12.58
I_3		0.05	3	4.45	8.89	17.27	-	7.42	6.82×10^{-4}	9.04	13.24
II_1		0.01	2	4.66	12.49	-	-	9.69	1.20×10^{-3}	6.11	10.32
II_2	1000	0.03	3	3.74	8.29	17.34	-	9.95	1.40×10^{-4}	7.52	11.73
II_3		0.05	3	4.45	8.89	17.27	-	8.04	6.82×10^{-4}	9.05	13.26
III_1		0.01	3	3.26	8.34	18.00	-	13.23	2.01×10^{-5}	5.20	9.40
III_2	10000	0.03	3	3.74	8.29	17.34	-	11.22	1.40×10^{-4}	7.52	11.73
III_3		0.05	4	3.58	7.21	11.40	18.38	10.81	1.00×10^{-4}	8.02	12.21

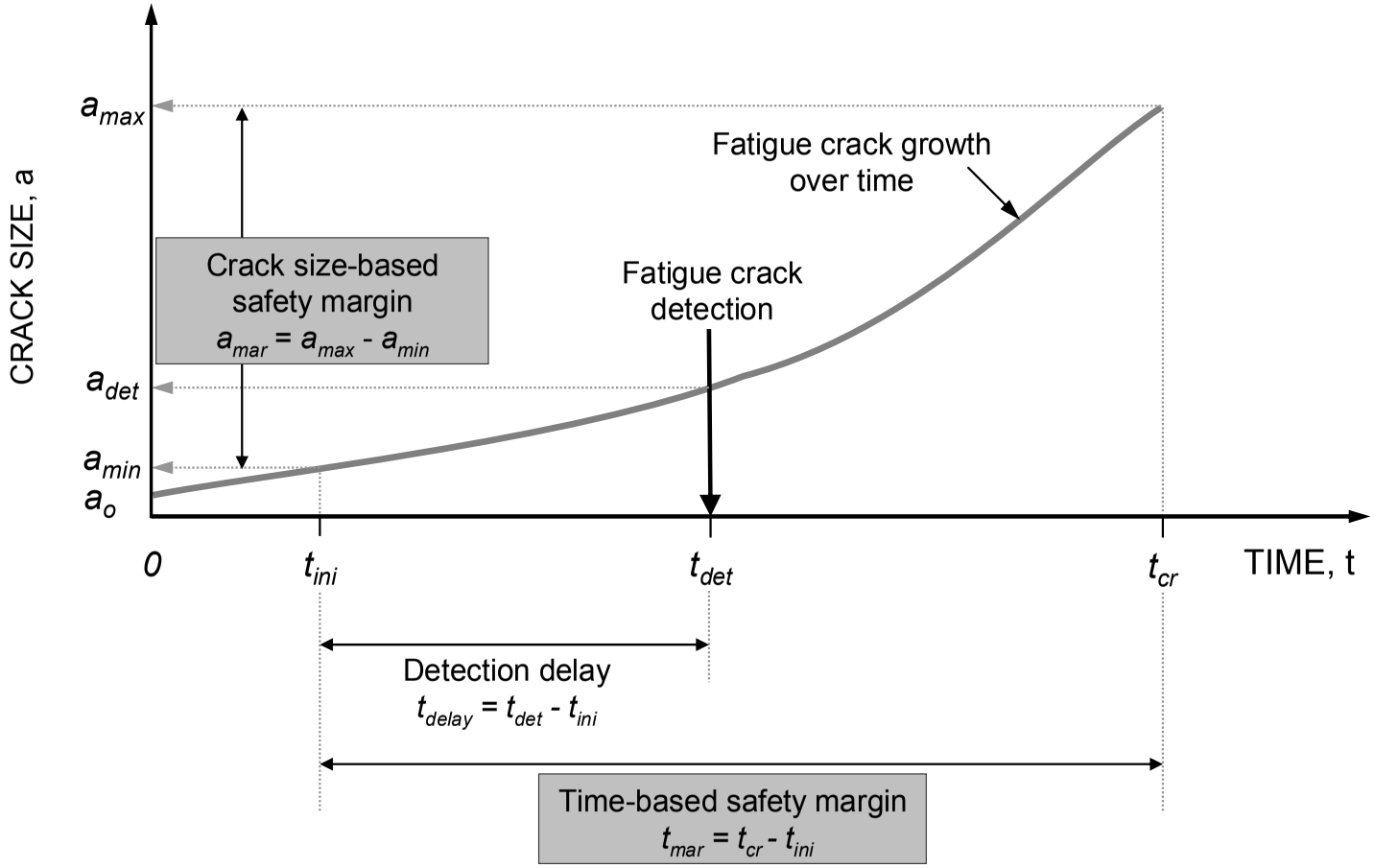

Figure 6.1 Crack size-based and time-based safety margin

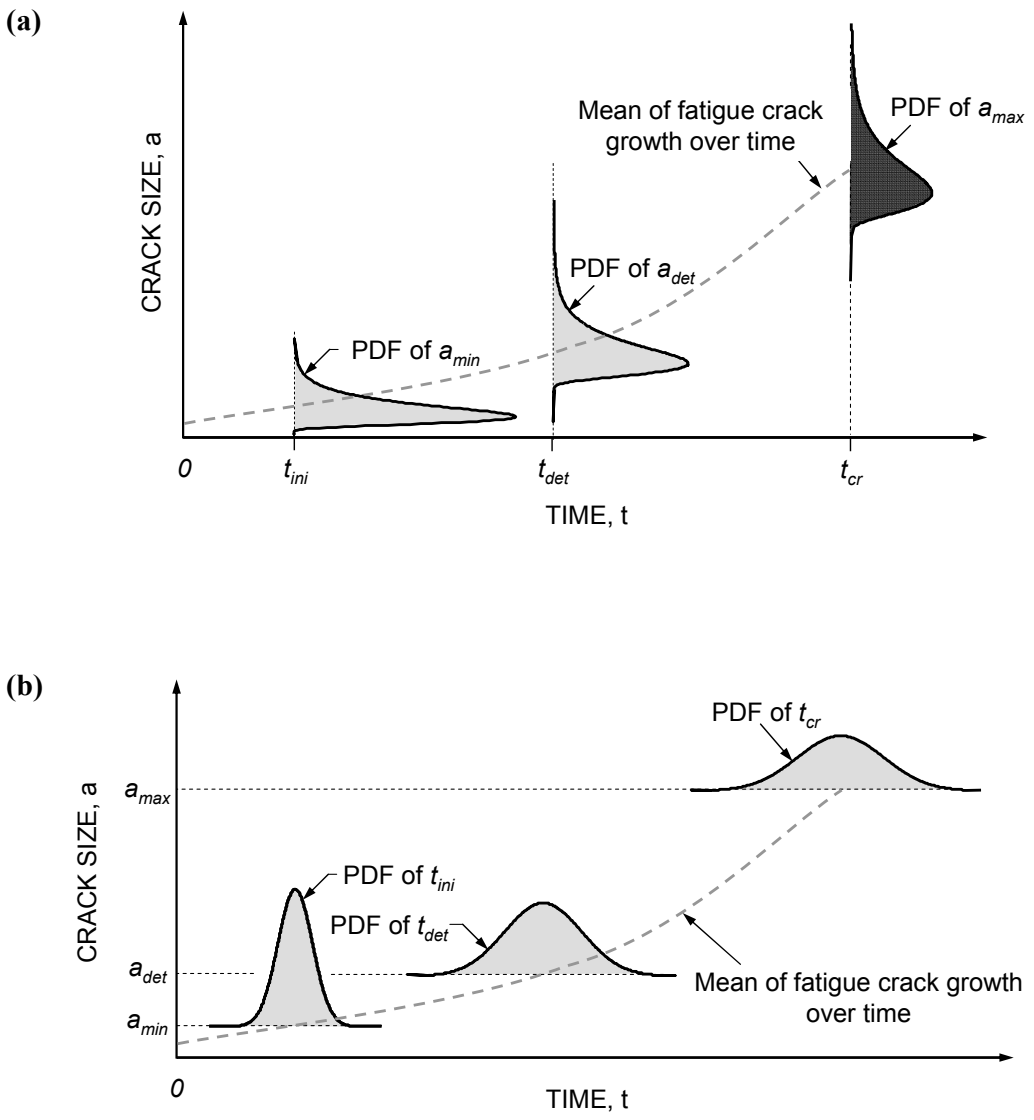

Figure 6.2 (a) PDFs of crack size a_{min}, a_{det}, a_{max}; and **(b)** PDFs of times t_{ini}, t_{det}, t_{cr}

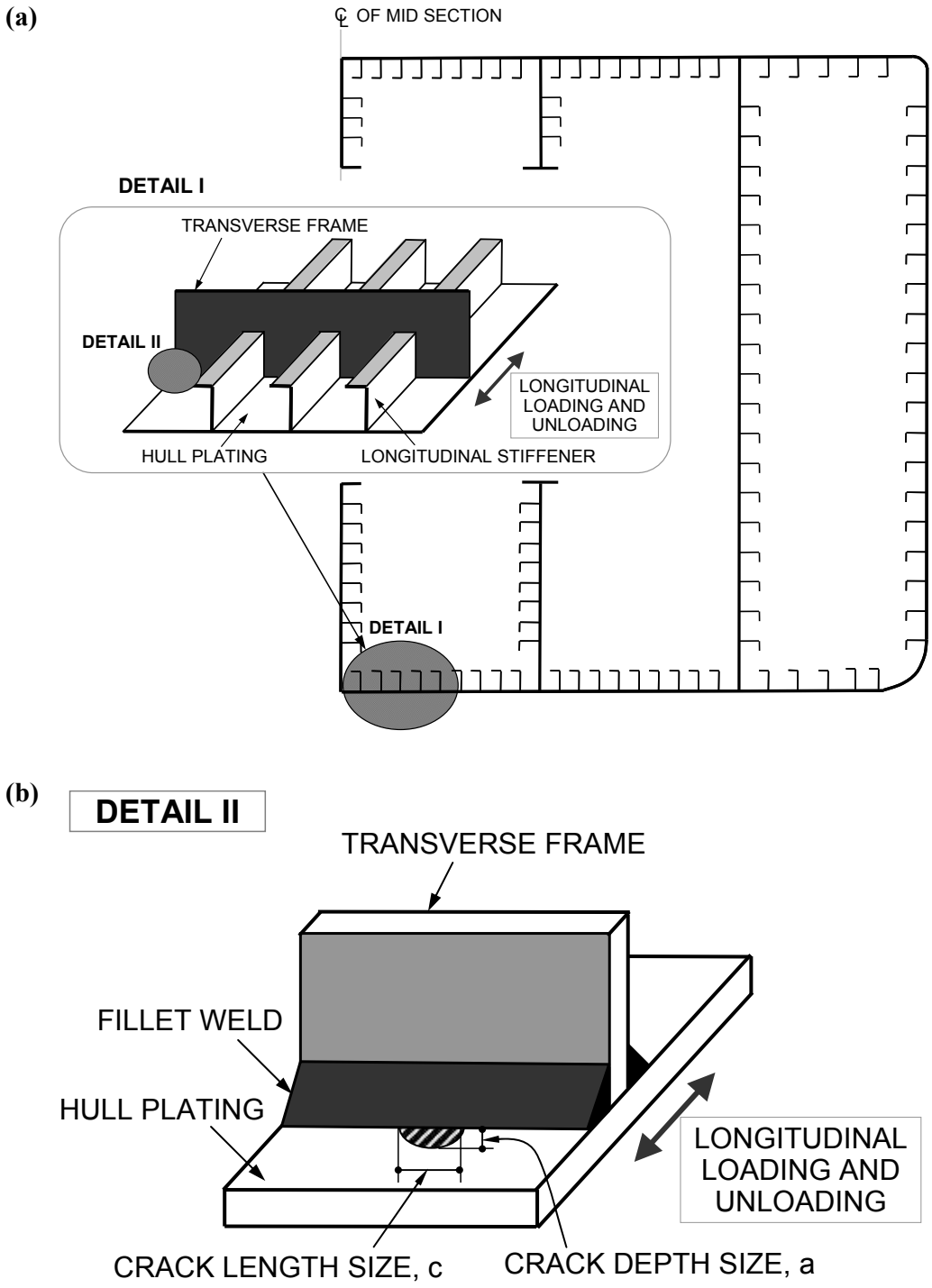

Figure 6.3 (a) Schematic representation of the mid-ship section of a ship; and **(b)** detail of the assumed crack location

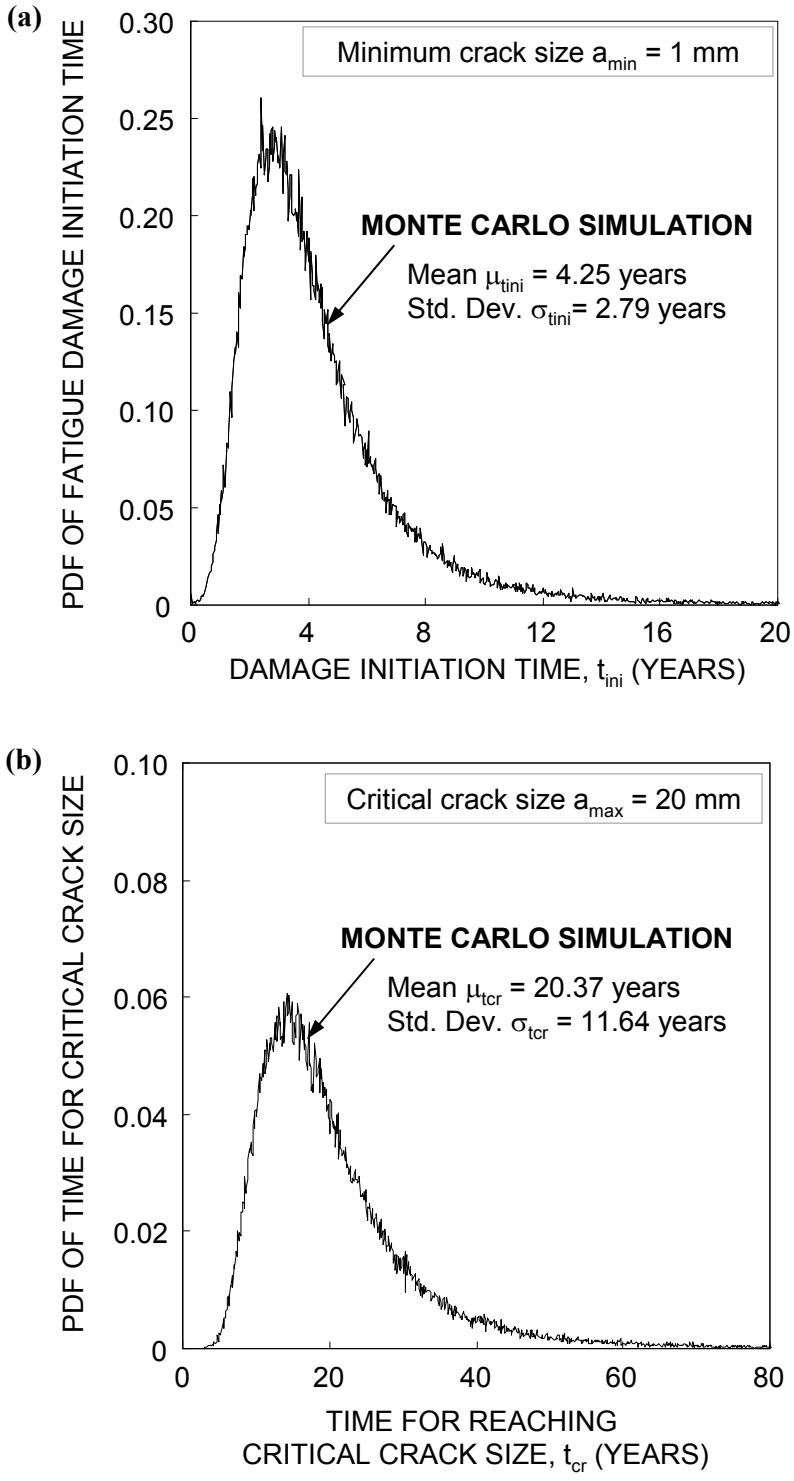

Figure 6.4 PDFs of **(a)** fatigue damage initiation time; and **(b)** time to reach the critical crack size

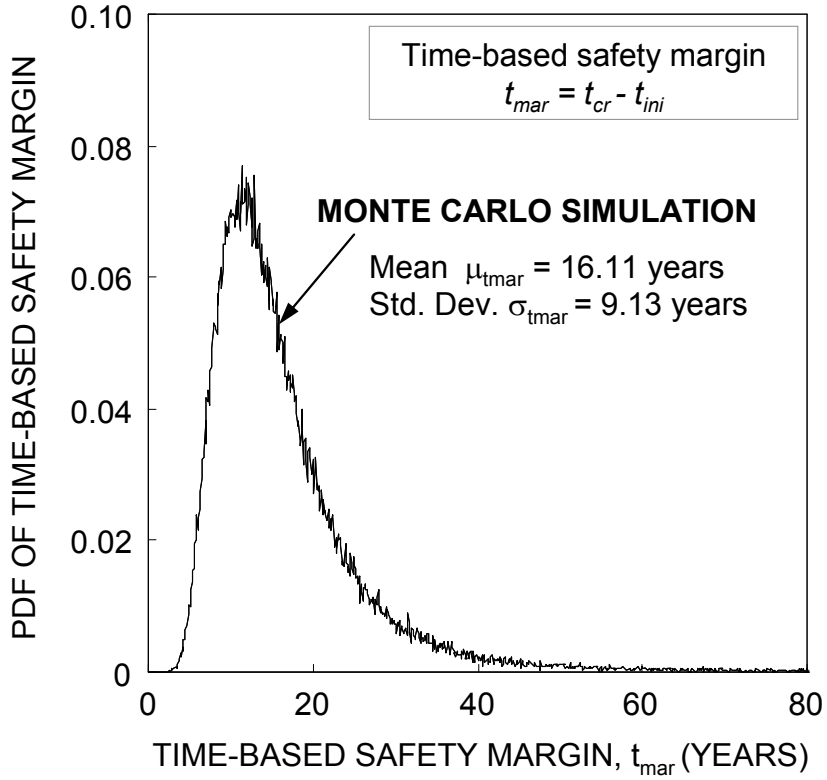

Figure 6.5 PDF of time-based safety margin

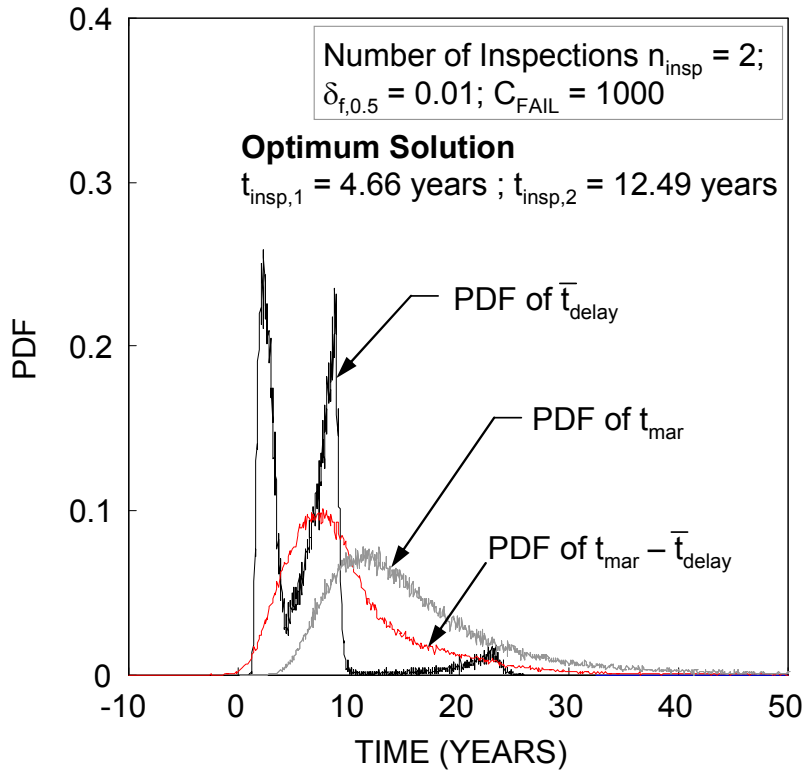

Figure 6.6 PDFs of $\bar{t}_{delay}$, t_{mar}, and $t_{mar} - \bar{t}_{delay}$ associated with the optimum solution for $\delta_{f,0.5} = 0.01$ in Table 6.2

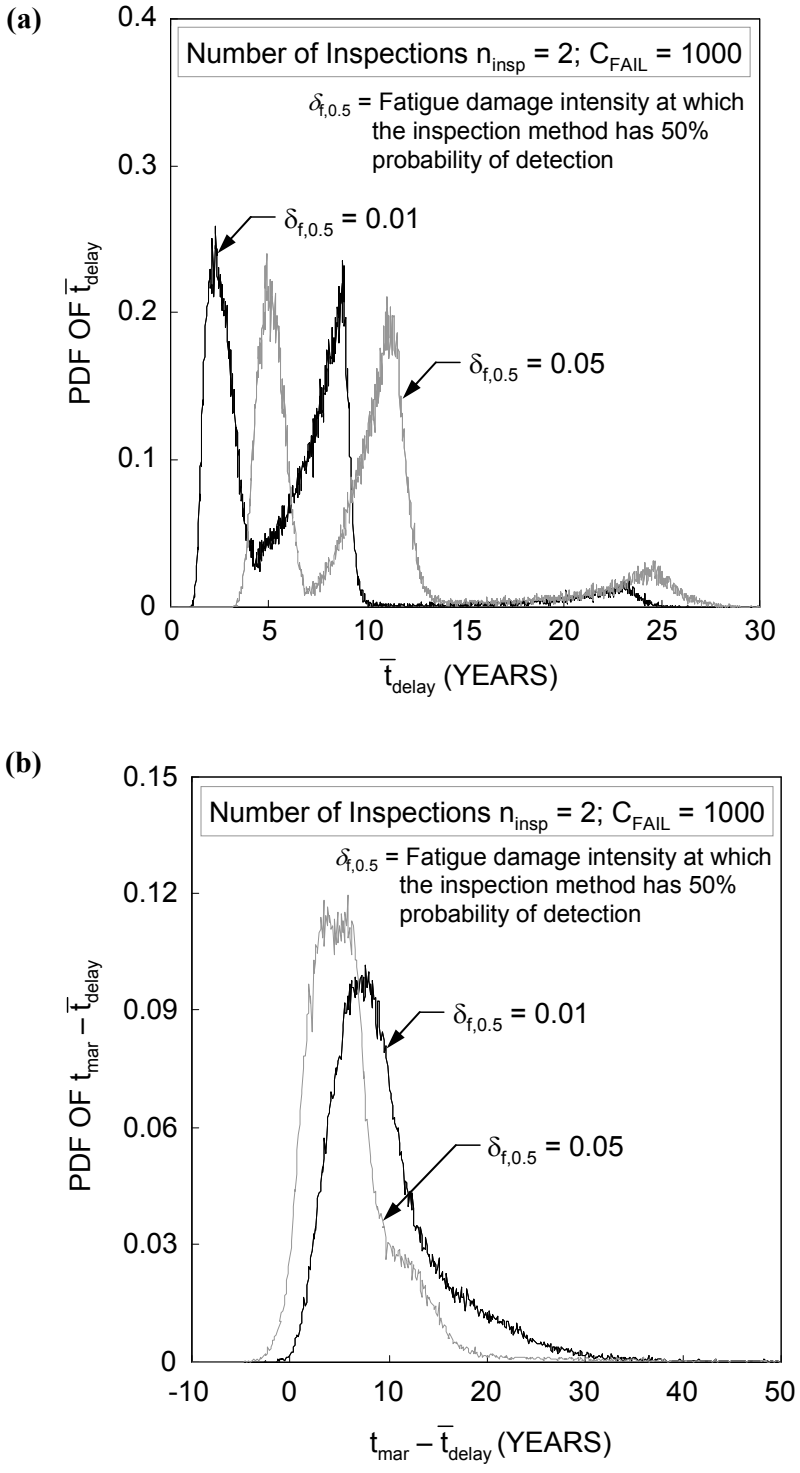

Figure 6.7 PDFs of **(a)** $\bar{t}_{delay}$, and **(b)** $t_{mar} - \bar{t}_{delay}$ associated with the optimum solutions for $\delta_{f,0.5} = 0.01$ and 0.05 in Table 6.2

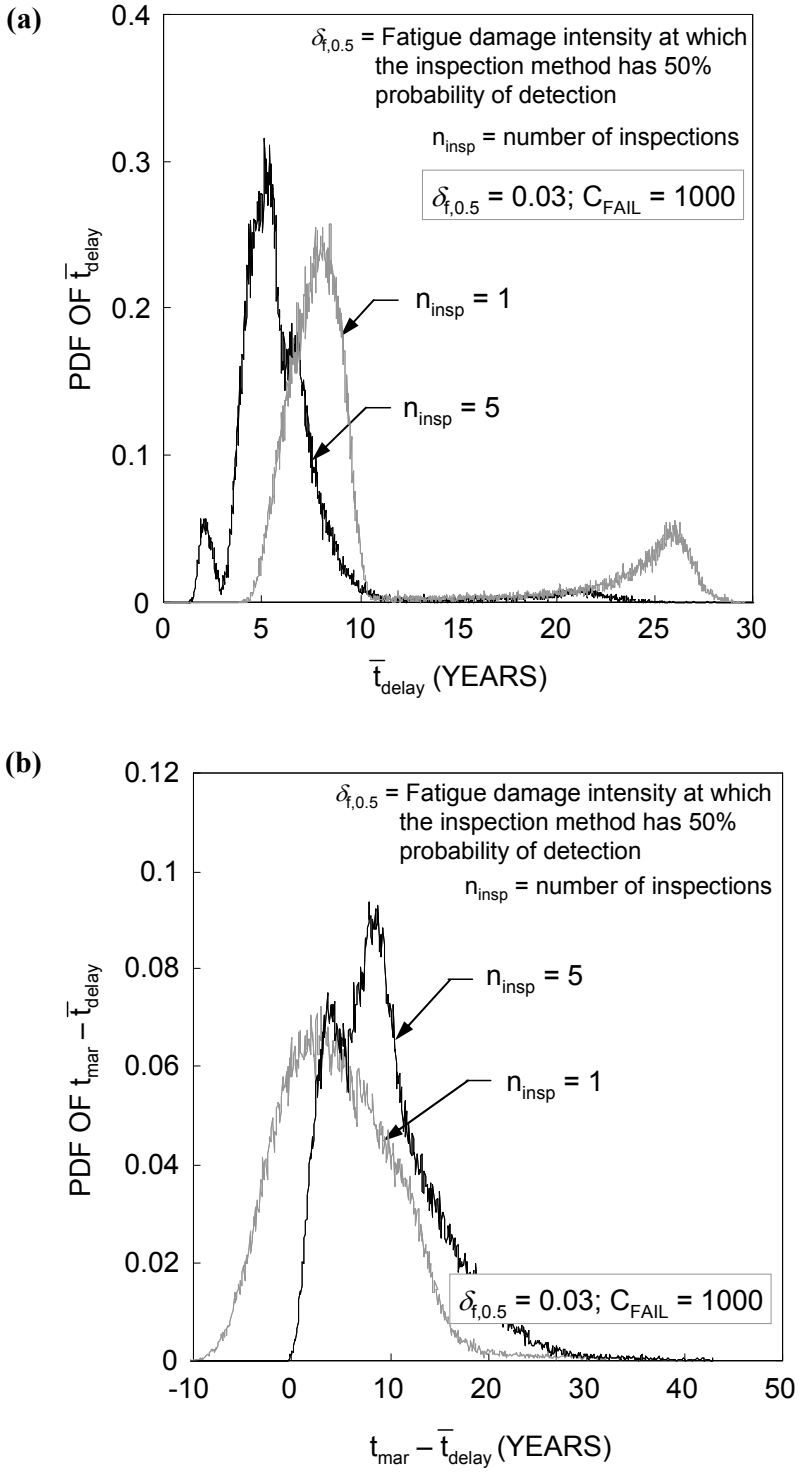

Figure 6.8 PDFs of (a) $\bar{t}_{delay}$ and (b) $t_{mar} - \bar{t}_{delay}$ associated with the optimum solutions for number of inspections n_{insp} = 1 and 5 in Table 6.3

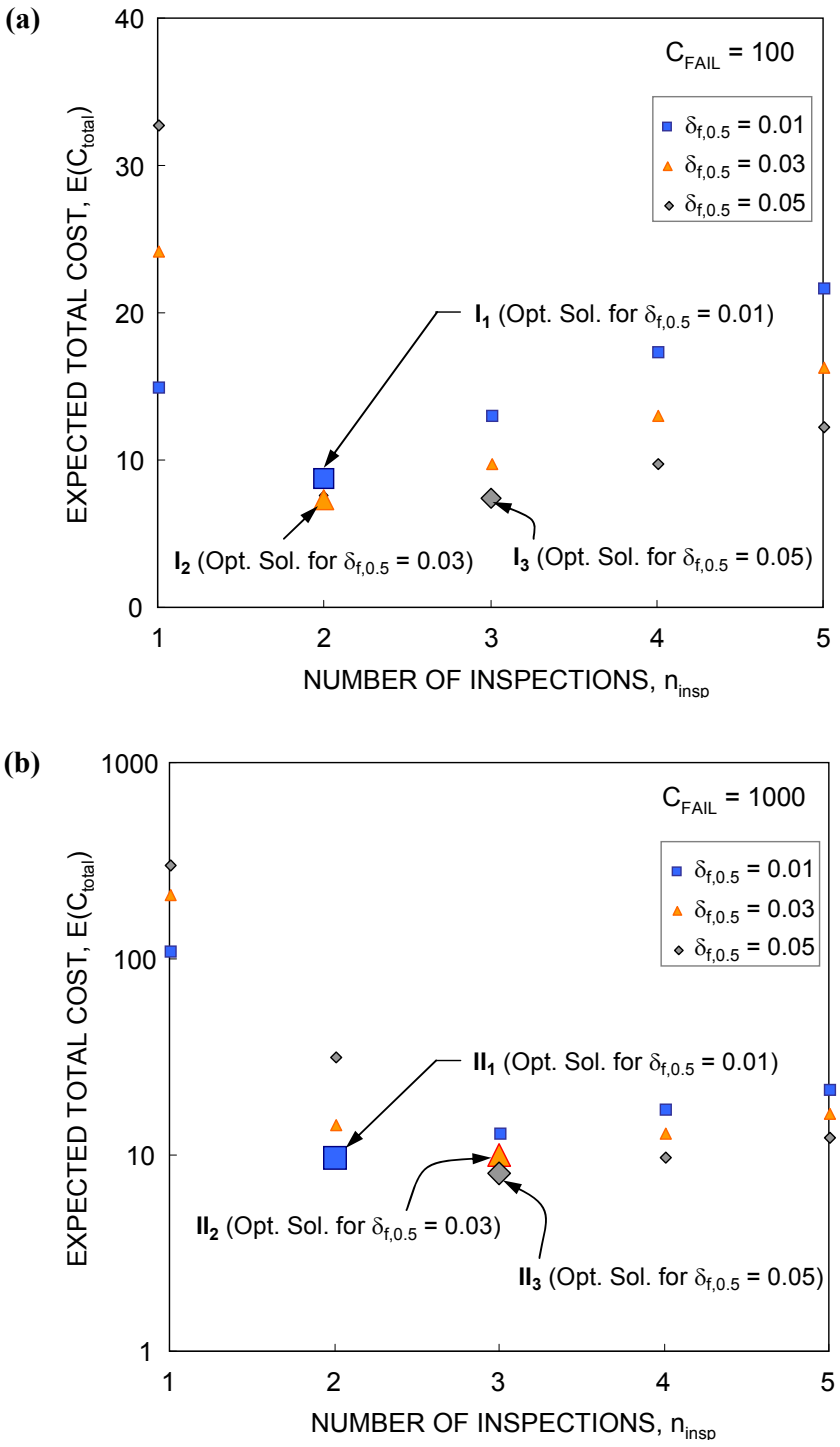

Figure 6.9 Expected total cost as function of number of inspections n_{insp} = 1 to 5 for **(a)** C_{FAIL} = 100, **(b)** C_{FAIL} = 1,000, and **(c)** C_{FAIL} = 10,000

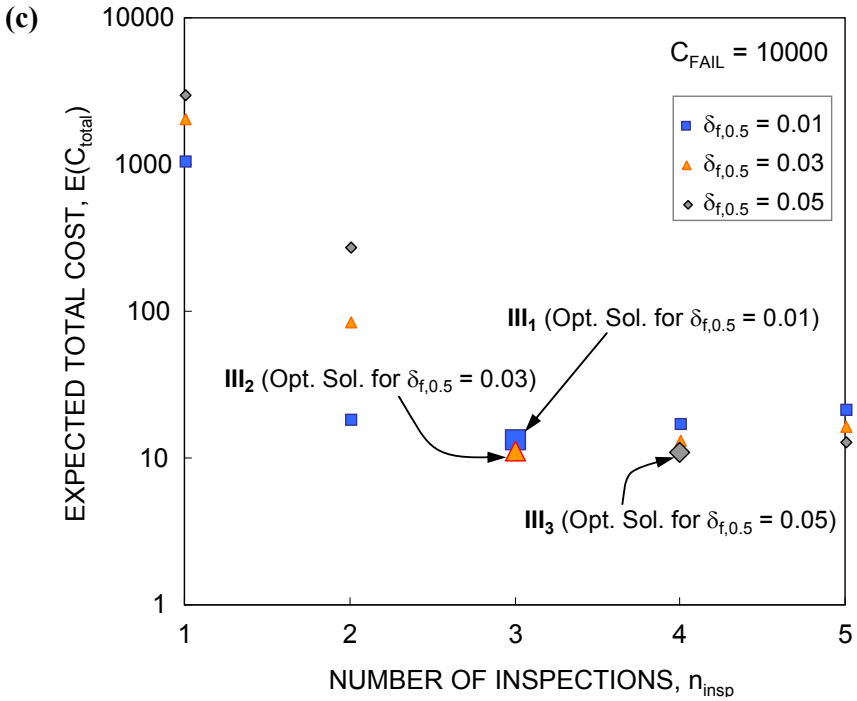

Figure 6.9 Expected total cost as function of number of inspections n_{insp} = 1 to 5 for **(a)** C_{FAIL} = 100, **(b)** C_{FAIL} = 1,000, and **(c)** C_{FAIL} = 10,000 (continued)

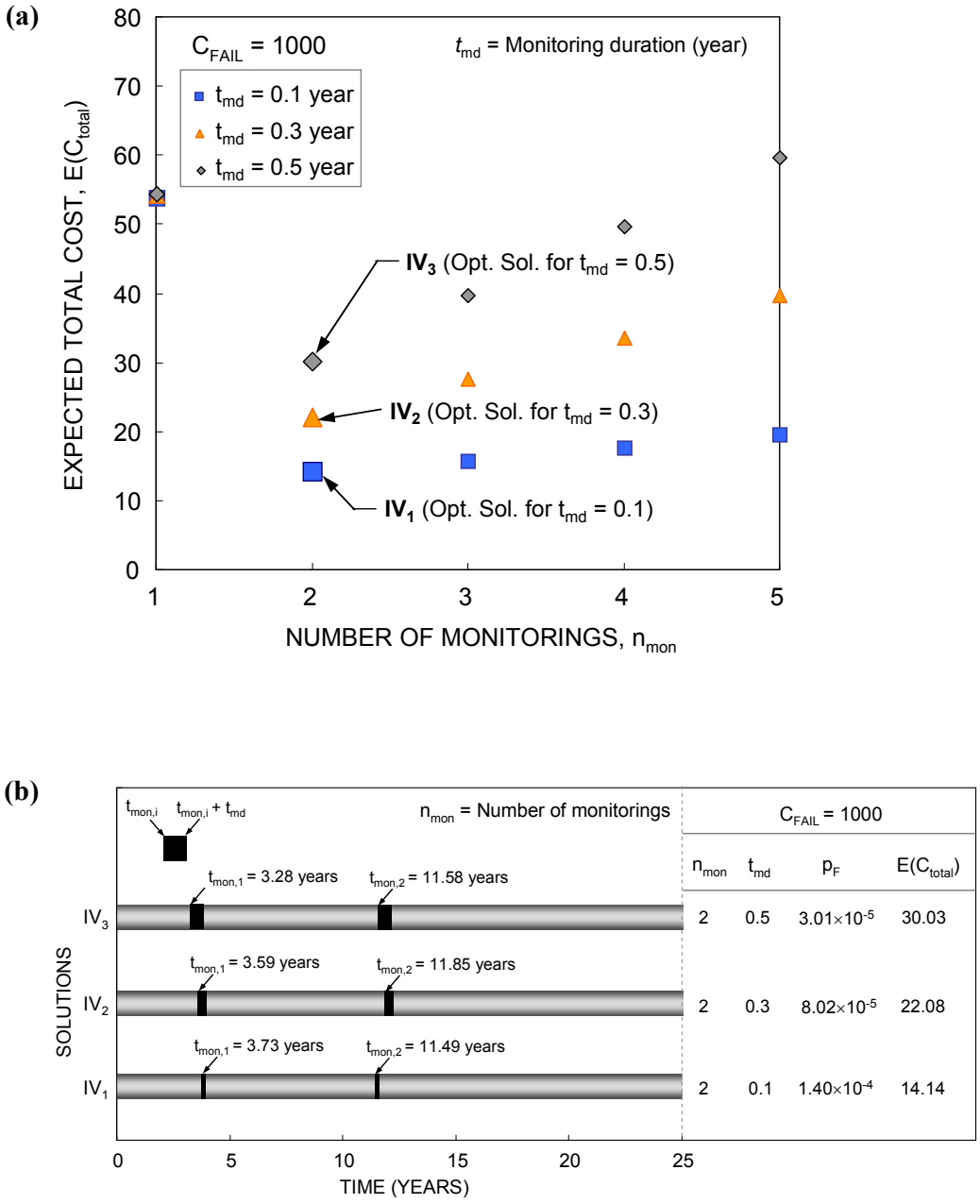

Figure 6.10 (a) Expected total cost as function of number of monitorings n_{mon} = 1 to 5 for C_{FAIL} = 1,000, and **(b)** monitoring schedules for optimum solutions IV_1, IV_2 and IV_3 in **(a)**

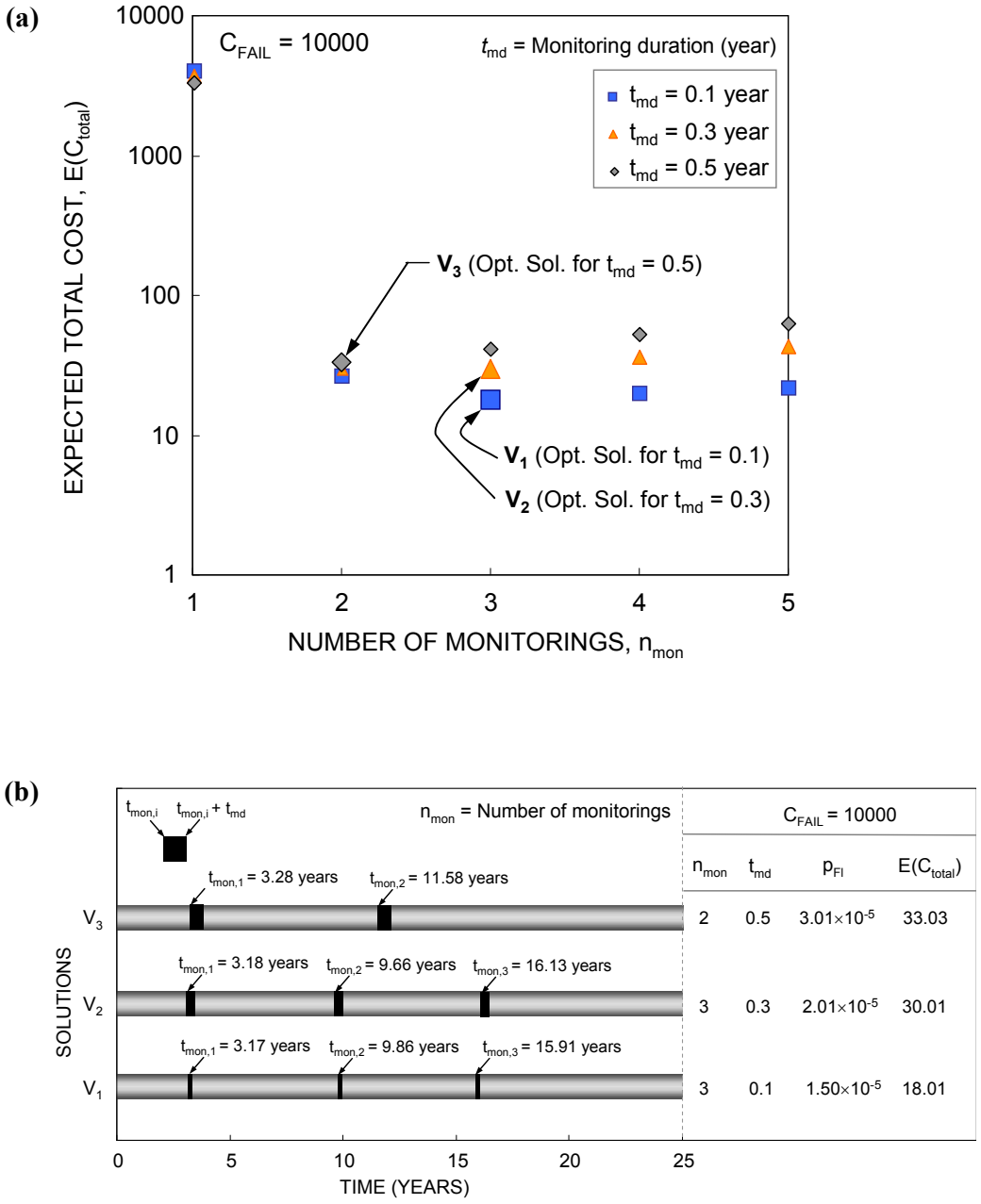

Figure 6.11 (a) Expected total cost as function of number of monitorings n_{mon} = 1 to 5 for C_{FAIL} = 10,000, and **(b)** monitoring schedules for optimum solutions V_1, V_2 and V_3 in **(a)**

CHAPTER 7

INSPECTION AND REPAIR PLANNING TO EXTEND LIFETIME OF STRUCTURES

7.1 Introduction

The lifetime of a structure can be extended through effective and timely inspection / repair. Optimization process has been considered as an essential tool to establish the inspection / repair planning during given target lifetime [Frangopol 2011]. In order to find the inspection / repair planning from an optimization process, damage initiation and propagation under uncertainty should be predicted in a rational way. The probability of damage detection can affect the repair action [Mori and Ellingwood 1994a]. Even though the damage is detected, the repair can be delayed according to availability of funds and/or importance of a structural component [Estes and Frangopol 2001]. Therefore, effects of uncertainties associated with damage initiation and propagation, and probabilities of damage detection and repair on structural performance should be considered to optimize the lifetime inspection / repair strategy.

This chapter presents a probabilistic approach to establish an optimum inspection / repair strategy for RC structures under pitting corrosion. This strategy is the solution of a bi-objective optimization problem under uncertainty considering the maximization of expected extended lifetime and minimization of expected total cost. The formulation of extended lifetime for a given number of inspections is based on a

decision tree analysis. In this decision tree, probabilities of damage detection and repair are considered. The relation among damage intensity, quality of an inspection method and probability of damage detection is expressed as a damage detectability function. The decision maker's willingness to make a repair after pitting corrosion detection is considered as the probability of repair. This is categorized into the following repair approaches: (a) delayed, (b) linear and (c) proactive. The solution obtained from the optimization problem provides the optimum inspection time for a given number of inspections. The effects of inspection quality, repair approach and/or number of inspections on the expected extended lifetime are investigated.

7.2 Lifetime Prediction of Deteriorating RC Structures

The performance of RC structures can deteriorate due to shrinkage, inadequate pouring procedures, freeze and thaw cycles, corrosion of reinforcement, fatigue and degradation of steel and concrete [Ellingwood 2005]. Among these stressors resulting in deterioration of RC structures, corrosion is considered as the most costly deterioration mechanism [Chaker 1992, Weyers et al. 1993, Kirkpatrick et al. 2002, NCHRP 2005). The deterioration process due to corrosion generally consists of the following two steps: corrosion initiation and corrosion propagation [Tuutti 1982, Al-Tayyib et al. 1988, Dhir et al. 1989, Stewart and Rosowsky 1998]. Based on the degree of damage (e.g., damage intensity, percent of cumulative damage, remaining reinforcement area) or structural capacity (e.g., flexure or shear strength), service life

of RC structures can be predicted.

The deteriorating mechanisms of RC structures are highly dependent on the environment and material properties under uncertainty. In order to predict the service life of RC structures considering uncertainties in a rational way, a probabilistic approach has to be applied [Frangopol et al. 1997a and 1997b, Stewart and Rosowsky 1998, Enright and Frangopol 1998a, Stewart 2004, Li et al. 2005]. Figure 7.1 illustrates the deterioration profile of a RC structure under uncertainty. By considering the uncertainties associated with parameters of corrosion deterioration model, PDFs of corrosion and crack initiation times (i.e., t_{corr} and t_{crack}, respectively) can be obtained. This figure also indicates the PDF of service life t_{life} defined as the time when the damage of a RC structure reaches its threshold.

7.3 Extended Lifetime with Inspection / Repair

Lifetime of a deteriorating structure can be extended through appropriate repair action after damage detection. In order to predict the lifetime of a deteriorating structure considering effects of inspections / repair, a decision tree model can be used. This model represents all the possible events. Every event has a particular outcome, and every path to the associated outcome has a probability of occurrence.

Figure 7.2(a) shows the decision tree to predict the lifetime of a deteriorating structure when an inspection is used at time $t_{insp,1}$. Decision tree begins with a decision node (i.e., denoted as a gray square node in Figure 7.2(a)), at which there

are alternatives. The decision tree of Figure 7.2(a) has two alternatives: inspection is performed after the time associated with the initial service life $t^{(0)}_{life}$ (i.e., $t_{insp,1} > t^{(0)}_{life}$), and inspection performed before the initial service life (i.e., $t_{insp,1} \leq t^{(0)}_{life}$). The first case is associated with a late inspection (branch 1 in Figure 7.2(a)). In the second case, there is a chance node (i.e., denoted as a black circle in Figure 7.2(a)) associated with damage detection and no detection (branch 2). The probabilities of detection and no detection are $P_{insp,1}$ and $1 - P_{insp,1}$, respectively. If damage is detected (branches 3 and 4), decision maker should decide whether immediate repair is necessary. The decision maker's willingness to make a repair can be quantified by the probability of repair [Estes and Frangopol 2001]. The probability of repair is defined as the conditional probability that repair is made immediately after damage is detected. Considering the probability of repair, there are two events (i.e., repair (branch 4) and no repair (branch 3)) after damage detection. As a result, the decision tree model has the four branches shown in Figure 7.2(a). Branch 4 represents the event of damage detection and repair. The associated lifetime and probability are $t^{(1)}_{life}$ and $P_{insp,1} \times P_{rep,1}$, respectively, where $P_{rep,1}$ is the probability of repair after the first inspection. Figure 7.2(b) illustrates the lifetimes of branches 1 to 4 in Figure 7.2(a). Considering the probabilities of inspection and repair, and the lifetime associated with all the branches, the extended lifetime t_{life} is defined as

$$t_{life} = t^{(0)}{}_{life} \qquad \text{for } t_{insp,1} > t^{(0)}_{life} \qquad (7.1a)$$

$$t_{life} = \left(1 - P_{insp,1}\right) \cdot t^{(0)}{}_{life} + P_{insp,1} \cdot \left(1 - P_{rep,1}\right) \cdot t^{(0)}{}_{life} + P_{insp,1} \cdot P_{rep,1} \cdot t^{(1)}{}_{life} \qquad \text{for } t_{insp,1} \le t^{(0)}{}_{life} \qquad (7.1b)$$

where $t^{(0)}{}_{life}$ = initial lifetime, and $t^{(1)}{}_{life}$ = extended lifetime by repair. Similarly, the extended lifetime t_{life} for the multi-inspection case can be formulated using the decision tree model.

The probability of damage detection P_{insp} in Equations (5.15) and (5.18) is used to formulate t_{life}. The probability of repair P_{rep} is expressed as [Estes and Frangopol 2001]

$$P_{rep} = \left(\frac{PT}{PT_{allow}}\right)^{r_p} \qquad \text{for } PT < PT_{allow} \qquad (7.2a)$$

$$P_{rep} = 1.0 \qquad \text{for } PT \ge PT_{allow} \qquad (7.2b)$$

where PT = maximum pit depth defined in Equation (5.5), PT_{allow} = allowable maximum pit depth, and r_p = power parameter. The relation between the maximum pit depth PT and the probability of repair P_{rep} in Equation (7.2) is illustrated in Figure 7.3. Depending on the value of r_p, the repair is (a) proactive (r_p < 1.0), (b) linear (r_p = 1.0), and (c) delayed (r_p > 1.0). The value of r_p is associated with availability of funds and competing priorities among others [Estes and Frangopol 2001]. For PT less than PT_{allow}, the proactive approach has the highest probability of occurrence. If the pit depth PT is larger than the allowable depth PT_{allow}, repair must be performed. The computational flowchart associated with the approach proposed in this chapter is presented in Figure A.6 (see Appendix).

7.4 Application to Existing Highway Bridges

7.4.1 Description of the I-39 Northbound Bridge

The proposed approach is applied to the I-39 Northbound Bridge over the Wisconsin River (Bridge-37-75) in Wisconsin, USA. This bridge was built in 1961. As shown in Figure 7.4, this bridge is a five span continuous steel plate girder bridge with slightly curved girders. The space between girders is 2.74m. The thickness of concrete deck is 190.5 mm (7.5 in), and the depth of cover is 50.8 mm (2 in). Details of this bridge are available in Mahmoud et al. (2005). This paper focuses on corrosion of the top transverse reinforcement bars of the deck between spans 1 and 2 (see Figure 7.4), where the maximum negative moment can occur.

7.4.2 Corrosion Initiation Time and Initial Lifetime

Corrosion initiation time is calculated using Equation (5.3). Pitting corrosion model of Equation (5.5) is used to predict pit depth over time. The parameters associated with predictions of corrosion initiation time and pit depth are assumed to be random. The descriptors of the random variables (i.e., mean value and coefficient of variation (COV)) are summarized in Table 7.1. The coefficient representing the ratio between maximum and average corrosion penetrations R_{pit} in Equation (5.5) is assumed to be normally distributed with mean value of 6.0 [Val and Melchers 1997] and COV of 0.1, considering that the range of R_{pit} can be from 4 to 8 [Gonzalez et al. 1995].

Effect of R_{pit} on structural reliability was investigated by Stewart (2004). As indicated in Table 7.1, the assumed distribution type of other variables is log-normal.

The time-dependent maximum pit depth *PT* defined in Equation (5.5) is obtained using Monte Carlo simulation with a sample size of 100,000 as shown in Figure 7.5. Figure 7.5(a) shows PDFs of the maximum pit depth *PT* at 10, 20, 30 and 40 years. PDFs of corrosion initiation time and time when *PT* reaches 4, 8 and 12 *mm* are presented in Figure 7.5(b). The mean and the standard deviation of *PT* increase over time due to increasing uncertainties. Figure 7.6 shows the PDFs of corrosion initiation time t_{corr} and initial lifetime $t^{(0)}_{life}$. As shown in Figure 7.6(a), mean and standard deviation of t_{corr} are 8.59 years and 2.34 years, respectively. According to Torres-Acosta and Martinez-Madrid (2003), the lifetime of RC structures can be estimated using the ratio of uniform (i.e., average) corrosion penetration to radius of initial reinforcement bar. The allowable ratio from 0.035 to 0.08 was suggested for lifetime estimation [Torres-Acosta and Martinez-Madrid 2003]. In this study, the allowable ratio is assumed to be 0.05, and the associated maximum pit depth *PT* is computed as 4.43 mm using Equations (5.6) and (5.7). It means that when the maximum pit depth reaches PT_{allow} of 4.43 mm, the equivalent uniform corrosion penetration is 5% of initial steel bar radius. Therefore, it is assumed that the lifetime $t^{(0)}_{life}$ of RC structure corresponds to the time when the maximum pit depth *PT* reaches 4.43 mm. As shown in Figure 7.6(b), the initial lifetime $t^{(0)}_{life}$ has the mean value of 21.52 years and the standard deviation of 4.06

years.

7.4.3 Optimum Inspection / Repair Planning to Extend Lifetime

After the damage is detected by an inspection method, a decision is made to repair or not according to the probability of repair. For given relation between probability of repair and degree of damage, the probability of damage detection can affect the type and timing of repair actions and, consequently the lifetime of the structure. The probability of damage detection is related to quality of inspection method, and damage intensity as indicated in Equation (5.15). In this study, the approach to establish the optimum inspection / repair planning is formulated considering probabilities of damage detection and repair.

The inspection planning is formulated as an optimization problem by maximizing the mean of extended lifetime $E(t_{life})$.

Find $\mathbf{t_{insp}} = \{t_{insp,1}, t_{insp,2}, \ldots, t_{insp,i}, \ldots, t_{insp,ninsp}\}$ (7.3)

to maximize $E(t_{life})$ (7.4)

such that $t_{insp,i} - t_{insp,i\text{-}1} \geq 1$ year (7.5)

given n_{insp}, $\delta_{c,0.5}$ and r_p (7.6)

where $\mathbf{t_{insp}}$ = vector of design variables (i.e., inspection times $t_{insp,1},\ldots, t_{insp,ninsp}$), $t_{insp,i}$= ith inspection time (years), n_{insp} = total number of inspections, and $\delta_{c,0.5}$ = corrosion damage intensity at which the given inspection method has 50%

probability of damage detection. The time interval between inspections is assumed to be at least one year as indicated in Equation (7.5). The number of inspections n_{insp}, $\delta_{c,0.5}$ representing the quality of inspection and power parameter r_p defined in Equation (7.2) are fixed (see Equation (7.6)). Using decision tree model, the extended lifetime t_{life} for $n_{insp} = 1$ is formulated as indicated in Equation (7.1). This formulation is extended to t_{life} for $n_{insp} \geq 2$. Considering uncertainties associated with corrosion initiation time and propagation, t_{life} is treated as a random variable. The objective is to maximize the expected t_{life} (see Equation (7.4)). In this chapter, partial-depth deck repair is applied. For this repair option, the top layer of reinforcement steel and concrete are replaced [NCHRP 2006]. It is assumed that the RC deck has original structural performance after repair. This problem is solved by the optimization toolbox provided in MATLAB® version R2009a [MathWorks Inc. 2009]. NSGA-II [Deb et al. 2002] was used to verify if the solution from the optimization toolbox of MATLAB® is a global minimum.

When an inspection with perfect detectability (i.e., $P_{insp,1} = 1.0$) is used, and probability of repair $P_{rep,1}$ is equal to 1.0, the optimum inspection time is 16.59 years. The objective value (i.e., maximum $E(t_{life})$) is 36.57 years. The associated PDF of the extended lifetime t_{life} has two modes as shown in Figure 7.7. The left side mode results from the late inspection associated with branch 1 in Figure 7.2. The right side mode is associated with branch 4. There is no effect of branches 2 and 3 on the extended lifetime in Figure 7.7, since detection and repair are certain event. The

probability that the extended lifetime t_{life} is less than 16.59 years is 0.093. This value is same as the probability that the initial lifetime $t^{(0)}_{life}$ in Figure 7.6(b) is less than 16.59 years.

Effect of repair approach on the expected extended lifetime

As indicated previously, according to the value of the power parameter r_p in Equation (7.2), the repair approach can be proactive ($r_p < 1.0$), linear ($r_p = 1.0$), or delayed ($r_p > 1.0$). Figures 7.8(a) and 7.8(b) show the relation between $\delta_{c,0.5}$ (representing the quality of inspection) and the expected extended lifetime $E(t_{life})$ for proactive and delayed approach, respectively, when the number of inspections $n_{insp} = 2$. Each point in Figure 7.8 is the solution of the optimization problem defined in Equations (7.3) to (7.6). As $\delta_{c,0.5}$ increases (i.e., probability of damage detection decreases), the expected extended lifetime $E(t_{life})$ is reduced (see Figure 7.8). Furthermore, $E(t_{life})$ increases as r_p decreases for given $\delta_{c,0.5}$. It should be noted that the decrease of r_p leads to higher probability of repair. From these results, it can be seen that use of a higher inspection quality (i.e., lower values for $\delta_{c,0.5}$) and/or repair with smaller r_p results in an increase of $E(t_{life})$. Figure 7.9 shows the two representative PDFs of the extended lifetime t_{life} associated with proactive (i.e, r_p =0.3) and delayed (i.e, r_p =5.0) repair approaches, when the number of inspections $n_{insp} = 2$ and $\delta_{c,0.5} = 0.04$. In the proactive case ($r_p = 0.3$), the inspections should be performed at 17.66 and 35.33 years as shown in Figure 7.9. The associated mean of

t_{life} is 45.65 years. When the delayed repair approach (r_p =5.0) is used, the inspection has to be performed at 20.11 and 40.22 years. In this case, the associated mean of t_{life} is 28.15 years.

Effect of number of inspections on the expected extended lifetime and total cost

The expected total cost $E(C_{total})$ associated with inspection / repair consists of total inspection cost C_{INS} and expected repair cost $E(C_{REP})$ as

$$E(C_{total}) = C_{INS} + E(C_{REP}) \tag{7.7}$$

The total inspection cost C_{INS} is defined in Equation (5.29). Based on a decision analysis tree, the expected repair cost $E(C_{REP})$ is estimated as the sum of the repair costs multiplied by the probability of the branch associated with repair. For a given number of inspections n_{insp}, the expected repair cost $E(C_{REP})$ considering the discount rate of money r_{dis} is

$$E(C_{REP}) = \sum_{s=1}^{n_b} \sum_{r=1}^{n_{rep,s}} \frac{C_{rep}}{(1+r_{dis})^{t_{insp,r}}} \cdot P_{b,s} \tag{7.8}$$

where C_{rep} = cost of a single repair, $P_{b,s}$ = probability of occurrence of the sth branch, $n_{rep,s}$ = number of repairs associated with this branch, and n_b = total number of branches in the decision tree. $t_{insp,r}$ is rth repair time, which is equal to the inspection time when damage is detected, and repair must be performed immediately. For example, when n_{insp} = 1 there are four branches (i.e., n_b = 4) as shown in Figure 7.2. The number of repairs associated with the branches 1, 2 and 3 is nil, and there is no

repair cost. Only branch 4 has a repair action at time $t_{insp,1}$, and the associated probability is $P_{b,4} = P_{insp,1} \times P_{rep,1}$ (see Figure 7.2(a)). Therefore, the expected repair cost $E(C_{REP})$ is $\left(C_{rep} \times P_{insp,1} \times P_{rep,1}\right) / \left(1+r_{dis}\right)^{t_{insp,1}}$. The constant α_{ins} in the inspection cost C_{ins} of Equation (5.28) and the cost of a single repair C_{rep} in Equation (7.8) are assumed 0.5 and 100, respectively. It should be noted that C_{ins} is a relative cost when the repair cost C_{rep} assumed to be 100.

Figure 7.10 shows the effect of number of inspections n_{insp} on the expected extended lifetime $E(t_{life})$ and the expected total cost $E(C_{total})$, considering r_p = 0.5, 0 $\leq \delta_{c,0.5} \leq$ 0.2 and r_{dis} = 0. The inspection times, and expected extended lifetime and total cost associated with $\delta_{c,0.5}$ = 0.04, 0.08, 0.12 and 0.16 in Figure 7.10 are provided in Table 7.2. Figure 7.10 indicates that for given $\delta_{c,0.5}$ increasing n_{insp} results in the increase of both $E(t_{life})$ and $E(C_{total})$.

7.4.4 Optimum Balance of the Expected Extended Life and Total Cost

In order to extend the lifetime of a structure, an increase in the number of inspections and inspection quality are needed. However, this requires additional financial resources. Therefore, it is necessary to formulate a bi-objective optimization problem with two conflicting criteria: maximizing the expected extended lifetime $E(t_{life})$ and minimizing expected total cost $E(C_{total})$ as follows

$$\text{Find} \qquad \mathbf{t_{insp}} = \{t_{insp,1}, t_{insp,2}, \ldots, t_{insp,i}, \ldots, t_{insp,,ninsp}\}, \text{ and } \delta_{c,0.5} \tag{7.9}$$

to maximize $E(t_{life})$ and minimize $E(C_{total})$ (7.10)

such that $t_{insp,i} - t_{insp,i-1} \geq 1$ year (7.11a)

$0.02 \leq \delta_{c,0.5} \leq 0.2$ (7.11b)

given n_{insp} and r_p (7.12)

The design variables of this problem are the inspection times and $\delta_{c,0.5}$. The formulation of $E(t_{life})$ in Equation (7.10) is identical with that of Equation (7.4). The expected total cost $E(C_{total})$ is provided in Equation (7.7). The constraints and known parameters are indicated in Equations (7.11) and (7.12), respectively. The Pareto optimal solution set of this bi-objective optimization problem is found using NSGA-II [Deb et al. 2002]. The maximum number of generations is fixed at 500 with population of 100.

The Pareto optimal solution set of the bi-objective optimization problem defined in Equation (7.9) to (7.12) is illustrated in Figure 7.11. Figures 7.11(a), 7.11(b) and 7.11(c) show the Pareto solution sets associated with n_{insp} = 1, 2 and 3, respectively. A proactive approach with r_p = 0.3 is used and the annual discount rate of money r_{dis} is considered as 0.03. Table 7.3 provides values of design variables and objectives of six representative solutions in Figure 7.11. Solution $N1_2$ leads to the largest expected extended life $E(t_{life})$ and highest expected total cost $E(C_{total})$ among Pareto solutions in Figure 7.11(a). The optimum inspection time of solution $N1_2$ is 17.56 years, and the associated $E(t_{life})$ and $E(C_{total})$ are 34.34 years and 43.64, respectively (see Table 7.3). In the Pareto solution set associated with n_{insp} = 3,

solution $N3_2$ requires the highest $E(C_{total})$, but its expected extended lifetime $E(t_{life})$ will be the largest as shown in Figure 7.11(c).

7.5 Conclusions

This chapter presents a probabilistic approach to establish optimum inspection / repair planning for deteriorating structures. The objective of the optimization is maximizing the expected extended lifetime. A decision tree model is used to formulate the extended lifetime considering probabilities of damage detection and repair. The probabilities of damage detection and repair are based on the degree of damage, and pitting corrosion is considered as the main factor affecting the deterioration of RC structures. The following conclusions can be drawn:

1. The probabilistic methodology proposed considers uncertainties associated with corrosion initiation time and lifetime of deteriorating structures. Additionally, inspection uncertainty and type of preference behavior of the decision maker for repair (proactive or delayed) are considered. The effects of inspection quality, repair approach and/or number of inspections on the expected extended lifetime are revealed.
2. Use of higher probabilities of damage detection and/or increasing number of inspections can lead to an increase of the expected lifetime. However, this increase requires additional financial resources. In order to establish a well-balanced cost-effective inspection / repair plan, a bi-objective optimization

formulation consisting of simultaneously maximizing the expected extended lifetime and minimizing the expected total cost has to be solved.

3. The extended lifetime of deteriorating structures and the cost of lifetime extension can be affected by repair types and associated costs. The proposed approach considers a single repair option. However, multiple repair options can be implemented into this approach by considering improvement of structural performance after repair and repair cost.
4. In order to implement the proposed approach, additional efforts are necessary for improving (a) probabilistic modeling of structural deterioration process, (b) accuracy of the prediction of lifetime of deteriorating structures, and (c) quantification of the relation between detectability and inspection methods including structural health monitoring. These improvements will reduce uncertainty and, in turn, will provide greater confidence in optimum inspection / repair strategies of deteriorating structures.

Table 7.1 Random variables for corrosion initiation and loss of reinforcement (Based on information provided in Gonzalez (1995), Val & Melchers (1997), Stewart (2004), Marsh & Frangopol (2008), and engineering judgement)

Random variables	Units	Mean	COV	Type of distribution
Depth from the concrete surface	x (mm)	50.8	0.1	Lognormal
Surface chloride concentration	$C_{ch,o}$ (g/mm^3)	0.15	0.1	Lognormal
Effective chloride diffusion coefficient	D_{ch} (mm^2/year)	110.0	0.1	Lognormal
Threshold chloride concentration	$C_{ch,th}$ (g/mm^3)	0.035	0.1	Lognormal
Initial diameter of reinforcement steel	d_{st0} (mm)	19.05	0.02	Lognormal
Rate of corrosion	r_{corr} (mm/year)	0.06	0.2	Lognormal
Coefficient representing ratio between maximum and average corrosion penetrations	R_{pit}	6	0.1	Normal

Table 7.2 Optimum inspection times, expected extended lifetime and total cost for the proactive repair approach associated with $r_p = 0.5$

$\delta_{c,0..5}$		0.04	0.08	0.12	0.16
Number of inspections $n_{insp} = 1$	$t_{insp,1}$ (years)	17.77	17.89	18.80	19.74
	$E(t_{life})$ (years)	33.27	32.88	31.62	29.05
	$E(C_{total})$	66.39	63.65	53.83	38.18
Number of inspections $n_{insp} = 2$	$t_{insp,2}$ (years)	35.54	36.51	37.90	39.70
	$E(t_{life})$ (years)	43.12	42.55	40.33	35.39
	$E(C_{total})$	121.73	115.23	99.28	69.89
Number of inspections $n_{insp} = 3$	$t_{insp,2}$ (years)	36.44	36.69	37.90	39.90
	$t_{insp,3}$ (years)	54.67	55.03	56.85	59.86
	$E(t_{life})$ (years)	51.44	50.81	47.96	40.97
	$E(C_{total})$	164.58	159.80	139.57	97.54

Table 7.3 Values of objectives and design variables for Pareto solutions in Figure 7.11

Pareto optimum solution	Objective function values		Design variables			
	$E(t_{life})$ (years)	$E(C_{total})$	$\delta_{c,0.5}$	Optimum inspection times (years)		
				$t_{insp,1}$	$t_{insp,2}$	$t_{insp,3}$
$N1_1$	22.53	1.52	0.20	28.52	-	-
$N1_2$	34.34	43.64	0.02	17.56	-	-
$N2_1$	23.47	2.00	0.16	29.49	59.05	-
$N2_2$	45.75	66.56	0.02	17.58	35.15	-
$N3_1$	24.10	2.27	0.11	29.63	56.30	82.86
$N3_2$	55.31	73.97	0.06	17.98	35.94	53.92

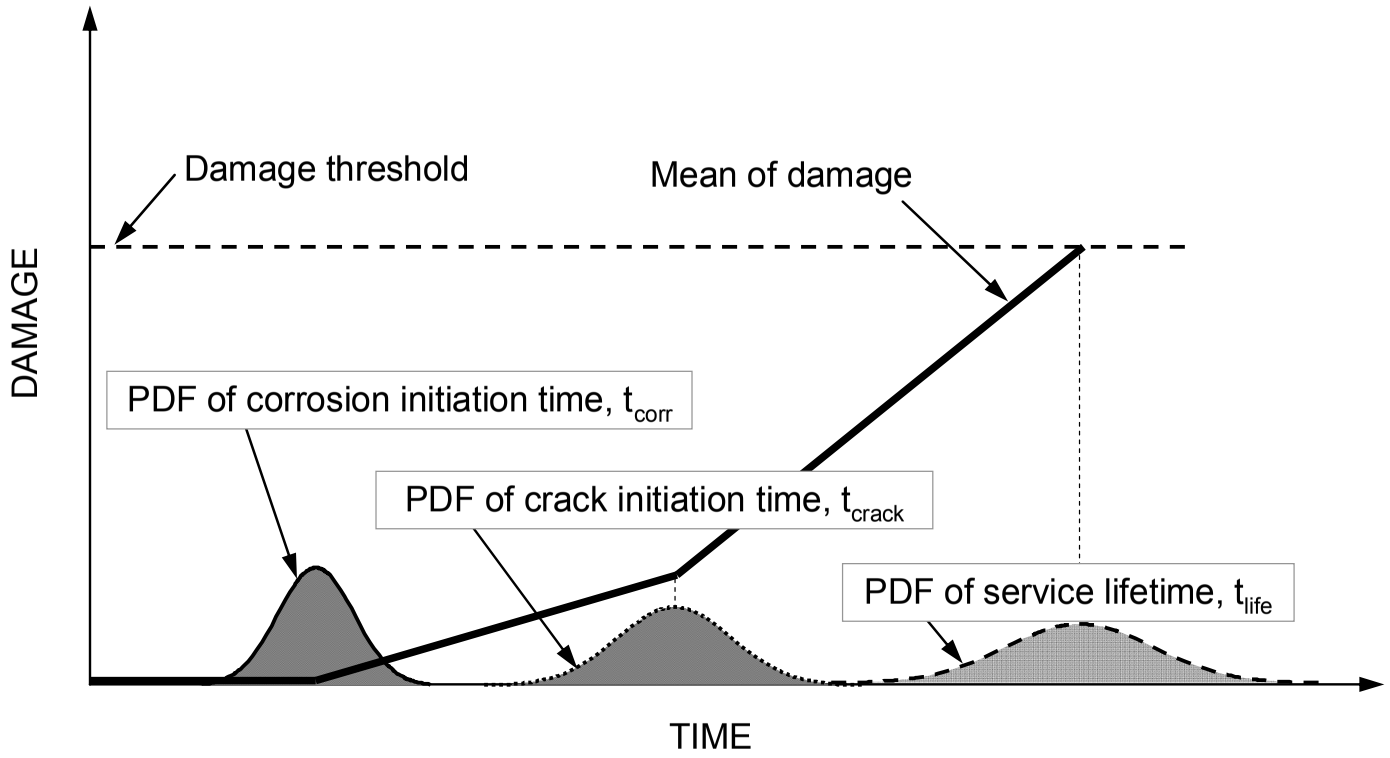

Figure 7.1 Deterioration profile of a RC structure under uncertainty

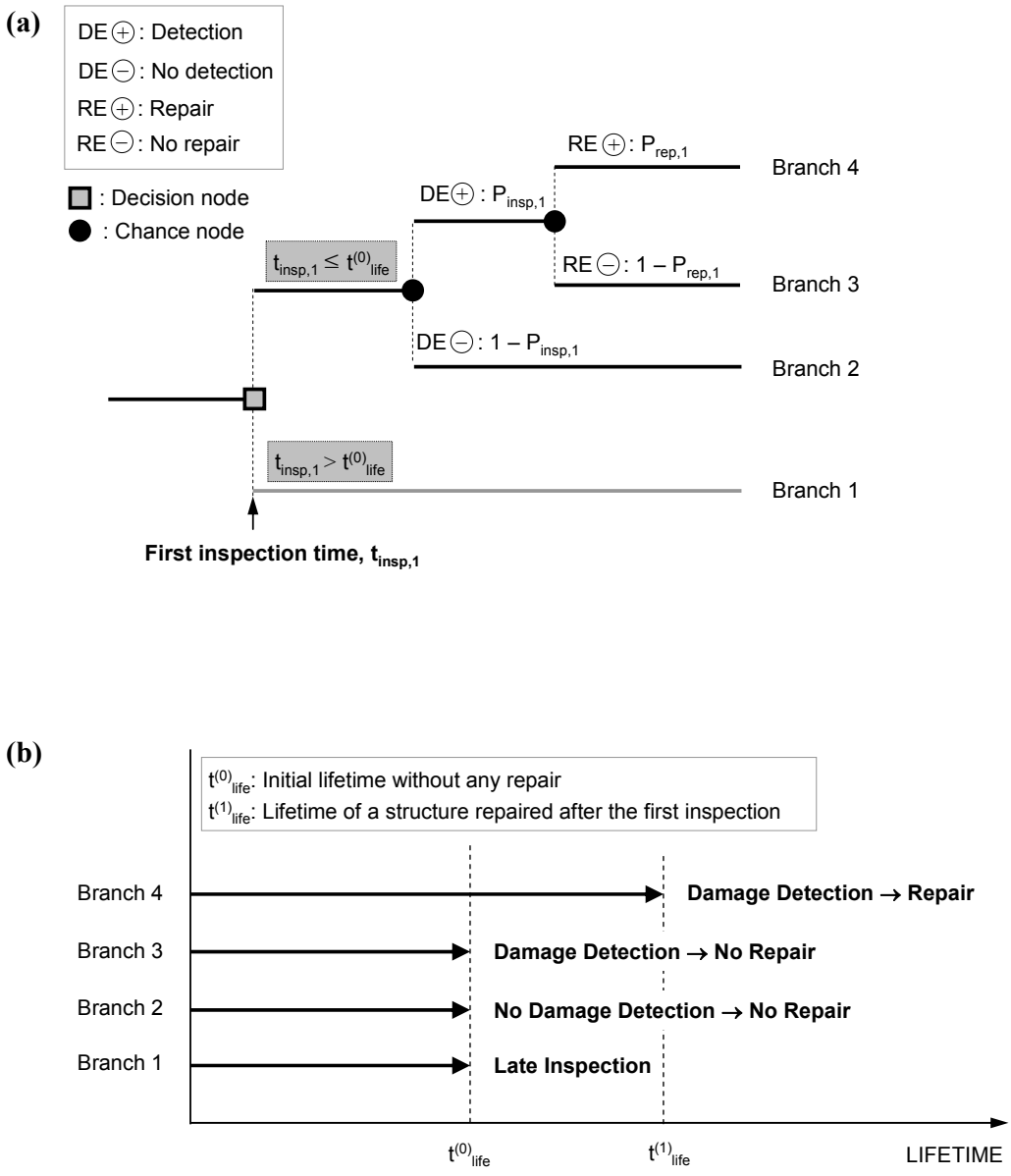

Figure 7.2 (a) Decision tree for prediction of lifetime with one inspection; and **(b)** extended lifetime of each branch in (a)

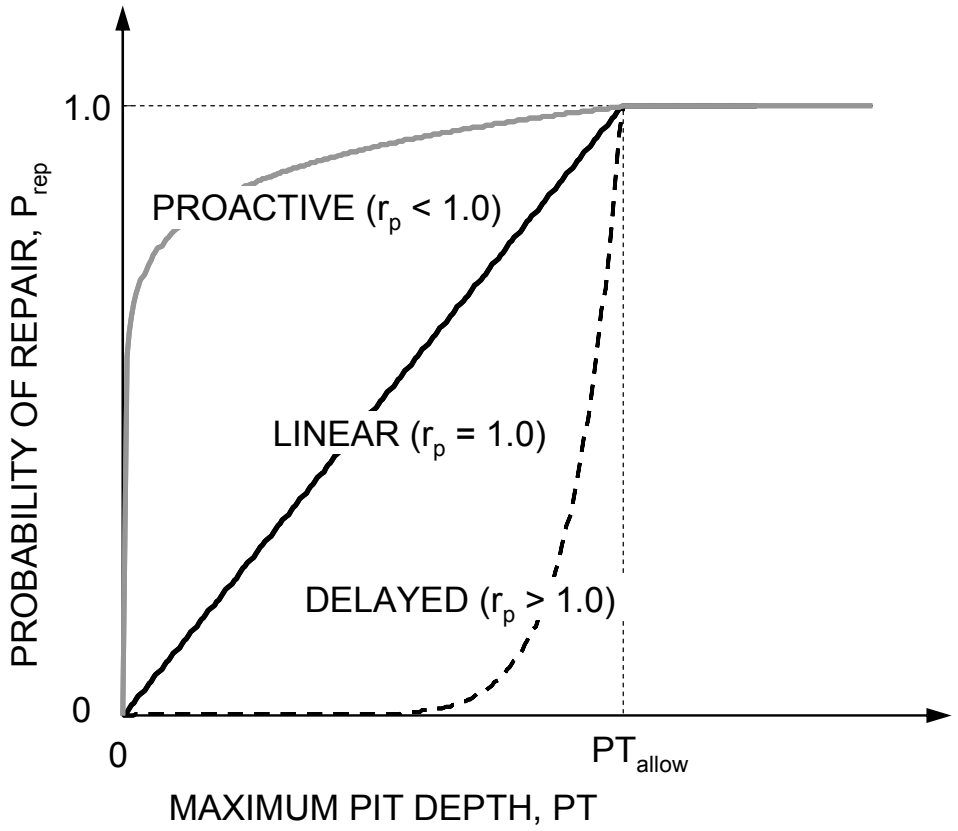

Figure 7.3 Relation between maximum pit depth and probability of repair

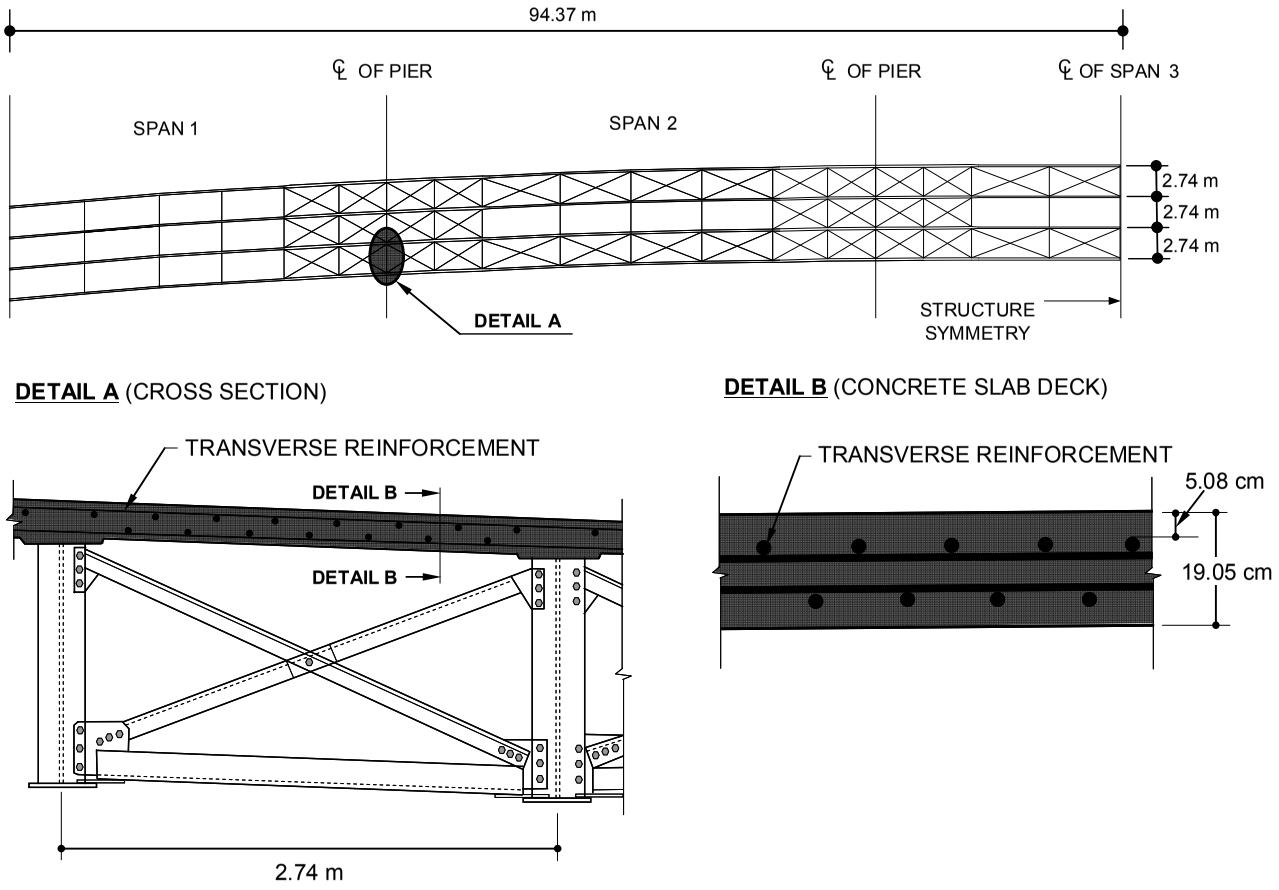

Figure 7.4 I-39 Northbound Wisconsin River Bridge: top view, cross sectional view (Detail A), and concrete slab (Detail B) (adapted from Mahmoud et al. 2005)

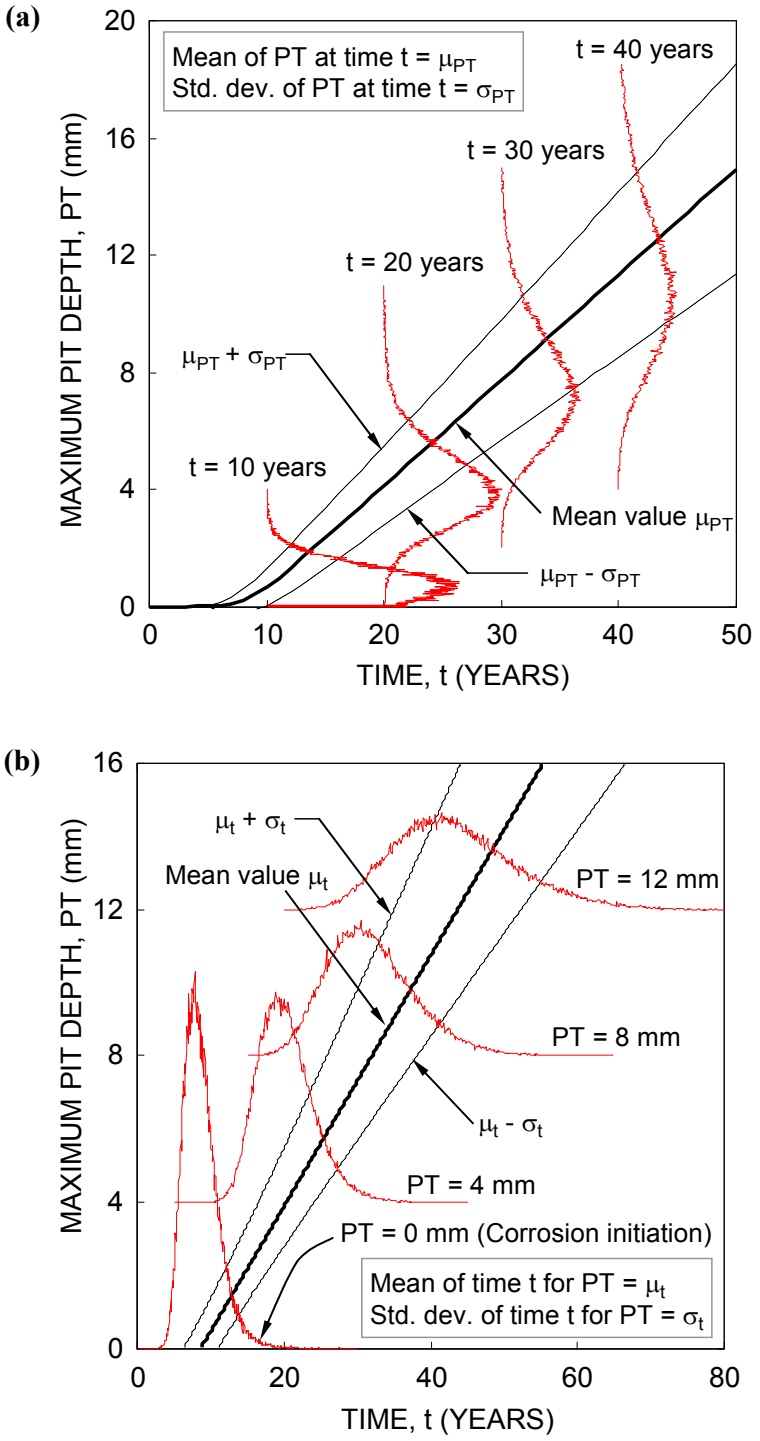

Figure 7.5 Time-dependent maximum pit depth *PT* of RC slab deck with **(a)** PDFs of *PT* at every 10 years; and **(b)** PDFs of corrosion initiation time and times when *PT* = 4, 8 and 12 mm

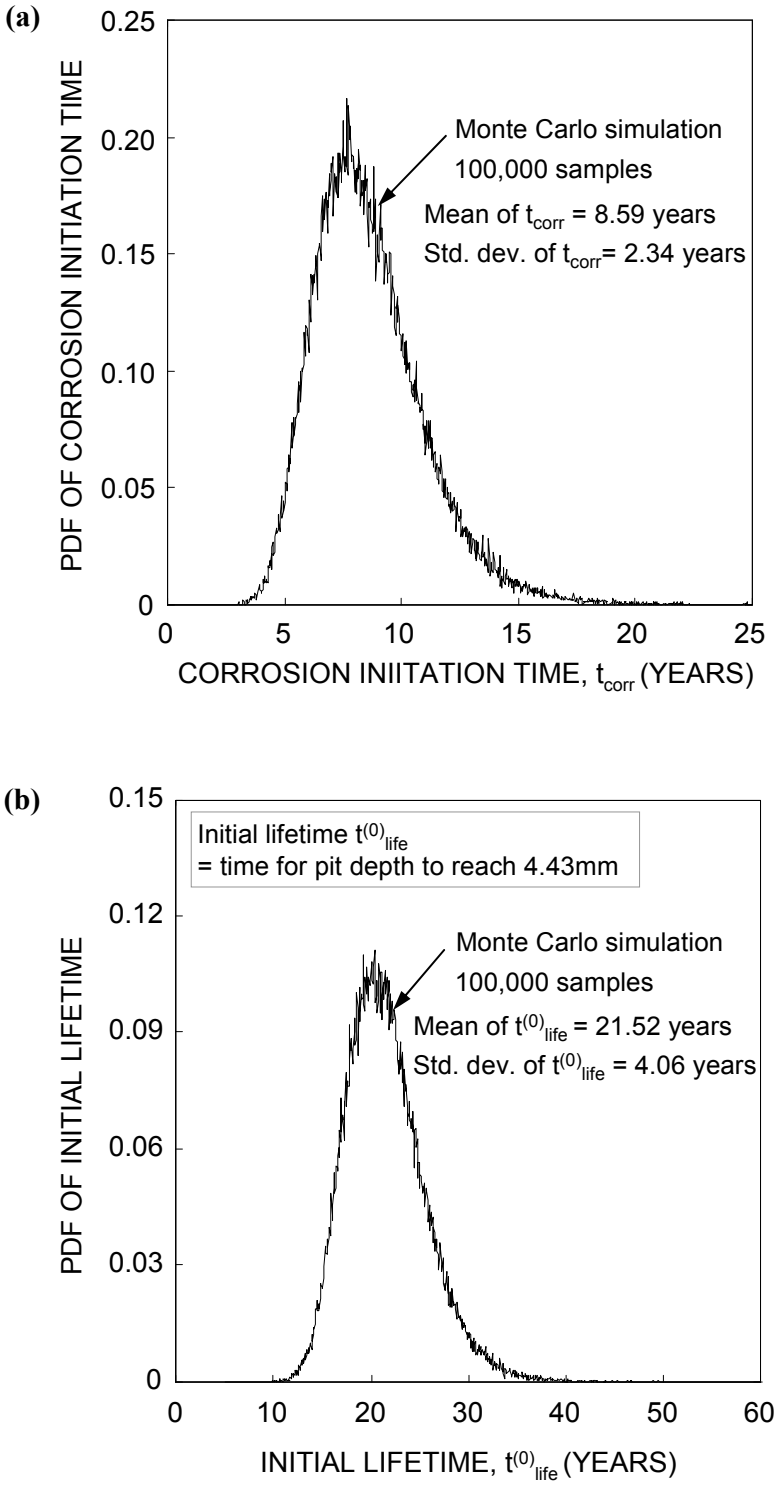

Figure 7.6 PDFs of **(a)** corrosion initiation; and **(b)** initial lifetime

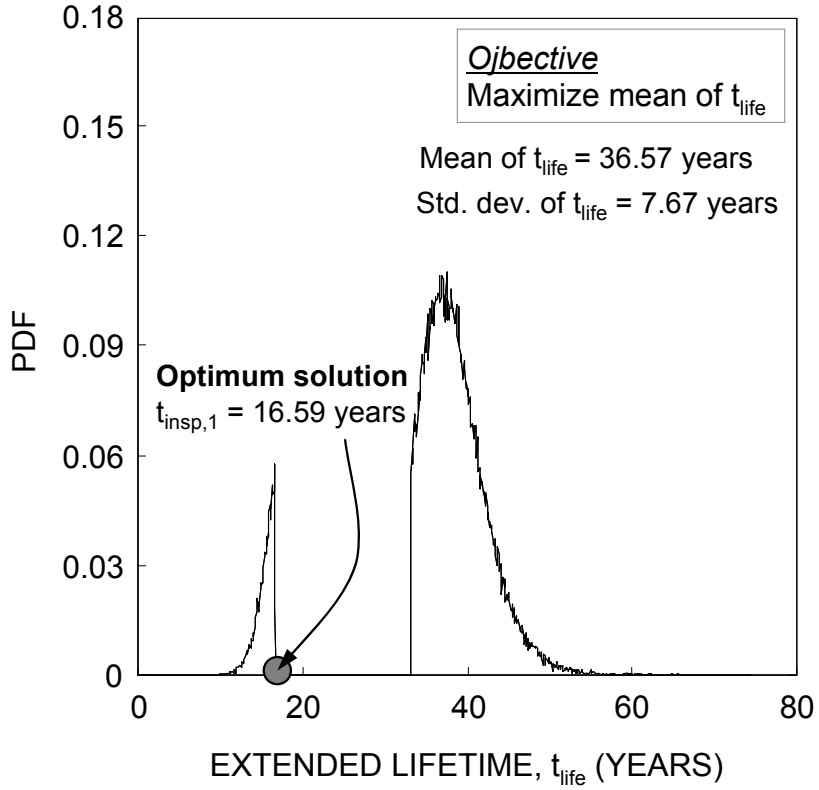

Figure 7.7 PDF of the extended lifetime associated with one inspection (i.e., $n_{insp} = 1$) assuming damage detection and repair as certain event (i.e., $P_{insp,1} = P_{rep,1} = 1.0$)

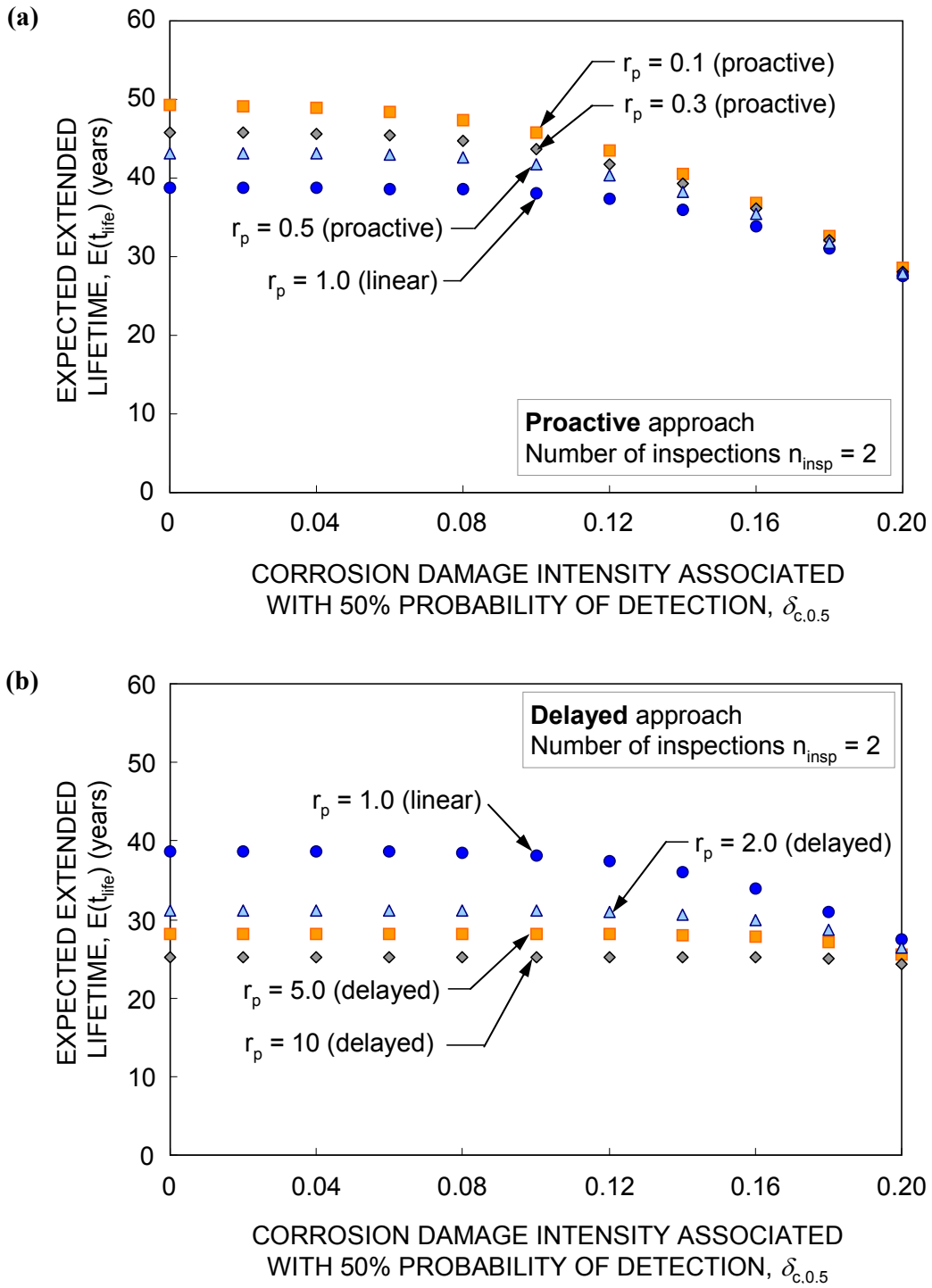

Figure 7.8 Relation between the corrosion damage intensity associated with 50% probability of damage detection and the expected extended lifetime based on **(a)** proactive; and **(b)** delayed approaches to the probability of repair

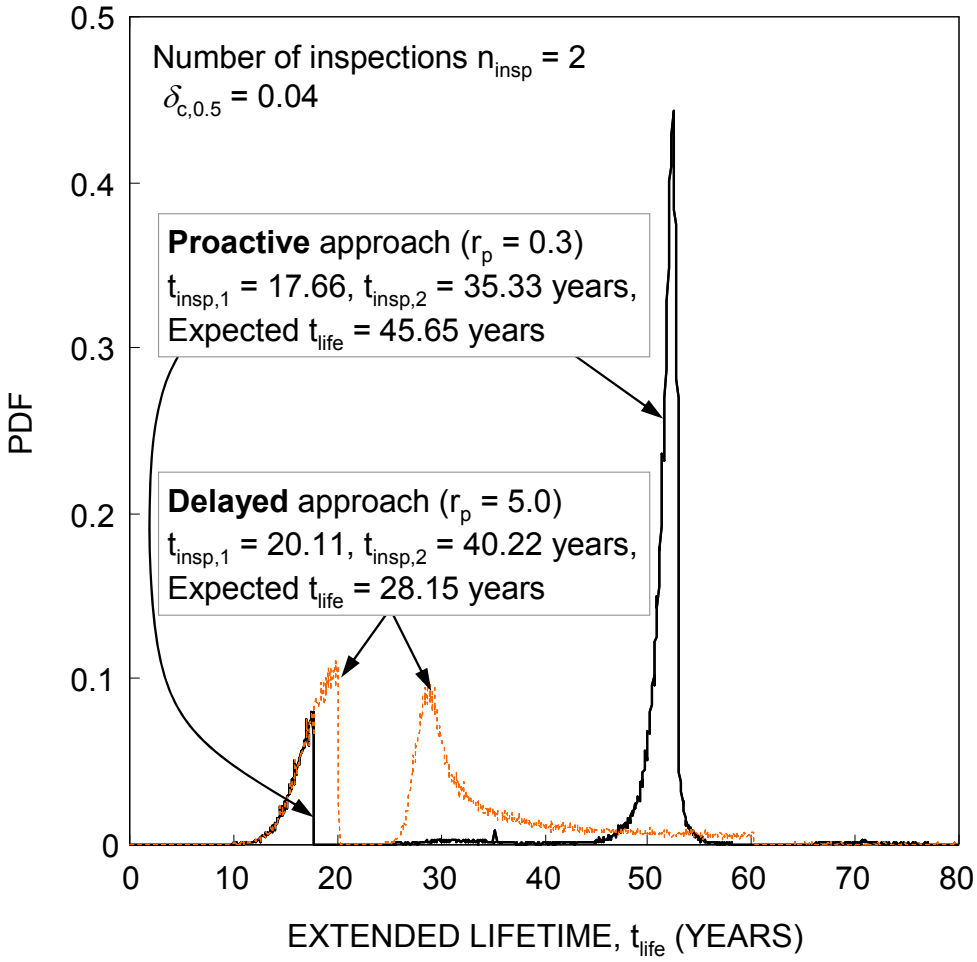

Figure 7.9 PDFs of the extended lifetime based on proactive and delayed approaches to the probability of repair

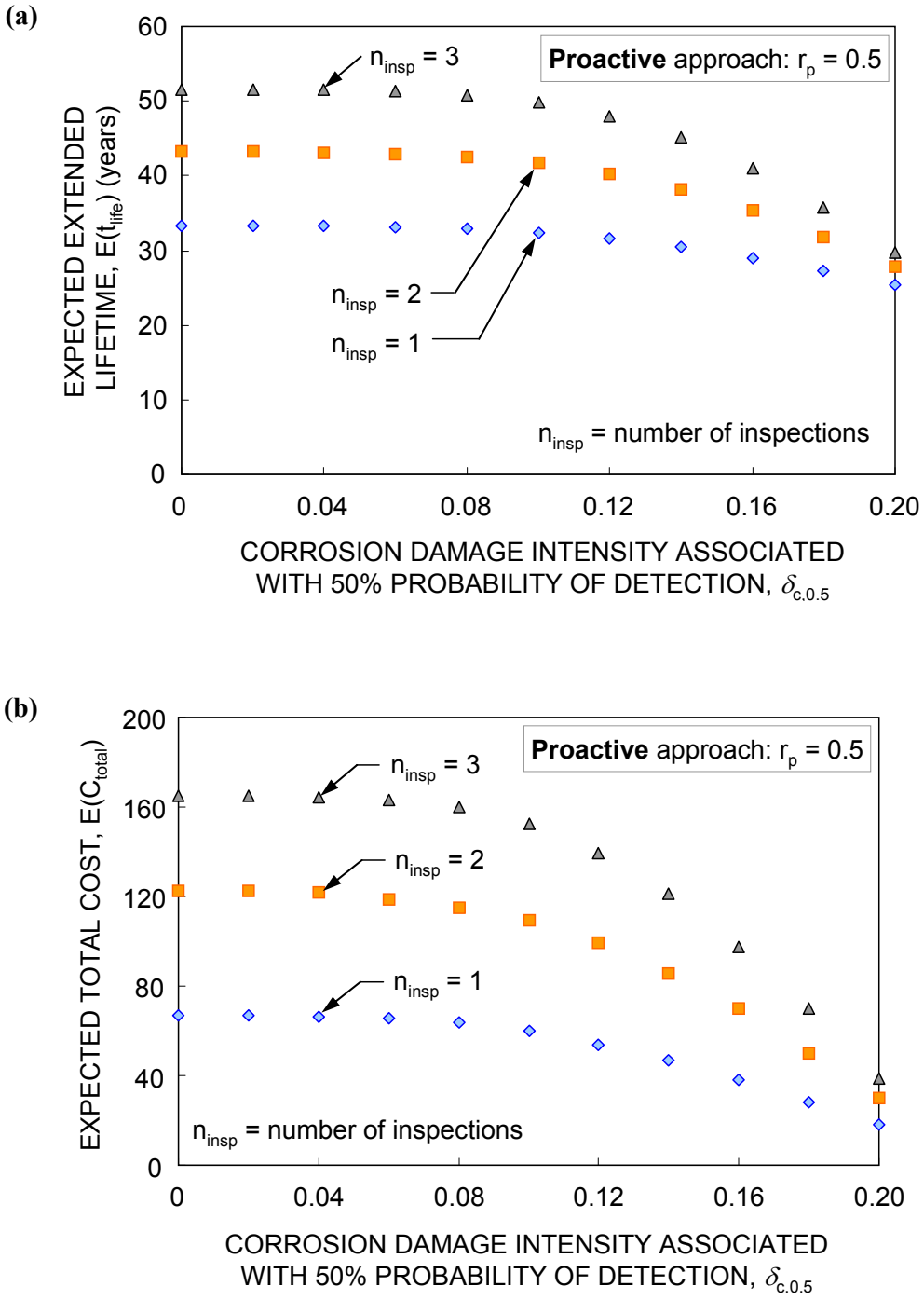

Figure 7.10 Effects of number of inspections on **(a)** expected extended lifetime; and **(b)** expected total cost

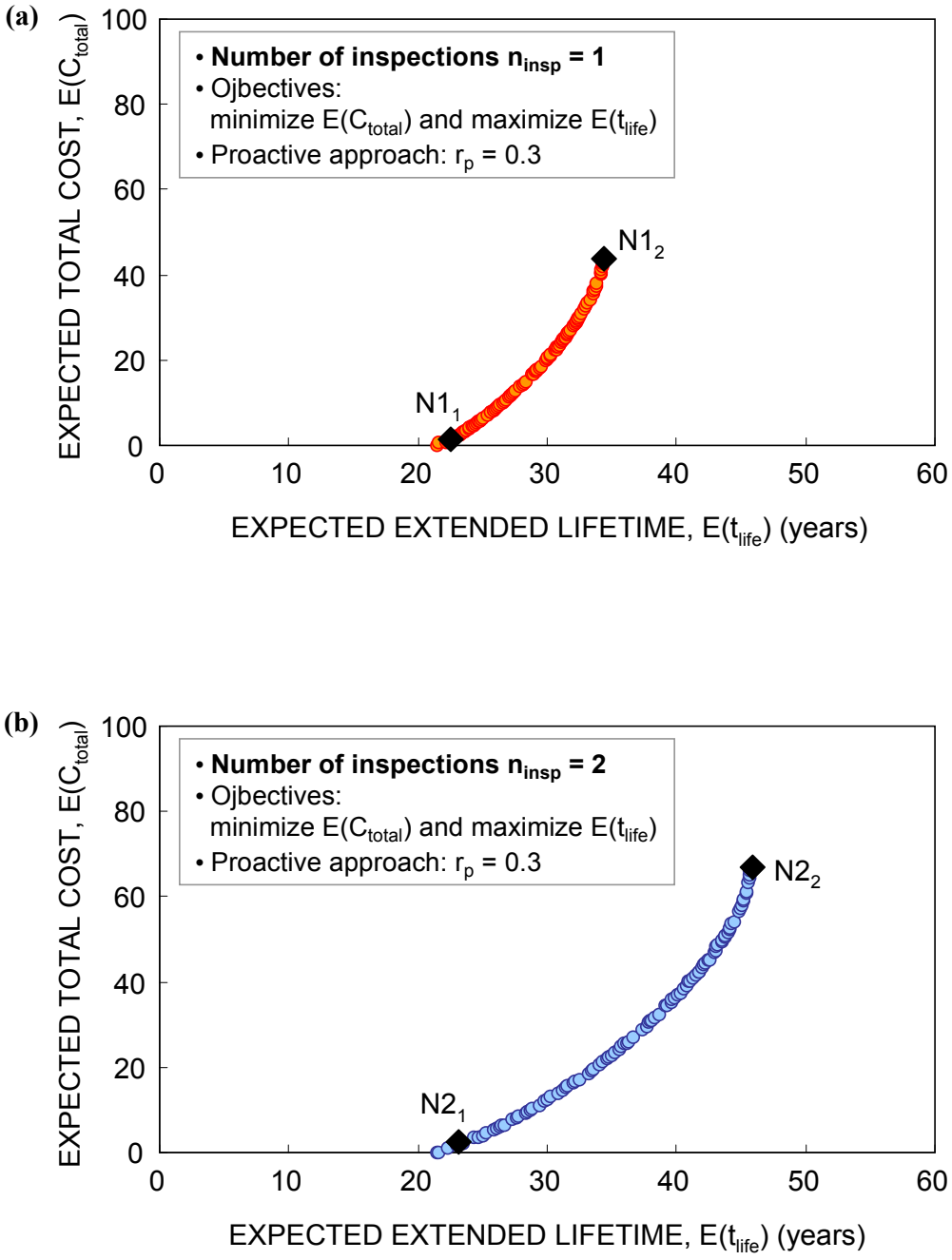

Figure 7.11 Pareto optimum solution sets for **(a)** number of inspections = 1; **(b)** number of inspections = 2; and **(c)** number of inspections = 3

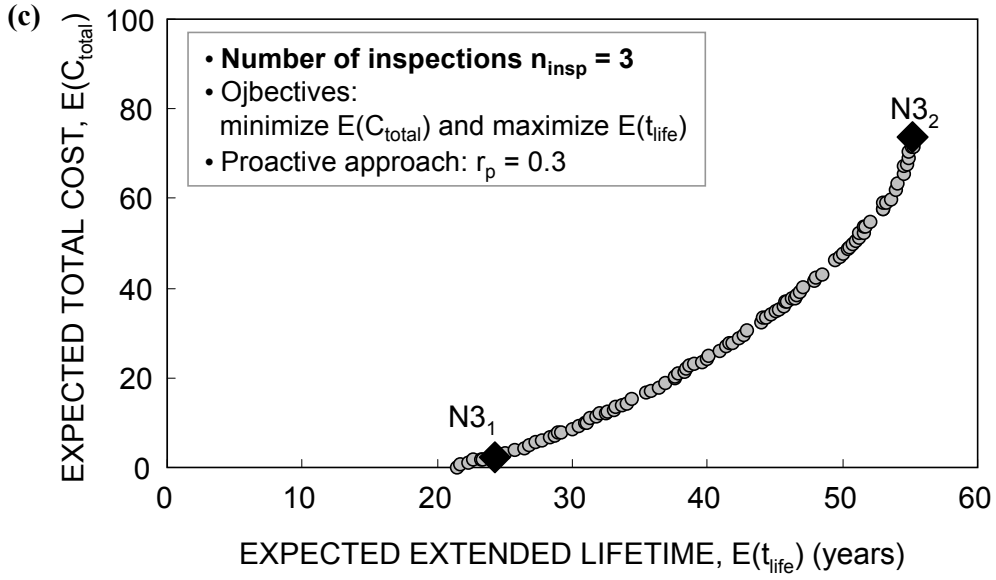

Figure 7.11 Pareto optimum solution set for **(a)** number of inspections = 1; **(b)** number of inspections = 2; and **(c)** number of inspections = 3 (continued)

CHAPTER 8

SUMMARY, CONCLUSIONS AND FUTURE WORK

8.1 Summary

The main goal of this study was to develop probabilistic approaches for optimal inspection, monitoring and maintenance planning of deteriorating structures. These approaches were based on a single-objective or bi-objective optimization formulation. The objectives of these optimization formulations include maximizing the expected average availability of monitoring data and extended lifetime of a structure, and minimizing the expected damage detection delay and expected total cost. In order to formulate these objectives, probabilistic and statistical concepts and methods are used. The approaches proposed in this study were applied to existing highway bridges and naval ship structures under several deterioration mechanisms (i.e., corrosion and fatigue).

Improvement of accuracy associated with assessment and prediction of structural performance through appropriate use of SHM data, results in the timely and appropriate maintenance interventions. These can lead to the reduction of the expected failure cost and the expected maintenance cost of deteriorating structural systems. Therefore, it is necessary to develop approaches to assess and predict the structural performance based on SHM data. Chapter 2 described the general concepts of reliability, service life of structures, and optimal management. Chapter 3

presented approaches to assess and predict the structural performance using SHM data. In Chapter 4, the optimization process for cost-effective monitoring planning was formulated as a bi-objective optimization problem associated with the availability of monitoring data for structural performance prediction and the cumulative cost. This formulation provides a monitoring plan with uniform time interval between monitorings for an individual structural component. Considering the reliability importance factors of structural components, the approach was extended to the optimal monitoring planning of structural systems. Chapter 5 proposed a probabilistic approach to establish the optimum inspection and monitoring plan to minimize the expected damage detection delay. The formulation of the expected damage detection delay considers uncertainties associated with the damage occurrence and propagation, and quality of inspection method. This approach provides inspection and monitoring planning with non-uniform time intervals between inspections or monitorings. Chapter 6 extended the approach presented in Chapter 5, considering the relationship between time-based safety margin and damage detection delay. The approach in Chapter 6 is associated with a single objective optimization process based on the minimization of the expected total cost. Chapter 7 presented an approach for the optimum inspection / repair strategy under uncertainty to extend the lifetime of a structure cost-effectively. Decision makers' willingness to make repair after damage detection as well as uncertainties associated with damage initiation and propagation, and quality of the inspection

method were considered in the optimization process. The approaches presented in this study were applied to deteriorating highway bridges and naval ship structures.

The detailed summary of each chapter is as follows:

- Chapter 2 reviewed the general concepts of the reliability and service life of civil structures, including (a) the system reliability approach and its applications, (b) the effects of time-dependent structural performance on the service life of a structure, and (c) the concepts of optimal management using multi-criteria optimization.
- Chapter 3 presented (a) an approach to develop and update prediction functions, and (b) a procedure for the assessment and prediction of structural performance using monitoring. The updating of prediction functions is based on mean square fitting to monitored extreme data assigned to monitoring periods, while the necessary monitoring periods are computed from acceptance sampling theory. Furthermore, in order to assess and predict the structural system performance through series-parallel system modeling, an efficient approach using the long-term monitored strain data was proposed. Sensitivity studies with respect to system modeling, correlations, and measurement errors were carried out.
- In Chapter 4, a probabilistic approach to establish an optimum monitoring plan based on availability was provided. The probability that the performance prediction model (introduced in Chapter 3) is usable in the future was computed by using the statistics of extremes. This probability represents the availability of the monitoring data over the future non-monitoring period. The optimum availability

of the monitoring data and monitoring cost was formulated as a bi-objective optimization problem with two conflicting objectives: minimization of the total monitoring cost and maximization of the availability of the monitoring data for performance prediction. The Pareto solution set from this problem provides the monitoring plan with uniform monitoring time intervals between monitoring activities for an individual structural component. Considering the normalized reliability importance factors of structural components, the approach to establish an optimal monitoring plan for a structural system was developed. In addition, as an alternative approach, decision analysis theory associated with the minimum monetary loss criterion was used.

- Chapter 5 proposed a probabilistic approach for an optimum inspection and monitoring planning with non-uniform time intervals between inspections or monitorings. This approach considers uncertainties associated with damage occurrence and propagation, and quality of the inspection method, and monitoring duration. The optimization problem was formulated with the objective of minimizing the expected damage detection delay. The effects of the quality of inspection method, number of inspections or monitorings, monitoring duration, and dispersion associated with damage occurrence on the minimization of the expected damage detection delay were investigated. A well-balanced inspection or monitoring plan was obtained from a bi-objective optimization problem by simultaneously minimizing both the expected damage detection delay and the total

inspection and monitoring cost. A comparison of the inspection plans based on the same type and different types of inspections was conducted. Furthermore, an optimum combined inspection / monitoring planning was investigated taking into account the Pareto solution sets associated with various combinations of inspection and monitoring.

- Chapter 6 extended the approach presented in Chapter 5 to cost-based optimum inspection and monitoring planning. This approach considers the relationship between time-based safety margin and damage detection delay, and the expected total cost including the costs of inspection and failure. The failure criterion is based on time-based safety margin defined as the difference between the time for damage to reach the critical fatigue crack size and the damage detection time. Uncertainty associated with time-based safety margin is included in the approach proposed in this chapter. Effects of the failure cost on inspection and monitoring scheduling were studied.
- Chapter 7 presented a probabilistic approach for an optimum inspection and repair strategy to extend service life of a deteriorating structure. This strategy is a solution of a bi-objective probabilistic optimization problem considering the maximization of expected extended lifetime and minimization of expected total cost. The formulation of extended lifetime for a given number of inspections is based on a decision tree analysis. Probabilities of damage detection and repair are considered in this decision tree. The decision makers' willingness to make a repair

after damage detection is categorized into: (a) delayed, (b) directly proportional and (c) proactive. The effects of inspection quality, repair approach, and number of inspections on the expected extended lifetime were investigated.

8.2 Conclusions

- The use of the proposed performance prediction function based on monitored extreme data provides the following benefits: (a) inclusion of environmental and degradation processes in the structural reliability assessment; and (b) flexible updating of performance functions associated with the reliability index or to any performance indicator by using acceptance criteria applied to monitoring extreme data.
- The approach for optimum monitoring planning based on availability of monitoring data provides uniform time intervals between monitorings for an individual component. This optimum monitoring plan is affected by the discount rate of money. A higher discount rate of money leads to an optimal monitoring plan with shorter monitoring duration and shorter time interval between monitoring activities. As an illustrative example, the proposed approach was applied to an existing bridge. However, it can also be applied to other types of monitored structure.
- The formulation of damage detection delay considers uncertainties associated with damage occurrence and propagation and quality of the inspection method. This approach provides optimum non-uniform time intervals between inspections or

monitoring activities. In the formulation of the expected damage detection delay, the determination of the lower and upper bounds for damage occurrence depends on the PDF of damage occurrence time. These bounds have a significant effect on the expected damage detection delay.

- Increase in the number of inspections and/or inspection quality (or number of monitorings and/or monitoring duration) may lead to reduction of the expected damage detection delay. However, this increase requires additional financial resources. Therefore, in order to consider cost-effective inspection and/or monitoring plans, a bi-objective optimization problem based on minimization of both expected damage detection delay and inspection cost has to be solved.
- For a predefined expected damage detection delay, an optimum inspection plan based on multiple inspection types is more economical than that based on a single type of inspection. Furthermore, damage may be detected with less delay by using monitoring than inspection. However, monitoring is usually more expensive than inspection. For this reason, combined inspection / monitoring plans were investigated.
- Damage detection delay leads to repair delay, and, therefore, to an increase in the probability of failure. Under the assumption that repair and retrofit methods are applied immediately after damage is detected, the failure criterion can be formulated using damage detection time and time for damage to reach the critical state. This time-based failure criterion is used for the cost-based inspection or

monitoring planning.

- The time-based failure criterion proposed in Chapter 6 is associated with the time-based safety margin. This safety margin considers uncertainty associated with the time for damage to reach a critical level. Alternatively, the time-based failure criterion can be associated with the crack size-based safety margin. The two approaches are expected to lead to identical results.
- A probabilistic approach for optimum inspection / repair planning for extending the service life of a deteriorating structure was proposed. In this approach, proactive and delayed repair actions were considered. The relationships among inspection quality, number of inspections, repair approach and the expected extended lifetime were revealed. As expected, the use of higher probabilities of damage detection and/or the increase in the number of inspections can lead to an increase of the expected lifetime. However, this increase requires additional financial resources so that a bi-objective optimization formulation consisting of simultaneously maximizing the expected extended lifetime and minimizing the expected total cost has to be solved.

8.3 Recommendation for Future Studies

- The results after each inspection or monitoring can be used to update the existing inspection, monitoring and/or maintenance schedule. The updating process after each inspection or monitoring will lead to a more reliable maintenance schedule.

Therefore, further studies are necessary to establish the optimum inspection and monitoring planning considering updating.

- The probabilistic approaches proposed in this study were applied to ship hull structures and bridge structures. These applications can be extended to include a wide range of structures under different deterioration processes. However, future efforts are needed to establish a methodology to consistently deal with lack of knowledge and data associated with deterioration mechanisms, inspection and monitoring methods, and time-dependent performance prediction.
- The accuracy of the approach based on the newly developed component state function using monitored data depends on how correctly and completely the structural system is modeled. In addition, in order to achieve accurate system performance assessment, it is important to obtain the actual coefficients of correlation among the random variables directly from the monitored data. Therefore, the system should be modeled appropriately, and the correlation should be considered based on monitoring data.
- Several assumptions in this study need to be further investigated. For example, the formulation of the expected damage detection delay for optimum monitoring planning is based on the assumption that the damage detection during monitoring is certain, when the sensors are installed properly. However, there are uncertainties associated with damage detection process. Further studies need to consider these uncertainties.

- In order to model damage occurrence and propagation of deteriorating RC structures more accurately, concrete carbonation, time-dependent effects associated with chloride diffusion coefficient and the initial chloride concentration, and loss of bond between concrete and reinforcing bars have to be considered.
- The fatigue damage occurrence and propagation are random processes involving intermittent growths and dormant periods. In order to consider these evolutionary features, Markov chains, jump process models and stochastic differential equations have been developed [Sobczyk 1987]. The scheduling of inspection and monitoring can be affected by the time evolution model of fatigue cracks. Therefore, further studies are needed to incorporate such advanced stochastic modelings into the approaches proposed in this study.
- A single repair option was considered in the approach presented in Chapter 7. However, multiple repair options can be implemented into this approach by considering improvement of structural performance after repair and repair cost.
- Further studies are necessary to develop the integrated approach to optimize monitoring location, type of monitoring, and monitoring duration for a life-cycle framework.

REFERENCES

AASHTO (1989). *Guide Specifications of Strength Evaluation of Steel and Concrete Bridges.* Specifications, American Association of State Highway and Transportation Officials, Washington D.C.

AASHTO (2007). *LRFD Bridge Design Specifications.* Specifications, American Association of State Highway and Transportation Officials, Washington D.C.

ACI 318 (2005). *Building Code Requirements for Structural Concrete.* Design Codes, American Concrete Institute, Farmington Hills, MI.

ACI 437R-03 (2003). *Strength Evaluation of Existing Concrete Buildings*. Specifications, American Concrete Institute, Farmington Hills, MI.

Ahmad, S. (2003). "Reinforcement corrosion in concrete structures, its monitoring and service life prediction - a review." *Cement & Concrete Composites*, Elsevier, 25(4-5), 459-471.

AISC 325 (2005). *Steel Construction Manual.* Manual, American Institute of Steel Constructions, Chicago, IL.

Akgül, F. (2002). "Lifetime system reliability prediction for multiple structure types in a bridge network." PhD thesis, Univ. of Colorado, Boulder, Colo.

Akiyama, M., Frangopol, D.M., and Suzuki, M. (2009). "Integration of the effects of airborne chlorides into reliability-based durability design of reinforced concrete structures in a marine environment." *Structure and Infrastructure Engineering*, Taylor & Francis, doi: 10.1080/15732470903363313, in press.

Akpan, U.O., Koko, T.S., Ayyub, B., and Dunbar, T.E. (2002). "Risk assessment of aging ship hull structures in the presence of corrosion and fatigue." *Marine Structures*, Elsevier, 15(3), 211-231.

Al-Tayyib, A.-H. J., and Khan, M.S. (1988). "Corrosion rate measurements of reinforcing steel in concrete by electrochemical techniques." *ACI Materials*

Journal, 85(3), 172-177.

Anderson, T.W., and Darling, D.A. (1952). "Asymptotic theory of certain "goodness-of-fit" criteria based on stochastic processes." *Annals of Mathematical Statistics*, 23(2), 193–212.

Ang, A.H.-S. and De Leon, D. (2005). "Modeling and analysis of uncertainties for risk-informed decisions in infrastructures engineering." *Structure & Infrastructure Engineering*, Taylor and Francis, 1(1), 19-31.

Ang, A.H.-S. and Tang, W.H. (1984). *Probability Concepts in Engineering Planning and Design Volume II*. John Wiley & Sons.

Ang, A.H.-S. and Tang, W.H. (2007). *Probability Concepts in Engineering: Emphasis on Applications to Civil and Environmental Engineering.* 2nd edn. New York, Wiley.

Arora, J.S. (2004). *Introduction to Optimum Design.* Elsevier Academic Press, 537-552.

Arora, P., Popov, B.N., Haran, B., Ramasubramanian, M., Popova, S. and White, R.E. (1997). "Corrosion initiation time of steel reinforcement in a chloride environment - A one dimensional solution." *Corrosion Science,* Elsevier, 39(4), 739-759.

ASCE (2000). *Guideline for Structural Condition Assessment of Existing Building, SEI/ASCE 11-99.* Specifications, American Society of Civil Engineers, Reston, Virginia.

Athan, T.W., and Papalambros, P.Y. (1996). "A note on weighted criteria methods for compromise solutions in multi-objective optimization." *Engineering Optimization*, Taylor & Francis, 27(2), 155-176.

Ayyub, B.M., Assakkaf, I.A., Kihl, D.P., and Siev, M.W. (2002). "Reliability-based design guidelines for fatigue of ship structures." *Naval Engineers Journal*, ASNE, 114(2), 113-138.

Bannantine, J.A., Comer, J.J., and Handrock, J.L. (1990). *Fundamentals of Metal Fatigue Analysis.* Prentice Hall.

Berens, A.P. (1989). "NDE reliability analysis." *Metal handbook*, 9th Edition, Vol. 17, ASM International, Material Park, Ohio, 689-701.

Berens, A.P., and Hovey, P.W. (1981). "Evaluation of NDE reliability characterization." *AFWAL-TR-81-4160*, Vol. 1, Air Force Wright Aeronautical Laboratory, Wright-Patterson Air Force Base, Dayton, Ohio.

Bertolini, L., Elsener, B., Pedeferri, P., and Polder, R. (2004). *Corrosion of Steel in Concrete: Prevention, Diagnosis, and Repair*. Wiley-VCH.

Boller, C., and Buderath, M. (2007). "Fatigue in aerostructures-where structure health monitoring can contribute to a complex subject." *Philosophical Transactions of the Royal Society A*, 365, 561-587.

BS7910 (2005) *Guidance on Methods for Assessing the Acceptability of Flaws in Fusion Welded Structures*. British Standards Institution (BSI), London.

Cabrera, J.G. (1996). "Deterioration of concrete due to reinforcement steel corrosion." *Cement & Concrete Composite*, Elsevier, 18(1), 47-59.

Cartz, L. (1995). *Nondestructive Testing: Radiography, Ultrasonics, Liquid Penetrant, Magnetic Particle, Eddy Current*. ASM International.

Chang, P.C., Flatau, A., and Liu, S.C. (2003). Review paper: Health monitoring of civil infrastructure. *Structural Health Monitoring*, SAGE, 2(3), 257-267.

Chaker, V., ed. (1992). "Corrosion forms & control for infrastructure." *ASTM STP 1137*, Philadelphia.

Chong, K.P., Carino, N.J., and Washer, G. (2003). "Health monitoring of civil infrastructures." *Smart Materials and Structures*, 12, 483-493.

Chung, H.-Y., Manuel, L., and Frank, K.H. (2006). "Optimal inspection scheduling of steel bridges using nondestructive testing techniques." *Journal of Bridge*

Engineering, ASCE, 11(3), 305-319.

Clark, J.D. (1991). "Fatigue Crack Initiation and Propagation in Warship Hulls." *Advances in Marine Structures – 2*, C.S. Smith and R.S. Dow, eds, Elsevier Applied Science, London, 42-60.

Cornell, C.A. (1967). "Bounds on the reliability of structural systems." *Journal of Structural Division*, ASCE, 93(ST1), 171-200.

Cramer, E.H., Schulte-Strauthaus, R., and Bea, R.G., (1992). "Structural maintenance project volume 1 – fatigue damage evaluation software theory documentation and verification." *SSC-386*, Ship Structure Committee.

Crank, J. (1975). The Mathematics of Diffusion. 2nd Ed. Oxford University Press.

Das, P. C. (1999). ''Prioritization of bridge maintenance needs.'' *Case studies in optimal design and maintenance planning of civil infrastructure systems*, D. M. Frangopol, ed., ASCE, Reston, Va., 26–44.

Deb, K., Pratap, A., Agarwal, S., and Meyarivan, T. (2002). "A Fast elitist multiobjective genetic algorithm: NSGA-II." *IEEE Transactions on Evolutionary Computation* 6 (2), 182-197.

Denton, S. (2002). "Data estimates for different maintenance options for reinforced concrete cross heads." Draft report for highways agency, U.K., Brinckerhoff Ltd.

Dexter, R.J., FitzPatrick, R.J., and St. Peter, D.L. (2003). "Fatigue strength and adequacy of weld repairs." *SSC-425*, Ship Structure Committee.

Dhir, R.K., Hewlett, P.C., and Chan, Y.N. (1989). "Near-surface characteristics of concrete: Prediction of carbonation resistance." *Magazine of Concrete Research,* 41(148), 137-143.

Ditlevsen, O. (1979). "Narrow reliability bounds for structural systems." *Journal of Structural Mechanics*, ASCE, 7(4), 453-472.

Dobson, W.G., Brodrick, R.F., Wheaton, J.W., Giannotti, J., and Stambaugh, K.A.

(1983). "*Fatigue considerations in view of measured load spectra.*" SSC-315, Ship Structure Committee.

Ellingwood, B.R. (2005). "Risk-informed condition assessment of civil infrastructure: state of practice and research issues." *Structure & Infrastructure Engineering*, Taylor and Francis, 1(1), 7-18.

Enright, M.P., and Frangopol, D.M. (1998a). "Probabilistic analysis of resistance degradation of reinforced concrete bridge beams under corrosion." *Engineering Structures*, Elsevier, 20(11), 960-971.

Enright, M.P., and Frangopol, D.M. (1998b). "Service-life prediction of deteriorating concrete bridges." *Journal of Structural Engineering*, ASCE, 124(3), 309-317.

Enright, M.P., and Frangopol, D.M. (1999a). "Condition prediction of deteriorating concrete bridges using Bayesian updating." *Journal of Structural Engineering*, ASCE, 125(10), 1118-1125.

Enright, M.P., and Frangopol, D.M. (1999b). "Maintenance planning for deteriorating concrete bridges." *Journal of Structural Engineering*, ASCE, 125(12), 1407-1414.

Estes, A.C., and Frangopol, D.M. (1998). "RELSYS: A computer program for structural system reliability analysis." *Structure Engineering & Mechanics*, Techno-Press, 6(8), 901-919.

Estes, A.C., and Frangopol, D.M. (1999). "Repair optimization of highway bridges using system reliability approach." *Journal of Structural Engineering*, ASCE, 125(7), 766–775.

Estes, A.C., and Frangopol, D.M. (2001). "Minimum expected cost-oriented optimal maintenance planning for deteriorating structures: application to concrete bridge decks." *Reliability Engineering & System Safety*, Elsevier, 73(3), 281-291.

Estes, A.C., and Frangopol, D.M. (2005). "Life-cycle evaluation and condition assessment of structures." *Chapter 36 in Structural Engineering Handbook*, 2nd

Edition, W-F. Chen and E. M. Lui, eds., CRC Press, 36-1 - 36-51.

Farhey, D.N. (2005). "Bridge instrumentation and monitoring for structural diagnostics." *Structural Health Monitoring*, SAGE, 4(4), 301-318.

Farrar, C.R., and Worden, K. (2007). "An introduction to structural health monitoring." *Philosophical Transactions of the Royal Society A*: *Mathematical, Physical and Engineering Sciences*, 365(1851), 303-315.

Fatemi, A., and Yang, L. (1998). "Cumulative fatigue damage and life prediction theories: a survey of the state of the art for homogeneous materials." *International Journal of Fatigue*, Elsevier, 20(1), 9-34.

Fisher, J. W. (1984). *Fatigue and Fracture in Steel Bridges*. John Willey & Sons.

Fisher, J.W., Kulak, G.L., and Smith, I.F. (1998). *A Fatigue Primer for Structural Engineers*. National Steel Bridge Alliance.

Floudas, C.A., Pardalos, P.M., Adjiman, C., Esposito, W., Gumus, Z., Harding, S., Klepeis, J., Meyer, C., and Schweiger C. (1999) *Handbook of Test Problems in Local and Global Optimization*. Kluwer, Dordrecht.

Frangopol, D.M. (2011). "Life-cycle performance, management, and optimization of structural systems under uncertainty: accomplishments and challenges." *Structure and Infrastructure Engineering*, Taylor & Francis, 7(6), 389-413.

Frangopol, D.M., and Estes, A.C. (1999). "Optimum lifetime planning of bridge inspection / repair programs." *Structural Engineering International*, Journal of IABSE, 9(3), 219-223.

Frangopol, D.M., Kong, J.S., and Gharaibeh, E.S. (2001). "Reliability-based life-cycle management of highway bridges." *Journal of Computing in Civil engineering*, ASCE, 15(1), 27–34.

Frangopol, D.M., Lin, K.Y., and Estes, A.C. (1997a). "Reliability of reinforced concrete girders under corrosion attack." *Journal of Structural Engineering*,

ASCE, 123(3), 286-297.

Frangopol, D.M., Lin, K.Y., and Estes, A.C. (1997b). "Life-cycle cost design of deteriorating structures." *Journal of Structural Engineering*, ASCE, 123(10), 1390-1401.

Frangopol, D.M., and Liu, M. (2006). "Life-Cycle Cost and Performance of Civil Structures," Article in McGraw-Hill 2006 Yearbook of Science and Technology, McGraw-Hill, New York, 183-185.

Frangopol, D.M., and Liu, M. (2007). "Maintenance and management of civil infrastructure based on condition, safety, optimization, and life-cycle cost." *Structure & Infrastructure Engineering*, Taylor and Francis, 3(1), 29-41.

Frangopol, D.M., and Messervey, T.B. (2007). "Risk assessment for bridge decision making." *Proceedings of the Fourth Civil Engineering Conference in the Asian Regions, CECAR 4, Taipei, Taiwan, June 25-28, 2008* (invited paper); in ASCE Tutorial & Workshop on Quantitative Risk Assessment, Taipei, Taiwan, June 25-28, 2007, 37-42.

Frangopol, D.M. and Messervey, T.B. (2009a) "Life-cycle Cost and Performance Prediction: Role of Structural Health Monitoring." *Chapter 16 in Frontier Technologies for Infrastructures Engineering*, S-S. Chen and A. H-S. Ang, eds., CRC Press-Balkema-Taylor & Francis Group, Leiden, The Netherlands, 361-381.

Frangopol, D.M., and Messervey, T.B. (2009b). "Maintenance principles for civil structures." *Chapter 89 in Encyclopedia of Structural Health Monitoring*, C. Boller, F-K. Chang, and Y. Fujino, eds., John Wiley & Sons Ltd, Chicester, UK, Vol. 4, 1533-1562.

Frangopol, D.M., Strauss, A., and Kim, S. (2008a). "Bridge reliability assessment based on monitoring." *Journal of Bridge Engineering,* ASCE, 13(3), 258-270.

Frangopol, D.M., Strauss, A., and Kim, S. (2008b). "Use of monitoring extreme data for the performance prediction of structures: General approach." *Engineering*

Structures, Elsevier, 30(12), 3644-3653.

Funahashi, M. (1990). "Predicting corrosion-free service life of a concrete structure in a chloride environment." *ACI Materials Journal*, ACI, 87(6), 581-587.

Furuta, H., Kameda, T., Nakahara, K., Takahashi, Y., and Frangopol, D.M. (2006). "Optimal bridge maintenance planning using improved multi-objective genetic algorithm." *Structure & Infrastructure Engineering*, Taylor and Francis, 2(1), 33-41.

Garbatov, Y., and Soares, C.G. (2001). "Cost and reliability based strategies for fatigue maintenance planning of floating structures." *Reliability Engineering and System Safety*, Elsevier, 73(3), 293-301.

Gharaibeh, E.S., Frangopol, D.M., and Onoufriou, T. (2002). "Reliability-based importance assessment of structural members with applications to complex structures." *Computers and Structures*, Elsevier, 80 (12), 1113-1131.

Ghosn, M., Moses, F., and Frangopol, D.M. (2010). "Redundancy and robustness of highway bridge superstructures and substructures." *Structure & Infrastructure Engineering,* Taylor and Francis, 6(1-2), 257-278.

Glen, L.F., Dinovitzer, A., Malik, L., Basu, R., and Yee, R. (2000). "Guide to damage tolerance analysis of marine structures." *SSC-409*, Ship Structure Committee.

Gonzalez, J.A., Andrade, C., Alonso, C., and Feliu, S. (1995). "Comparison of rate of general corrosion and maximum pitting penetration on concrete embedded steel reinforcement." *Cement and Concrete Research*, Elsevier, 25(2), 257-264.

Gumbel, E.J. (1958). *Statistics of Extremes.* Columbia Univ. Press.

Haimes, Y.Y., Lasdon, L.S., and Wismer, D.A. (1971). "On a bicriterion formulation of the problems of integrated system identification and system optimization." *IEEE Transactions on Systems, Man, and Cybernetics*, 1(3), 296-297.

Harris, D.O. (1977). "A means of assessing the effects of NDT on the reliability of

cyclically loading structures." *Materials Evaluation*, 35(7), 57–69.

Huang, B.-S., and Chiu, H.-N. (1995). "The quality management of the imperfect production process under two monitoring policies." *International Journal of Quality & Reliability Management*, Emerald, 12(3), 19-31.

Irwin, G. R. (1958). "The Crack-extension-force for a crack at a free surface boundary." NRL report 5120.

Kim, A.T., and Stewart, M.G. (2000). "Structural reliability of concrete bridges including improved chloride-induced corrosion models." *Structural Safety*, Elsevier, 22(4), 313-333.

Kim, S., and Frangopol, D.M. (2010). "Optimal planning of structural performance monitoring based on reliability importance assessment." *Probabilistic Engineering Mechanics*, Elsevier, 25(1), 86-98.

Kim, S., and Frangopol, D.M. (2011a). "Cost-effective lifetime structural health monitoring based on availability." *Journal of Structural Engineering*, ASCE, 137(1), 22-33.

Kim, S., and Frangopol, D.M. (2011b). "Inspection and monitoring planning for RC structures based on minimization of expected damage detection delay," *Probabilistic Engineering Mechanics*, Elsevier, 26(2), 308-320.

Kim, S., and Frangopol, D.M. (2011c). "Optimum inspection planning for minimizing fatigue damage detection delay of ship hull structures," *International Journal of Fatigue*, Elsevier, 33(3), 448-459.

Kim, S., and Frangopol, D.M. (2011d). "Probabilistic bi-objective optimum inspection / monitoring planning: applications to naval ships and bridges under fatigue," *Structure and Infrastructure Engineering*, Taylor & Francis, accepted.

Kim, S., and Frangopol, D.M. (2011e). "Cost-based optimum scheduling of inspection and monitoring for fatigue sensitive structures under uncertainty," *Journal of Structural Engineering*, doi: 10.1061 / (ASCE) ST. 1943 - 541X.0000365, ASCE,

in press.

Kim, S., Frangopol, D.M., and Zhu, B. (2011). "Probabilistic optimum inspection / repair planning to extend lifetime of deteriorating RC structures," *Journal of Performance of Constructed Facilities*, ASCE, doi: 10.1061 / (ASCE) CF. 1943 - 5509.0000197, in press.

Kirkpatrick, T.J., Weyers, R.E., Anderson-Cook, C.M., and Sprinkel, M.M. (2002). "Probabilistic model for the chloride-induced corrosion service life of bridge decks." *Cement and Concrete Research*, Elsevier, 32(12), 1943-1960.

Kong, J.S., Akgul, F., and Frangopol, D.M. (2000). "User's Manual, Monte Carlo Simulation Program." Report No. 00-1, Structural Engineering and Structural Mechanics Research series No. CU/SR-00/1, Department of Civil, Environmental, and Architectural Engineering, University of Colorado, Boulder, November 2000.

Kong, J.S., and Frangopol, D.M. (2003a). "Evaluation of expected life-cycle maintenance cost of deteriorating structures." *Journal of Structural Engineering*, ASCE, 129(5), 682–691.

Kong, J.S., and Frangopol, D.M. (2003b). "Life-cycle reliability based maintenance cost optimization of deteriorating structures with emphasis on bridges." *Journal of Structural Engineering,* ASCE, 129(6), 818–828.

Kong, J. S., and Frangopol, D. M. (2005). "Probabilistic optimization of aging structures considering maintenance and failure cost." *Journal of Structural Engineering*, ASCE, 131(4), 600–616.

Kulkarni, S.S., and Achenbach, J.D. (2008). "Structural health monitoring and damage prognosis in fatigue." *Structural Health Monitoring*, SAGE, 7(1), 37-49.

Kwon, K., and Frangopol, D.M. (2010). "Bridge fatigue reliability assessment using probability density functions of equivalent stress range based on field monitoring data." *International Journal of Fatigue*, Elsevier, 32(8), 1221-1232.

Lee, L.Y., Pan, J., Hathaway, R., and Barkey, M. (2005). *Fatigue Testing and Analysis: Theory and Analysis*. Elsevier Butterworth-Heinemann, UK.

Leemis, L.M. (1995). *Reliability: Probabilistic Models and Statistical Methods.* Prentice Hall.

Levine, D.M., Ramsey, P.P., Smidt, R.K. (2001). *Applied Statistics for Engineers and Scientists.* Prentice Hall.

Li, C.Q., Lawanwisut, W., and Zheng, J.J. (2005). "Time-dependent reliability method to assess the serviceability of corrosion-affected concrete structures." *Journal of Structural Engineering*, ASCE, 131(11), 1674-1680.

Liu. M., and Frangopol, D.M. (2004). "Optimal bridge maintenance planning based on probabilistic performance prediction." *Engineering Structures*, 26(7), 991–1002.

Liu. M., and Frangopol, D.M. (2005a). "Bridge annual maintenance prioritization under uncertainty by multiobjective combinatorial optimization." *Computer-aided Civil and Infrastructure engineering*, 20(5), 343–353.

Liu. M., and Frangopol, D.M. (2005b). "Multiobjective maintenance planning optimization of deteriorating bridges considering condition, safety, and life-cycle cost." *Journal of Structural Engineering*, ASCE, 131(5), 833–842.

Liu, M., and Frangopol, D.M. (2005c). "Time-dependent bridge network reliability: Novel Approach." *Journal of Structural Engineering*, ASCE, 131(2), 329-337.

Liu, M., Frangopol, D.M., and Kim, S. (2009a). "Bridge safety evaluation based on monitored live load effects." *Journal of Bridge Engineering*, ASCE, 14(4), 257-269.

Liu, M., Frangopol, D.M., and Kim, S. (2009b). "Bridge system performance assessment from structural health monitoring: A case study." *Journal of Structural Engineering*, ASCE, 135(6), 733-742.

Liu, P.-L., Lin, H.-Z., and Der Kiureghian A. (1989). "CalREL user manual." Report No. UCB/SEMM-89/18, Structural Engineering, Mechanics and Materials, Department of Civil Engineering, University of California, Berkeley, CA.

Maage, M., Helland, S., Poulsen, E., Vennesland, O., and Carlsen, J.E. (1996). "Service life predictions of existing concrete structures exposed to marine environment." *ACI Material Journal*, 93 (6), 602-608.

Maage, M., Helland, S., and Carlsen, J.E. (1999). "Chloride penetration into concrete with light weight aggregates." Brite Euram project BE96-3942, Report R3. CUR, Gouda, The Netherlands.

Madsen, H.O., Krenk, S., and Lind, N.C. (1985). *Methods of Structural Safety.* Prentice-Hall, Englewood Cliffs, N.J.

Madsen, H.O., Skjong, R.K, Tallin, A.G., and Kirkemo, F. (1987). "Probabilistic fatigue crack growth analysis of offshore structures, with reliability updating through inspection." *Proceedings of the Marine Structural Reliability Symposium***,** SSC/SNAME, Arlington, VA., 45-55.

Madsen, H.O., and Sørensen J.D. (1990). "Probability-based optimization of fatigue design, inspection and maintenance." *Proceedings of the Fourth International Symposium on Integrity of Offshore Structures*, London, Elsevier, 421 – 432.

Madsen, H.O., Torhaug, R., and Cramer E.H. (1991). "Probability-based cost benefit analysis of fatigue design, inspection and maintenance." *Proceedings of the Marine Structural Inspection, Maintenance and Monitoring Symposium***,** SSC/SNAME, Arlington, VA., II.E.1- 12.

Mahmoud, H.N., Connor, R.J. and Bowman, C.A. (2005). "Results of the fatigue evaluation and field monitoring of the I-39 Northbound Bridge over the Wisconsin River." *ATLSS Report No. 05-04*, Lehigh University, Bethlehem, PA.

Marsh, P.S., and Frangopol, D.M. (2007). "Lifetime multi-objective optimization of cost and spacing of corrosion rate sensors embedded in a deteriorating reinforced

concrete bridge deck." *Journal of Structural Engineering*, ASCE, 133(6), 777–787.

Marsh, P.S., and Frangopol, D.M. (2008). "Reinforced concrete bridge deck reliability model incorporating temporal and spatial variations of probabilistic corrosion rate sensor data." *Reliability Engineering and System Safety*, Elsevier, 93(3), 364-409.

MathWorks Inc. (2009). *Optimization Toolbox™ 4 User's Guide*. The MathWorks, Inc., USA.

Meo, M., and Zumpano, G. (2005). "On the optimal sensor placement techniques for a bridge structure." *Engineering Structures*, Elsevier, 27(10), 1488-1497.

Miki, C. (2007). "Retrofitting engineering for steel bridge structures." XIII WG5-74-07, International Institute of Welding.

MINITAB release 15 statistical software. (2007), Minitab Inc., 1829 Pine Hall Rd, State College, PA 16801, USA

Moan, T. (2005). "Reliability-based management of inspection, maintenance and repair of offshore structures." *Structure & Infrastructure Engineering*, Taylor and Francis, 1(1), 33-62.

Mohanty, J.R., Verma, B.B., and Ray, P.K. (2009). "Prediction of fatigue crack growth and residual life using an exponential model: Part I (constant amplitude loading)." *International Journal of Fatigue*, Elsevier, 31(3) 418−424.

Mori, Y., and Ellingwood, B.R. (1993). "Reliability-based service-life assessment of aging concrete structures." *Journal of Structural Engineering*, ASCE, 119(5), 1600-1621.

Mori, Y., and Ellingwood, B.R. (1994a). "Maintaining reliability of concrete structures. I: Role of inspection / repair." *Journal of Structural Engineering*, *ASCE*, 120(3), 824-845.

Mori, Y., and Ellingwood, B.R. (1994b). "Maintaining reliability of concrete

structures. II: Optimum inspection / repair." *Journal of Structural Engineering*, *ASCE*, 120(3), 846-862.

Murthy, V.K., and Swartz, G.B. (1974). "Cumulative fatigue damage." *Statistical Papers*, Springer Berlin/Heidelberg, 15(2-3), 202-231.

NCHRP (2005). "Concrete bridge deck performance." NCHRP-synthesis 333, *Transportation Research Board*, *National Cooperative Highway Research Program*, Washington D.C.

NCHRP (2006). "Manual on service life of corrosion-damaged reinforced concrete bridge superstructure elements." NCHRP-report 558, *Transportation Research Board*, *National Cooperative Highway Research Program*, Washington D.C.

Neves, L.A.C., Frangopol, D.M., and Cruz, P.J.S. (2004). "Cost of life extension of deteriorating structures under reliability-based maintenance." *Computers and Structures*, 89 (13-14), 1077–1089.

Neves, L.A.C., Frangopol, D.M., and Cruz, P.J.S. (2006a). "Probabilistic lifetime-oriented multiobjective optimization of bridge maintenance: Single maintenance type." *Journal of Structural Engineering*, ASCE, 132(6), 991–1005.

Neves, L.A.C., Frangopol, D.M., and Petcherdchoo, A. (2006b). "Probabilistic lifetime-oriented multiobjective optimization of bridge maintenance: Combination of maintenance types." *Journal of Structural Engineering*, ASCE, 132(11), 1821–11834.

Okasha, N.M., and Frangopol, D.M. (2009). "Lifetime-oriented multi-objective optimization of structural maintenance considering system reliability, redundancy and life-cycle cost using GA." *Structural Safety*, Elsevier, 31(6), 460-474.

Okasha, N.M., and Frangopol, D.M. (2010a). "Time-variant redundancy of structural systems." *Structure & Infrastructure Engineering*, Taylor and Francis, 6(1-2), 279-301.

Okasha, N.M., and Frangopol, D.M. (2010b). "Novel approach for multi-criteria optimization of life-cycle preventive and essential maintenance of deteriorating structures." *Journal of Structural Engineering*, ASCE, 136(8), 1009-1022.

Osyczka, A. (2002). *Evolutionary Algorithms for Single and Multicriteria Design Optimization*. Physica Verlag, Berlin, Germany.

Packman, P. F., Pearson, H. S., Owens, J. S., and Young, G. (1969). "Definition of fatigue cracks through nondestructive testing." *Journal of Materials*, 4(3), 666-700.

Papazian, J.M., Nardiello, J., Silberstein, R.P., Welsh, G., Grundy, D., Craven, C., Evans, L., Goldfine, N., Michaels, J.E., Michaels, T.E., Li, Y., and Laird, C. (2007). "Sensors for monitoring early stage fatigue cracking." *International Journal of Fatigue*, Elsevier, 29(9-11), 1668-1680.

Paris, P.C., and Erdogan**,** F.A. (1963). **"**Critical analysis of crack propagation laws." *Journal of Basic Engineering*, TRANS ASME, 85(Series D), 528–534.

Peil, U. (2005). "Assessment of bridges via monitoring." *Structure and Infrastructure Engineering*, Taylor & Francis, 1(2), 101-117.

Qian, S. (2005). "Testing Steel Corrosion in Reinforced Concrete." Inspection and Monitoring Techniques for Bridges and Civil Structures. *Woodhead Publishing Ltd. Cambridge*, England.

Rafiq, M.I. (2005). "Health monitoring in proactive reliability management of deteriorating concrete bridges." PhD thesis, School of Engineering, Civil Engineering, University of Surrey, Surrey, UK.

Raupach, M., and Schießl, P. (2001). "Macrocell sensor systems for monitoring of the corrosion risk of the reinforcement in concrete structures." *NDT & E International*, Elsevier, 34(6), 435-442.

Roberge, P.R. (1999) *Handbook of Corrosion Engineering.* McGraw-Hill, NewYork,

USA.

Roberge, P.R. (2007). *Corrosion Inspection and Monitoring.* Wiley-Interscience, New Jersey, USA.

Rolfe, S.T., Hays, K.T., and Henn, A.E. (1993). "Fracture mechanics methodology for fracture control in VLCC's." *Ship Structures Symposium 1993*, November 16-17, 1993, Arlington, VA, available from SNAME, Jersey City, NJ.

Rosenkrantz. W.A. (1997). *Introduction to Probability and Statistics for Scientists and Engineers.* McGraw-Hill Companies, Inc.

Schijve, J. (2003). "Fatigue of structures and materials in the 20th century and the state of the art." *International Journal of Fatigue*, Elsevier, 25(8), 679-702.

Schuëller, G. I. 1998. "Structural reliability - Recent advances." *Proceedings of the 7th International Conference on Structural Safety and Reliability* (ICOSSAR'97), N. Shiraishi, M Shinozuka, and Y.K. Wen, eds., Kyoto, Japan, November 1998. A.A. Balkema Publications, Rotterdam, The Netherlands, pp. 3-35 (Freudenthal lecture).

Shetty, N.K., and Baker, M.J. (1990). "Fatigue reliability of tubular joints in offshore structures: reliability analysis." *Proceedings of the 9th International Conference on Offshore Mechanics and Arctic Engineering*, ASME, Vol. 2, Houston, USA, 223-230.

Shi, Z.Y., Law, S.S., and Zhang, L.M. (2000). "Optimum sensor placement for structural damage detection." *Journal of Engineering Mechanics*, ASCE, 126(11), 1173-1179.

Smoak, W.G. (2002). *Guide to Concrete Repair*. Books for Business, New York - Hong Kong.

Soares, C.G., and Garbatov, Y. (1996a). "Fatigue reliability of the ship hull girder accounting for inspection and repair." *Reliability Engineering and System Safety*,

Elsevier, 51(3), 341-351.

Soares, C.G., and Garbatov, Y. (1996b). "Fatigue reliability of the ship hull girder." *Marine Structures*, Elsevier, 9(3-4), 495-516.

Sobczyk, K. (1987). "Stochastic models for fatigue damage of materials." *Advances in Applied Probability*, Applied Probability Trust, 19(3), 652-673.

Stehno, G., Straninger, W., Bergmeister, K. (1987). "Verfahren zur Vorhersage des Umfanges von Brückensanierungen." Bundesministerium für wirtschaftliche Angelegenheiten, Straßenforschung, Heft 338.

Stewart, M.G. (2004). "Spatial variability of pitting corrosion and its influence on structural fragility and reliability of RC beams in flexure." Structural Safety, Elsevier, 26(4), 453-470.

Stewart, M.G., and Rosowsky, D.V. (1998). "Time-dependent reliability of deteriorating reinforced concrete bridge decks." *Structural Safety*, Elsevier, 20(1), 91-109.

Strauss, A., Kala, Z., Bergmeister, K., Hoffmann, S., and Novak, D. (2006). Technologische Eigenschaften von Stählen im europäischen Vergleich. Stahlbau, Ernst & Sohn, 75(1), 55-60.

Strauss, A., Frangopol, D.M., and Kim, S. (2008). "Use of monitoring extreme data for the performance prediction of structures; Bayesian updating." *Engineering Structures*, Elsevier, 30(12), 3654-3666.

Teplý, B., Chromá, M., Matesová, D., and Rovnaník, P. (2006). "FReET-D. Program Documentation, Part 1 and Part 2." Institute of Structural Mechanics, Fakulty Stavebni, Vysoké Uceni Technické v Brne.

Thoft-Christensen, P., and Murotsu, Y. (1986). *Application of Structural System Reliability Theory.* Springer-Verlag.

Thoft-Christensen, P. (2003). "Corrosion and cracking of reinforced concrete."

Life-Cycle Performance of Deteriorating Structures (edited by D.M. Frangopol, E. Brühwiler, M.H. Faber, B. Adey), ASCE, 26-36.

Torres-Acosta, A.A., and Martinez-Madrid, M. (2003). "Residual life of corroding reinforced concrete structures in marine environment." *Journal of Materials in Civil Engineering*, ASCE, 15(4), 344-353.

Tuutti, K. (1982). *Corrosion of Steel in Concrete*, Swedish Cement and Concrete Research Institute, 17–21.

Val, D.V., and Melchers, R.E. (1997). "Reliability of deteriorating RC slab bridges." *Journal of Structural Engineering*, ASCE, 123(12), 1638-1644.

Weyers, R.E., Prowell, B., Sprinkel, M.M., and Vorster, M. (1993). "Concrete bridge protection, repair, and rehabilitation relative to reinforcement corrosion: A methods application manual." SHRP-S-360, *Strategic Highway Research Program*, Washington. DC.

Worden, K., and Burrows, A.P. (2001). "Optimal sensor placement for fault detection." *Engineering Structures*, Elsevier, 23(8), 885-901.

White, G.J. and Ayyub, B.M. (1987). "Reliability-based fatigue design for ship structures." *Naval Engineers Journal*, Wiley Interscience, 99(3) 135-149.

Zhang, J. and Lounis, Z. (2006). "Sensitivity analysis of simplified diffusion-based corrosion initiation model of concrete structures exposed to chlorides." *Cement and Concrete Research*, Elsevier, 36(7), 312-323.

Zhang, R., and Mahadevan, S. (2000). "Model uncertainty and Bayesian updating in reliability-based inspection." *Structural Safety*, Elsevier, 22(2), 145-160.

Zheng, R., and Ellingwood, B.R. (1998). "Role of non-destructive evaluation in time-dependent reliability analysis." *Structural Safety*, Elsevier, 20(4), 325-339.

APPENDIX

A.1 Notation

a = crack size

a_{mar} = crack-based safety margin during damage process

A_{st} = cross-section area of reinforcement

$\overline{A}$ = average availability of monitoring data for structural performance prediction

$C_{ch}(x, t)$ = chloride concentration at depth x from the surface at time t

$C_{ch,o}$ = chloride concentration at the concrete surface

$C_{ch,th}$ = threshold chloride concentration

C_{COM} = total inspection and/or monitoring cost (i.e., $C_{INS} + C_{MON}$)

C_e = measurement error factor

C_{level} = confidence level

C_{ET} = expected total life-cycle cost

C_{INI} = initial cost including design and construction cost

C_{ins} = cost of a single inspection

C_{INS} = expected total cost of inspection

C_{FAIL} = expected cost of failure

C_{main} = maintenance cost

$C_{main,i}$ = ith maintenance cost

C_{mon} = cost of a single monitoring

C_{MON} = total monitoring cost

C_{PM} = expected cost of routine maintenance

C_{REP} = expected cost of repair

d_{st0} = initial diameter of reinforcement

D_{ch} = effective chloride diffusion coefficient

$E(X)$ = expected value of random variable X

f_{exm} = monitored extreme data

f_p = prediction function

$f_X(x)$ = probability density function of random variable X

$f_{X,Y}(x,y)$ = joint probability density function of random variables X and Y

$F_X(x)$ = cumulative distribution function of random variable X

$g(\boldsymbol{X})$ = state function

M = safety margin

n_{insp} = number of inspections

n_{main} = number of maintenance actions

n_{mon} = number of monitorings
n_{op} = order of the polynomial function
N_{an} = annual number of cycles
N_{cycle} = total number of cycles
N_{lt} = total number of heavy trucks which crossed the bridge on the left lane during monitoring period
N_{rt} = total number of heavy trucks which crossed the bridge on the right lane during monitoring period
N_{ss} = total number of heavy trucks which crossed bridge side-by-side during monitoring period
N_{tt} = total number of heavy trucks which crossed the bridge during monitoring period
$NRIF_i$ = normalized reliability importance factor of component i
p_F = probability of failure
p_S = probability of survival
P_{exd} = exceedance probability
P_{insp} = probability of damage detection
P_{rep} = probability of repair
$\boldsymbol{PS}$ = Pareto solution set
PT = maximum penetration of pitting
$q_{limit,i}$ = predefined upper limit of physical quantity of component i
$q_{mon,i}$ = physical quantity obtained from monitoring system of component i
r_{cycle} = annual increase rate of number of cycles
r_{dis} = discount rate of money
r_{md} = ratio of monitoring duration and prediction duration
R = resistance
R_{pit} = ratio of maximum pit depth to average pit depth
RIF_i = reliability importance factor of ith component
S = load effect
t_{delay} = damage detection delay
t_{det} = time for damage to be detected
t_e = upper bound of damage occurrence
t_i = ith time interval
$t_{insp,i}$ = ith inspection time
t_{life} = service life of a structure
t_{mar} = time-based safety margin
$t_{md,i}$ = ith monitoring period
$t_{mon,i}$ = ith monitoring starting time
t_s = lower bound of damage occurrence

T_{corr} = corrosion initiation time

$T_{main,i}$ = ith maintenance application time

X' = reduced random variable X

$Y(a)$ = geometry function

r_{corr} = corrosion rate

r_{dis} = discount rate of money

$r^{(0)}_{det}$ = deterioration rate without effect of maintenance

r_{det} = deterioration rate with effect of maintenance

β = reliability index

$\beta_{imp,i}$ = improved reliability index due to ith maintenance

β_p = reliability profile

$\beta_{system,IN}$ = system reliability index when all components are independent

$\beta_{system,PC}$ = system reliability index when all components are perfectly correlated

β_{target} = target value of reliability index

δ_c = corrosion damage intensity

$\delta_{c,0.5}$ = corrosion damage intensity at which the inspection method has a 50% probability of damage detection

δ_f = fatigue damage intensity

$\delta_{f,0.5}$ = fatigue damage intensity at which the inspection method has a 50% probability of damage detection

ΔK = stress intensity factor

λ_{par} = location parameter

ξ_{par} = shape parameter

ρ_{par} = scale parameter

Φ = standard normal cumulative distribution function

Φ^{-1} = inverse standard normal cumulative distribution function

μ_X = mean value of X

ρ_{sys} = system correlation matrix

σ_{limit} = predefined stress limit

σ_{max} = maximum stress

σ_X = standard deviation of X

σ_{yield} = yield strength

$\zeta(t)$ = ratio of the expected largest value during future time period t to the largest value obtained during the monitored period

A.2 Detailed Flowchart of Computation Platform for Optimum Inspection, Monitoring and Maintenance Planning under Uncertainty

This section presents detailed computational flowchart for optimum inspection, monitoring and maintenance planning.

- Figure A.1 shows the detailed flowchart to assess and predict the structural system performance, and normalized reliability importance factors of individual components.
- The detailed flowchart for optimum monitoring planning for a structural component is provided in Figure A.2.
- The detailed flowchart for optimum monitoring planning for a structural system is provided in Figure A.3. The outputs from Figures A.1 and A.2 serves as input in Figure A.3, as shown in this figure. These three flowcharts are used to compute the results in Chapter 4.
- Figure A.4(a) shows the detailed computational procedure for inspection and maintenance planning for minimizing the expected damage detection delay. The detailed optimization procedure is provided in Figure A.4(b). All the results of single and bi-objective optimization in Chapter 5 are obtained from computational procedure in Figure A.4.
- Figure A.5 presents the detailed flowchart for inspection and maintenance planning for minimizing the expected total cost. This figure is associated with the results in Chapter 6.
- Figure A.6 provides the detailed computational flowchart for the approach in Chapter 7.

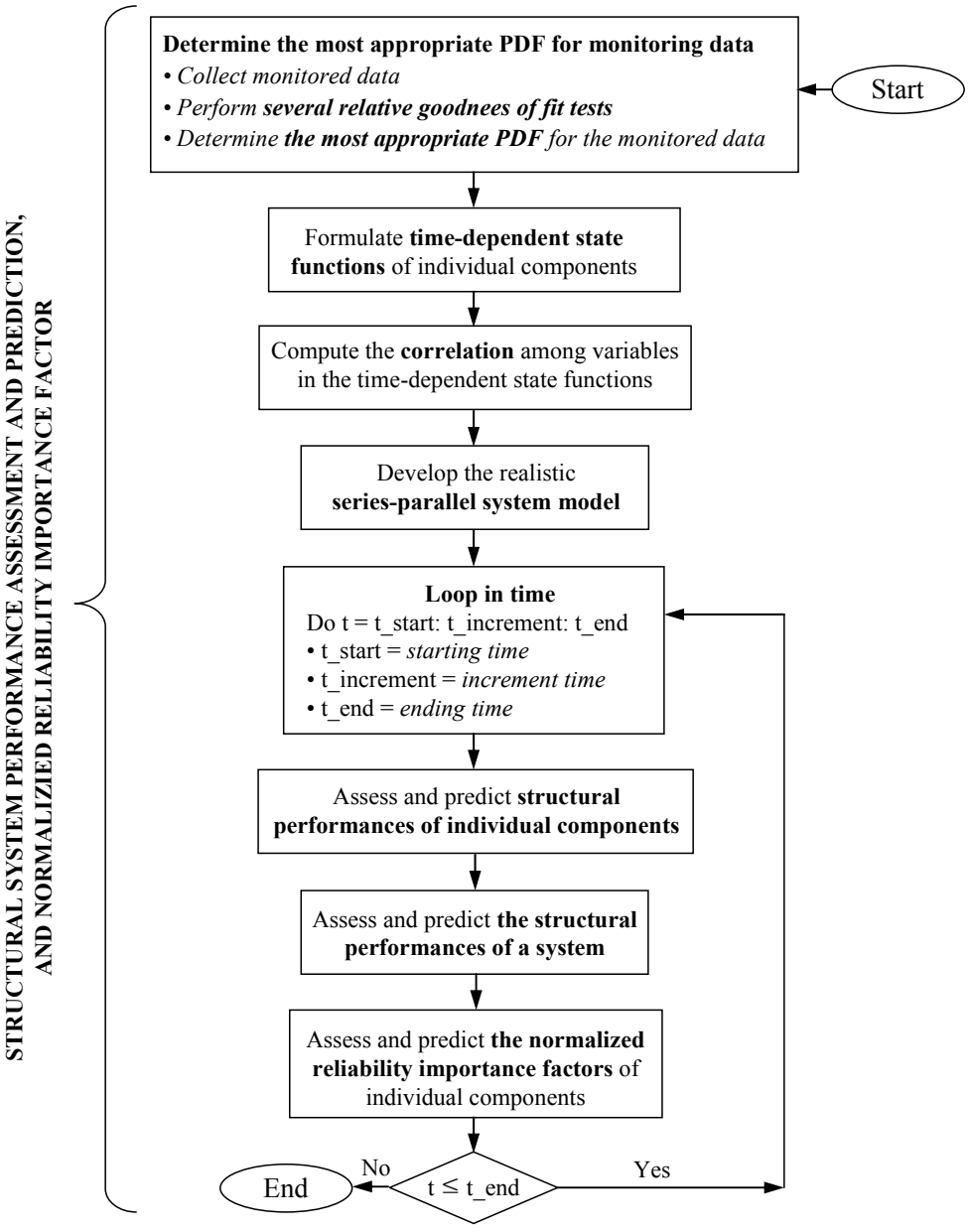

Figure A.1 Detailed flow chart for assessment and prediction of structural system performance and normalized reliability importance factors of individual components

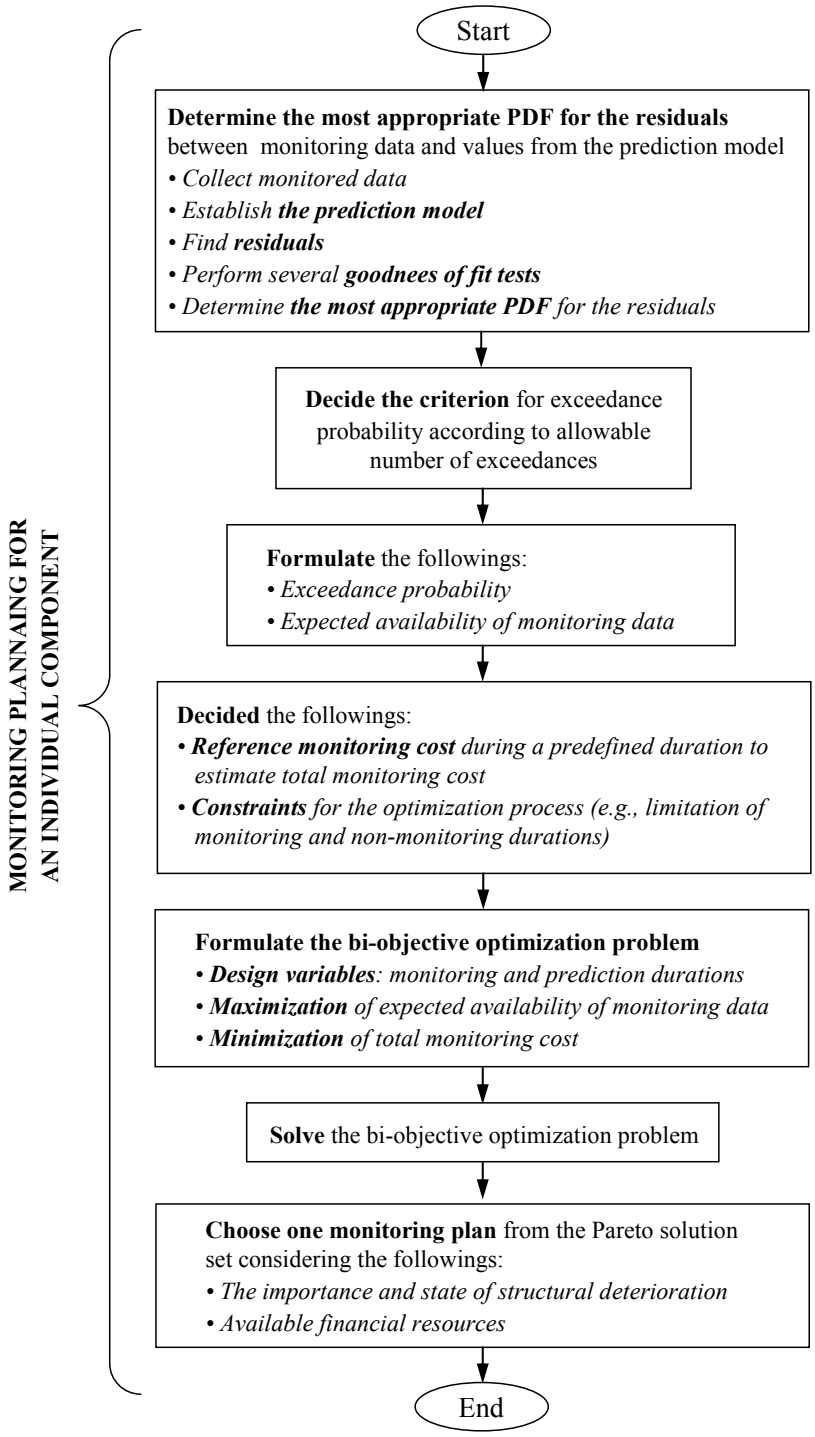

Figure A.2 Detailed flow chart for optimum monitoring planning of individual components based on availability

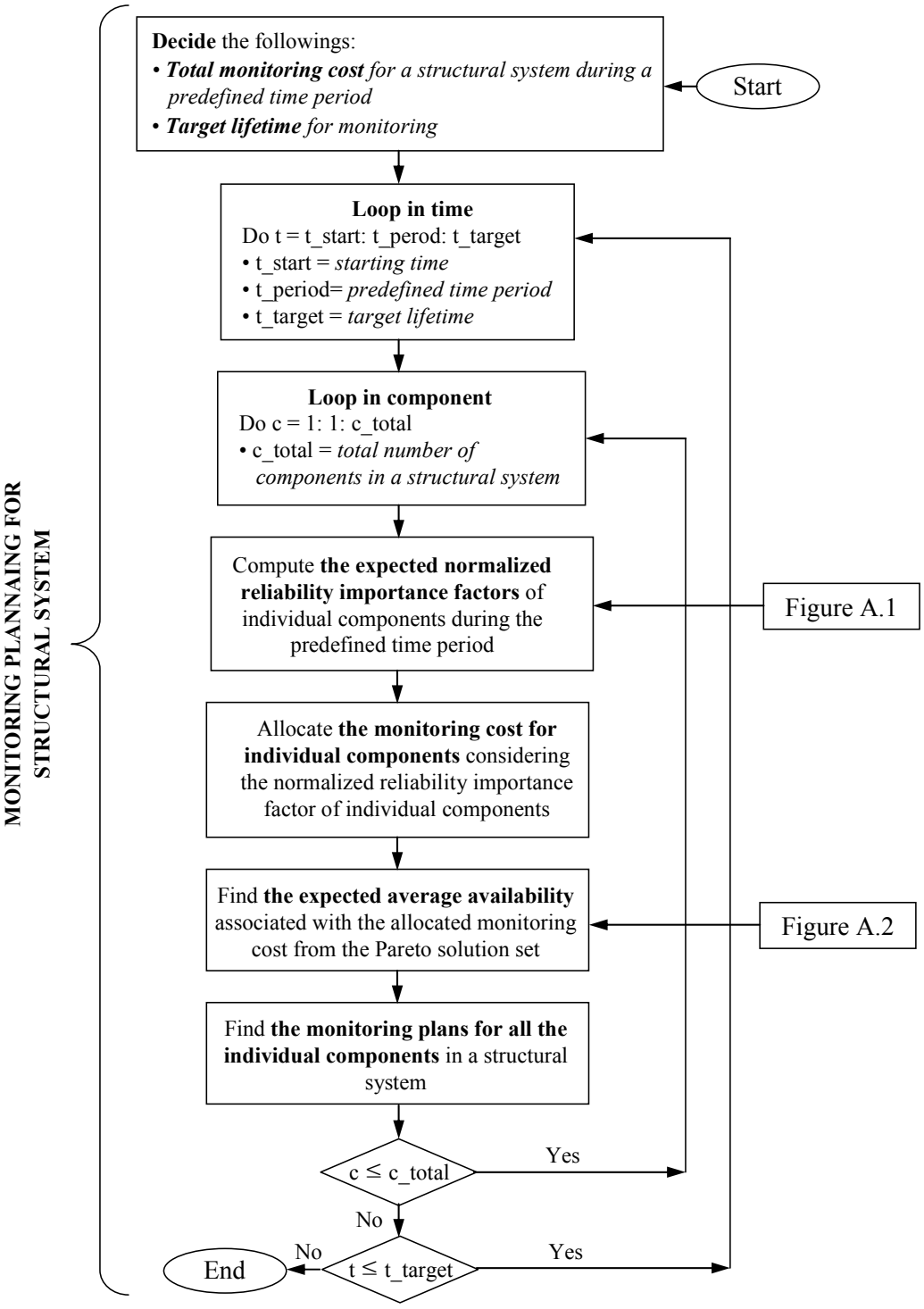

Figure A.3 Detailed flow chart for optimum monitoring planning of a structural system based on availability

(a)

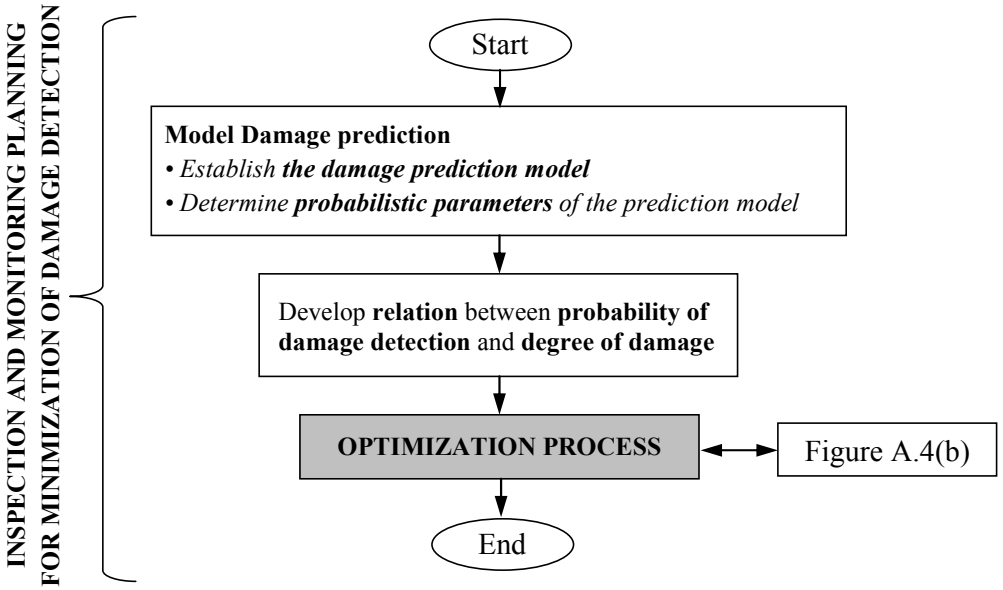

Figure A.4 Detailed flow chart for optimum inspection and maintenance planning for minimizing the expected damage detection delay: (a) general process; and (b) optimization process in (a)

(b)

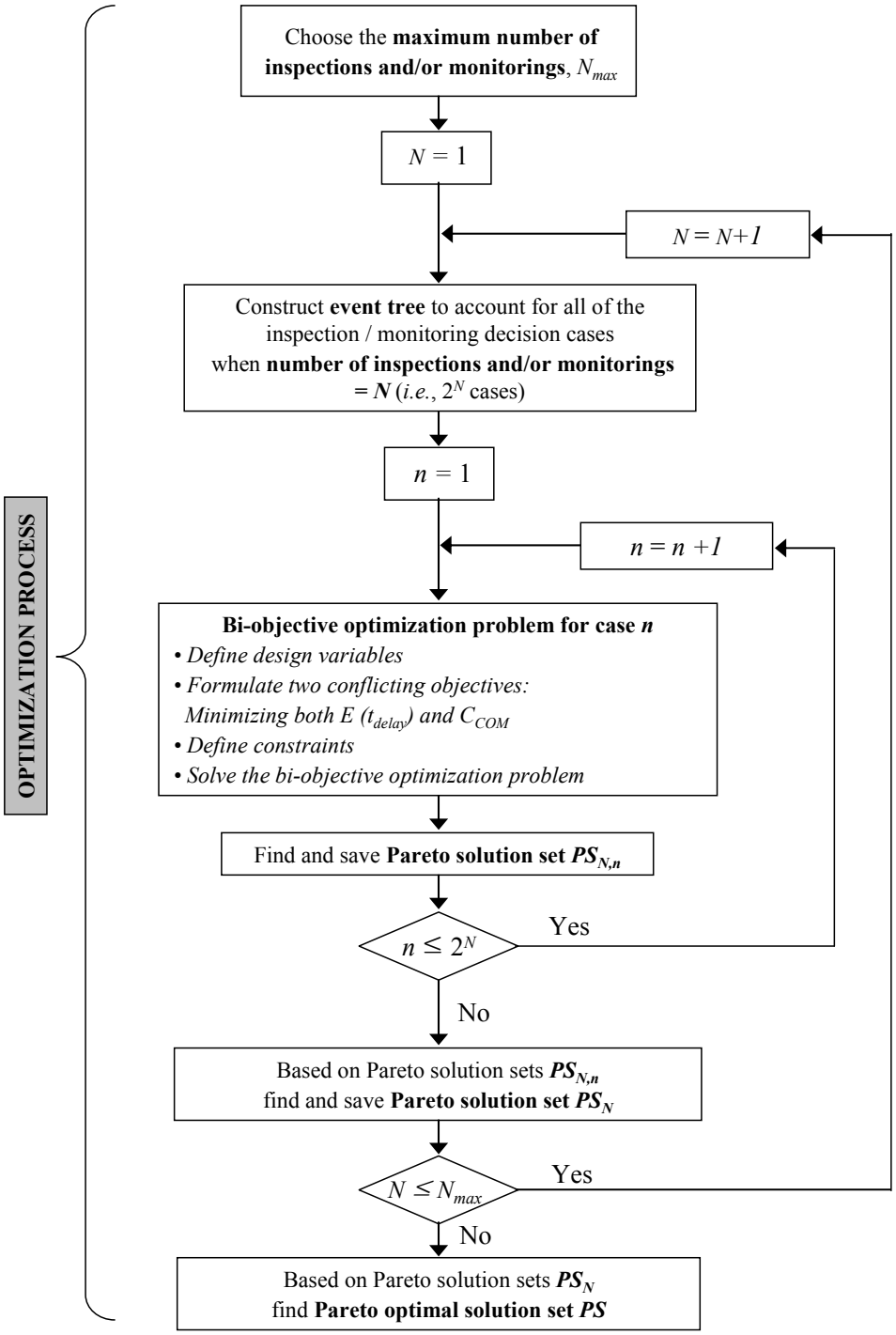

Figure A.4 Detailed flow chart for optimum inspection and maintenance planning for minimizing the expected damage detection delay: (a) general process; and (b) optimization process in (a) (continued)

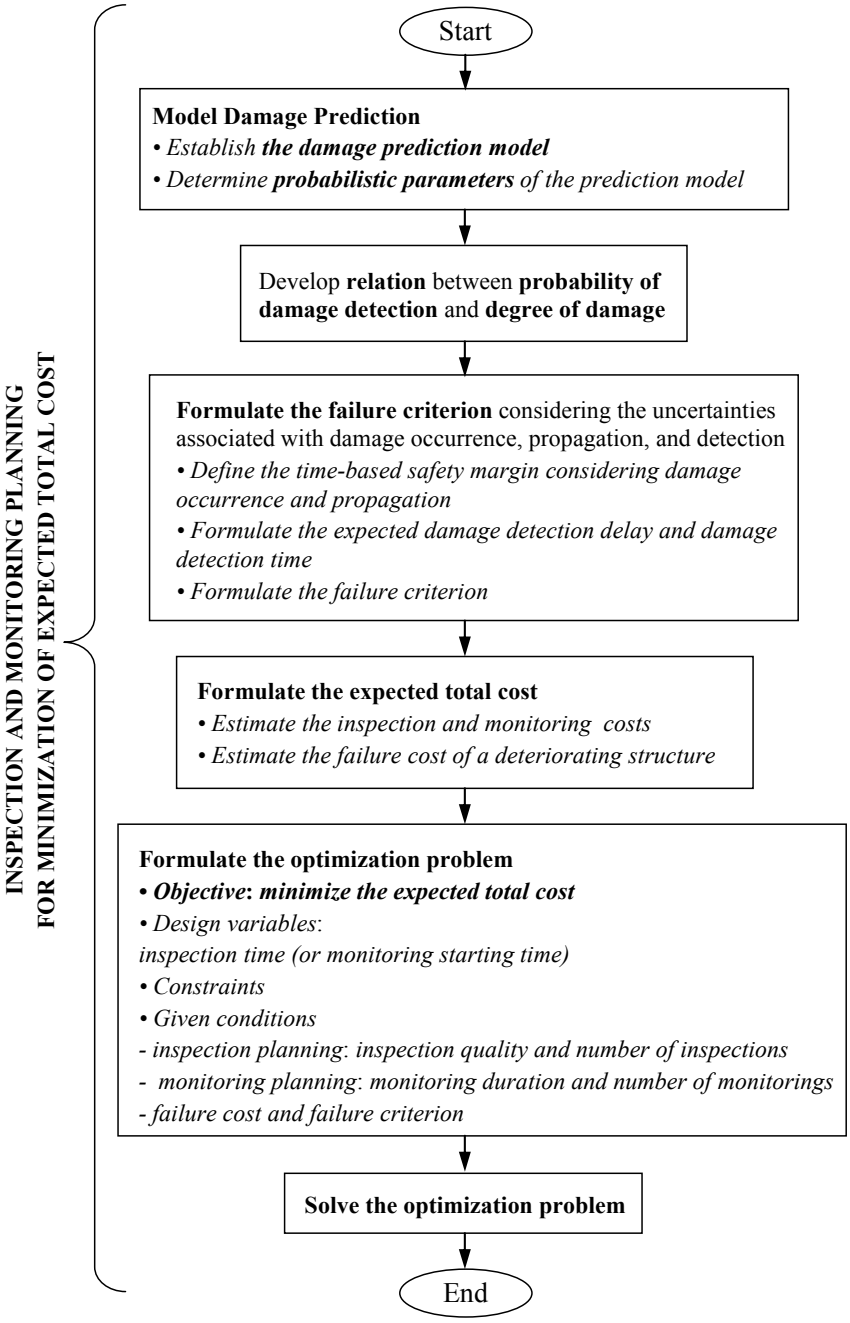

Figure A.5 Computational Procedure for optimum inspection and monitoring planning for minimizing the expected total cost

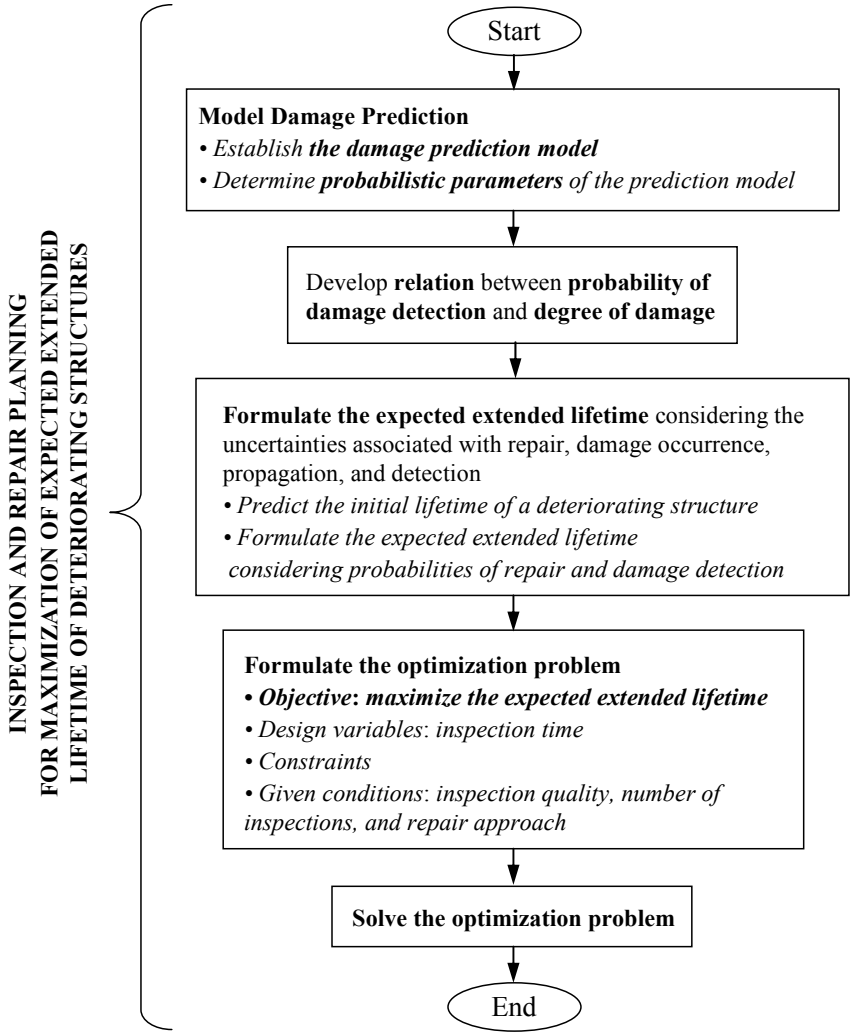

Figure A.6 Procedure for optimum inspection and repair planning for maximizing the expected extended lifetime

VITA

Sunyong Kim was born on September 17, 1976 in Seoul, Republic of Korea to Chuljoong Kim and his wife, Younghee Oh. He received his Bachelor of Science Degree in Civil Engineering from Yonsei University, Seoul, Republic of Korea in February 1999. He attended the Graduate School of Civil and Environmental Engineering in Korea Advanced Institute of Science and Technology (KAIST), Daejeon, Republic of Korea in March 2002, and received his Mater of Science Degree from KAIST in February 2004. He started his Ph.D. program at University of Colorado, Boulder, CO, USA in 2005. He joined Lehigh University, Bethlehem, PA in 2006.